



**HAL**  
open science

# Experimental and numerical study on passive building envelope integrated by PCM and bio-based concrete

Dongxia Wu

► **To cite this version:**

Dongxia Wu. Experimental and numerical study on passive building envelope integrated by PCM and bio-based concrete. Engineering Sciences [physics]. Université de Lorraine, 2022. English. NNT : 2022LORR0104 . tel-03889576

**HAL Id: tel-03889576**

**<https://hal.univ-lorraine.fr/tel-03889576>**

Submitted on 8 Dec 2022

**HAL** is a multi-disciplinary open access archive for the deposit and dissemination of scientific research documents, whether they are published or not. The documents may come from teaching and research institutions in France or abroad, or from public or private research centers.

L'archive ouverte pluridisciplinaire **HAL**, est destinée au dépôt et à la diffusion de documents scientifiques de niveau recherche, publiés ou non, émanant des établissements d'enseignement et de recherche français ou étrangers, des laboratoires publics ou privés.



**UNIVERSITÉ  
DE LORRAINE**

**BIBLIOTHÈQUES  
UNIVERSITAIRES**

## AVERTISSEMENT

Ce document est le fruit d'un long travail approuvé par le jury de soutenance et mis à disposition de l'ensemble de la communauté universitaire élargie.

Il est soumis à la propriété intellectuelle de l'auteur. Ceci implique une obligation de citation et de référencement lors de l'utilisation de ce document.

D'autre part, toute contrefaçon, plagiat, reproduction illicite encourt une poursuite pénale.

Contact bibliothèque : [ddoc-theses-contact@univ-lorraine.fr](mailto:ddoc-theses-contact@univ-lorraine.fr)  
*(Cette adresse ne permet pas de contacter les auteurs)*

## LIENS

Code de la Propriété Intellectuelle. articles L 122. 4

Code de la Propriété Intellectuelle. articles L 335.2- L 335.10

[http://www.cfcopies.com/V2/leg/leg\\_droi.php](http://www.cfcopies.com/V2/leg/leg_droi.php)

<http://www.culture.gouv.fr/culture/infos-pratiques/droits/protection.htm>



## Thèse

Présentée et soutenue publiquement pour l'obtention du titre de

**DOCTEUR DE L'UNIVERSITE DE LORRAINE**

Mention : **Énergie et Mécanique**

par **Dongxia WU**

Sous la direction de **Mohammed EL GANAOU**

**Experimental and numerical study on passive building envelope integrated by PCM and bio-based concrete**

**Soutenance le 5 juillet 2022**

### Membres du jury :

Directeur de thèse :	<b>M. Mohammed EL GANAOU</b>	Professeur, Université de Lorraine, Longwy
Co-directeur de thèse :	<b>M. Mourad RAHIM</b>	Maître de conférences, Université de Lorraine, Longwy
Rapporteurs :	<b>Mme. Monica SIROUX</b>	Professeur, Université de Strasbourg, Strasbourg
	<b>M. Laurent ROYON</b>	Professeur, Université Paris Cité, Paris
Président du jury :	<b>M. Rachid BENNACER</b>	Professeur, Université Paris-Saclay, Gif sur Yvette
Examineurs :	<b>M. Bin LIU</b>	Professeur, Tianjin University of Commerce, Tianjin
	<b>Mme. Alexandra BOURDOT</b>	Maître de conférences, Université Paris-Saclay, Gif sur Yvette
	<b>Mme. Ahlem ARFAOUI</b>	Maître de conférences, Université de Reims Champagne-Ardenne, Reims
Membres invités :	<b>Mme. Halima ALEM-MARCHAND</b>	Maître de conférences, Université de Lorraine, Nancy
	<b>M. Henri VAHABI</b>	Maître de conférences, Université de Lorraine, Saint-Avold
	<b>M. Olivier CASPARY</b>	Maître de conférences, Université de Lorraine, Saint-Dié-des-Vosges

## **Abstract**

With the development of society, the demand for energy saving and carbon emission reduction in buildings as well as the indoor thermal and humidity environment comfort is gradually increasing. Using Phase change materials (PCMs) or bio-based hygroscopic materials as building envelopes are promising solutions. PCMs can improve indoor thermal comfort and reduce energy consumption, while bio-based hygroscopic materials are environment-friendly materials that enable indoor humidity regulation and thermal insulation. However, only a few studies have explored the integrated application of the two types of materials and comprehensively analyzed the energy and hygrothermal performance. This dissertation proposed a passive envelope solution that integrates PCM and bio-based hemp concrete (HC) to simultaneously improve the energy, thermal, and hygric performances of buildings. The main objectives of this study are to investigate the feasibility of the integrated envelopes, to comprehensively study the hygrothermal and energy performance as well as the advantages and disadvantages of different configurations with PCM placed in different locations of the HC, and to conduct the parametric analysis and evaluate the application risks of the integrated envelope.

First, experiments were conducted by comparing the hygrothermal performance of a reference envelope (HC only) and three integrated envelopes with PCM placed in different locations under two typical boundary conditions. The results demonstrated the feasibility of the integrated envelopes. The presence of PCM increased the thermal and hygric inertia of the envelope. As a result, the time delay was increased and the temperature/relative humidity amplitude was decreased. Different configurations had different advantages and disadvantages. The configurations with PCM placed in the middle of the HC was worth noting as it had small temperature/relative humidity fluctuation, long temperature time delay, and large energy savings.

Then, the mathematical model of the integrated envelope that couples heat and moisture transfer

and considers the temperature dependence of HC's hygroscopic characteristic was developed. The accuracy of the model was validated by comparison with the experimental data. Based on the validated model, the simulations were performed in a Mediterranean climate to comprehensively investigate the hygrothermal and energy performance of the integrated envelope. The results highlighted the indispensable role moisture transfer plays in determining the indoor hygric environment and heat load, as well as the valuable effect of the integrated envelope on improving both energy and hygrothermal performance. Besides, the integrated envelope with PCM close to (but not in contact with) the interior showed great potential for saving energy and adapting to climate humidity variation while guaranteeing moisture equilibrium within the HC.

Finally, the parametric analysis was performed from the perspective of PCM properties (thickness, latent heat, and phase transition range), and the application (condensation and mold growth) risk was evaluated. The results of the parametric analysis illustrated that the performance of the integrated envelope could be improved by increasing the thickness and latent heat and identifying the appropriate phase transition range of the PCM. The risk evaluation results confirmed that the integrated envelope was free from the risk of condensation and mold growth.

## **Keywords**

Phase change material (PCM); Bio-based concrete; Passive building envelope; Heat and moisture transfer; Hygrothermal and energy performance; Parametric analysis; Risk evaluation

## Acknowledgement

Time is a file that wears and makes no noise.

It all started in July 2017. The International Conference on Materials & Energy was held in Tianjin, China. I met Prof. Ganaoui and Prof. Bennacer, who were enthusiastic. Four months later, I contacted Prof. Ganaoui and started to apply for the CSC (China Scholar Council) funding. Fortunately, I successfully applied for the CSC funding on May 30, 2018 and arrived in France on Jan 21, 2019.

Three years have elapsed in a flash and I am about to finish my doctoral career. I would like to express my sincere gratitude to my supervisor, Prof. Mohammed El Ganaoui, who opened the doors of his laboratory and gave me the opportunity to study in France. He has provided me with great support and help in my research, including professional advice, meticulous arrangements, and valuable guidance. His dedication and enthusiasm for research greatly encouraged my motivation.

I am also grateful to my extramural academic supervisor, Prof. Rachid Bennacer, who spent a lot of time guiding my research work. He provided advice on the selection of research directions. He provided guidance in the progress of research work and publication of papers. His professional knowledge and rigorous research attitude are invaluable resources worthy learning.

Thanks to Dr. Mourad Rahim, who is the co-director of my PhD thesis. He gave me detailed guidance and help in doing experiments, implementing simulations, writing papers, arranging defenses, etc. The frequent discussions and communication between us guaranteed the completion of the PhD thesis. The same thanks also to Dr. Rabah Djedjig, an excellent young researcher in our institute.

Thanks also to Prof. Bin Liu, who is also my extramural academic supervisor. Despite the difficulties of time difference between China and France, he contributed a lot of constructive comments to our research work. Most importantly, he was the one who built an academic bridge between my Chinese university and the French universities, and I was the third lucky one to step on that bridge.

I would like to express my sincere gratitude to all the jury members during my PhD defense. Thanks to their professional questions and constructive suggestions, I have gained a lot during the defense period. Special thanks to my reviewers: Monica SIROUX and Laurent ROYON, for their patient revisions and professional suggestions on my thesis.

I received a lot of help from the researchers and PhD/master students in our lab. They are Dr. Damien Guilbert, Dr. Monireh Asadi, Dr. Lahoucine Ouhsaine, Dr. Vittorio Guida, Dr. Ferial Mustapha, Maoulida Fahad, Mohamed Amine Tounsi, Salma Kouzzi, etc. Thanks also to the staff of our department. Thanks also to my French friend Ilias El Ganaoui, who often comes to chat with me.

I am very grateful to my Chinese friends who are also studying in France. They are Xinyi Chen, Xiaoyu Ma, Bengang Zhang, Wendong Li, Bin Guo, etc. I will always remember the happy times we had together in traveling, having dinner, and playing balls.

I would also like to thank my friends and teammates at the A.S.T.T. Herserange Table Tennis Club. I miss the days when we played together. Thanks: Michel Penicaud, Michel Durey, Jose Mateos, Matthieu Penicaud, Stephane Digirolamo, Yannick Charlot, David Michelin, Yan Pan, Guillaume Dubuy, Clement Delboccio, Pascal Maison, Stephane Cazzaro, Jerome Clin, Kevin Mougeot, Jeremy Parve, Patou Patrick, Lionel Replinger, Mathieu Colson, Marco Delavega, Stef Chok, etc.

Special thanks to my family. My dad, Henghai Wu, my mom, Juan Liu, and my wife, Chaofan Wang. My parents gave me enough energy and encouragement to overcome difficulties. My wife gave me full understanding, support, and motivation to carry out my scientific research for a better future. They are the harbor and motivation for me to move forward in my life.

Finally, I give my heartfelt gratitude to my motherland, China. Without the support of national strength and CSC funding from my homeland, I would not have been able to pursue my PhD in France. I wish my great motherland prosperity forever!

# Table of contents

<b>Abstract</b> .....	i
<b>Acknowledgement</b> .....	iii
<b>Table of contents</b> .....	v
<b>List of figures</b> .....	xi
<b>List of tables</b> .....	xvi
<b>Nomenclature</b> .....	xvii
<b>Chapter 1 Introduction</b> .....	1
1.1 Background .....	1
1.2 Motivation, objective, and approach .....	4
1.2.1 Motivation .....	4
1.2.2 Objective.....	6
1.2.3 Approach and research frame .....	7
1.3 Thesis outline .....	8
<b>Chapter 2 Literature review and basic theoretical considerations</b> .....	9
2.1 Indoor thermal and humid environment.....	9
2.1.1 Thermal and humid comfort .....	9
2.1.2 Global Climate and interior environment.....	12
2.2 Bio-based materials as building envelope .....	13
2.2.1 Bio-based materials as building structure.....	13

2.2.2	Thermal insulation characteristics .....	14
2.2.3	Hygroscopic characteristics .....	17
2.2.4	Temperature dependence of hygroscopic characteristics .....	19
2.2.5	Impact of hygrothermal behavior on energy consumption.....	21
2.3	PCMs as building envelope.....	22
2.3.1	PCMs as part of building construction .....	22
2.3.2	Adaptability of PCMs.....	28
2.3.3	Location and property dependence of PCM performance.....	29
2.4	Integration of hygroscopic materials and PCMs .....	32
2.4.1	Preparation and characterization of the integrated materials.....	32
2.4.2	Application of the integrated materials .....	33
2.5	Heat and mass transfer theory and model .....	35
2.5.1	Moisture transfer in porous media.....	35
2.5.2	Heat transfer in porous media.....	36
2.5.3	Coupled heat and moisture transfer in porous media .....	37
2.5.4	Heat transfer in PCM.....	43
2.6	Conclusion.....	46
Chapter 3	Experimental study on hygrothermal performance of integrated envelope .....	48
3.1	Objectives of experimental study.....	48
3.2	Material and methodology .....	49
3.2.1	Experimental materials .....	49

3.2.2	Experimental facilities .....	51
3.2.3	Experiment setup .....	55
3.2.4	Envelope configurations .....	55
3.2.5	Installation of sensors .....	58
3.2.6	Boundary conditions.....	59
3.3	Temperature and relative humidity stabilization validation.....	63
3.4	Results, analysis, and discussion of static boundary condition.....	65
3.4.1	Hygrothermal behavior of configuration without PCM .....	65
3.4.2	Hygrothermal behavior of configurations with PCM.....	68
3.4.3	Heat flux and heat store/release capacity .....	75
3.5	Results, analysis, and discussion of dynamic boundary condition .....	80
3.5.1	Hygrothermal behavior of the configuration without PCM .....	80
3.5.2	Hygrothermal behavior of the configurations with PCM.....	83
3.5.3	Summary of temperature/relative humidity amplitudes and time delay.....	87
3.5.4	Heat flux and released/absorbed heat on the interior/exterior surface .....	90
3.5.5	Energy storage/release by the whole envelope and the PCM.....	92
3.5.6	PCM activation and storage/release efficiency .....	94
3.6	Conclusion.....	97
3.6.1	Results of static boundary condition .....	98
3.6.2	Results of dynamic boundary condition .....	99
3.6.3	Over conclusion and recommendation .....	100

Chapter 4	Numerical study on hygrothermal performance of integrated envelope .....	101
4.1	Objectives of numerical study.....	101
4.2	Description of the integrated envelope.....	102
4.2.1	Multilayer envelope.....	102
4.2.2	Properties of materials .....	103
4.3	Model derivation and boundary conditions.....	105
4.3.1	Moisture transfer equation of HC .....	105
4.3.2	Heat transfer equation of HC.....	108
4.3.3	Heat transfer equation of PCM.....	109
4.3.4	Boundary conditions.....	110
4.4	Numerical principle and tool.....	112
4.4.1	Commonly used numerical methods .....	113
4.4.2	COMSOL Multiphysics.....	114
4.5	Model validation .....	116
4.6	Climate and interior conditions .....	119
4.7	Metric parameters.....	121
4.8	Results, analysis, and discussion.....	123
4.8.1	Impact of moisture transfer on energy and hygrothermal performance .....	123
4.8.2	Relationship between energy, thermal, and hygric performance .....	125
4.8.3	Impact of PCM and its location on energy and hygrothermal performance .....	127
4.8.4	Evaluation of annual energy and hygric performance.....	130

4.9	Conclusion.....	134
Chapter 5 Parametric analysis and application risk evaluation of integrated envelope ..... 137		
5.1	Objectives of parametric analysis and risk evaluation.....	137
5.2	Methodology of parametric analysis and application risk evaluation.....	138
5.2.1	Methodology of parametric analysis .....	138
5.2.2	Methodology of application risk evaluation.....	140
5.3	Parametric analysis of integrated envelope.....	141
5.3.1	Impact of PCM thickness .....	141
5.3.2	Impact of PCM latent heat.....	143
5.3.3	Impact of PCM phase transition range .....	145
5.4	Evaluation of condensation and mold growth risk.....	148
5.4.1	Evaluation of condensation risk .....	148
5.4.2	Evaluation of mold growth risk.....	151
5.5	Conclusion.....	154
Chapter 6 Conclusions, contributions and future work..... 156		
6.1	Findings and conclusions .....	156
6.2	Contributions.....	160
6.3	Future work .....	161
Appendix ..... 162		
Appendix A: Résumé de la thèse en français ..... 162		
A.1	Résumé .....	162

A.2 Constatations et conclusions.....	164
A.3 Contributions .....	167
A.4 Travaux futurs.....	168
Appendix B: List of publications .....	169
Reference.....	171

©

## List of figures

Fig. 1.1. Primary energy demand and CO <sub>2</sub> emissions .....	1
Fig. 1.2. Buildings and construction's percentage of global energy and CO <sub>2</sub> emissions .....	2
Fig. 1.3 Working principle of (a) hygroscopic material with moisture adsorption/desorption [8] and (b) PCM with latent heat store/release [9].....	4
Fig. 2.1 Optimum relative humidity ranges for minimizing adverse health effects [20].....	10
Fig. 2.2. Dependence of <i>PPD</i> on <i>PMV</i> [21]2.9 .....	11
Fig. 2.3. Recommended operative temperature and humidity [23] .....	11
Fig. 2.4. Köppen climate classification with different climate classifications [24].....	13
Fig. 2.5. Carbon release and store by different material [48] .....	14
Fig. 2.6. Building insulation avoiding external environmental impact [49].....	15
Fig. 2.7 MBVs of hemp concrete (HLC) and flax concrete (FLC) and conventional materials [76]..	18
Fig. 2.8 First desorption isotherms for a mature mortar at four temperatures [86] .....	20
Fig. 2.9. Different methods to incorporate the PCM into construction: (a) microencapsulation; (b)macroencapsulation; (c) shape-stabilization; (d) immersion. [127, 132, 135-137] .....	24
Fig. 2.10. Schematic diagram of a PCM wallboard [140] .....	25
Fig. 2.11. Floor panel incorporated with PCM [142] .....	25
Fig. 2.12. PV-PCM roof [143] .....	26
Fig. 2.13 Ventilated cooling ceiling with PCM [150] .....	27
Fig. 2.14. Glazing systems with/without PCM (left figure) [152] and a schematic of double-glazed PCM window (right figure) [155].....	28
Fig. 2.15 Different walls: (a) No-PCM; (b) PCM close to interior; (c) PCM close to exterior [169].	30
Fig. 3.1. Finished shape-stabilized PCM: (a) PCM panel; (b) aluminum sheet and the mixture of paraffin wax and ethylene-based polymer .....	49

Fig. 3.2. Specific heat capacity of the PCM [222].....	50
Fig. 3.3. Bio-based material: (a) hemp concrete; (b) hemp shives [94].....	50
Fig. 3.4 Climatic chamber (LabEvent L C/64/40/3).....	52
Fig. 3.5 Type K thermocouple and HMP-110 sensor .....	53
Fig. 3.6 Heat flux sensor .....	53
Fig. 3.7 Keithley 2700 data acquisition equipment .....	54
Fig. 3.8 Experimental setup: (a) sketch view; (b) actual experiment .....	55
Fig. 3.9 Four envelope configurations of integrating HC and PCM.....	57
Fig. 3.10 Monitoring points for temperature, relative humidity, and heat flux of (a) configuration X = 0 L in full view and (b) all the configurations .....	58
Fig. 3.11 Installation and arrangement of different monitoring sensors in the actual experiment .....	59
Fig. 3.12 Static boundary condition: (a) temperature and relative humidity condition provided by the climatic chamber; (b) temperature and relative humidity in the psychrometric chart.....	60
Fig. 3.13 Dynamic boundary condition: (a) temperature and relative humidity condition provided by the climatic chamber; (b) temperature and relative humidity in the psychrometric chart.....	62
Fig. 3.14 Temperature behavior of configuration without PCM .....	65
Fig. 3.15 Relative humidity behavior of configuration without PCM.....	66
Fig. 3.16. Temperature behavior of the configuration X = 0 L .....	69
Fig. 3.17. Relative humidity behavior of the configuration X = 0 L .....	70
Fig. 3.18. Temperature behavior of configuration X = 1 L .....	72
Fig. 3.19. Relative humidity behavior of configuration X = 1 L .....	73
Fig. 3.20. Temperature behavior of configuration X = 0.5 L .....	74
Fig. 3.21. Temperature behavior of configuration X = 0.5 L .....	74
Fig. 3.22. (a) Heat flux on the interior surface of the envelope; (b) heat flux difference between each side of the envelope and the imposed temperature (right).....	76

Fig. 3.23. (a) Heat store/release by interior surface; (b) heat store/release by the envelope and ratio value (right).....	78
Fig. 3.24. (a) Temperature in both side of PCM; (b) dynamic specific heat capacity of PCM.....	79
Fig. 3.25. Temperature behavior of the configuration without PCM .....	81
Fig. 3.26. Relative humidity behavior of the configuration without PCM.....	83
Fig. 3.27. Temperature behavior of the configuration X = 0 L .....	83
Fig. 3.28. Relative humidity behavior of the configuration X = 0 L .....	84
Fig. 3.29. Temperature behavior of the configuration X = 1 L .....	85
Fig. 3.30. Relative humidity behavior of the configuration X = 1 L .....	86
Fig. 3.31. Temperature behavior of the configuration X = 0.5 L .....	87
Fig. 3.32. Relative humidity behavior of the configuration X = 0.5 L .....	87
Fig. 3.33. Temperature and relative humidity amplitudes of HC in different configurations .....	88
Fig. 3.34. Temperature amplitude and time delay at different configurations and measurement points .....	89
Fig. 3.35. (a) Heat flux on the exterior and interior surface; (b) heat absorption/release on the exterior/interior surface.....	91
Fig. 3.36. (a) Heat flux difference of the envelope and the PCM; (b) energy storage/release and the proportion of the PCM.....	93
Fig. 3.37. PCM's mean T and melt fraction .....	96
Fig. 3.38. PCM's storage/release efficiency .....	97
Fig. 4.1. Two-dimensional layout of envelope: Baseline and integrated configurations .....	103
Fig. 4.2. Thermal properties of PCM: (a) specific heat capacity; (b) thermal conductivity.....	105
Fig. 4.3. Comparison between the simulation and experimental results of (a) configuration without PCM and (b) configuration X = 0.5 L .....	118
Fig. 4.4. Annual climate and interior conditions: (a) exterior climate in Rome; (b) interior temperature	

and relative humidity .....	120
Fig. 4.5. Representative climate during one week in (a) summer and (b) winter .....	121
Fig. 4.6. Comparison between HMT and HT models: (a) heat fluxes; (b) heat loads.....	124
Fig. 4.7. Relationship between temperature, relative humidity, partial water vapor pressure, moisture flux, and latent heat flux .....	126
Fig. 4.8. Impact of PCM presence and location: (a) cumulative heat load and moisture load; (b) variation of temperature and partial water vapor pressure; (c) reduction of heat load, temperature fluctuation, and partial water vapor pressure fluctuation compared to configuration baseline .....	129
Fig. 4.9. Annual heat gain and loss for HMT and HT models.....	131
Fig. 4.10. Annual heat load for different configurations .....	132
Fig. 4.11. Annual hygric performance for different configurations: (a) moisture load and (b) net moisture load.....	134
Fig. 5.1. Thermal properties of PCMs with different phase transition ranges and latent heats: (a) specific heat capacity; (b) thermal conductivity .....	139
Fig. 5.2. Impact of PCM thickness: (a) cumulative heat load and moisture load; (b) variation of temperature and partial water vapor pressure; (c) reduction of heat load, temperature fluctuation, and partial water vapor pressure fluctuation compared to configuration baseline .....	143
Fig. 5.3. Impact of PCM latent heat: (a) cumulative heat load and moisture load; (b) variation of temperature and partial water vapor pressure; (c) reduction of heat load, temperature fluctuation, and partial water vapor pressure fluctuation compared to configuration baseline .....	145
Fig. 5.4. Middle temperature and melt fraction of PCMs for different PCM phase transition ranges .....	146
Fig. 5.5. Impact of PCM phase transition range: (a) cumulative heat load and moisture load; (b) variation of temperature and partial water vapor pressure; (c) reduction of heat load, temperature fluctuation, and partial water vapor pressure fluctuation compared to configuration baseline.....	148

Fig. 5.6. Condensation risk evaluation of (a) configuration baseline; (b) configuration 1/5; (c) configuration 2/5; (d) configuration 3/5; (e) configuration 4/5 .....151

Fig. 5.7. Mold growth risk evaluation of (a) configuration baseline; (b) configuration 1/5; (c) configuration 2/5; (d) configuration 3/5; (e) configuration 4/5 .....154

## List of tables

Table 3.1. Dimensions and hygrothermal properties of the PCM and the HC .....	51
Table 3.2 Apparatus and sensors .....	55
Table 3.3 Different envelope configurations .....	56
Table 3.4 Temperature and relative humidity combinations for static boundary condition .....	60
Table 3.5 Temperature and relative humidity in the interior (laboratory environment) for static boundary condition .....	61
Table 3.6 Temperature and relative humidity in the interior (laboratory ambient) for dynamic boundary condition .....	63
Table 3.7. Temperature and relative humidity (mean value $\pm$ SD) within the envelope two hours before the start with static boundary condition .....	64
Table 3.8. Temperature and relative humidity (mean value $\pm$ SD) within the envelope two hours before the start with dynamic boundary condition.....	64
Table 4.1 Physical properties of HC [94, 236] and PCM [222] .....	104
Table 4.2 Summary of relative error, RMSE, and $CV_{(RMSE)}$ for configurations without PCM and $X = 0.5 L$ .....	119
Table 4.3 Difference between the HMT and HT models.....	123
Table 5.1 Initial and final temperature of different phase transition ranges .....	139
Table 5.2 Relationship between $\beta$ and latent heat of PCM.....	139
Table 5.3 PCM properties settings for parametric analysis .....	140

## Nomenclature

Symbol	Explanation	Units
$A$	area of envelope	$m^2$
$C_a$	specific heat capacity of air	$J/(kg \cdot K)$
$C_{hc}$	specific heat capacity of HC	$J/(kg \cdot K)$
$C_l$	specific heat capacity of liquid PCM	$J/(kg \cdot K)$
$C_{pcm}$	specific heat capacity of PCM	$J/(kg \cdot K)$
$C_{s,o}$	initial value of parameter under study for characteristic time	-
$C_s$	specific heat capacity of solid PCM	$J/(kg \cdot K)$
$C_{stu}$	parameter under study for characteristic time calculation	-
$C^*$	effective heat capacity of PCM	$J/(kg \cdot K)$
$E_{st}$	actual latent thermal energy stored/released by the PCM	$J/kg$
$F_{sky}$	radiation view factor from sky to the envelope	-
$h_{t,e}$	convective heat transfer coefficient on the exterior surface	$W/(m^2 \cdot K)$
$h_{t,i}$	convective heat transfer coefficient on the interior surface	$W/(m^2 \cdot K)$
$h_{m,e}$	convective mass transfer coefficient on the exterior surface	$kg/(m^2 \cdot s \cdot Pa)$
$h_{m,i}$	convective mass transfer coefficient on the interior surface	$kg/(m^2 \cdot s \cdot Pa)$
$I_{rad}$	solar radiation on exterior surface	$W/m^2$
$J$	moisture load	$kg/m^2$
$J_{gain}$	moisture gain load	$kg/m^2$
$J_{loss}$	moisture loss load	$kg/m^2$
$j$	total moisture flux ( $kg/(m^2 \cdot s)$ )	$kg/(m^2 \cdot s)$
$j_{gain}$	moisture gain flux ( $kg/(m^2 \cdot s)$ )	$kg/(m^2 \cdot s)$

$j_{loss}$	moisture loss flux (kg/(m <sup>2</sup> .s))	kg/(m <sup>2</sup> .s)
$j_l$	liquid moisture flux (kg/(m <sup>2</sup> .s))	kg/(m <sup>2</sup> .s)
$j_v$	vapor moisture flux (kg/(m <sup>2</sup> .s))	kg/(m <sup>2</sup> .s)
$K_w$	liquid water permeability (kg/(Pa·m·s))	-
$L$	PCM's total latent thermal energy	J/kg
$Le$	Lewis number	-
$L_v$	latent heat of evaporation	J/kg
$M_w$	molar mass of water	kg/mol
$m_{pcm}$	mass of PCM	kg/mol
$p_c$	capillary pressure	Pa
$p_v$	partial water vapor pressure	Pa
$p_{v,amp}$	partial water vapor pressure amplitude	Pa
$p_{v,e}$	partial water vapor pressure of exterior	Pa
$p_{v,i}$	partial water vapor pressure of interior	Pa
$p_{v,x=0}$	partial water vapor pressure on the exterior surface	Pa
$p_{v,x=l}$	partial water vapor pressure on the interior surface	Pa
$p_{v,sat}$	saturation vapor pressure	Pa
$q$	heat flux	W/m <sup>2</sup>
$q_{gain}$	heat gain flux	W/m <sup>2</sup>
$q_{loss}$	heat loss flux	W/m <sup>2</sup>
$Q$	heat load	W·h/m <sup>2</sup>
$Q_{gain}$	heat gain load	W·h/m <sup>2</sup>
$Q_h$	stored or released heat	J

$Q_{loss}$	heat loss load	$W\cdot h/m^2$
$R$	universal gas constant	$J/(kg\cdot K)$
$R_e$	experimental results	-
$R_s$	simulation results	-
$T$	temperature	$^{\circ}C$
$T_{amp}$	temperature amplitude	$^{\circ}C$
$T_e$	temperature of exterior	$^{\circ}C$
$T_i$	temperature of interior	$^{\circ}C$
$T_{ini}$	initial temperature of PCM phase transition range	$^{\circ}C$
$T_{fin}$	final temperature of PCM phase transition range	$^{\circ}C$
$T_{\overline{pcm}}$	mean temperature of PCM	$^{\circ}C$
$T_{sky}$	temperature of sky	$^{\circ}C$
$T_{x=0}$	temperature on the exterior surface	$^{\circ}C$
$T_{x=l}$	temperature on the interior surface	$^{\circ}C$
$t$	time	s
$w$	volumetric moisture content	$kg/m^3$

***Greek symbols***

$\alpha$	solar absorptivity on exterior surface	-
$\beta$	PCM latent heat dependent factor	-
$\delta_p$	water vapor permeability	$kg/(Pa\cdot m\cdot s)$
$\varepsilon$	infrared emittance of the exterior wall surface	-
$\theta$	relative error	-

$\xi$	sorption capacity	-
$\rho_a$	density of air	kg/m <sup>3</sup>
$\rho_{hc}$	density of HC	kg/m <sup>3</sup>
$\rho_{pcm}$	density of PCM	kg/m <sup>3</sup>
$\rho_w$	density of water	kg/m <sup>3</sup>
$\sigma$	Stefan-Boltzmann constant	W/(m <sup>2</sup> ·K <sup>4</sup> )
$\lambda_{hc}$	thermal conductivity of HC	W/(m·K)
$\lambda_l$	thermal conductivity of liquid PCM	W/(m·K)
$\lambda_s$	thermal conductivity of solid PCM	W/(m·K)
$\lambda^*$	effective thermal conductivity of PCM	W/(m·K)
$\varphi$	relative humidity	%
$\varphi_{crit}$	critical relative humidity	%
$\Omega$	computational domain	-

## Abbreviation

ASHRAE	American Society of Heating, Refrigerating and Airconditioning Engineers
CO <sub>2</sub>	Carbon Dioxide
CV <sub>(RMSE)</sub>	Coefficient of Variation of the Root Mean Square Error
FDM	Finite Difference Method
FEM	Finite Element Method
FLC	Flax Lime Concrete
FVM	Finite Volume Method
HC	Hemp Concrete

HLC	Hemp Lime Concrete
HMT	Heat and Moisture Transfer
HT	Heat Transfer
HVAC	Heating, Ventilation, and Air Conditioning
MBV	Moisture Buffer Value
PCM	Phase Change Material
PDE	Partial Differential Equation
PMV	Predicted Mean Vote
PPD	Predicted Percentage of Dissatisfied
RMSE	Root Mean Square Error
SD	Standard Deviation
TIM	Transparent Insulation Material
XPS	Extruded Polystyrene

# Chapter 1 Introduction

## 1.1 Background

With the rapid development of the world economy, energy demand is increasing and energy reserves are becoming scarce. The contradiction between energy demand and supply is becoming more and more prominent. However, most of the energy consumed (e.g., coal, oil, and natural gas) by humans is non-renewable energy, meaning that their consumption is irreversible. In addition, unprecedented amounts of CO<sub>2</sub> are being released into the earth's atmosphere with the use of these energy sources [1]. Therefore, the global energy system will face a double challenge in the future as described in Fig. 1.1: the demand for more energy and less carbon [2].

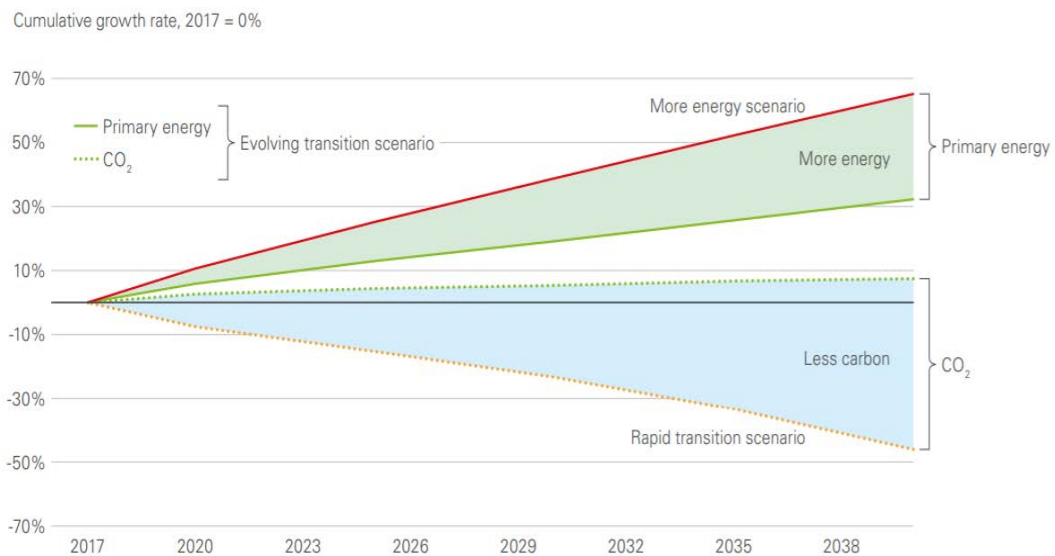


Fig. 1.1. Primary energy demand and CO<sub>2</sub> emissions

As places where people live, work, and play, buildings are responsible for higher energy consumption and CO<sub>2</sub> emissions. According to the *2021 Global Status Report for Building and*

*Construction*, building and construction account for 36% and 37% of the energy consumption and CO<sub>2</sub> emissions (Fig. 1.2) [3], respectively. Building energy consumption consists of energy consumption from envelopes, HVAC (Heating, Ventilation, and Air Conditioning), appliances, and lighting, with envelopes and HVAC accounting for about 69% (52% for envelopes + 17% for HVAC [4]) of the building energy consumption. Therefore, the innovation and development of the envelope play a significant role in achieving energy saving and emission reduction. Generally, strengthening the insulation performance of the envelope is the most effective way to save energy in buildings. The heat transfer characteristics of the envelope determine its thermal insulation performance, including the blocking, attenuation, and delaying effect on the exterior temperature, which has an important impact on indoor comfort and building energy efficiency.

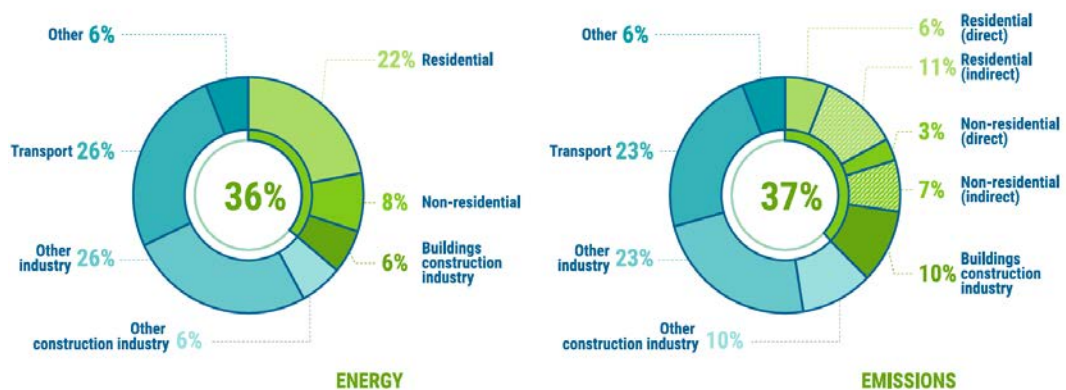


Fig. 1.2. Buildings and construction’s percentage of global energy and CO<sub>2</sub> emissions

Furthermore, there is an increasing demand for indoor thermal and humidity comfort. People spend most of their time in the indoor environment in modern society, so indoor thermal and humid environmental comfort is crucial. A comfortable indoor environment ensures the physical and mental health of the occupants and improves their work efficiency. In order to meet occupants’ requirements for indoor environmental comfort, a variety of electrical equipment is used to manage indoor

temperature and humidity. For example, heating/cooling equipment is used to regulate indoor temperature and humidification/dehumidification equipment is used to control indoor humidity. However, there are some drawbacks if electrical equipment is greatly relied upon. Firstly, in order to continuously maintain a comfortable interior environment, a large amount of energy is inevitably consumed, which is a great challenge to the current state of the world energy shortage. Secondly, carbon emission during the operation of electrical equipment is not conducive to environmental protection. Finally, the high requirement of airtightness for the building in order to save energy will aggravate the accumulation of indoor CO<sub>2</sub> and organic gases released from furniture, which affects the health of the occupants.

Passive building solutions can save more than 50% of energy compared with traditional building solutions [5-7]. They are considered the most promising solution to reduce building energy consumption and carbon emissions, and improve indoor thermal and humidity comfort. Therefore, research on passive building technologies has received increasing attention in recent years.

Using bio-based materials or phase change materials (PCMs) as building envelopes is one of the passive building technologies. Bio-based materials are environment-friendly materials. As building envelopes, some bio-based materials have thermal insulation properties that can regulate the indoor thermal environment and save building energy. Besides, some bio-based materials with porous structures have hygroscopic properties, which can reversibly adsorb and desorb moisture from the surrounding environment to regulate the relative humidity (Fig. 1.3 (a)). PCMs have excellent thermal energy storage properties. They can store and release large amounts of latent heat with small temperature changes in the phase transition range (Fig. 1.3 (b)). As part of building envelope, PCMs can reduce indoor temperature fluctuation, shift peak temperature, and save energy consumption. Saving energy usually means reducing carbon emissions, which conforms to the current theme and context of energy saving and emission reduction. In addition, the regulation of the indoor thermal and

humidity environment by both materials is completely autonomously, without human intervention.

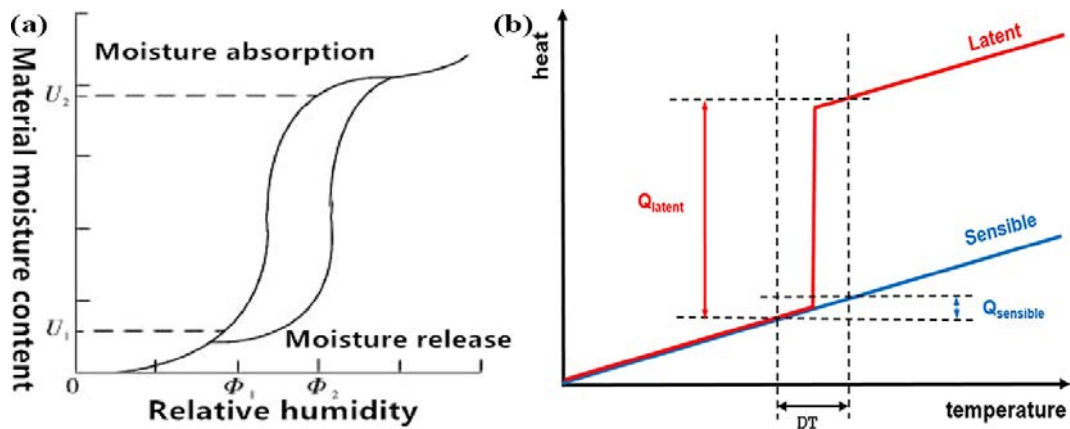


Fig. 1.3 Working principle of (a) hygroscopic material with moisture adsorption/desorption [8] and (b) PCM with latent heat store/release [9]

Therefore, based on the above background, this study explores the technology of passive solutions in the field of building envelope technology, aiming to improve the indoor thermal and humidity environment and save energy by using green and low-carbon building materials.

## 1.2 Motivation, objective, and approach

### 1.2.1 Motivation

As mentioned previously, there is a high percentage of energy consumption and carbon emission in the building envelope. Besides, demand from occupants for comfortable indoor thermal and humid environments is increasing. Therefore, it is necessary and urgent to innovate in the building envelope to achieve the goals of low energy consumption and carbon emission, as well as high indoor comfort in buildings, especially if these goals can be achieved simultaneously.

Bio-based hygroscopic materials have high hygric inertia and excellent hygroscopic properties,

which can regulate the indoor humid environment and affect the energy consumption of buildings. PCMs have a great capacity to store and release thermal energy (i.e., high thermal inertia), which improves indoor thermal comfort and saves energy of buildings. It is interesting and meaningful to integrate and utilize the advantages simultaneously of the two materials.

Till date, few studies have covered the integration of the two materials, and these studies generally fall into two categories. The first category deals with the integration and preparation of the two materials as well as the characterization of the integrated samples. In the preparation process, the PCMs are often integrated into the hygroscopic materials in the capsulation form, which ensures the uniform distribution of PCM encapsulations and the efficient transport of moisture in the envelope. However, this approach has disadvantages such as complicated preparation, small total thermal storage capacity, and low mechanical properties [10]. It is necessary to develop a simple assembly approach that could take full advantage of the PCM's thermal storage capacity and has high mechanical strength. Thus, the integration of the two materials by a multilayer assembly approach is proposed in this study. The multilayer assembly approach has been mentioned several times when studying the performance of PCM building envelopes. However, these studies have focused only on the thermal and energy performance while neglecting the hygric performance. The second category focuses on the application of the integrated materials, involving the behavior of temperature, relative humidity, and energy consumption of the buildings. Nevertheless, there is a lack of comprehensive analysis regarding thermal, hygric, and energy performance, especially the interactions between PCMs and hygroscopic materials. Therefore, the feasibility of multilayer assembly of the two materials needs to be explored. Besides, the thermal, hygric, and energy performance of the multilayer envelope in the real climate are required to be investigated. On the one hand, the principle that PCMs affect the hygric performance of the envelope by influencing its thermal performance needs to be investigated. On the other hand, the effect of hygroscopic materials on hygric and energy performance is worth studying.

Furthermore, considering that the PCM's locations and properties affect the temperature distribution in the envelope, it is meaningful to conduct the parametric analysis by studying the impact of PCM parameters on the performance of the integrated envelope. In addition, since PCMs are moisture impermeable material, they block the moisture transfer and result in a moisture accumulation on both sides of the PCM within the multilayer envelope. Therefore, it is necessary to evaluate the risk of condensation and mold growth at key locations within the integrated envelope.

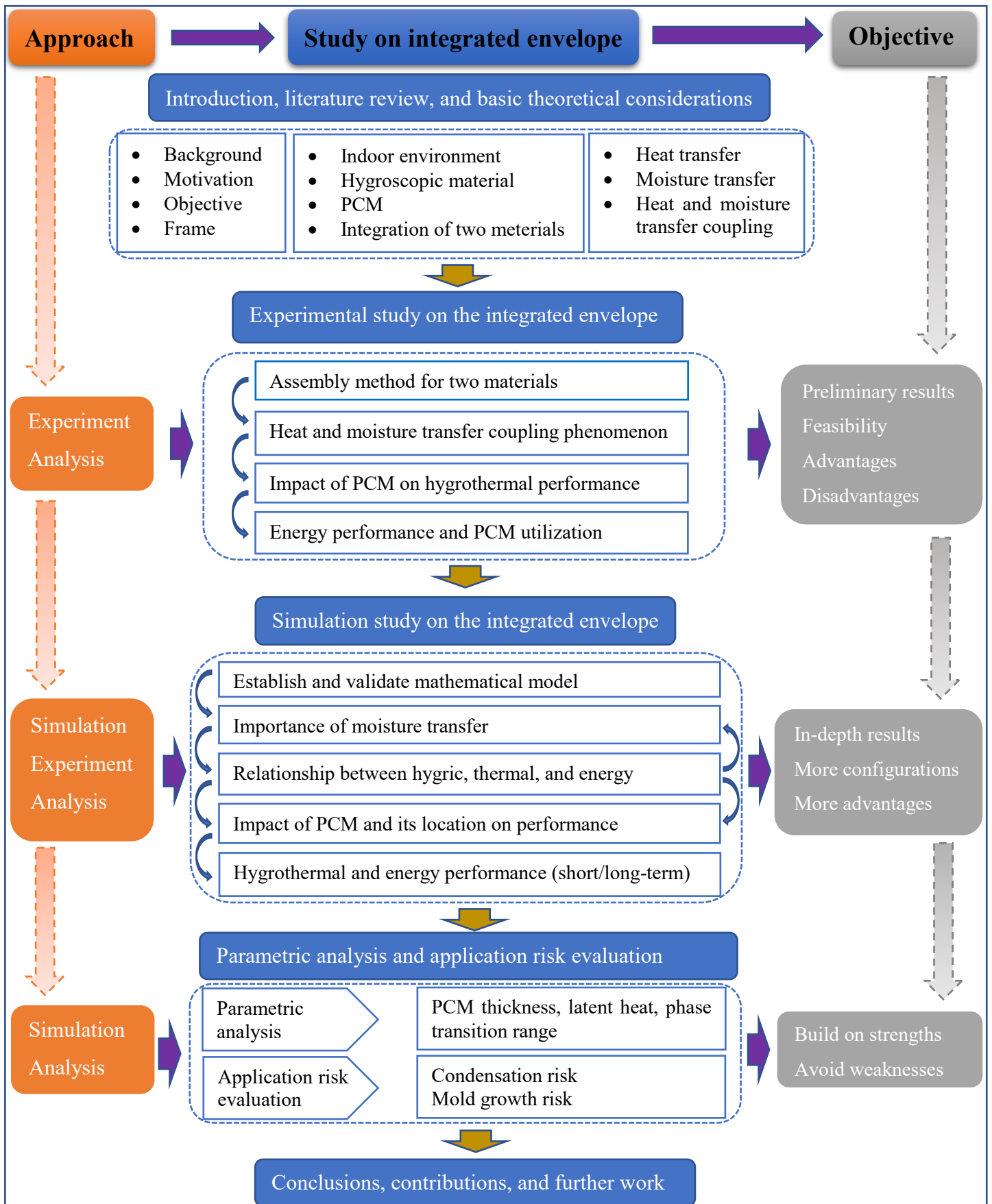
### **1.2.2 Objective**

In this study, PCM and bio-based hygroscopic concrete (hemp concrete) are integrated into a novel passive building envelope. The aim of this research is to develop an integrated passive envelope capable of both temperature and humidity regulation as well as energy savings, and to explore its application potential, principle, and risk. The main objectives are as follows:

- 1) Explore the feasibility of the integrated envelope by multilayer assembling PCM and bio-based hygroscopic material.
- 2) Study the coupling behavior of heat and moisture transfer within the hygroscopic material and the effect of adding PCM.
- 3) Explore the assembly configuration of bio-based hygroscopic material and PCM, and study the advantages and disadvantages of different configurations.
- 4) Study comprehensively the thermal, hygric, and energy performance of the integrated envelope with different configurations under real climate.
- 5) Conduct the parametric analysis of the integrated envelope for performance improvement; evaluate the application risk of the integrated envelope.

In addition, the detailed sub-objectives can be seen in the first section of Chapters 3, 4, and 5.

### 1.2.3 Approach and research frame



### **1.3 Thesis outline**

The thesis consists of 6 chapters, the main content of each chapter is as follows

- Chapter 1: the background, motivation, objective, and frame of the thesis.
- Chapter 2: the literature review and basic theoretical considerations, including indoor thermal and humid environments, hygroscopic materials and PCM as building envelopes, integration of two types of materials, and development of heat and mass transfer theory.
- Chapter 3: the experimental study on the integrated envelope. The preliminary analysis on the hygrothermal and energy performance of the integrated envelope under steady and dynamic boundary conditions.
- Chapter 4: the derivation and validation of mathematical models, the simulation study on the integrated envelope. The comprehensive investigation on the thermal, hygric, and energy performance of the integrated envelope in real climate.
- Chapter 5: the parametric analysis and application risk evaluation of the integrated envelope.
- Chapter 6: the major conclusions, contributions, and future work.

## **Chapter 2      Literature review and basic theoretical considerations**

### **2.1    Indoor thermal and humid environment**

#### **2.1.1   Thermal and humid comfort**

Indoor environment includes indoor thermal and humid environment as well as indoor air quality, which affects (directly or indirectly) the physical and psychological health of the occupants [11, 12]. In the early 1930s, thermal comfort was already given priority attention. ASHRAE (American Society of Heating, Refrigerating and Airconditioning Engineers) [13] has defined thermal comfort as the condition of the mind in which satisfaction is expressed with the thermal environment. The human body can adapt to the environment temperature and maintain the temperature balance, while the inappropriate temperature will affect blood vessels, pulse, and immunity [14].

However, the role of humidity on indoor comfort and occupants was not emphasized in the early studies [15]. In summer, excessive humidity inhibits evaporative heat dissipation and makes the body feel more humid and uncomfortable. In winter, excessive humidity accelerates heat transfer and makes people feel cold. Besides, excessive humidity also promotes mold growth [16-18]. Conversely, lower humidity causes human discomfort, such as dry eye and throat symptoms from prolonged exposure to a low relative humidity environment [19]. Fig. 2.1 shows the relationship between adverse health effects and relative humidity [20], the optimal relative humidity range of 40% to 60% is beneficial to occupants. Therefore, both temperature and humidity need to be maintained within a suitable range for occupant comfort. The comfort temperature range is around 23–28°C in summer and 18–25°C in winter.

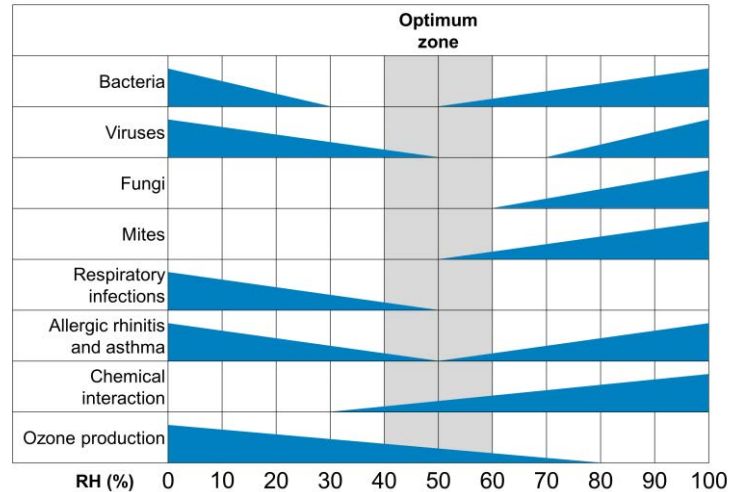


Fig. 2.1 Optimum relative humidity ranges for minimizing adverse health effects [20]

Two indexes are usually used to quantify whether a certain thermal and humid environment would be acceptable to a large group of people. The first index is PMV (predicted mean vote) [21], which is detected by six parameters: air temperature, mean radiant temperature, relative air velocity, air humidity, activity level, and clothing insulation. The PMV index reflects the degree of deviation of the human thermal balance. The second index, derived from PMV, is PPD (predicted percentage of dissatisfied), which predicts the percentage of the total number of people in a group who are uncomfortable with a given thermal environment on the average scale of thermal sensation (i.e., the percentage of the people who inclined to complain about the environment). The thermal sensation can be scaled from  $-3$  to  $+3$ . Fig. 2.2 indicates the dependence of PPD on PMV. The PPD curve is symmetrical of thermal neutrality ( $PMV = 0$ ) with the minimum PPD of 5%, indicating that even in the thermal neutrality state, about 5% are still dissatisfied. According to ASHRAE Standard 55-2010, the recommended PMV range for indoor thermal comfort is from  $-0.5$  to  $+0.5$ , corresponding to a PPD of less than 10% of dissatisfied people. The PMV–PPD model has been adopted by various national and international standards [22, 23].

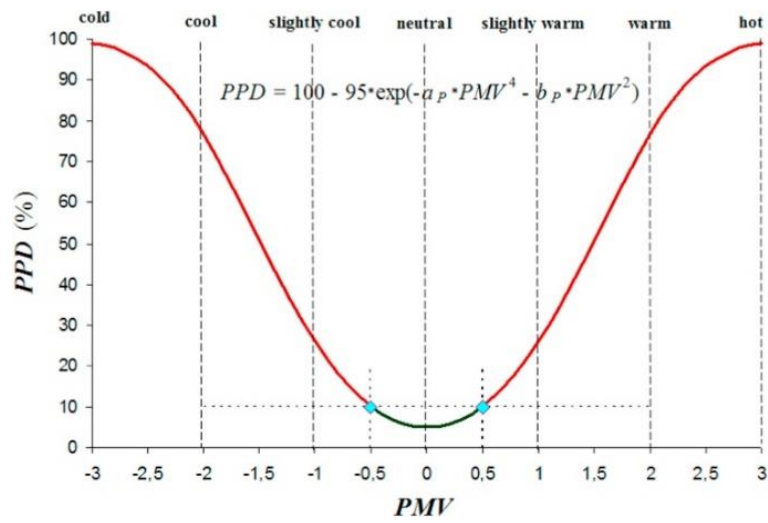


Fig. 2.2. Dependence of *PPD* on *PMV* [21]

Fig. 2.3 shows the operative temperature and humidity ranges for the comfort zone recommended by ASHRAE 55-2013 [23]. The comfort zone corresponds to thermal conditions acceptable to 80% of the personnel, based on a *PPD* from 5% to 10% (i.e., *PMV* from -0.5 to +0.5). For example, the appropriate temperature range is approximately 20 to 27°C at a state of 50% relative humidity.

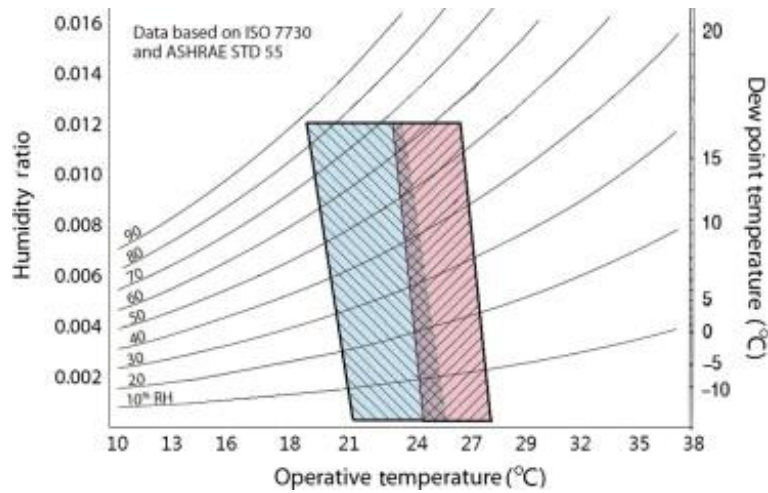


Fig. 2.3. Recommended operative temperature and humidity [23]

### **2.1.2 Global Climate and interior environment**

There are different climate types worldwide due to longitude, latitude, oceans, mountains, woods, and deserts, etc. The Köppen climate classification [24] is one of the most widely used climate classification systems, which divides climate into five major climate groups (Fig. 2.4), including A (tropical), B (dry), C (temperate), D (continental), and E (polar). Buildings in different climatic conditions require different solutions for indoor temperature and humidity. Napp [25] developed different control systems adapted to the humidity of different seasons to cope with the maritime climate in Estonian. Li [26] investigated the characteristics of five different climatic zones in China (severe cold, cold, hot summer and cold winter, hot summer and warm winter, and mild) and developed thermal environment evaluation criteria applicable to each zone to save energy and improve the indoor thermal environment. Qin [27] investigated a new material capable of controlling humidity in different climates (hot desert, semi-arid, Mediterranean, temperate and subtropical humid) and proved the ability of the material to control humidity varied with different climates. The climate in Turpan is severe, with extremely hot summers and cold winters, and extremely dry all year round. Some scholars [28-30] proposed interior environmental solutions for this extreme climate by integrating earth brick and active/passive solar technology with shading, ventilation, insulation.



insulation, humidity regulation, low cost, and energy savings [38-40].

Bio-based concretes are also one of the fastest growing bio-based materials in recent years. They are made from a mixture of bio-based materials (e.g., hemp, straw, and flax), water, and lime. They weigh only 15% of conventional concretes [41]. In recent years, structures made of bio-based concretes have started to become a substitute for many old wooden frames. Bio-based concretes are environmental-friendly materials that eliminate greenhouse gas emissions by avoiding the need to burn fuel. The advantages of wood and concrete over steel in CO<sub>2</sub> release and storage can be seen in Fig. 2.5. As a building envelope, bio-based concretes improve the thermal resistance of the building and ensure indoor thermal comfort [42, 43]. Besides, their hygroscopic performance is also beneficial to improve the indoor humid comfort [44-46]. The common bio-based concretes are hemp concrete, followed by straw and flax concrete [47].

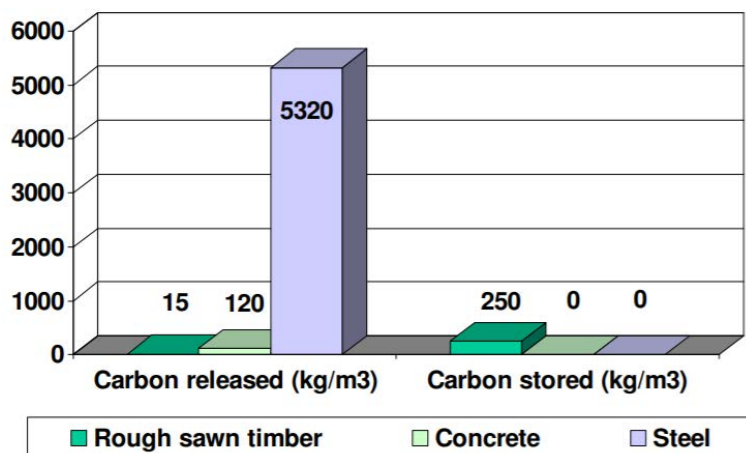


Fig. 2.5. Carbon release and store by different material [48]

### 2.2.2 Thermal insulation characteristics

As part of the envelope of residential and commercial buildings, insulation materials can improve indoor thermal comfort and reduce energy consumption. Insulation materials are materials that provide

thermal insulation or reduce the transfer of heat between objects. As shown in Fig. 2.6, insulation materials impede the cold temperatures from the outdoors and keep the interior environment warm during the cold winter. Conversely, insulation materials impede the huge heat flow from the outdoors in summer.

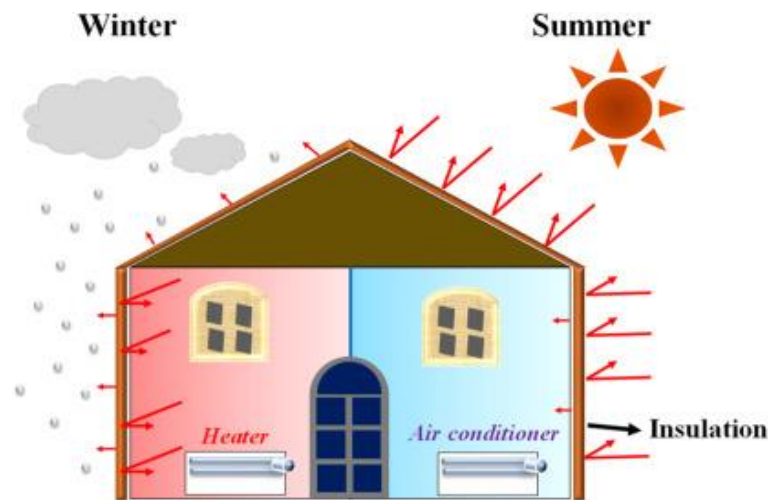


Fig. 2.6. Building insulation avoiding external environmental impact [49]

Bio-based materials come from nature, their high porosity and low thermal conductivity make them possible for thermal insulation of buildings. Liu [47] reviewed the development history of bio-based materials as building insulation and listed the four most popular bio-based materials: hemp, straw, flax, and wood.

Sassoni [50] developed a novel hemp-based composite material using a new hybrid organic-inorganic binder; the composites showed a good thermal behavior with a low thermal conductivity of  $0.078 \text{ W}/(\text{m}\cdot\text{K})$ . Bennai [51] studied the hygrothermal performance of hemp concrete and compared it to conventional building materials. The results proved the good hygrothermal properties of the bio-based material, especially its high thermal resistance of  $3.08 (\text{m}^2\cdot\text{K})/\text{W}$ . Liu [52] prepared a bio-insulating material with wheat straw as aggregate and measured its physical properties. The

measurement results indicated that the material has a low thermal conductivity from 0.092 to 0.186 W/(m·K). Belhadj [53] investigated the effect of barley straw addition on the thermophysical properties of sand concrete. The results revealed that the addition of barley straw reduced the thermal conductivity and thermal diffusivity by 5.71% and 21.97%, respectively. Benmahiddine [54] studied the effect of flax shives content size on the hygrothermal properties of flax concrete. The results showed that the thermal conductivity of flax concrete was low (0.082–0.127 W/(m·K)) and that the higher the flax shives content, the lower the thermal conductivity. Kymäläinen [55] collected and summarized the thermal conductivity of flax from numerous studies, and they ranged from 0.033 to 0.075 W/(m·K).

Woods or wood-based materials also have low thermal conductivity. Li [56] measured the insulating properties of nanowood; the results showed that their thermal conductivity ranged from 0.03 to 0.06 W/(m·K). Bianco [57] compared the thermal performance of synthetic (XPS and polyurethane) and natural (wood fiber) insulation materials in Turin, Italy. It was found that the wood fiber indicated better thermal insulation properties when applied to a larger roof surface. Kočí [58] analyzed the insulating performance of two different wood-fiber thermal insulations. The results showed that the two insulation systems reduced the annual energy from 66.35% to 79.53% compared to the unprotected wall.

In addition to these popular bio-based materials, there are other bio-based materials that have gained attention for their thermal insulation properties. Zhou [59] developed a binderless cotton stalk fiberboard using cotton stalk fiber without resin and chemical additives. It was found that the thermal conductivity ranged between 0.0585 and 0.0815 W/(m·K). Panyakaew [60] added coconut husk and bagasse to thermal insulation wallboards without chemical binding additives, resulting in their thermal conductivity ranging from 0.046 to 0.068 W/(m·K). Wei [61] developed a new thermal insulation material by rice straw and found that the thermal conductivity of the insulation material was

low, ranging from 0.051 to 0.053 W/(m·K). Ali [62] studied the potential of date palm trees surface fibers as insulation material and revealed that they have good thermal conductivity from 0.0475 to 0.0697 W/(m·K). Zou [63] developed a novel bio-based composite material fabricated with geopolymers as adhesives and sawdust wastes as aggregates. The results indicated that the composite material had a low thermal conductivity of 0.112–0.125 W/(m·K). There are also some similar studies on thermal insulation using other bio-based materials such as sugarcane fiber [64], corn [65], sunflower [66], palm [67], cork [68], and olive [69].

### 2.2.3 Hygroscopic characteristics

The porous structure of hygroscopic materials can reversibly adsorb and desorb water molecules from the surrounding environment. Some bio-based materials are porous media materials, which provide the necessary structural conditions for moisture regulation [70, 71].

In 1998, Padfield [72] proposed the term "moisture buffer" to describe the effect of porosity and adsorption/desorption on the humidity balance in a room. The moisture buffer value (MBV) is a value that measures the effect of material on the surrounding humid environment, and it can be tested by the Nordtest protocol [78]. Therefore, MBV is an important hygroscopic characteristic of bio-based material [73]. Chen [74] fabricated a hygroscopic phase change material using microencapsulated PCM and diatomite. The composite showed excellent hygroscopic properties with an MBV of 1.57 g/(m<sup>2</sup>%RH), which was higher than diatomaceous earth (0.33 g/(m<sup>2</sup>%RH)), gypsum (0.26 g/(m<sup>2</sup>%RH)), and pure wood (0.4 g/(m<sup>2</sup>%RH)). Chennouf [75] measured the MBV of a date palm fiber-reinforced cement composite. The MBV of 2.97 g/(m<sup>2</sup>%RH) indicated that the composite was a good hygroscopic material. Rahim [76] measured the MBV of hemp concrete and flax concrete; the results proved the "excellent" moisture buffer capacity of them with the MBVs of 2.02 and 2.27 g/(m<sup>2</sup>%RH), respectively (Fig. 2.7).

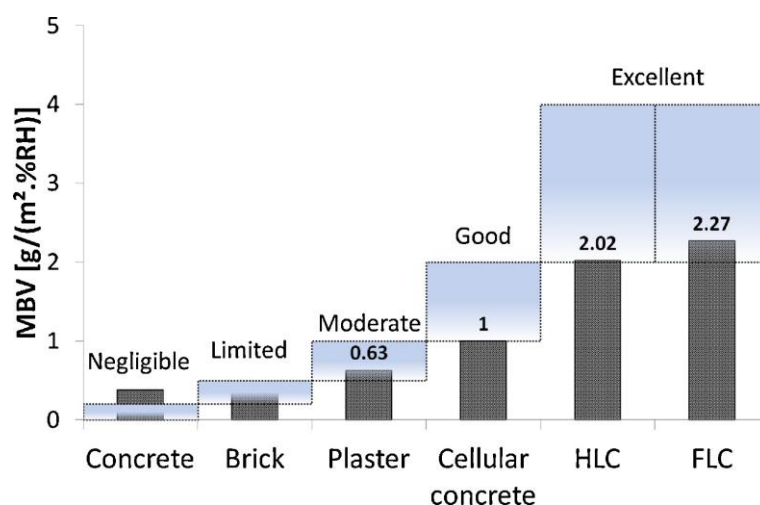


Fig. 2.7 MBVs of hemp concrete (HLC) and flax concrete (FLC) and conventional materials [76]

In addition to characterizing and measuring the MBV, several studies have investigated the actual effects of hygroscopic materials by experimental or simulation methods. Collet [77] experimentally investigated the hygrothermal behavior of hemp concrete walls. The results highlighted the hygric behaviors such as homogeneous vapor diffusion and huge vapor pressure variations. Rahim [78] studied the hygrothermal behavior of hemp and straw rape concrete walls on an experimental scale. The results proved the ability of the bio-based concrete walls to reduce fluctuations in temperature and relative humidity. Maalouf [79] numerically studied the hygrothermal behavior of the hemp concrete wall in three French cities. The results showed that the indoor temperature fluctuations and maximum indoor relative humidity in buildings with hemp concrete walls were reduced by 3 °C and 10%, respectively, compared to buildings with plain concrete walls. Tran Le [80] numerically studied the ability of hemp concrete to regulate indoor humidity and found that the humidity fluctuation in the room with hemp concrete was significantly less than that of cellular concrete. Moujalled [81] experimentally and numerically evaluated the hygrothermal performance of a hemp lime concrete building for four years. The results showed that the hemp lime concrete contributed to good

hygrothermal comfort in both winter and summer. In addition, the concrete with 30 cm dampened daily temperature and relative humidity variations by 90% and delayed the peak effect by about 12 h.

#### **2.2.4 Temperature dependence of hygroscopic characteristics**

In some experimental studies [82-85] on hygroscopic materials, the high coupling between heat and moisture transfer within the material can be observed due to evaporation or condensation phenomena. In addition, another phenomenon worth noting is that the hygroscopic properties of hygroscopic materials are more susceptible to temperature than relative humidity. Therefore, several studies have investigated the effect of temperature on the hygroscopic properties. Hundt [86] measured the first desorption isotherm of different cementitious materials at four different temperatures of 20, 45, 57.5, and 70 °C. The results shown in Fig. 2.8 revealed that the higher the temperature, the less the water adsorbed at equilibrium and the less the water at saturation. Daian [87, 88] measured the adsorption isotherms of water-cured mortars at four different temperatures (20, 35, 45, and 55 °C) and found that the adsorption isotherms were not the same for different temperatures and that the higher was the temperature, the less water was adsorbed. Poyet [89] investigated the effect of temperature on the first desorption isotherm of concrete at 30 and 80 °C. It was found that the water content at equilibrium was drastically reduced at 80 °C and was significantly lower than that of 30 °C.

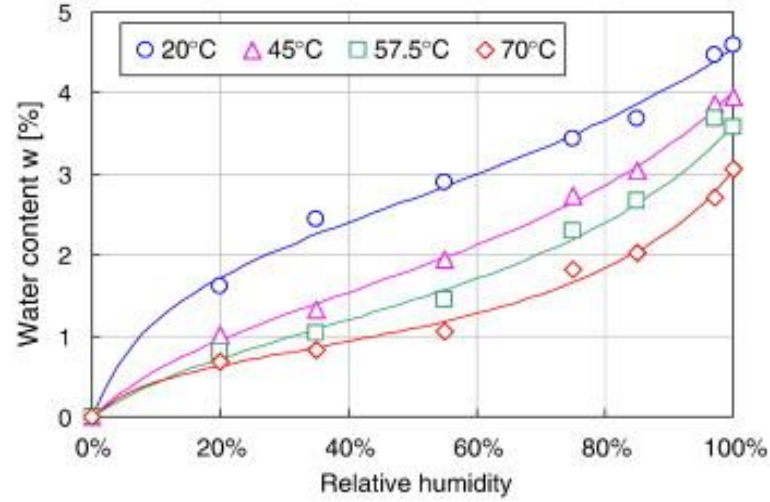


Fig. 2.8 First desorption isotherms for a mature mortar at four temperatures [86]

Poyet [90] presented the theoretical background to describe the relationship between temperature and properties based on the Clausius-Clapeyron equation and the isosteric heat of sorption. The desorption isotherm at any temperature can be accurately estimated by using the following model:

$$\varphi(T_1, w) = \varphi(T_2, w) \frac{p_{v,sat}(T_2)}{p_{v,sat}(T_1)} \exp \left[ \frac{Q_{st}(w)}{R} \left( \frac{T_1 - T_2}{T_1 T_2} \right) \right] \quad (2.1)$$

where

$T_i$  = temperature of condition  $i$  (with  $i = 1$  or  $2$ , meaning the state 1 or state 2), (K);

$w$  = moisture water content, (kg/kg);

$\varphi(T_i, w)$  = relative humidity at equilibrium with the adsorbed water content  $w$  at the temperature  $T_i$ ;

$p_{v,sat}(T_i)$  = saturation pressure at the temperature of  $T_i$ , (Pa);

$Q_{st}(w)$  = isosteric heat of sorption, (J/mol);

$R$  = ideal gas constant, (8.314 J/mol/K).

This theory and model were then validated by Colinart [91, 92], who experimentally studied the

influence of temperature on relative humidity variations within three building materials. Moreover, Chennouf [75], Feng [85], and Oumeziane [93] experimentally confirmed that the sorption-desorption process and MBV were highly affected by temperature. Rahim [94] and Le [95] found by simulation that the relative humidity behavior could be predicted accurately by taking into account the influence of temperature.

### **2.2.5 Impact of hygrothermal behavior on energy consumption**

Heat and moisture transfer within the envelope affects the interior heating and cooling loads, which in turn affects the overall energy consumption of the buildings. Mendes [96, 97] numerically studied the hygrothermal performance in different geographical areas. The results showed that the effect of moisture transfer on the total heat load of the building could not be neglected because of the latent heat load. Osanyintola [98] studied the effect of hygroscopic materials on building energy consumption. It was found that buildings with hygroscopic materials saved 2–3% and 5–30% of the heating and cooling energy consumption, respectively. Barbosa [99] evaluated the heat load and energy consumption of a multi-zone building. The results highlighted the significance of moisture transfer. When moisture transfer was not considered, the HVAC system was overestimated by 13% in structural size and underestimated by 4% in cooling energy consumption. Similarly, Liu [100, 101] found that the total cooling, heating, and annual loads were underestimated by 9.9–34.4%, 1.7–4.0%, and 5.2–6.8%, respectively, when moisture transfer was neglected. Besides, moisture transfer neglect also led to an underestimation of life-cycle costs/savings and overestimation of payback periods. Woloszyn [102] analyzed indoor air quality and energy efficiency by combining a relative humidity-sensitive ventilation system with humidity buffering materials. The results suggested that the ventilation system equipped with humidity buffering materials reduced energy consumption by 12–17% during cold periods. Qin [103, 104] developed a model coupling heat, moisture, and airflow to study the energy

consumption of a building. The energy savings were found to be 1.7–5.8% for heating and 8–16% for cooling.

## **2.3 PCMs as building envelope**

### **2.3.1 PCMs as part of building construction**

Phase change materials (PCMs) as building envelopes are also promising due to their high thermal inertia [105, 106]. Research and development of PCM have been going on for many years. In 1982, PCM was first used by the U.S. Department of Energy in encapsulated form for the walls of passive solar buildings [107, 108]. In 1989, Kedl and Stoval [109] successfully applied phase change wallboards immersed with octadecane for passive solar applications. Since the 1990s, a great deal of research has been conducted on PCM applications in building envelopes. And by the 20th century, this technology has made tremendous and comprehensive progress.

PCM as a building material needs to meet different properties, including thermal-physical, kinetic, chemical, economic, and environmental properties [110-117]. A detailed description is shown below

#### 1) Thermal-physical properties

- Small volume change during phase transition
- High specific heat to store more latent heat energy
- Suitable phase change temperature for application
- High latent heat of fusion per unit volume to reduce the size
- High thermal conductivity to improve the charging and discharging efficiency of PCM
- Small vapor pressure during application
- Completely melted in the phase change process to improve PCM efficiency
- Thermally reliable (i.e., cycling stability) for long-term use

## 2) Kinetic properties

- High rate of nucleation to avoid PCM subcooling in the liquid phase
- High rate of crystal to ensure optimal heat recovery for storage systems

## 3) Chemical properties

- Chemically compatible with construction/encapsulated materials
- Corrosion resistant to construction/encapsulated materials
- No degradation after a large number of charging/discharging cycles
- Non-toxic, non-flammable and non-explosive

## 4) Economic properties

- Cost effective
- Commercially available

## 5) Environmental properties

- Low environmental impact and no pollution
- Recyclable potential

There are many ways to incorporate the PCM into construction envelope (Fig. 2.9), including direct incorporation [118], immersion [115, 119], encapsulation (microencapsulation [120-122] and macroencapsulation [123-125]), shape-stabilization (with polyethylene[126, 127], styrene-acrylic emulsion, and dry cement powder [128]), and form-stabilization composite (with diatomite [129], expanded perlite [130], and waste glass [131]). Different methods have different advantages and shortcomings [132-134]. As part of building construction, PCM can be used for building walls/wallboards, doors, windows, ceilings, and even glasses.

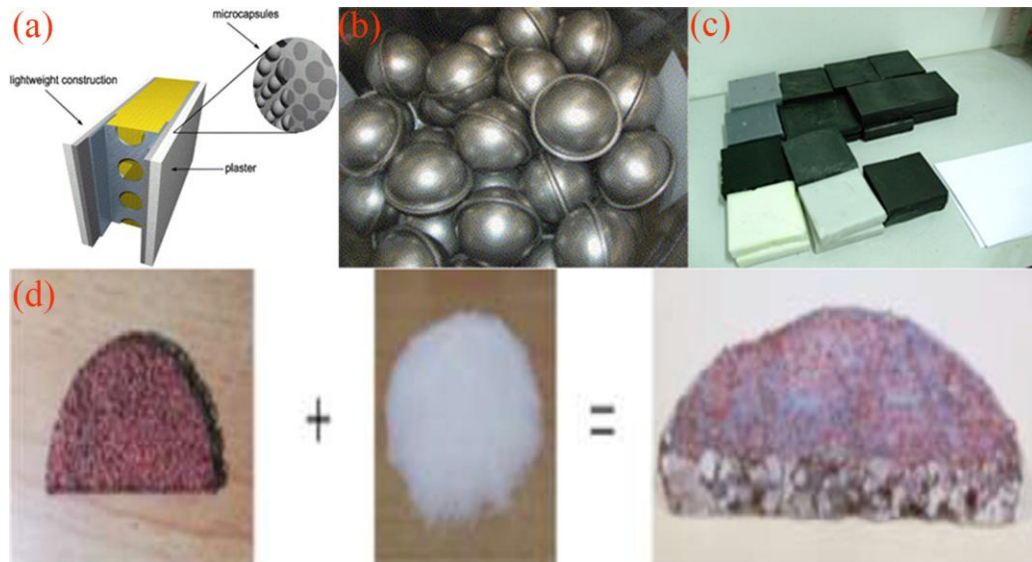


Fig. 2.9. Different methods to incorporate the PCM into construction: (a) microencapsulation; (b) macroencapsulation; (c) shape-stabilization; (d) immersion. [127, 132, 135-137]

Installing PCM wallboards or integrated PCMs into the wall is a common and convenient way to implement PCM in buildings (Fig. 2.10). Kuznik [138] compared two rooms with and without PCM wallboards and found that the thermal comfort was better for the room with PCM wallboards. Li [139] characterized the thermal properties of PCM wallboards and found that the apparent heat capacity of the PCM wallboards was 2.71 times higher than that of gypsum wallboards during the temperature amplitude from 26°C to 32°C.

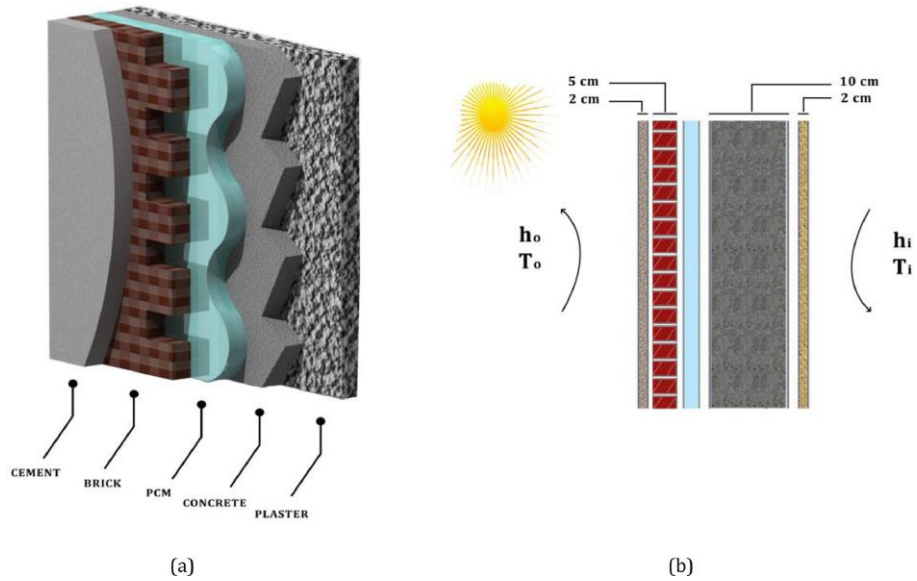


Fig. 2.10. Schematic diagram of a PCM wallboard [140]

PCM can also be used in floors (Fig. 2.11), roofs (Fig. 2.12), and ceilings (Fig. 2.13). Karim [141] designed and developed a PCM floor having high inertia that could transfer thermal peaks. Royon [142] studied the temperature amplitude at the upper face of a room equipped with a PCM floor and found that the amplitude was reduced by about 2°C.



Fig. 2.11. Floor panel incorporated with PCM [142]

Kosny [143] evaluated the thermal behavior of a natural ventilated solar roof with PCM. The results showed that the cooling load in summer and the heating load in winter is reduced by about 55%

and 30%, respectively, compared to the conventional roof. Li [144] investigated the thermal performance of different roofs with and without PCM in China. The results indicated that the delay time of peak temperature in the room with PCM roof was 3 hours longer than that of the normal room. Xaman [145] studied roofs including three different PCMs (paraffin-MG29, N-eicosane, and salt hydrate) in Merida. The results showed that the roof with a PCM layer of paraffin-MG29 reduced the heat load by 57% on the hottest day compared to a conventional concrete roof.



Fig. 2.12. PV-PCM roof [143]

Yahay [146] compared the indoor temperature with and without PCM ceiling panels and found that the PCM-based ceiling panels effectively reduced the energy consumption of buildings. Abden [147] fabricated a novel ceiling panel integrated by form-stabilized PCM and gypsum; the ceiling panel was proven to reduce the cooling energy by 16.2%. Weinlader [148, 149] studied the thermal behavior of two PCM cooling ceiling configurations (PCM on the top and below the water pipes). It was found that the ceiling with the PCM below the water pipes had a better thermal connection with the indoor room as the PCM was utilized more efficiently.

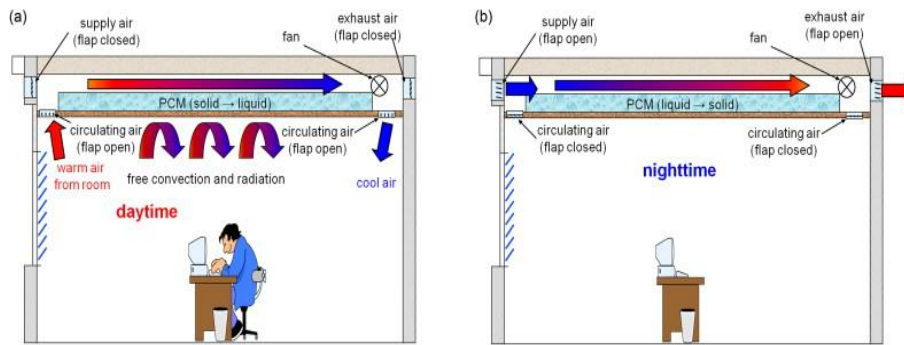


Fig. 2.13 Ventilated cooling ceiling with PCM [150]

Windows in rooms suffer from high heat leakage and energy consumption. For example, up to 10–25% heat loss from the hot indoor environment to the cold outdoor environment in cold climates. Therefore, the application of windows integrated with PCM has been investigated in recent years (Fig. 2.14). Alawadhi [151] investigated the feasibility of using window shutters with PCM to reduce the heat gain under solar radiation. The results showed that the heat gain of the windows was reduced by 23.39% for the shutters with PCM. Goia [152, 153] designed a double-glazed unit containing PCM and found that it improved the thermal environment of the room. Besides, the PCM double-glazed unit reduced the energy gain by more than 50% compared to the conventional double-glazed unit in summer. Li [154] used nanoparticles as supporting material for PCM in PCM-filled windows to improve thermal conductivity. It was found that the energy consumption can be reduced by 4% by appropriate nanoparticle concentration and diameter.

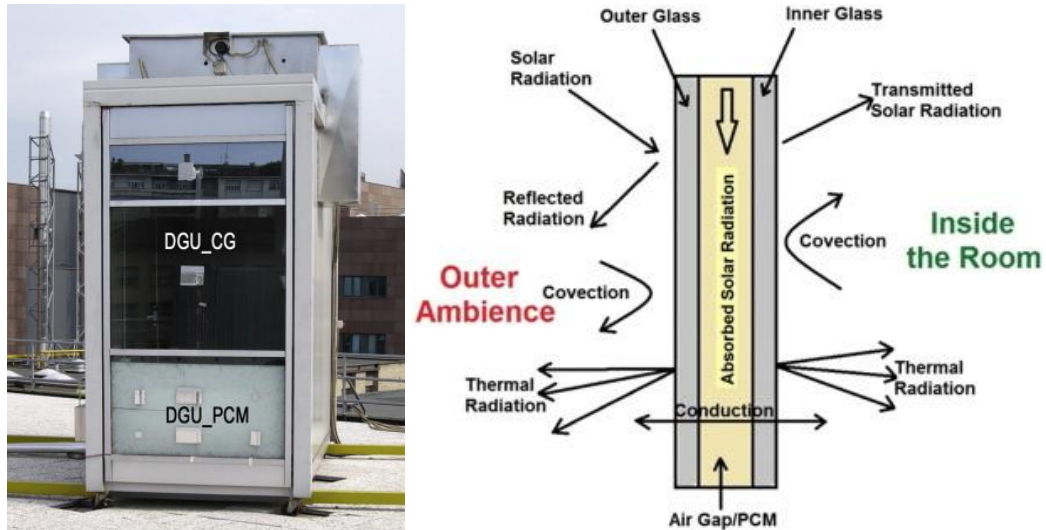


Fig. 2.14. Glazing systems with/without PCM (left figure) [152] and a schematic of double-glazed PCM window (right figure) [155]

### 2.3.2 Adaptability of PCMs

PCMs have shown their great potential as different parts of the building constructions, and their adaptability to different climates, cities, and urban areas is also of interest [156]. Fateh [157] studied the thermal and energy performance of PCM-enhanced-light-walls in two climates (Würzburg, Germany and Denver, USA). The results showed that although the PCM walls had different effects on buildings in the two climates, comfortable thermal environments and energy savings were both achieved. Souayfane [158] analyzed the economic benefits of TIM-PCM walls in different climates and found that the TIM-PCM walls affected the indoor temperature in all climates. Besides, the TIM-PCM walls induce high economic value in polar and subarctic climates, but not in Sacramento (Mediterranean climate) and Toronto (humid continent). Ahangari [159] investigated an innovative double layer PCM system in five different climatic zones in Iran. The results showed that the double layer PCM system increased the thermal comfort period from 73% to 93% in Yazd and from 63% to 75% in Tehran. Yu [160] investigated the pipe-embedded ventilation roof with outer-layer shape stabilized PCM in five representative climatic conditions (severe cold region, cold region, hot-

summer-winter-cool region, hot-summer-winter-warm region, and mild region) in China. It was found that excellent thermal performance could be achieved by varying the phase transition temperature range and thickness of the PCM layer and the airflow rate in the ventilation duct.

### **2.3.3 Location and property dependence of PCM performance**

The fact that PCMs can be applied to different climates and regions means that PCMs can motivate the ability to store and release heat by changing their characteristics. The location (Fig. 2.15) in the building structure and the thermophysical properties are the crucial characteristics of PCM.

Jin [161-164] investigated the thermal performance of the building envelope when PCM was placed in different locations. The results showed that the state, heat flux, amplitude, and time delay of the PCM differed with its location. Besides, the optimal location of PCM was affected by different factors such as thickness, heat fusion, and melting temperature. Lee [165] studied the thermal behavior of the south and west wall with PCMs placed at different locations. It was found that the optimal location in the south wall was closer to the external environment than the west wall. Lagou [166] revealed that the optimal locations were located on the interior side in different European continent climatic conditions. Kishore [167, 168] found that the optimal location of PCM was in the middle of the envelope in five U.S. cities. Li [169] discovered that the heat transfer reduction was higher when PCM was placed close to the outdoors. Murathan [170] evaluated the energy consumption of the envelope with PCMs placed at different locations. The results showed that the envelope consumed less energy when the PCM was placed between the middle and the outside of the envelope. Rai [171] studied the energy performance of a building assembled with PCM enhanced walls by placing the PCM on the outer and inner sides of the walls. The results suggested that the maximum latent heat could be used with PCM placed on the outer side. However, the PCM was recommended to be placed on the inner side with a melting point close to the indoor set-point temperature, accompanied by

sufficient insulation to shield the outdoor temperature.

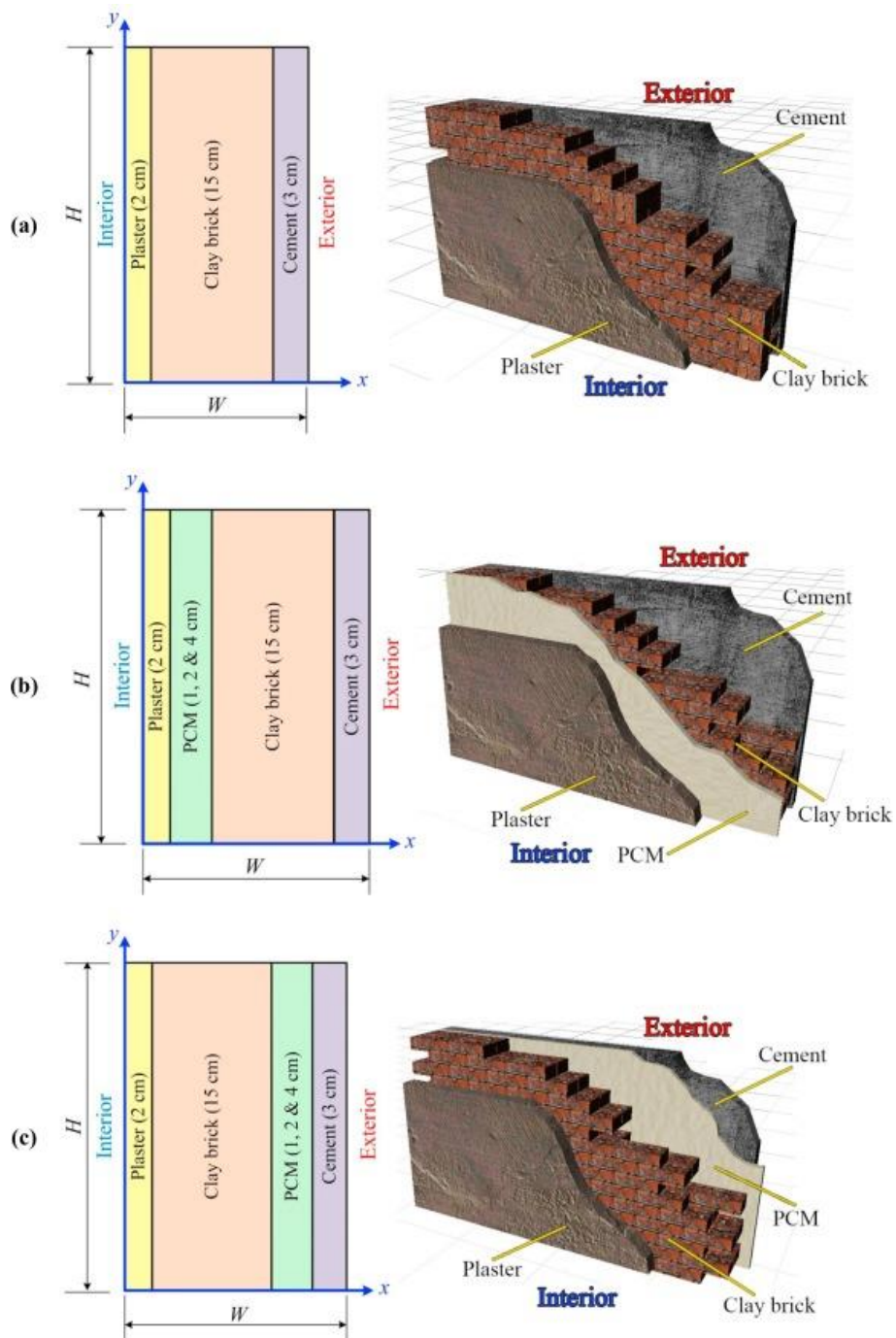


Fig. 2.15 Different walls: (a) No-PCM; (b) PCM close to interior; (c) PCM close to exterior [169]

In addition to the location, the thermophysical properties of the PCM also affect the thermal

performance of the building structure. Yu [172] studied the performance of PCM with different phase transition ranges in five climate regions. It was found that the optimal phase transition temperature was 31–33 °C, 34–36 °C, 36–38 °C, 34–36 °C, and 29–31 °C in severe cold region, cold region, hot summer and cold winter region, hot summer and warm winter region, and mild region, respectively. Kishore [167, 168] investigated the effect of PCM transition temperature, thickness, latent heat, and mass density on the heat gain reduction. The results showed that the peak heat gain reduction increased with the thickness, latent heat, and mass density. Besides, sensitivity analysis revealed that PCM transition temperature was the strongest parameter affecting thermal load modulation. Mohseni [173] evaluated the impact of PCM thickness and melting temperature on the cooling and heating energy consumptions of buildings. The results showed that with the increase in thickness from 5 mm to 10 mm, the energy consumption for cooling and heating decreased by 23% and 12%, respectively. Besides, the optimal melting temperature varied with the season, with 25°C and 21°C in summer and winter, respectively. Li [174] explored the effect of PCM melting temperature on the thermal performance of buildings. The results showed that the optimal PCM melting points were 26–30°C, 24°C, and 20–24°C for cities located in hot climates (e.g., summer of Las Vegas), moderate climates cold climates (e.g., summer of Seattle), and cold climates (e.g., summer of Seattle), respectively. Lei [175] studied the effect of PCM phase change temperature and range, location, and shape of enthalpy–temperature curve on the building energy performance in Singapore. The results revealed that the heat gain decreased with the increase of PCM thickness. The optimal phase change temperature was comprehensively affected by the location, phase transition temperature range, and shape of the enthalpy-temperature curve of the PCM. When PCM was placed on the exterior surface, the optimal phase transition temperature was the minimum temperature that allowed the full melting-solidification cycle of the entire PCM layer. When PCM was placed on the interior surface, the optimal phase transition temperature was the average temperature of the interior surface. Moreover, a larger phase change range improved the adaptability of the PCM to environment variations.

## **2.4 Integration of hygroscopic materials and PCMs**

According to the previous statements, it is valuable to integrate the thermal inertia of PCMs and the hygric inertia of hygroscopic materials, making it possible for the envelope to improve the energy, thermal, and hygric performance simultaneously. However, till date, few studies related to this topic have been conducted, and they are summarized as follows.

### **2.4.1 Preparation and characterization of the integrated materials**

Integrated materials (composites) were usually prepared by combining a hygroscopic material with an encapsulated PCM. The characterization of the composites includes morphological, thermal, hygroscopic properties, and chemical structure. Specifically, the morphology properties were measured by scanning electron microscope or transmission electron microscopy; the thermal properties were measured by differential scanning calorimetry or thermo gravimetric analysis; the hygroscopic properties were measured by dynamic vapor sorption; the chemical structure was measured by Fourier transform infrared or X-ray diffraction.

He [176] prepared phase change microcapsule composites with different substrates (gypsum, zeolite, expanded vermiculite, and shell powder) and characterized their thermal properties, apparent morphology, and pore distribution characteristics. The results revealed the superiority of the zeolite-based phase change microcapsule composites compared to other composites. They had a large phase latent heat and their moisture buffering performance index was 2 to 10 times that of other composites.

Wu [177] and Chen [74, 178] prepared a novel phase change humidity control material (PCHCM) by using PCM microcapsules with some hygroscopic materials (diatomite, vesuvianite, sepiolite, and zeolite). The hygroscopic, thermal properties, and thermal stability of PCHCMs were measured. The

results showed that the super-cooling degree of PCCHCMs was lower than that of pure PCMs, which were more conducive to temperature stabilization. Moreover, the moisture transfer coefficients of PCHCMs were 1.47–1.83 times higher than those of pure hygroscopic materials.

Hou [179] prepared and characterized a novel hygrothermal MOF/MicroPCM composite material by using Metal-Organic Frameworks (MOFs) and n-octadecane-based microencapsulated phase change material (MicroPCM). The physical and chemical properties of the synthesized materials were experimentally characterized; the hygrothermal performance of a building using the composite material containing 50% MicroPCM in a Mediterranean climate (Rome, Italy) was studied numerically. The characterization results showed that the composites had both thermal and humidity buffer capacity. Besides, the numerical results revealed that the MOF/MicroPCM composites significantly reduced the temperature and humidity fluctuations compared to the gypsum board.

Park [180] prepared a composite material from PCM and functional gypsum board (FGB) by direct impregnation method, where the FGB was prepared from gypsum, water, and porous materials (expanded vermiculite, expanded perlite, and carbon nanomaterials). According to the results of FTIR analysis, the composites containing FGB and PCM could maintain the heat storage properties of PCM with no chemical interactions during the compositing process. Besides, the hygrothermal performance of the wall applied with the composite material was evaluated. The results indicated that the heat storage capacity of the composite wall was improved and that there was no potential for condensation, mold growth, and structural damage during the application.

#### **2.4.2 Application of the integrated materials**

Compared with the studies of preparation and characterization, there are fewer studies on the application performance of the integrated materials.

Chang [181] evaluated the hygrothermal performance of wood frame walls containing Macro-

packed PCM under Korean climate conditions by numerical methods. It was revealed that such walls could improve hygrothermal performance and reduce the mold growth risk.

Shi [182] experimentally investigated the effect of incorporating macro encapsulated PCM into concrete walls on indoor temperature and humidity by placing PCM in different positions (externally bonded, laminated within, and internally bonded). The results showed that PCM laminated inside concrete walls and placed on the inner of concrete walls showed the best ability of temperature and humidity control, with a maximum temperature and relative humidity reduction of 4°C and 16%, respectively, compared to the control group.

Fraine [183] investigated the hygrothermal performance of a sintered hollow brick filled with a new phase change humidity control material (PCHCM) prepared from microencapsulated phase change material (MPCM) and diatomite. The results showed that the fluctuations in temperature and relative humidity and the total heat flux on the inner surface were reduced. Besides, the optimum effect could be obtained by filling the PCHCM in the center of the sintered hollow brick.

Similarly, Wu [184] prepared a PCHCM comprising phase change material microcapsules and hygroscopic material (diatomite). The effect of PCHCM on the temperature, relative humidity, and energy consumption in buildings under different climatic conditions (Atlanta, Beijing, Paris, and Guangzhou) were investigated. The results showed a significant impact of PCHCM on the hygrothermal performance as it reduced and moderated the indoor temperature and relative humidity. The study also indicated that the PCHCM could reduce building energy consumption, especially in Paris (temperate maritime climate). In contrast, the energy savings potential in Guangzhou (subtropical humid climate) was limited.

Zhu [185] proposed a double-layer wallboard with phase change humidity control material (PCHCM) to manage indoor temperature and relative humidity environment. The hygrothermal and energy performance of a PCHCM building in Wuhan, China, was numerically evaluated. The results

showed that the PCHCM wallboard effectively regulated the indoor hygrothermal environment. Compared to the building with air conditioning, the indoor temperature of the PCHCM building remained almost unchanged, but the relative humidity was reduced by 5%. Besides, the energy consumption of the PCHCM building was reduced by 8.3% in summer and 24.9% in winter.

## 2.5 Heat and mass transfer theory and model

Building envelopes are typical porous media; the heat and moisture transfer in the building envelope can be regarded as the transfer in porous materials. Common substances such as soil, bricks, and rocks are porous materials, and they have the same mechanisms of heat and moisture transfer.

### 2.5.1 Moisture transfer in porous media

The total moisture transfer in porous materials includes vapor diffusion and liquid transport, which follow different transfer mechanisms.

#### 2.5.1.1 Vapor transfer

The molecular diffusion theory can describe the vapor transport in the pore space. At the pore scale, Fick's law [186] is used to describe the phenomenon of molecular diffusion. According to this law, the concentration gradient is proportional to the flow rate per unit area and time.

$$N_c = -D_c \nabla C_v \quad (2.2)$$

where

$N_c$  = rate of molecular moisture diffusion, (mol/(m<sup>2</sup>/s))

$D_c$  = molecular diffusion coefficient proportional to the mean free path, (m<sup>2</sup>/s)

$C_v$  = molar concentration of vapor, (mol/m<sup>3</sup>).

### 2.5.1.2 Liquid transfer

The liquid phase transfer is driven by capillary pressure gradients and gravity force. Normally, the effect of gravity force is small and can be neglected [187-189]. When gravity is neglected, the liquid transfer can be described by Darcy's law [190], which describes the volume flow of incompressible fluid through the unit cross section of porous media.

$$j_w = -D_w \nabla w \quad (2.3)$$

where

$j_w$  = flow density of water content, (m<sup>3</sup>/(m<sup>2</sup>·s))

$D_w$  = moisture water diffusion coefficient, (m<sup>2</sup>/s)

$w$  = moisture water content, (m<sup>3</sup>/m<sup>3</sup>).

### 2.5.2 Heat transfer in porous media

Normally, under continuous media assumption, heat transfer process can be quantified by a rate equation based on Fourier's law of thermal conduction. This law states that the heat transfer rate through a material is proportional to the negative gradient in the temperature and the area (perpendicular to the gradient) of the surface through which the heat flows. It is expressed by

$$q = -\lambda \nabla T \quad (2.4)$$

where

$q$  = thermal flux, (W/m<sup>2</sup>)

$\lambda$  = thermal conductivity, (W/(m·K))

$T$  = temperature, (K).

Heat transfer in the porous material can be described as a change in enthalpy caused by a change in temperature, and it consists of two parts. First, the heat flux gradient is directly proportional to the temperature gradient and the conductivity as defined by Fourier's law. Second, the heat flux gradient can also be transported by the moisture flux, defined as a source term in the general heat equation [96]. Thus, the energy conservation equation [191] can be expressed by

$$\rho C_p \frac{\partial T}{\partial t} = \nabla(\lambda \nabla T) - \nabla(L_v \nabla j_v) \quad (2.5)$$

where

$\rho$  = density of material, (kg/m<sup>3</sup>)

$C_p$  = specific heat capacity of material, (J/(kg·K))

$\lambda$  = thermal conductivity of material, (W/(m·K))

$L_v$  = latent heat of evaporation, (J/kg)

$j_v$  = moisture flux of moisture vapor diffusion, (kg/(m<sup>2</sup>·s)).

### 2.5.3 Coupled heat and moisture transfer in porous media

The study of coupled heat and moisture transfer models within porous media has been conducted for many years. Different theories and models of moisture transfer have been proposed by different scholars. Different driving forces, such as moisture content, capillary pressure, relative humidity, and partial water vapor pressure, have been applied to these models. Some representative models such as Philip and De Vries model, Luikov model, Whitaker model, Kunzel model, and Mendes model [192] are presented below.

### 2.5.3.1 Philip and De Vries model

In 1957, Philip and De Vries [193-195] proposed a coupled heat and moisture model based on the hypothesis of the relationship between moisture transport and temperature in the soil. In this model, the volumetric water content and temperature are the driving forces for moisture and heat transfer, respectively. The general differential equations for moisture and heat transfer are written as

$$\frac{\partial \theta}{\partial t} = \nabla(D_{\theta} \nabla \theta) + \nabla(D_T \nabla T) + \frac{\partial k_h}{\partial z} \quad (2.6)$$

$$C \frac{\partial T}{\partial t} = \nabla(\lambda \nabla T) - L_v \nabla(D_{\theta, vap} \nabla \theta) \quad (2.7)$$

$$D_{\theta} = D_{\theta, liq} + D_{\theta, vap} \quad (2.8)$$

$$D_T = D_{T, liq} + D_{T, vap} \quad (2.9)$$

where

$\theta$  = volumetric water content, ( $\text{m}^3/\text{m}^3$ )

$T$  = temperature, (K)

$D_{\theta}$  = moisture diffusion coefficient related to the moisture gradient, ( $\text{m}^2/\text{s}$ )

$D_T$  = moisture diffusion coefficient related to the temperature gradient, ( $\text{m}^2/\text{s}\cdot\text{K}$ )

$k_h$  = hydraulic conductivity which generally related to the gravity forces

$C$  = volumetric heat capacity of material, ( $\text{J}/(\text{kg}\cdot\text{K})$ )

$\lambda$  = thermal conductivity, ( $\text{W}/(\text{m}\cdot\text{K})$ )

$L_v$  = latent heat of evaporation, ( $\text{J}/\text{kg}$ )

$D_{T, liq}$  = liquid diffusion coefficient related to the temperature gradient, ( $\text{m}^2/\text{s}\cdot\text{K}$ ) or ( $\text{kg}/\text{m}\cdot\text{s}\cdot\text{K}$ )

$D_{T, vap}$  = vapor diffusion coefficient related to the temperature gradient, ( $\text{m}^2/\text{s}\cdot\text{K}$ ) or ( $\text{kg}/\text{m}\cdot\text{s}\cdot\text{K}$ )

$D_{\theta,liq}$  = liquid diffusion coefficient related to the moisture gradient, (m<sup>2</sup>/s)

$D_{\theta,vap}$  = vapor diffusion coefficient related to the moisture gradient, (m<sup>2</sup>/s).

### 2.5.3.2 Luikov model

In 1966, Luikov [196-198] proposed a coupled heat and moisture model based on irreversible thermodynamics, macroscopic mass conservation, and energy conservation. The driving forces for moisture and heat transfer in the model are relative moisture concentration and temperature, respectively. Under non-isothermal conditions, the partial differential equations for heat and moisture transfer are written as

$$\frac{\partial u}{\partial t} + \tau_{rm} \frac{\partial^2 u}{\partial t^2} = D_m \nabla (\nabla u + \delta \nabla T) \quad (2.10)$$

$$\frac{\partial T}{\partial t} = \alpha \nabla (\lambda \nabla T) + \frac{E}{c_p} L_v \frac{\partial u}{\partial t} \quad (2.11)$$

where

$u$  = relative moisture concentration, (kg/kg)

$T$  = temperature, (K)

$\tau_{rm}$  = time of moisture propagation in the capillary porous media, (s)

$D_m$  = moisture diffusion coefficient of the porous media, (m<sup>2</sup>/s)

$\delta$  = thermogradient coefficient, (K<sup>-1</sup>)

$\alpha$  = thermal diffusion coefficient

$E$  = phase conversion number

$C_p$  = volumetric heat capacity of material, (J/(kg·K))

$\lambda$  = thermal conductivity, (W/(m·K))

$L_v$  = latent heat of evaporation, (J/kg).

### 2.5.3.3 Whitaker model

In 1977, Whitaker [199] proposed a more detailed theory of heat and moisture transfer based on local average volume behavior. The model describes the transport equations of each phase (solid, liquid, and vapor) at macroscopic and microscopic levels based on two variables, moisture and temperature. The coupled heat and moisture equations are shown as

$$\rho_s \frac{\partial X}{\partial t} = \nabla(\rho_s f D_v \nabla W_v + D_b \nabla \rho_v + \rho_w \bar{V}_w) \quad (2.12)$$

$$\frac{\partial(\varepsilon_w \rho_w H_w + \varepsilon_v \rho_v H_v + \varepsilon_s \rho_s H_s + \bar{\rho}_b H_b)}{\partial t} = \nabla(\lambda \nabla T) + H_v \rho_g f D_v \nabla W_v + H_b D_b \nabla \rho_v - H_w \rho_w \bar{V}_w \quad (2.13)$$

where

$X$  = mass moisture content, (kg/kg)

$T$  = temperature, (K)

$f$  = dimensionless diffusivity tensor

$\rho_w, \rho_v, \rho_s$  = density of the liquid phase, vapor phase, solid phase of water, (kg/(m<sup>3</sup>))

$D_v, D_b$  = water vapor and bound water diffusivity, (m<sup>2</sup>/min)

$W_v$  = vapor mass fraction

$H_w, H_v, H_s, H_b$  = enthalpy of the liquid phase, vapor phase, solid phase of water, bound water, (J/kg)

$V_w$  = liquid phase velocity, (m/min)

$\varepsilon_w, \varepsilon_v, \varepsilon_s$  = volume fraction of liquid, vapor, solid

$\lambda$  = thermal conductivity, (W/(m·K)).

#### 2.5.3.4 Kunzel model

In 1995, Kunzel [187] proposed a model based on Kieβl's theorem. Relative humidity and temperature were chosen as driving forces to describe the coupled model of heat and moisture.

$$\frac{dw}{d\varphi} \frac{\partial \varphi}{\partial t} = \nabla \left( D_{\varphi} \nabla \varphi + \delta_p \nabla (\varphi P_{sat}) \right) \quad (2.14)$$

$$\frac{dH}{dT} \frac{\partial T}{\partial t} = \nabla (\lambda \nabla T) + L_v \nabla \left( \delta_p \nabla (\varphi P_{sat}) \right) \quad (2.15)$$

where

$\varphi$  = relative humidity

$T$  = temperature, (K)

$w$  = water content, (kg/m<sup>3</sup>)

$dw/d\varphi$  = moisture storage capacity of porous material

$D_{\varphi}$  = liquid conduction coefficient, (kg/m·s)

$\delta_p$  = water vapor permeability of the porous material, (kg/m·s·Pa)

$P_{sat}$  = water vapor saturation pressure, (Pa)

$H$  = total enthalpy, (J/m<sup>3</sup>)

$dH/dT$  = heat storage capacity of the porous material

$\lambda$  = thermal conductivity, (W/(m·K))

$L_v$  = latent heat of evaporation, (J/kg).

#### 2.5.3.5 Mendes model

In 1999, Mendes [200] proposed a model by improving and correcting the model of Philip and

De Vries. It is presented as:

$$\frac{\partial \theta}{\partial t} = \nabla(D_{\theta} \nabla \theta + D_T \nabla T) \quad (2.16)$$

$$\rho C \frac{\partial T}{\partial t} = \nabla(\lambda \nabla T) + L_v \nabla(D_{\theta, vap} \nabla \theta + D_{T, vap} \nabla T) \quad (2.17)$$

where

$\theta$  = volumetric water content, ( $\text{m}^3/\text{m}^3$ )

$T$  = temperature, (K)

$D_{\theta}$  = moisture diffusion coefficient related to the moisture gradient, ( $\text{m}^2/\text{s}$ )

$D_T$  = moisture diffusion coefficient related to the temperature gradient, ( $\text{m}^2/\text{s}\cdot\text{K}$ )

$\rho$  = density of material, ( $\text{kg}/\text{m}^3$ )

$C$  = volumetric heat capacity of material, ( $\text{J}/(\text{kg}\cdot\text{K})$ )

$\lambda$  = thermal conductivity of material, ( $\text{W}/(\text{m}\cdot\text{K})$ )

$L_v$  = latent heat of evaporation, ( $\text{J}/\text{kg}$ )

$D_{T, vap}$  = vapor diffusion coefficient related to the temperature gradient, ( $\text{m}^2/\text{s}\cdot\text{K}$ ) or ( $\text{kg}/\text{m}\cdot\text{s}\cdot\text{K}$ )

$D_{\theta, vap}$  = vapor diffusion coefficient related to the moisture gradient, ( $\text{m}^2/\text{s}$ ).

### 2.5.3.6 Other models

There are some other models on heat and humidity coupling, but they are mostly based on the above models. Diasty [201] proposed a model for moisture absorption and desorption in porous media based on the driving forces of water vapor partial pressure. Santos [202] developed a partial differential equation to describe the heat and moisture transfer by lumped parameter method based on temperature, moist air pressure, and water vapor partial pressure. Haupl [203] established a coupled nonlinear

differential equation for heat transfer, moisture transfer, and air permeation in porous media. Matsumoto [204] developed moisture and energy conservation equations to predict and analyze models using the moist chemical potential as the driving force.

#### 2.5.4 Heat transfer in PCM

PCMs contain three different states, i.e., solid, liquid, and solid-liquid coexistence states, which makes the phase change heat transfer problem more complicated compared to common materials. The main difficulty is that the two-phase interface of the region moves with time and is accompanied by storage and release of latent heat. The moving boundary problem is also known as Stefan's problem [205]. Thus, there are three heat transfer equations corresponding to different states in the control region. The equations are expressed based on the following assumptions [206]:

- 1) Thermal properties (e.g., thermal conductivity, specific heat capacity, and density) are constant in the solid-liquid coexistence state.
- 2) Free convection in the liquid state is neglected.
- 3) Subcooling during freezing is neglected.

For the solid state of PCM, the equation is

$$\rho_s C_s \frac{\partial T_s}{\partial t} = \nabla(\lambda_s \nabla T_s) \quad (2.18)$$

For the liquid state of PCM, the equation is

$$\rho_l C_l \frac{\partial T_l}{\partial t} = \nabla(\lambda_l \nabla T_l) \quad (2.19)$$

For the two-phase interface ( $x = S(t)$ ) of PCM, the equation is

$$-\rho_s L \frac{\partial S(t)}{\partial t} = \lambda_l \nabla T_l - \lambda_s \nabla T_s \quad (2.20)$$

where

$\rho_s, \rho_l$  = density of solid and liquid state, ( $\text{kg}/\text{m}^3$ )

$\lambda_s, \lambda_l$  = thermal conductivity of solid and liquid state, ( $\text{W}/(\text{m}\cdot\text{K})$ )

$C_s, C_l$  = specific heat capacity of solid and liquid state, ( $\text{J}/(\text{kg}\cdot\text{K})$ )

$S(t)$  = two-phase interface

$L$  = latent heat, ( $\text{J}/\text{kg}$ ).

The solution of the Stefan problem can be achieved by analytical or numerical methods. The analytical formulation of the classical Stefan problem is the Neumann solution, but it is only applicable to a few cases. In most cases, the Stefan problem has to be solved by numerical methods. The numerical method allows to express mathematically the thermal properties of PCM such as specific heat capacity, enthalpy, thermal conductivity, etc., which are usually expressed as a function of temperature. These thermal properties can be measured by different technical methods, such as DSC (differential scanning calorimetry) method [207-209], T-history method [210-212], heat flow meter method [117, 213], cut bar/flat slab method [213], hot wire method [214, 215]. There are two commonly used numerical methods: the enthalpy and the effective heat capacity method.

#### 2.5.4.1 Enthalpy method

The enthalpy model [216-218] takes enthalpy and temperature as dependent variables. Thus, the solution process of the enthalpy model does not need to consider the movement and change of the transition interface, making it possible to establish the unified equations in the three states of PCM. The enthalpy model is expressed as

$$\rho \frac{\partial H}{\partial t} = \nabla(\lambda \nabla T) \quad (2.21)$$

The total enthalpy ( $H$ ) is the sum of the sensible and latent heats of the PCM and is related to the temperature of the PCM:

$$H(T) = \int_{T_m}^T \rho C_p dT + \rho f_l L \quad (2.22)$$

where

$\rho$  = density, ( $kg/m^3$ )

$\lambda$  = thermal conductivity, ( $W/(m \cdot K)$ )

$C_p$  = specific heat capacity, ( $J/(kg \cdot K)$ )

$L$  = latent heat, ( $J/kg$ )

$f_l$  = liquid fraction.

$$f_l = \begin{cases} 0 & T < T_s \\ \frac{T-T_s}{T_l-T_s} & T_s \ll T \ll T_l \\ 1 & T > T_l \end{cases} \quad (2.23)$$

where

$T_s, T_l$  = initial and final temperature of phase transition range, (K) or ( $^{\circ}C$ ).

Thus, combining Eqs. (2.24) and (2.25),

$$H(T) = \begin{cases} \int_{T_s}^T \rho C_p dT & T < T_s \\ \rho \frac{T-T_s}{T_l-T_s} & T_s \ll T \ll T_l \\ \int_{T_l}^T \rho C_p dT + \rho L & T > T_l \end{cases} \quad (2.24)$$

#### 2.5.4.2 Effective heat capacity method

The effective heat capacity model [219-221] treats the latent heat of the phase change as a large amount of heat in the sensible form in the phase transition temperature interval. The heat transfer problem of PCM described by three equations for three states can be transformed into a "single-media" nonlinear conduction problem for the entire computational region. The model is expressed as:

$$\rho C_{eff} \frac{\partial T}{\partial t} = \nabla(\lambda_{eff} \nabla T) \quad (2.25)$$

The effective heat capacity ( $C_{eff}$ ) is

$$C_{eff}(T) = \begin{cases} C_{p,s} & T < T_s \\ (1 - f_l)C_{p,s} + f_l C_{p,l} + \frac{L}{T_l - T_s} & T_s \ll T \ll T_l \\ C_{p,l} & T > T_l \end{cases} \quad (2.26)$$

The effective thermal conductivity ( $\lambda_{eff}$ ) is

$$\lambda_{eff}(T) = \begin{cases} \lambda_s & T < T_s \\ f_l \lambda_l + (1 - f_l) \lambda_s & T_s \ll T \ll T_l \\ \lambda_l & T > T_l \end{cases} \quad (2.27)$$

where

$T_s, T_l$  = initial and final temperature of phase transition range, (K) or (°C)

$\rho$  = density, ( $kg/m^3$ )

$C_{p,s}, C_{p,l}$  = specific heat capacity of solid and liquid state, (J/(kg·K))

$\lambda_s, \lambda_l$  = thermal conductivity of solid and liquid state, W/(m·K)

L = latent heat, (J/kg)

$f_l$  = liquid fraction.

## 2.6 Conclusion

In this chapter, the literature review is conducted and the theory theoretical considerations about heat and moisture transfer is presented.

Indoor heat and humidity environments affect the physical and psychological health of occupants. As the intermediary of heat and humidity transfer between indoor and outdoor, envelopes play an important role in influencing indoor heat and humidity comfort and energy consumption. Therefore, the innovation of the envelope helps to improve the hygrothermal and energy performance of the

buildings.

Bio-based materials are environmental-friendly materials taken from nature. Due to the high porosity and low density, some bio-based materials have received attention as thermal insulation envelopes in recent years. Moreover, bio-based materials are also worth emphasizing as hygroscopic envelopes; they can adsorb and desorb moisture to regulate the humid environment and affect the building energy consumption. However, the physical hygroscopic properties are highly temperature dependent, and temperature affects the ability to adsorb and desorb moisture. Considering the effect of temperature on the hygroscopic properties helps to reach accurate simulation results.

PCMs are also an envelope technology to maintain thermal comfort in buildings as they can store and release a great amount of thermal energy during the phase change process. PCM has a wide range of applicability to improve indoor thermal comfort and save building energy in different climates. However, thermal performances of PCM vary with different properties (e.g., thickness, phase transition range, latent heat, and mass density) or locations in the building structure.

It is valuable to integrate the PCMs and the bio-based hygroscopic materials. However, to date, only a few studies related to this topic, and these studies generally fall into two categories. The first one deals with the integration and preparation of PCM and hygroscopic materials as well as the characterization and analysis of the integrated samples. The second one focuses mainly on the application of the integrated materials. More detailed and comprehensive studies need to be conducted.

The moisture transfer in porous media consists of vapor and liquid transfer, following Fick's law and Darcy's law, respectively. The heat transfer follows Fourier's law. There is a coupling between heat and moisture transfer within porous media. Therefore, different models with different driving forces are proposed to describe the coupling. The most commonly used models include Philip and De Vries, Luikov, Whitaker, Kunzel, and Mendes model. There are two common models to describe the heat transfer in PCM: the enthalpy and the effective heat capacity model.

# **Chapter 3      Experimental study on hygrothermal performance of integrated envelope**

## **3.1    Objectives of experimental study**

As stated in the literature review, bio-based material has the advantage of hygroscopic properties which leads to good hygric inertia, while PCM has the advantage of thermal storage and promotes the thermal inertia. It would be interesting and valuable to integrate and utilize their respective advantages simultaneously. In addition, temperature has a significant influence on the hygroscopic properties. Moreover, PCM can dampen the heat transfer and change the temperature field and this property varies with the location of the PCM in the envelope. Therefore, it is necessary to use the experimental approach to generate a reference for the assembly of the two materials and to investigate the hygrothermal behavior of the integrated envelope.

Based on the above motivation, the main objectives are presented as follows:

- 1) Explore the assembly method of hygroscopic material and PCM.
- 2) Study the coupling phenomena of heat and moisture transfer within the hygroscopic materials.
- 3) Study the effect of PCM on the hygrothermal behavior of hygroscopic material.
- 4) Study the hygrothermal and energy behavior of the integrated envelopes under different boundary conditions.
- 5) Provide experimental data for mathematical model validation for simulation studies in Chapter 4.

## 3.2 Material and methodology

### 3.2.1 Experimental materials

The PCM panel [222] used in this study shown in Fig. 3.1 (a) and (b) is a finished shape-stabilized PCM wrapped on both sides in an aluminum sheet with a thickness of 0.1 mm, preventing deformation and leakage during use. The main element producing the phase change is a mixture of 60% paraffin wax and 40% ethylene-based polymer.



Fig. 3.1. Finished shape-stabilized PCM: (a) PCM panel; (b) aluminum sheet and the mixture of paraffin wax and ethylene-based polymer

Fig. 3.2 shows the specific heat capacity of the PCM. It remains in the liquid-solid coexistence state during the phase transition range from 10 to 28 °C, making its latent heat deduced as 136.2 kJ/kg. The maximum specific heat capacity of 15.8 kJ/(kg · K) occurs at a temperature of 22°C. When the temperature of PCM is below 10 °C or above 28 °C, it remains in solid and liquid state with the constant specific heat capacity of 4.0 kJ/(kg · K) and 3.8 kJ/(kg · K), respectively.

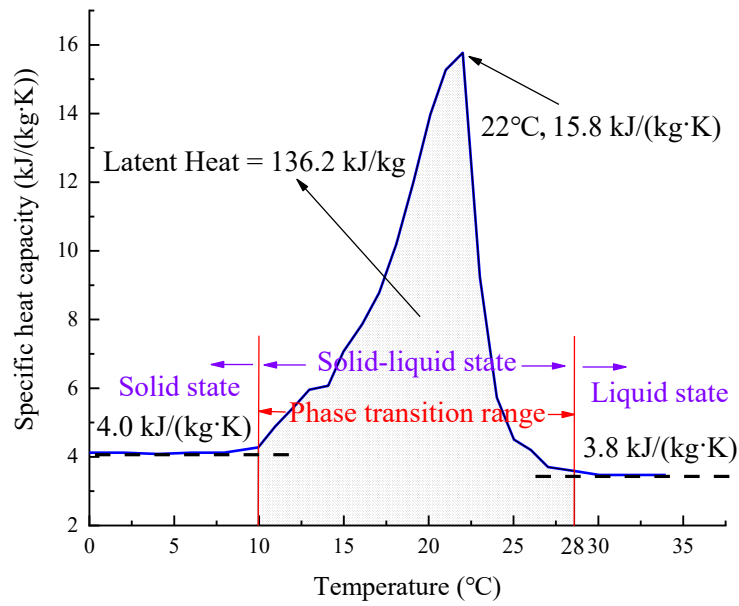


Fig. 3.2. Specific heat capacity of the PCM [222]

Fig. 3.3 (a) shows the hemp concrete (HC) panel, which was used as the bio-based hygroscopic material in this study. The HC panel was composed of hemp shives (shown in Fig. 3.3 (b)), water, and lime-based binder in the volume proportions of 64%, 24%, and 12%, respectively. Table 3.1 lists the dimensions and basic hygrothermal properties of the PCM and the HC.

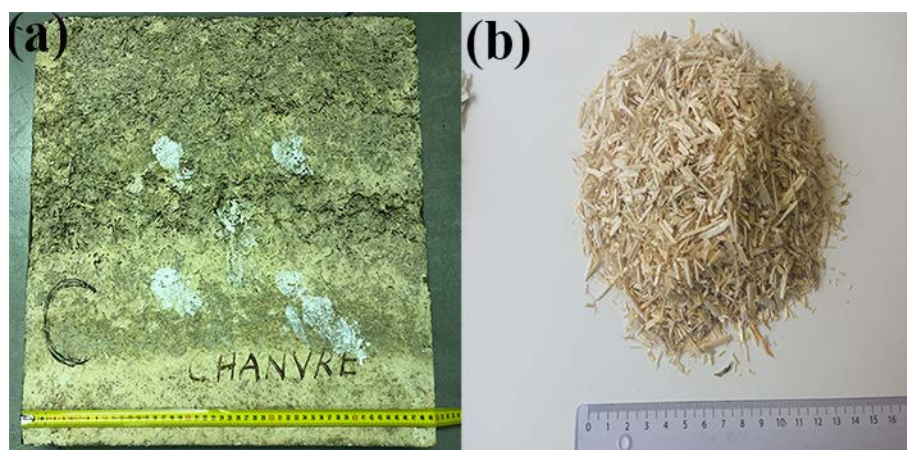


Fig. 3.3. Bio-based material: (a) hemp concrete; (b) hemp shives [94]

	PCM [222]	HC [94]
Dimensions (L × W) (cm)	50 × 50	50 × 50
Thickness (cm)	2.12	7
Density (kg/m <sup>3</sup> )	810	478
Thermal conductivity (W/(m · K))	Solid: 0.18; Liquid: 0.14	0.12
Specific heat capacity (kJ/(kg · K))	Solid: 4.0; Liquid: 3.8	1.08
Porosity (%)	—	76.44

Table 3.1. Dimensions and hygrothermal properties of the PCM and the HC

### 3.2.2 Experimental facilities

#### 3.2.2.1 Climatic chamber

The climatic chamber used in this investigation is LabEvent L C/64/40/3 with a dimension of  $109 \times 78.1 \times 97.8 \text{ cm}^3$  as shown in Fig. 3.4. The climatic chamber is equipped with a heating/cooling system and a humidification/dehumidification system that enables it to provide temperature control from  $-40$  to  $180 \text{ }^\circ\text{C}$  and relative humidity control from 10% to 95%. The accuracy of temperature and relative humidity were  $\pm 0.3\text{--}1 \text{ }^\circ\text{C}$  and  $\pm 1\text{--}3\%$ , respectively. The climatic chamber can provide a static or dynamic environment inside the chamber. It automatically reaches the set parameters by self-regulating of heating/cooling and humidification/dehumidification system once the temperature and relative humidity are manually entered.



Fig. 3.4 Climatic chamber (LabEvent L C/64/40/3)

### 3.2.2.2 Temperature/humidity sensor

The sensors for measuring temperature and relative humidity were Type K thermocouples and HMP-110 sensors, they are shown in Fig. 3.5. The diameter of the thermocouples is 0.25 mm; they could measure a temperature range from  $-70$  to  $200$  °C with an accuracy of  $\pm 0.1$  °C. The HMP-110 sensors had an elongated cylindrical shape with a length of 71 mm and a diameter of 12 mm. They were inserted into the HC layer from the lateral side to measure the temperature and relative humidity simultaneously, and the measurement ranges of temperature and relative humidity were from  $-40$  to  $80$  °C and from 0 to 100% with an accuracy of  $\pm 0.2$  °C ( $0-40$  °C) and  $\pm 1.5\%$  ( $0-90\%$ ), respectively.

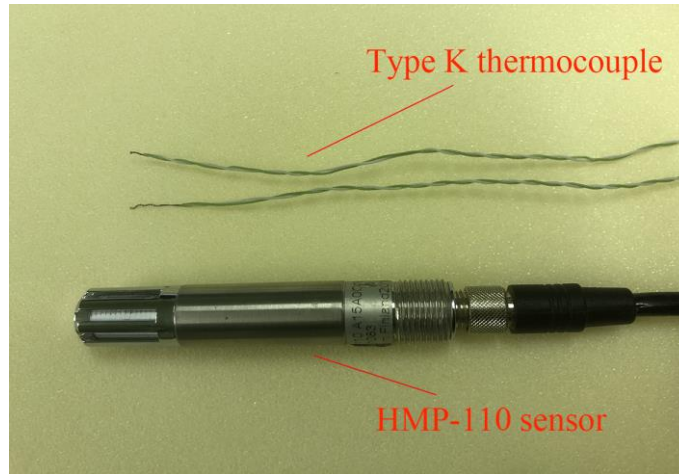


Fig. 3.5 Type K thermocouple and HMP-110 sensor

### 3.2.2.3 Heat flux sensor

The heat flux is monitored by HFS sensors (Fig. 3.6) with dimensions of  $50 \times 50 \times 0.5 \text{ mm}^3$ ; the measurement range is  $-2.0$  to  $2.0 \text{ kW/m}^2$  with an accuracy of  $\pm 2\%$ .



Fig. 3.6 Heat flux sensor

### 3.2.2.4 Date acquisition equipment

A Keithley 2700 data acquisition equipment (Fig. 3.7) with a resolution of 6.5-digit (22-bit) is used to collect and record data from temperature/humidity sensors, thermocouples, and heat flux sensors. When receiving voltage signals from sensors, the voltage range of Keithley 2700 is from 0.1  $\mu\text{V}$ –1000 V with an accuracy of  $\pm 0.002\%$ .

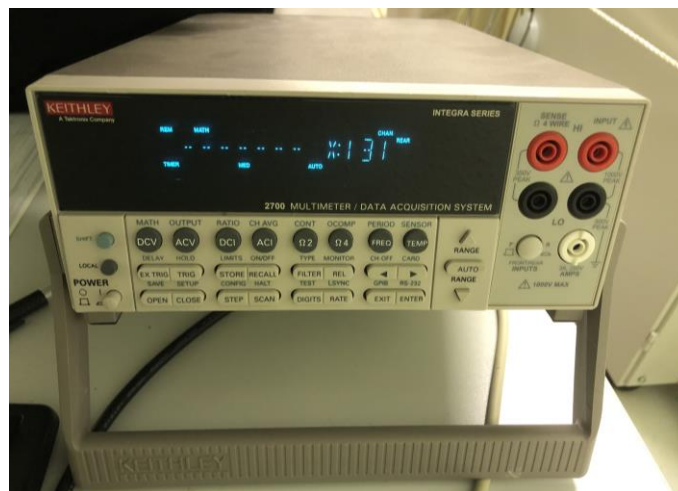


Fig. 3.7 Keithley 2700 data acquisition equipment

On the other side, the Keithley 2700 is connected to a computer to record experimental data with a time step of 120 s. Table 3.2 summarizes the experiment facilities and sensors as well as their ranges and accuracies.

Apparatus	Type	Range	Accuracy
Climatic chamber	LabEvent L C/64/40/3	Temperature: $-40$ – $180$ °C	Temperature: $\pm 0.3$ – $1$ °C
		Relative humidity: 10–95%	Relative humidity: $\pm 1$ – $3\%$
Thermocouple	K type	$-70$ – $200$ °C	$\pm 0.1$ °C
Temperature/Humidity sensor	HMP-110	Temperature: $-40$ – $80$ °C	Temperature: $\pm 0.2$ °C ( $0$ – $40$ °C); $\pm 0.4$ °C

		Relative humidity: 0–100%	(–40–0 °C; 40–80 °C)
			Relative humidity: ±1.5% (0–90%); ±2.5% (90–100%)
Heat flux sensor	HFS	–2000–2000 W/m <sup>2</sup>	±2%
Data acquisition equipment	Keithley 2700	0.1 μV–1000 V (Voltage)	±0.002% (Voltage)

Table 3.2 Apparatus and sensors

### 3.2.3 Experiment setup

The overview schematic of the experiment is shown in Fig. 3.8 (a). One side of the envelope was connected to the climatic chamber to imitate the exterior environment. The other side of the envelope was exposed to the laboratory environment with a relatively stable hygrothermal environment to imitate the interior environment of a real building. Fig. 3.8 (b) shows the actual experimental setup. To ensure thermal and moisture insulation in the transversal plan (perpendicular to the thickness), polystyrene foam and polyethylene film were wrapped around the lateral envelope sides.

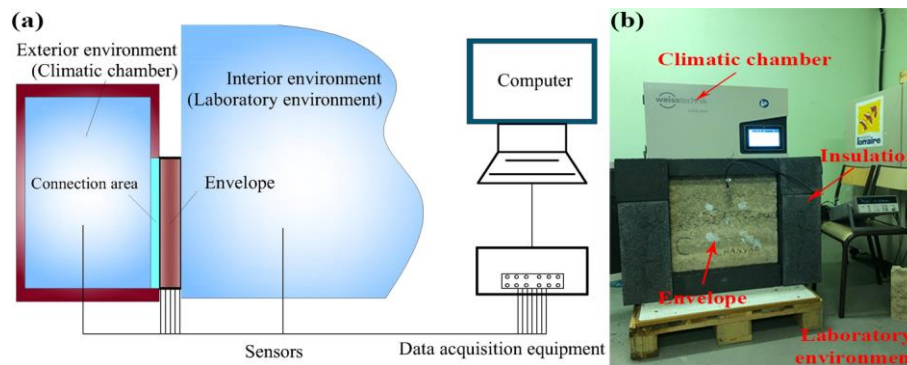


Fig. 3.8 Experimental setup: (a) sketch view; (b) actual experiment

### 3.2.4 Envelope configurations

Two HC layers and one PCM layer were used as the envelope elements. Four envelope

configurations were considered according to the PCM's presence and its location. A configuration without PCM is used as a reference, which is assembled by two HC layers. While for the integrated configurations, the PCM layer was arranged on both sides and in the middle of the two HC layers. The description and dimensions of the different configurations are shown in Table 3.3. Besides, Fig. 3.9 plots the schematic of four configurations, the exterior (climatic chamber) and interior (laboratory environment) are on the left and right side of each configuration, respectively.

It should be noted that the transferability of heat/moisture or the accuracy of experimental results were not affected when two HC layers are in direct contact (configuration without PCM,  $X = 0$  L, and  $X = 1$  L), because the temperature and relative humidity were constant on the interface of the two HCs [80, 103, 223].

Configuration	Description	Multilayer from climatic chamber to ambient	Area [cm <sup>2</sup> ]	Total thickness [cm]
(L: the thickness of HC)				
Without PCM	HC only	HC + HC	50 × 50	14
X = 0 L	PCM on the exterior side	PCM + HC + HC	50 × 50	16.12
X = 0.5 L	PCM in the middle of HCs	HC + PCM + HC	50 × 50	16.12
X = 1 L	PCM on the interior side	HC + HC + PCM	50 × 50	16.12

Table 3.3 Different envelope configurations

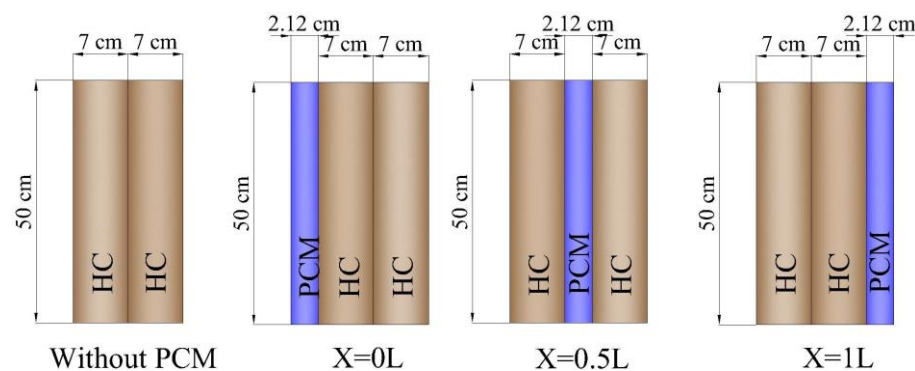
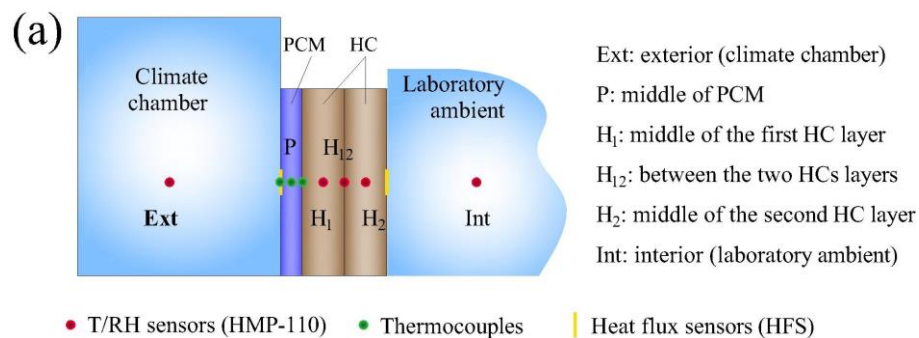


Fig. 3.9 Four envelope configurations of integrating HC and PCM

The main measurement points are shown in Fig. 3.10 (a) and (b), their names are given below :

- Ext: exterior environment (i.e., climatic chamber)
- Int: interior environment (i.e., laboratory environment)
- H<sub>1</sub>: middle of the first HC layer
- H<sub>12</sub>: between the two HC layers
- H<sub>2</sub>: middle of the second HC layer
- P: middle of the PCM layer

Furthermore, some heat flux sensors were affixed on each side of the PCM and the whole envelope.



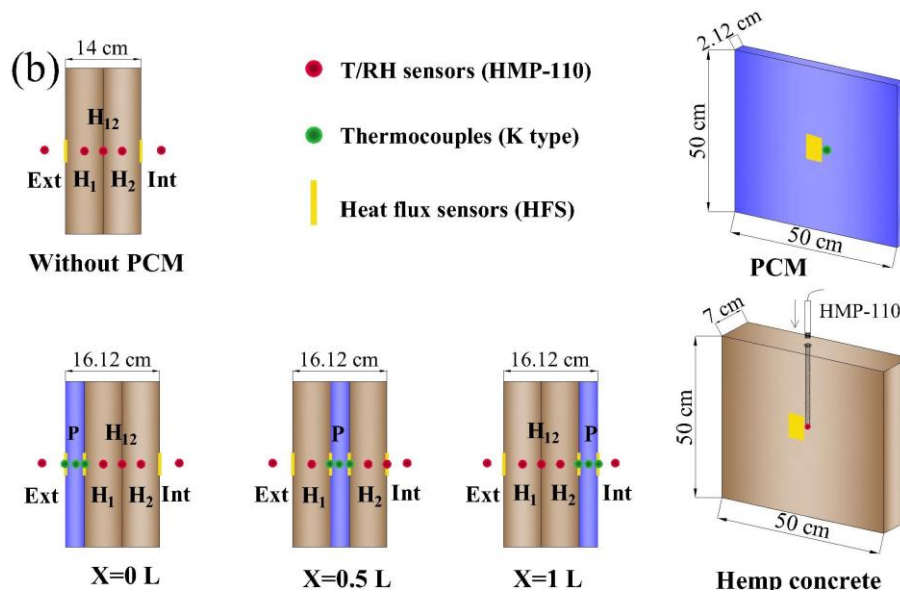


Fig. 3.10 Monitoring points for temperature, relative humidity, and heat flux of (a) configuration  $X = 0 L$  in full view and (b) all the configurations

### 3.2.5 Installation of sensors

Fig. 3.11 shows the installation and arrangement of different monitoring sensors in the actual experiment. Heat flux sensors (HFS) were affixed to the interior and exterior surfaces of the envelope, and each side was sealed and affixed to the surface with polyvinyl chloride tape to avoid air infiltration that could affect measurement results. Similarly, the thermocouples were also affixed to the surfaces of PCM and HC with polyvinyl chloride tape. In addition, HMP-110 sensors were inserted into each HC's geometrical center through drilled holes from the lateral side. Meanwhile, the cable of HMP-110 sensor was sealed by polyethylene film and polystyrene foam, and the hole was sealed by polyvinyl chloride tape, avoiding temperature and humidity interference from cable heat and the laboratory hygrothermal environment.

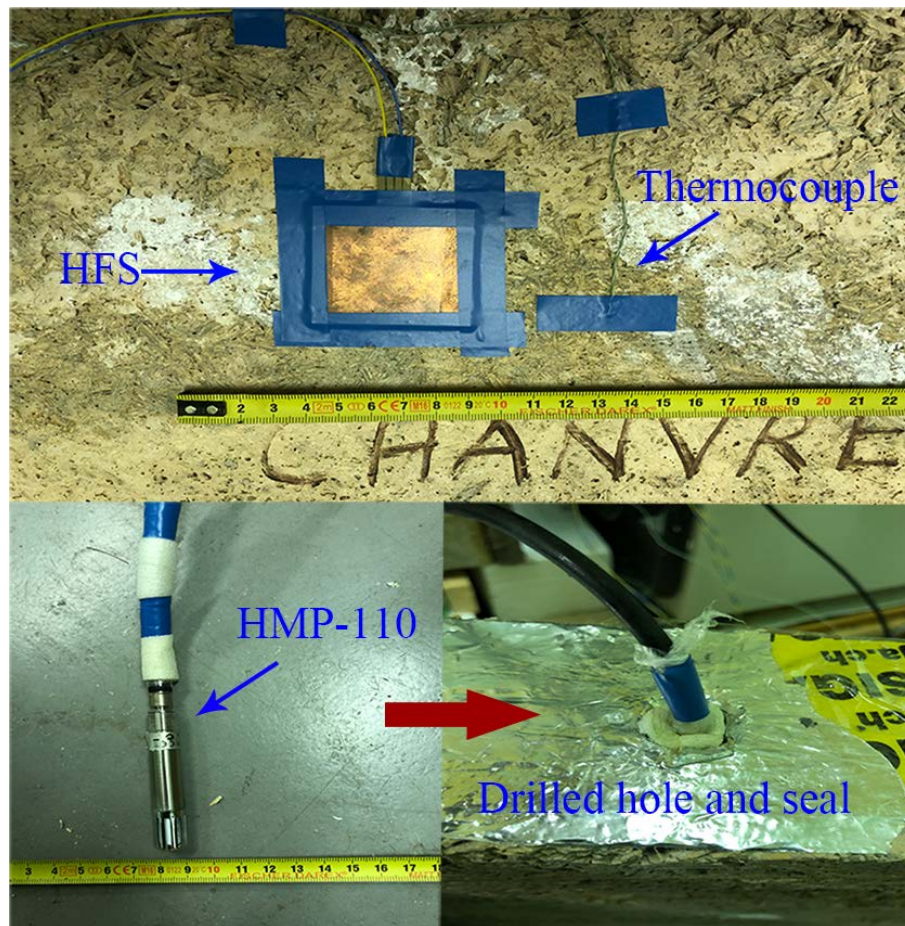


Fig. 3.11 Installation and arrangement of different monitoring sensors in the actual experiment

### 3.2.6 Boundary conditions

The laboratory is a small room located in a large building, so there are two building envelopes between the laboratory environment and the exterior environment, ensuring a relatively stable temperature and relative humidity in the laboratory during the experiment. In addition, due to natural convection in the laboratory, the convective heat/mass transfer coefficient between the envelope and the laboratory environment is small, ensuring little heat and moisture transfer between the two. Under these circumstances, the temperature and relative humidity variations within the envelopes were dominated by the climatic chamber. Therefore, the boundary condition inside the climatic chamber is important. In this study, two types of exterior boundary conditions were considered and performed in

the climatic chamber, they are static and dynamic boundary conditions.

### 3.2.6.1 Static boundary condition

Fig. 3.12 (a) shows the temperature and relative humidity changes for static boundary condition. Before starting, the temperature and relative humidity were set as 15 °C and 85% for two days to ensure heat and moisture stabilization in the envelope. Four combinations of temperature and relative humidity changes were then made with each combination being kept for one day, including two identical and two opposite trends as shown in Table 3.4.

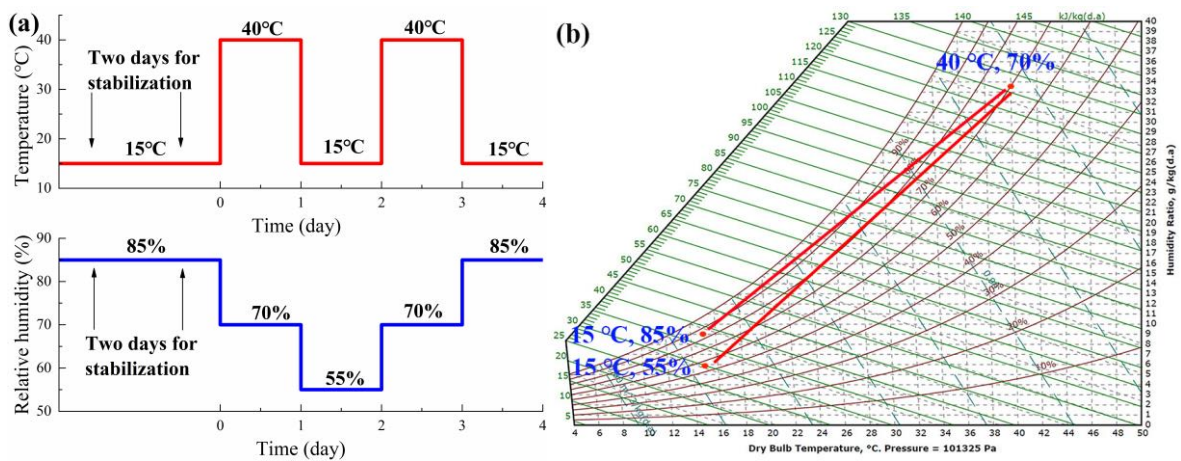


Fig. 3.12 Static boundary condition: (a) temperature and relative humidity condition provided by the climatic chamber; (b) temperature and relative humidity in the psychrometric chart

Days	Temperature	Relative humidity	Temperature and relative humidity combination
1st day	↑ <sup>a</sup>	↓ <sup>b</sup>	Opposite trend
2nd day	↓	↓	Identical trend
3rd day	↑	↑	Identical trend
4th day	↓	↑	Opposite trend

<sup>a</sup>↑ represents increased trend and <sup>b</sup>↓ represents decreased trend

Table 3.4 Temperature and relative humidity combinations for static boundary condition

The wide temperature and relative humidity range (Fig. 3.12 (b)) provided the dynamic change of boundary conditions and guaranteed clear hygrothermal feedback within the envelope. With this boundary condition, it is possible to analyze measurement results and link the integrated envelope's hygrothermal behavior to the obvious changes in temperature-humidity coupling.

Table 3.5 summarizes the mean values of interior temperature and relative humidity and their standard deviation (SD) of each configuration and of the overall experimental period. The SDs of temperature and relative humidity for each configuration are small with the values less than 0.8 °C and 4.0%, respectively. From an overall perspective, the SDs of temperature and relative humidity are also small with the values of 1.5 °C and 3.7%, respectively, indicating a relatively stable hygrothermal environment in the laboratory environment.

Configurations	Temperature [°C]	Relative humidity [%]
Without PCM	24.4 ± 0.4	42.4 ± 1.7
X = 0 L	26.0 ± 0.4	38.3 ± 3.8
X = 0.5 L	27.1 ± 0.8	38.4 ± 3.2
X = 1 L	26.3 ± 0.8	41.1 ± 3.9
Overall	25.9 ± 1.5	40.1 ± 3.7

Table 3.5 Temperature and relative humidity in the interior (laboratory environment) for static boundary condition

### 3.2.6.2 Dynamic boundary condition

Fig. 3.13 (a) shows the dynamic boundary condition. Due to the large phase change range of the PCM as shown in Fig. 3.2, a large diurnal temperature range of 15 to 40 °C (e.g., summer climate of Ruoqiang, China) was chosen to better observe the temperature and relative humidity fluctuations at different locations within the HC. The overall temperature range contains five smaller temperature

ranges to cover various weather conditions: cool (15–20 °C ), temperate (20–25 °C ), warm (25–30 °C ), hot (30–35 °C ), and very hot (35–40 °C ) [224]. On the one hand, the large temperature range helps to observe the feedback of the envelope to cold temperature, very hot temperature, and the temperatures between them. On the other hand, if the integrated envelope is shown to be applicable over a large temperature range, it is also applicable over a small temperature range. The relative humidity was set to a range of 25% to 95%, which represented the variation centered on a comfortable level (60%) and fluctuating between extremely dry (25%) and humid (95%) conditions. The combination of temperature and relative humidity represented dynamic boundary conditions in the exterior environment with a wide temperature/relative humidity range but little vapor pressure fluctuations (Fig. 3.13 (b)). In the beginning, the temperature and relative humidity were held at 27.5 °C and 60% for two days until stabilization. Then the temperature and relative humidity evolved periodically for seven days according to the sinusoidal function with time (day) as the variable:

$$T = 27.5 + 12.5 \times \sin\left(\frac{\pi}{12} t\right) \quad (3.1)$$

$$\varphi = 60\% - 35\% \times \sin\left(\frac{\pi}{12} t\right) \quad (3.2)$$

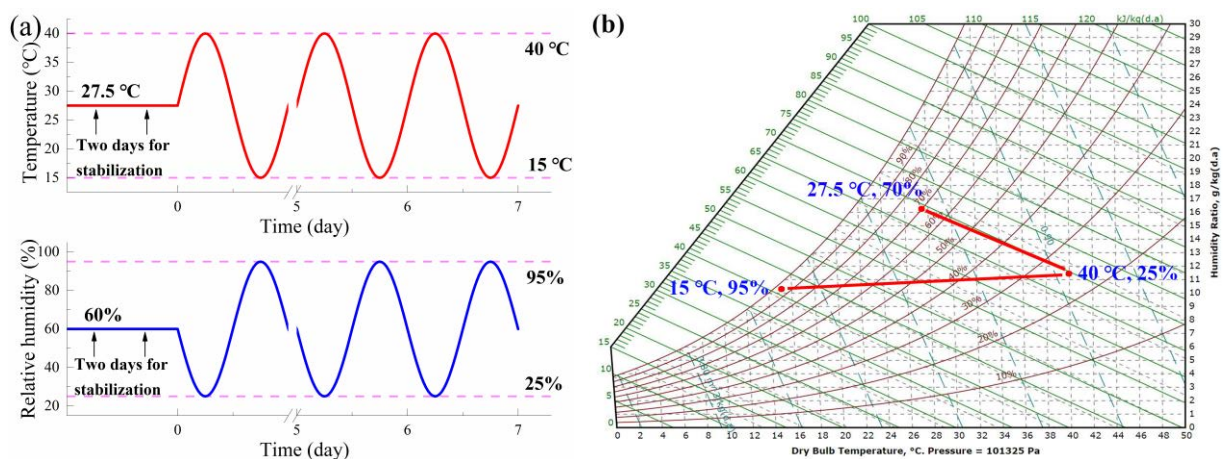


Fig. 3.13 Dynamic boundary condition: (a) temperature and relative humidity condition provided by the climatic chamber; (b) temperature and relative humidity in the psychrometric chart

Table 3.6 shows the mean values of interior temperature and relative humidity and their SD of each configuration. The interior temperature and relative humidity were relatively stable during the whole experimental period with a temperature of  $21.4 \pm 0.7$  °C and relative humidity of  $45.2 \pm 5.1\%$ , indicating a relatively stable hygrothermal environment in the laboratory environment. Thus, one side of the envelope was exposed to a dynamic condition, while the other side faced a relatively stable condition. The condition considered is similar to the real situation, i.e., exterior fluctuations do not show the same increasing/decreasing trend as interior conditions.

Days	Temperature [°C]	Relative humidity [%]
Without PCM	$21.9 \pm 0.4$	$44.6 \pm 4.7$
X = 0 L	$21.0 \pm 0.5$	$49.7 \pm 4.6$
X = 0.5 L	$21.3 \pm 0.6$	$47.5 \pm 4.3$
X = 1 L	$21.1 \pm 0.4$	$38.9 \pm 1.4$
Overall	$21.4 \pm 0.7$	$45.2 \pm 5.7$

Table 3.6 Temperature and relative humidity in the interior (laboratory ambient) for dynamic boundary condition

### 3.3 Temperature and relative humidity stabilization validation

In order to validate that the temperature and relative humidity within the HC and PCM started in a steady state, the temperature and relative humidity (mean value  $\pm$  SD) at the main locations (point H<sub>1</sub>, H<sub>12</sub>, H<sub>2</sub>, and P) within the envelope two hours before the start of the dynamic change were calculated. The results for static and dynamic boundary conditions are shown in Table 3.7 and Table 3.8, respectively.

It can be seen that the SDs of temperature and relative humidity for both boundary conditions are less than 0.08°C and 0.17%, respectively, indicating that the experimental process started with a

hygrothermal stabilization.

Configurations	Point H <sub>1</sub>		Point H <sub>12</sub>		Point H <sub>2</sub>		Point P
	Temperature	Relative	Temperature	Relative	Temperature	Relative	Temperature
	(°C)	humidity	(°C)	humidity	(°C)	humidity	(°C)
		(%)		(%)		(%)	
Without PCM	19.3 ± 0.03	54.5 ± 0.11	20.7 ± 0.04	47.0 ± 0.09	22.2 ± 0.04	43.7 ± 0.06	\
X = 0 L	22.2 ± 0.06	41.1 ± 0.07	23.7 ± 0.04	39.5 ± 0.07	25.0 ± 0.02	38.9 ± 0.07	19.0 ± 0.06
X = 0.5 L	20.7 ± 0.02	65.7 ± 0.04	\	\	26.6 ± 0.02	45.1 ± 0.08	23.7 ± 0.03
X = 1 L	18.9 ± 0.03	48.1 ± 0.15	20.2 ± 0.02	42.0 ± 0.14	21.6 ± 0.03	39.5 ± 0.06	23.0 ± 0.05

Table 3.7. Temperature and relative humidity (mean value ± SD) within the envelope two hours before the start with static boundary condition

Configurations	Point H <sub>1</sub>		Point H <sub>12</sub>		Point H <sub>2</sub>		Point P
	Temperature	Relative	Temperature	Relative	Temperature	Relative	Temperature
	(°C)	humidity	(°C)	humidity	(°C)	humidity	(°C)
		(%)		(%)		(%)	
Without PCM	26.9 ± 0.01	49.1 ± 0.04	26.2 ± 0.02	53.8 ± 0.05	25.1 ± 0.03	40.4 ± 0.05	\
X = 0 L	25.4 ± 0.03	51.7 ± 0.12	24.1 ± 0.05	52.3 ± 0.11	23.1 ± 0.08	47.3 ± 0.09	26.7 ± 0.03
X = 0.5 L	26.3 ± 0.02	58.9 ± 0.03	\	\	23.3 ± 0.02	46.8 ± 0.04	24.6 ± 0.03
X = 1 L	26.5 ± 0.02	54.7 ± 0.10	25.5 ± 0.02	51.0 ± 0.13	24.5 ± 0.02	51.4 ± 0.17	22.9 ± 0.03

Table 3.8. Temperature and relative humidity (mean value ± SD) within the envelope two hours before the start with dynamic boundary condition

### 3.4 Results, analysis, and discussion of static boundary condition

The hygrothermal behavior within the HC of the envelope configuration without PCM (two HC layers) is presented as a reference and compared to the configurations with PCM. The discussion was conducted base on changes in the overall trend, value, amplitude, and hygrothermal behavior differences between different locations of PCM. Finally, the energy behavior is analyzed.

#### 3.4.1 Hygrothermal behavior of configuration without PCM

Fig. 3.14 presents the temperature behavior at different monitoring points. The temperature amplitude applied on the exterior side decreases towards the constant interior condition over successive layers. The temperature amplitude obtained at points  $H_1$ ,  $H_{12}$ , and  $H_2$  varied, with values of 8.3, 6.2, and 4.1 °C respectively.

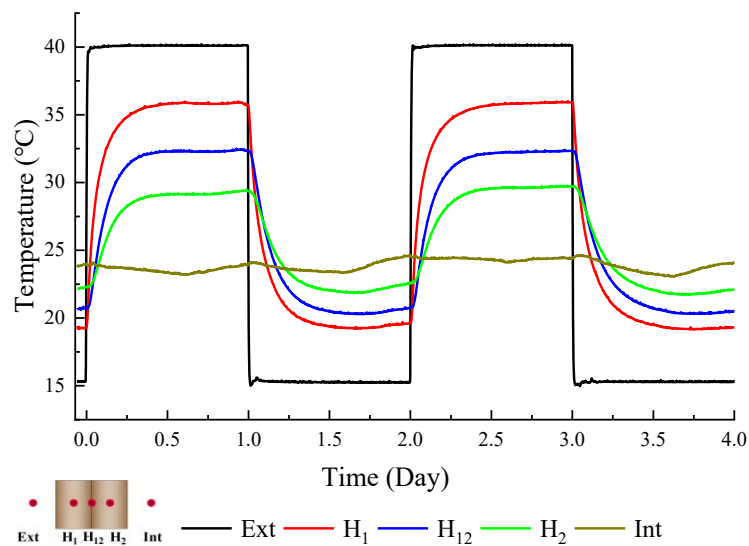


Fig. 3.14 Temperature behavior of configuration without PCM

Fig. 3.15 shows the relative humidity behavior within the HC. As regards relative humidity values, there were noticeable differences between the three points. They changed in descending order

from the exterior to the interior, i.e.,  $H_1$  has the highest relative humidity while  $H_2$  has the lowest. The amplitude was 6.5, 6.5, and 4% at  $H_1$ ,  $H_{12}$ , and  $H_2$ , respectively. In the following discussion we will keep in mind that moisture transfer is continuous from the exterior toward the interior, whereas the heat transfer changes direction depending on heating and cooling period.

According to the boundary condition setup in Section 3.2.6.1, the exterior relative humidity change underwent two successive decreases followed by two successive increases. However, the relative humidity change within the HC was highly consistent with temperature at all times. For example, even though the boundary temperature and relative humidity changed in opposite directions (one increased and the other decreased) on the first and fourth days, the relative humidity trend was still consistent with the temperature. That is, the relative humidity change was dominated by temperature change. The psychrometric chart (Fig. 3.12 (b)) summarizes this phenomenon: a positive relative humidity difference plus a temperature difference may be equivalent to negative partial pressure. It shows that vapor transfer is the consequence of water vapor pressure, and so a consequence of both temperature and relative humidity differences.

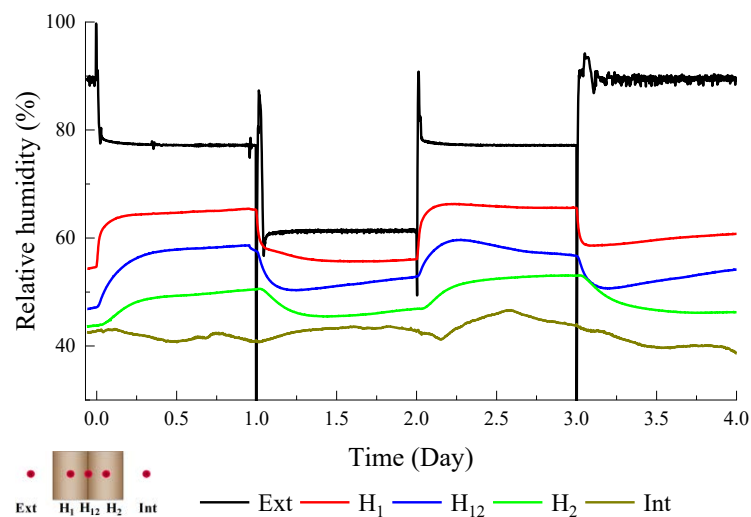


Fig. 3.15 Relative humidity behavior of configuration without PCM

As for the relative humidity on different days and in different locations, it generally obeyed some principles even if there were small differences between them. For example, in most days at  $H_1$  and  $H_{12}$ , relative humidity increased/decreased sharply at the beginning of each step because temperature feedback was faster than relative humidity. Therefore, after the sudden temperature change in the exterior, the temperature at  $H_1$  and  $H_{12}$  also changed sharply. It induced the vapor phase change within HC because the temperature change induce the evaporation/condensation phenomenon, which led to the increased/decreased relative humidity [82, 84, 225]. As for point  $H_2$  away from the exterior, feedback to the temperature in the exterior was relatively weak and less vapor phase change phenomenon occurred. On the other hand, the relative humidity in the exterior also affected the relative humidity within HC, and the effect was stronger if the location was closer to the exterior. For example, at  $H_1$ , the relative humidity on the second and fourth day suffered from the decrease in temperature. However, after the sharp decrease caused by temperature, it kept decreasing on the second day while started to increase on the fourth day. Because the decrease in relative humidity in the exterior on the second day led to evacuation of vapor from the HC and a decrease in relative humidity within the HC. Conversely, the increased relative humidity in the exterior on the fourth day caused moisture diffusion from the exterior to the envelope and increased the relative humidity within the HC. This phenomenon was not observed at  $H_{12}$ , which was farther from the exterior than  $H_1$  and was less affected. Therefore, the coupling effect between temperature and relative humidity within the HC was highlighted according to the relative humidity change at  $H_1$ , and temperature played a dominant role.

To evaluate how quickly temperature and relative humidity change, the characteristic time ( $\tau$ ) was referred to in our study. Characteristic times have been widely used in many fields, including electrical pollutants [226], thermal physics [227], and neuroscience [228], etc. General time ( $t$ ) evolution versus characteristic time is expressed as [229]:

$$C_{stu}(t) = C_{s,0} + \Delta C \cdot \exp(-t/\tau) \quad (3.3)$$

where

$C_{stu}$  = parameter under study;

$C_{s,0}$  = initial value of parameter under study;

$\Delta C$  = applied difference.

In this study, characteristic time changes from one stable state to the other can quantify the dynamic thermal/hygric response under the sudden change in boundary conditions and characterize the material's thermal/hygric inertia. Therefore, the curve fitting of temperature and relative humidity was first conducted according to the formula above, and then the characteristic time was obtained from the fitting result. To simplify the analysis, only the temperature and relative humidity curves at H<sub>1</sub>, H<sub>12</sub>, and H<sub>2</sub> on the first day were taken into consideration.

By calculation, temperature characteristic times were  $7.7 \times 10^3$ ,  $8.5 \times 10^3$ , and  $9.9 \times 10^3$  s at locations H<sub>1</sub>, H<sub>12</sub>, and H<sub>2</sub> respectively. The change in value was expected, as was the linear change from the exterior to the interior based on the consecutive thermal resistances of the envelope as it changed the initial value and applied difference. As with relative humidity, characteristic times at H<sub>1</sub>, H<sub>12</sub>, and H<sub>2</sub> were  $1.0 \times 10^4$ ,  $1.2 \times 10^4$ , and  $1.6 \times 10^4$  s respectively, all higher than the corresponding temperature points. This phenomenon indicated quantitatively that the relative humidity within the HC requires more time to stabilize than temperature, along with a smoother curve, which was due to the dominant effect of temperature and the HC's low moisture diffusion.

### **3.4.2 Hygrothermal behavior of configurations with PCM**

#### **3.4.2.1 PCM placed on the exterior side (X = 0 L)**

The temperature behavior of configuration with PCM placed on the exterior (climatic chamber) side (configuration X = 0 L) is shown in Fig. 3.16. It was noted that the PCM was moisture

impermeable and there was only heat transfer on the exterior side. While for the interior side, heat and moisture transfer can occur simultaneously.

Unlike the configuration without PCM, the temperature did not reach a stable state at the end of each day. Temperature amplitudes at  $H_1$ ,  $H_{12}$ , and  $H_2$  were 6.5, 4.4, and 2.6 °C respectively, a significant decrease compared to the configuration without PCM. Meanwhile, the temperature difference between the three points was significantly reduced. These phenomena were caused by the existence of PCM, as high PCM thermal inertia was available to prevent the temperature from rising/dropping during the heating/cooling period, i.e., it damped the temperature change and fluctuation.

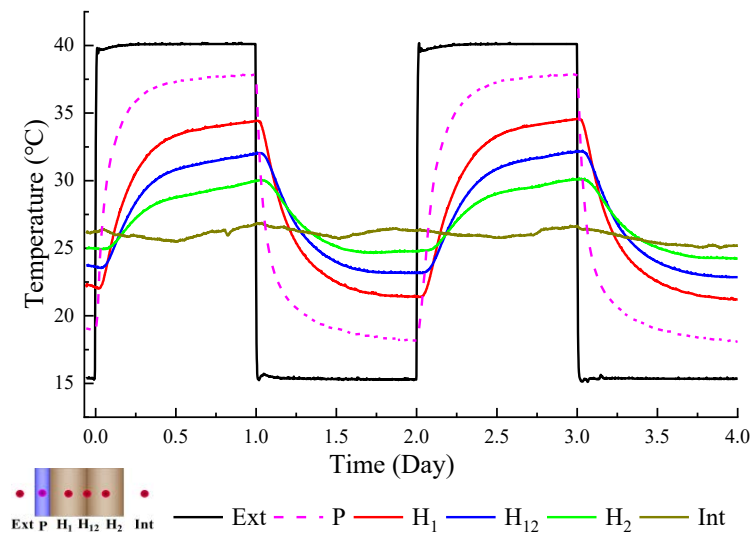


Fig. 3.16. Temperature behavior of the configuration  $X = 0$  L

Fig. 3.17 shows the relative humidity variation of configuration  $X = 0$  L. Focusing on the relative humidity comparison to the configuration without PCM, the overall value (around 40%) of the three locations within HC was lower, and the three curves almost overlapped, leading to the smaller difference between them. The PCM is impermeable and blocks the moisture transfer between the

exterior and the other layers. Such decoupling in moisture will mostly keep the effect of temperature change on the relative humidity. Relative humidity amplitude was then reduced by 50% due to the influence of PCM. Specifically, the PCM thermal inertia weakened the temperature change and affected the characteristic time. The temperature characteristic times at  $H_1$ ,  $H_{12}$ , and  $H_2$  were  $1.5 \times 10^4$ ,  $2.0 \times 10^4$ , and  $2.6 \times 10^4$  s respectively, which was higher than the configuration without PCM. As discussed previously, the characteristic time of relative humidity was higher than for temperature. So, the characteristic time of relative humidity ( $1.6 \times 10^4$ ,  $2.5 \times 10^4$ ,  $4.3 \times 10^4$  s for  $H_1$ ,  $H_{12}$ , and  $H_2$ ) was high enough to evolve the relative humidity smoothly. Looking at the three points' initial relative humidity, they were also similar due to the PCM's blocking effect. On the other hand, the moisture transfer between interior and HC was very slow and small, making the initial relative humidity within the HC almost the same as the interior. As a result, the relative humidity evolved almost based on the initial value and then fluctuated smoothly with small amplitude.

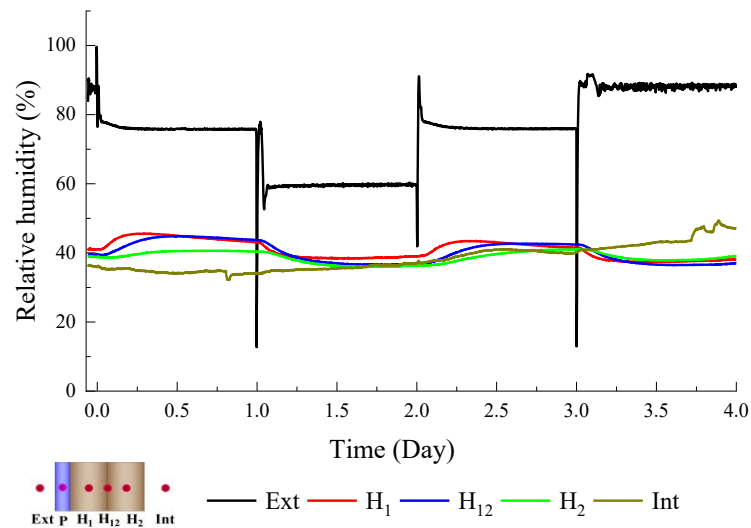


Fig. 3.17. Relative humidity behavior of the configuration  $X = 0$  L

It is worth noting that the overall trend of relative humidity was slightly downward, mainly due to the moisture release. On the one hand, the PCM hampered moisture gain from exterior to HC. On

the other hand, only a small amount of moisture was released from HC to the interior because it was an intercoupling and separated from the exterior change by the impermeable PCM. Therefore, the PCM placed on the exterior side damped the temperature and humidity changes, ensuring the effect of thermal and hygric inertia on the interior environment.

#### **3.4.2.2 PCM placed on the interior side (X = 1 L)**

Fig. 3.18 shows the temperature behavior when the PCM was placed on the interior side (configuration X = 1 L). As with configuration X = 0 L, the temperature evolution did not reach a steady state at the end of each day, and the difference between the three locations was significantly reduced. Compared with the configuration without PCM, the amplitudes were significantly increased with values of 9.2, 7.5, and 5.4 °C at H<sub>1</sub>, H<sub>12</sub>, and H<sub>2</sub> respectively. These phenomena were related to the PCM, which damped the heat loss/gain between HC and interior. Meanwhile, the continuous heat transfer between HC and the exterior also increased the temperature amplitude. Therefore, the PCM's barrier effect on heat and humidity fluxes weakened the difference between three points, which can be proven by the higher characteristic time ( $1.0 \times 10^4$ ,  $1.0 \times 10^4$ , and  $1.7 \times 10^4$  s at H<sub>1</sub>, H<sub>12</sub>, and H<sub>2</sub>, respectively) compared to the configuration without PCM.

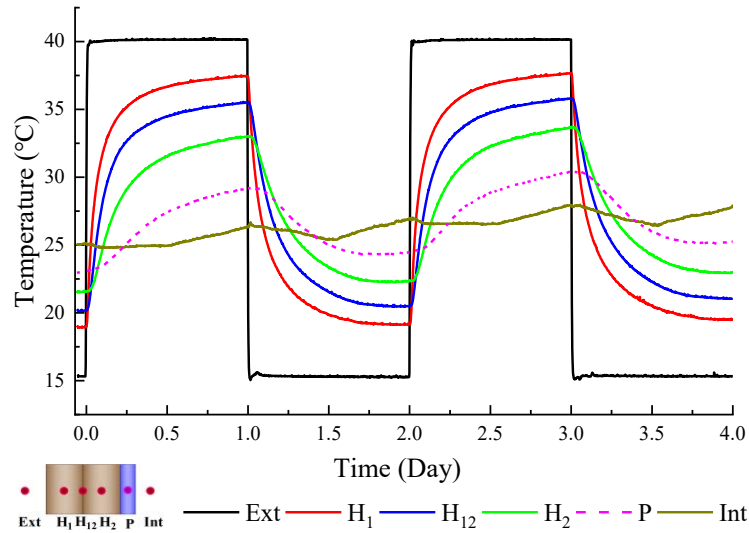


Fig. 3.18. Temperature behavior of configuration X = 1 L

For relative humidity (Fig. 3.19), the curve was relatively smooth and accompanied by small fluctuations as with configuration X = 0 L. Nevertheless, the coupling (the change) was more pronounced as the HC was coupled with the exterior and decoupled from the interior due to the impermeable behavior of PCM on moisture. Compared with the configuration without PCM, the characteristic time for relative humidity was higher ( $2.6 \times 10^4$ ,  $2.2 \times 10^4$ , and  $7.8 \times 10^4$  s at H<sub>1</sub>, H<sub>12</sub>, and H<sub>2</sub>, respectively), so lesser differences between each location and smaller amplitude of the curves were observed. It should be noted that although the initial relative humidity between the three locations was closer than with the configuration without PCM, it was a little more incompact compared to configuration X = 0 L. Moreover, the initial value at H<sub>12</sub> and H<sub>2</sub> was close and slightly lower than H<sub>1</sub>. Since no moisture transferred between HC and interior, the initial value at H<sub>12</sub> and H<sub>2</sub> was mainly affected by the envelope's original relative humidity (around 40%, like X = 0 L) and hardly affected by the exterior over a short time. In contrast, the initial value at H<sub>1</sub> was mainly affected by the exterior and consequently higher than the other two points (unidirectional diffusion with impermeable on interior side).

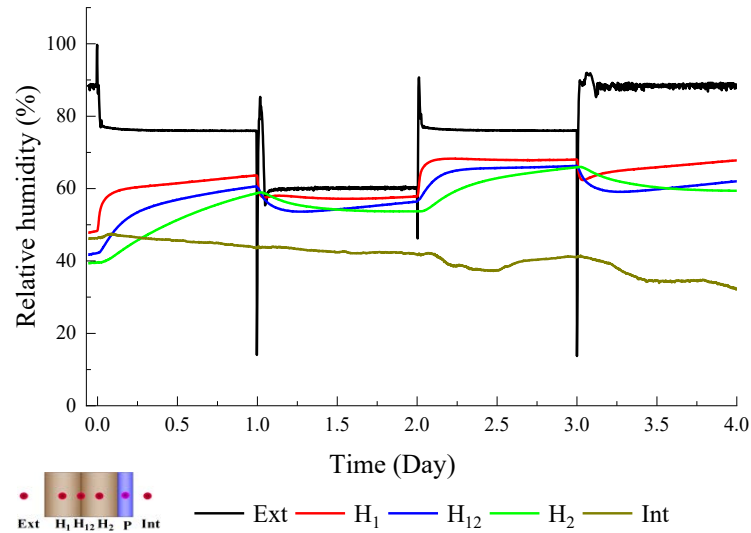


Fig. 3.19. Relative humidity behavior of configuration  $X = 1$  L

Likewise, due to the PCM's blocking effect, the moisture accumulation phenomenon occurred within HC, which made the relative humidity's overall trend an upward trend in order to reach equilibrium between the oscillation within HC and the average value in the exterior.

### 3.4.2.3 PCM placed between two HC layers ( $X = 0.5$ L)

The previous PCM integration illustrated one-sided (between the interior and the HC or between the exterior and the HC) temperature-humidity coupling. The temperature-humidity coupling between HC and both sides is discussed in this section for configuration  $X = 0.5$  L. The temperature and relative humidity behavior of configuration  $X = 0.5$  L is plotted in Fig. 3.20 and Fig. 3.21, respectively. The main feature of this configuration was that temperature and relative humidity difference between  $H_1$  and  $H_2$  were increased. Taking the end of the first day as an example, the temperature and relative humidity difference between  $H_1$  and  $H_2$  were  $5.9$  °C and 35.3%, higher than the other configurations (temperature difference were 5.8, 4.5, 4.4 °C and relative humidity difference were 14.8, 5, 2.7% for the configuration without PCM,  $X = 1$  L, and  $X = 0$  L respectively). On the one hand, PCM at  $X = 0.5$

L damped heat and moisture transfer from one HC to another. On the other hand, the initial difference and evolution process were also worth noting. The initial temperature and relative humidity differences were large due to the presence of PCM. In addition, temperature and relative humidity evolved smoothly, as was deduced by the characteristic times of temperature and relative humidity ( $1.2$  and  $2.4 \times 10^4$  s for temperature and  $3.6 \times 10^4$  and  $4.9 \times 10^4$  s for relative humidity at  $H_1$  and  $H_2$ ).

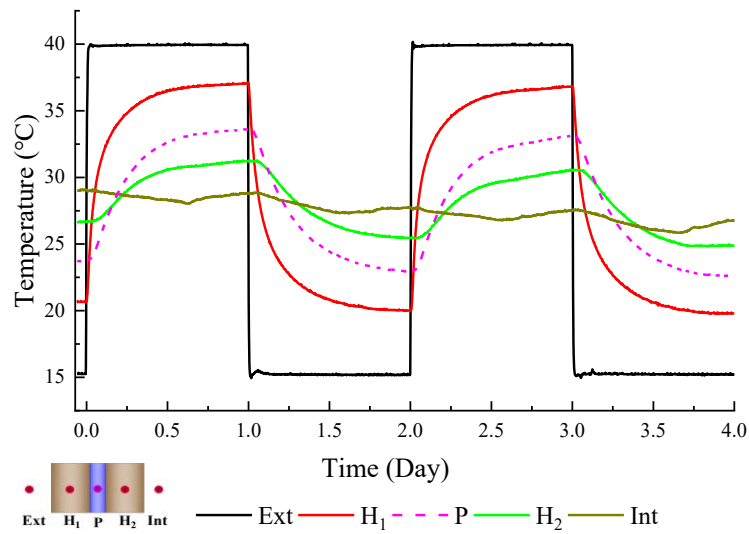


Fig. 3.20. Temperature behavior of configuration X = 0.5 L

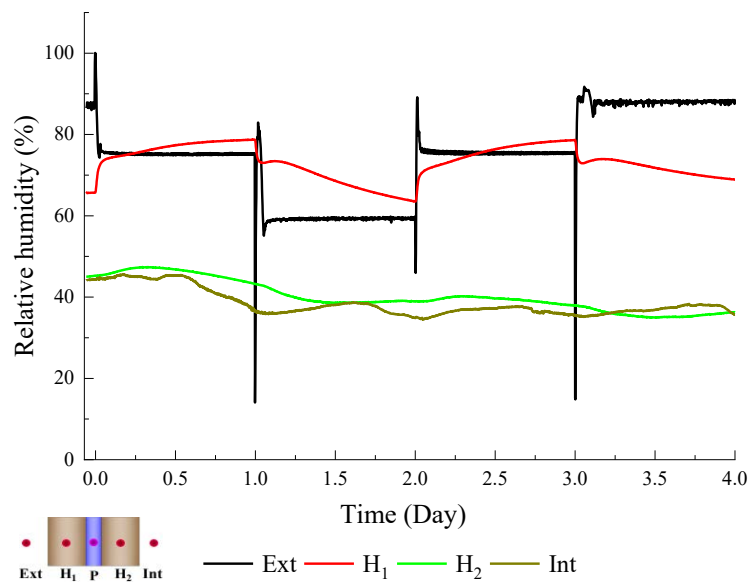


Fig. 3.21. Temperature behavior of configuration X = 0.5 L

The relative humidity's slightly upward and downward trend can also be observed. Evolution at  $H_1$  had a slight upward trend as with  $X = 1$  L while  $H_2$  trended downward like  $X = 0$  L, caused by moisture accumulation and moisture loss at  $H_1$  and  $H_2$  respectively.

### **3.4.3 Heat flux and heat store/release capacity**

The heat flux and heat store/release were analyzed and calculated in this section. Fig. 3.22 (a) shows the heat flux on the interior surface of the envelope for different configurations; it reflects the heat flux from the interior envelope surface to the interior environment after damping by the envelope. The heat flux of the configurations with PCM was lower than the configuration without PCM due to its damping effect. Configurations  $X = 0$  L and  $X = 0.5$  L had a small heat flux fluctuation in the two cycles of heating and cooling period among all the configurations, especially the latter, whose value was almost half of the configuration without PCM. Fig. 3.22 (b) shows the heat flux difference between each side of the envelope for different configurations. Configurations with PCM had a higher heat flux difference than the configuration without PCM. For configurations with PCM, the heat flux difference of  $X = 0$  L was the highest, followed by configurations  $X = 0.5$  L and  $X = 1$  L. The closer the PCM to the exterior, the greater the transient heat flux difference.

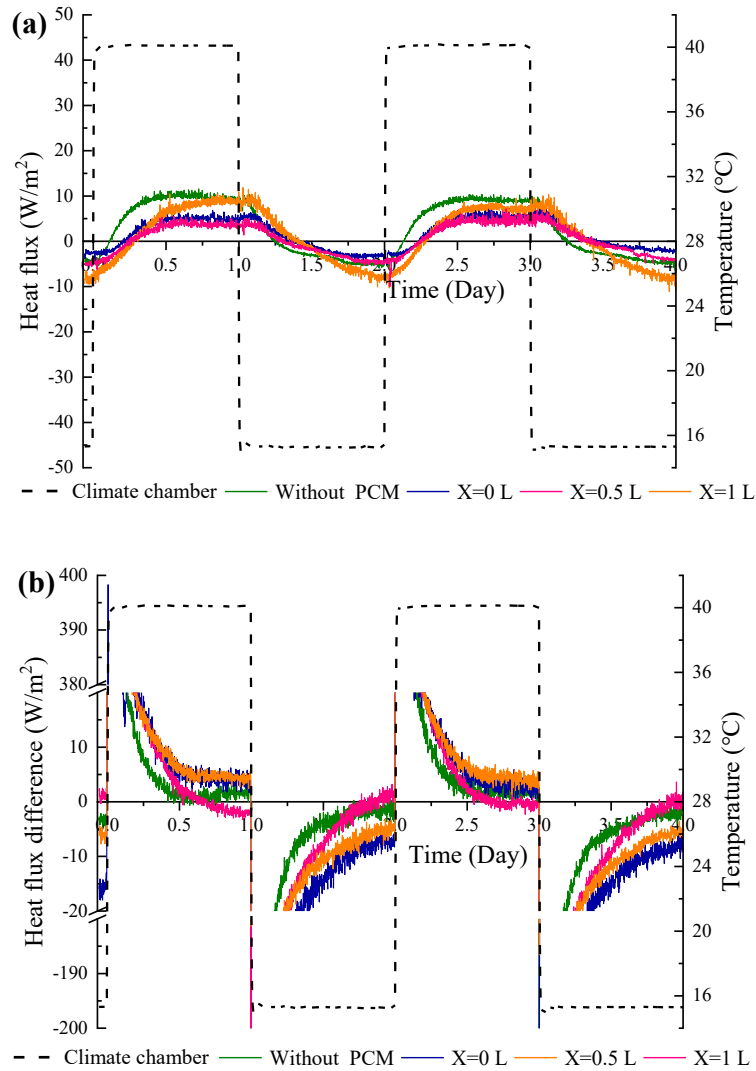


Fig. 3.22. (a) Heat flux on the interior surface of the envelope; (b) heat flux difference between each side of the envelope and the imposed temperature (right)

Since the area between heat flux curves and x-axis (time) was the heat store/release, the integral calculation of stored and released energy was implemented in accordance with the following formula,

$$Q_h = \int_{t_1}^{t_2} q A dt \quad (3.4)$$

where

$Q_h$  = stored/released heat, (J);

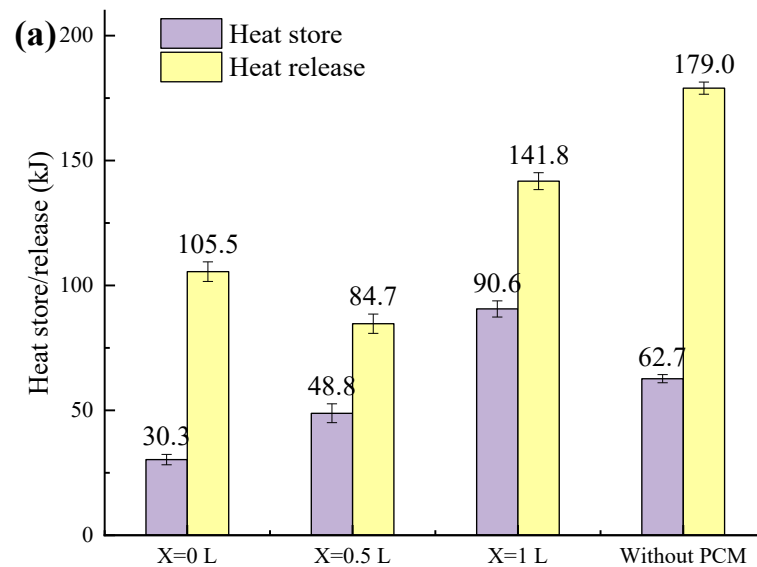
$t_1, t_2$  = start and end time of calculation, (s);

$q$  = heat flux, ( $W/m^2$ );

$A$  = area of the envelope, ( $m^2$ );

$t$  = time, ( $s$ ).

Heat store and release at the interior side for different configurations is presented in Fig. 3.23 (a); it reflects the heat gain and loss between the interior environment and the envelope, which is directly proportional to the building's cooling and heating load. The lowest stored heat was generated by configuration  $X = 0$  L with the value of 30.3 kJ; the lowest released heat value was produced by configuration  $X = 0.5$  L with the value of 84.7 kJ. That is, configurations  $X = 0$  L and  $X = 0.5$  L result in the lowest heat and cooling loads, respectively, which undoubtedly saves energy consumption in a real building.



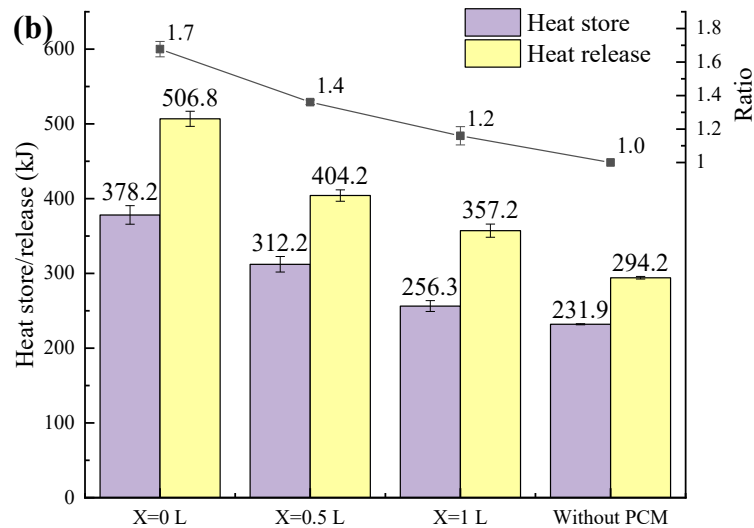


Fig. 3.23. (a) Heat store/release by interior surface; (b) heat store/release by the envelope and ratio value (right)

Fig. 3.23 (b) presents the heat store/release capacity of the whole envelope for different configurations. The capacity of configurations with PCM was stronger than the one without PCM. Configuration  $X = 0$  L showed excellent thermal control capacity. It had the highest heat store/ release capacity, with a value nearly 1.7 times greater than the configuration without PCM. In contrast, the heat store/release capacity of configuration  $X = 1$  L was the lowest, but still 1.2 times higher than the configuration without PCM. Therefore, the configuration with less distance between PCM and exterior had a higher heat store/release capacity. Moreover, the ordering relationship of heat store/release capacity showed some regularity, which could be deduced from the ratio value (the sum of heat store and release of each configuration divided by the configuration without PCM) on the right axis. The ratio maintained almost linear decreasing from configuration  $X = 0$  L to configuration without PCM, indicating the linear relation between PCM's location and heat store/release capacity. From the analysis above, regardless of the heat store/release from the interior side or the heat store/release capacity of the envelope itself, configurations  $X = 0$  L and  $X = 0.5$  L both need to be emphasized. In addition, another phenomenon worth mentioning is that the thermal energy released during the cooling period was more than that stored during the heating period.

Fig. 3.24 (a) shows the temperature distribution on both sides of PCM, and the 22 °C of y-axis corresponds to the starting point of the x-axis. Since 22 °C was the temperature at which maximum specific heat capacity was reached, the location closer to the x-axis in the vertical direction had a higher specific heat capacity. Due to the dynamic temperature change, the equivalent specific heat capacity also changes instantaneously.

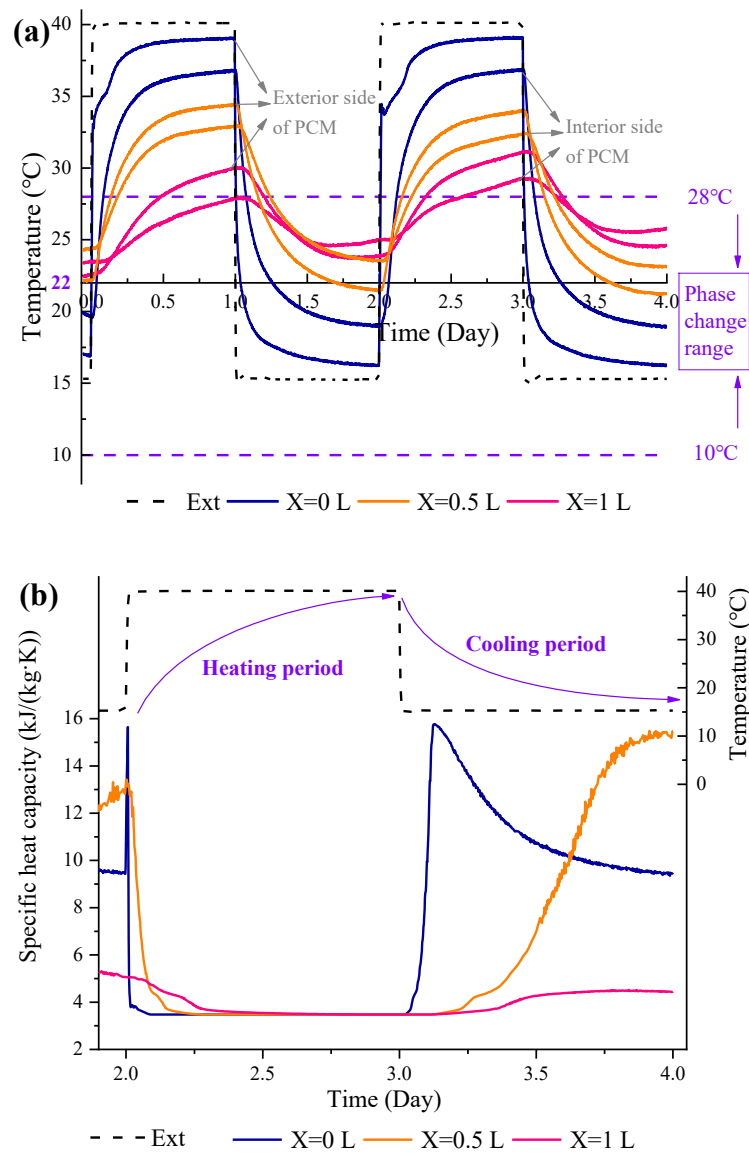


Fig. 3.24. (a) Temperature in both side of PCM; (b) dynamic specific heat capacity of PCM

In order to better observe the dynamic characteristics, the transient specific heat capacity based on the middle temperature of PCM is reflected in Fig. 3.24 (b), and is related to the phenomena observed in Fig. 3.23. At the beginning of the heating period, the temperature gradient and specific heat capacity of configuration  $X = 0$  L were the highest, contributing to major heat storage even though it was low in the middle period. In the last period, the specific heat capacity and temperature gradients were almost the same. This characteristic was more evident during the cooling period because most of the temperature was in the phase transition range and had a higher specific heat capacity than the heating period. For configuration  $X = 0$  L in particular, the specific heat capacity was much higher than for configurations  $X = 0.5$  L and  $X = 1$  L most of the time. This explains the heat store/release difference between different configurations and the higher released heat than stored heat.

### **3.5 Results, analysis, and discussion of dynamic boundary condition**

Since the dynamic boundary conditions are more like the actual climate environment, more detailed results and analysis are performed compared to the static boundary conditions. First, the hygrothermal behavior of configuration without PCM is studied. Then, three envelope configurations combining a PCM and HC are compared with the configuration without PCM. Special attention is paid to the temperature/relative humidity amplitude and time delay, especially in the case where the location within the envelope is close to the interior. Next, the energy performance of the whole envelope and of the PCM layer is studied. Finally, the activation and energy storage/release efficiency of the PCM in different locations are analyzed.

#### **3.5.1 Hygrothermal behavior of the configuration without PCM**

Fig. 3.25 represents the temperature behavior of the configuration without PCM. The

temperature amplitudes at points H<sub>1</sub>, H<sub>12</sub>, and H<sub>2</sub> decreased sequentially, with values of 6.1, 4.2, and 2.4 °C, respectively. There was a response time delay between the exterior environment and the envelope, with average time delays of 2.1, 3.0, and 3.7 h at points H<sub>1</sub>, H<sub>12</sub>, and H<sub>2</sub>, respectively.

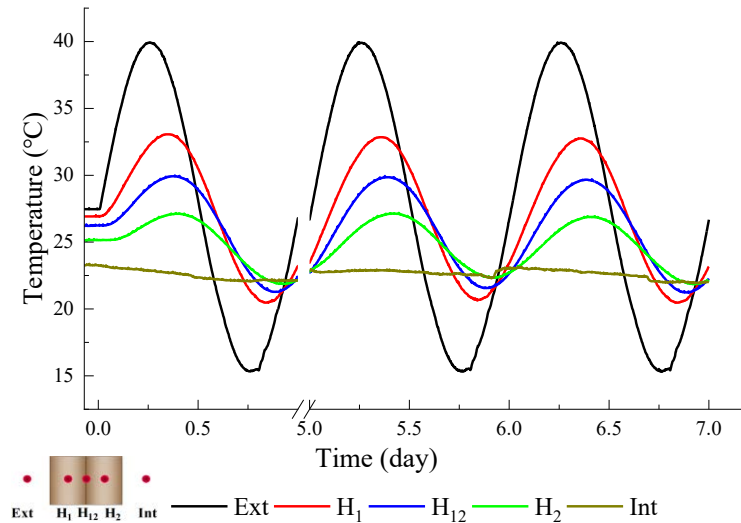


Fig. 3.25. Temperature behavior of the configuration without PCM

Fig. 3.26 plots the relative humidity behavior. Compared to the temperature, the relative humidity variation was more complex, which can be inferred from the relative humidity at H<sub>1</sub> and H<sub>12</sub>. Both the overall value (45.5–52.7%) and the amplitude (3.6%) of relative humidity at H<sub>1</sub> were lower than those at H<sub>12</sub> (48–58.1% and 5.1%). These phenomena were caused by the superposition effect within the HC.

Specifically, the increase of exterior temperature led to the instantaneous moisture evaporation and the increase of the relative humidity within the HC. Conversely, the decrease in exterior temperature led to moisture condensation and a decrease in the relative humidity within the HC. On the other hand, the increase in exterior relative humidity led to moisture diffusion from the outdoors to the envelope, and therefore increased the relative humidity within the HC. Conversely, the decrease

in exterior relative humidity caused the evacuation of the vapor out of the HC and decreased the relative humidity within the HC. Thus, the dynamically opposite variations of boundary temperature and relative humidity had opposite transient effects on the relative humidity variation within the HC.

As for different points, the effect of exterior relative humidity was strong at points close to the outdoors ( $H_1$ ) but weak at points far away from the outdoors ( $H_{12}$  and  $H_2$ ), which can be inferred from two aspects. First, the overall values and amplitudes of relative humidity at  $H_1$  were smaller than that of  $H_{12}$ . Because the decreased/increased exterior relative humidity inhibited the increase/decrease of relative humidity within the HC caused by the increased/decreased exterior temperature. Second, the time difference between peak/valley relative humidity and temperature was longer at point  $H_1$  than that of point  $H_{12}$  and  $H_2$ , and the longer time difference implied stronger competition between the effects of exterior relative humidity and temperature. At point  $H_1$ , the peak relative humidity appeared 6.3 h earlier than the peak temperature. In contrast, at points  $H_{12}$  and  $H_2$ , the corresponding values were 1.9 and 0.03 h, respectively. Therefore, relative humidity variations at point  $H_1$  were affected by the superposition effect of temperature and relative humidity, while at point  $H_{12}$  and especially  $H_2$ , relative humidity variations were mainly affected by temperature.

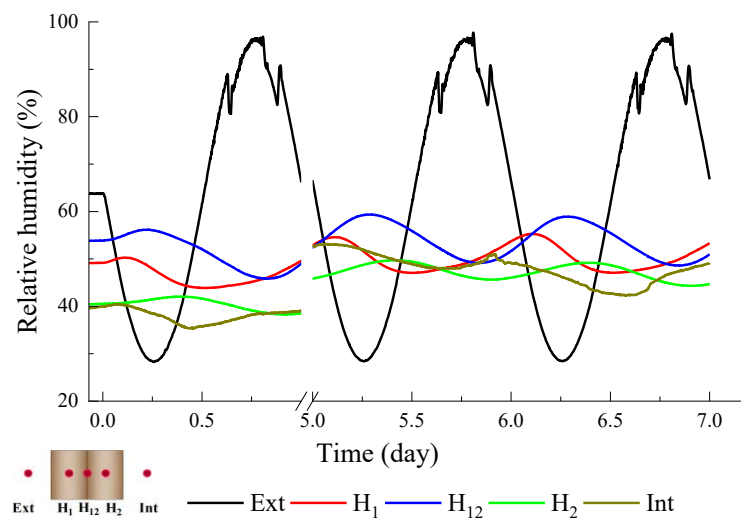


Fig. 3.26. Relative humidity behavior of the configuration without PCM

In this research, the points close to the indoor side ( $H_{12}$  and especially  $H_2$ ) are the main interest to us, because their temperature and relative humidity behavior influences indoor hygrothermal comfort. Therefore, the temperature and relative humidity behavior of  $H_{12}$  and  $H_2$  will be the focus of the following sections.

### 3.5.2 Hygrothermal behavior of the configurations with PCM

#### 3.5.2.1 PCM placed on the exterior side ( $X = 0$ L)

Fig. 3.27 shows the temperature behavior of the configuration  $X = 0$  L. The temperature amplitude was smaller and the time delay was longer than in the configuration without PCM. At  $H_1$ ,  $H_{12}$ , and  $H_2$ , the temperature amplitudes were reduced by 1.6, 1.2, and 0.4 °C, and the time delays were extended by 2.4, 2.4, and 2.1 h, respectively, because PCM damped the heat transfer between the HC and the exterior side.

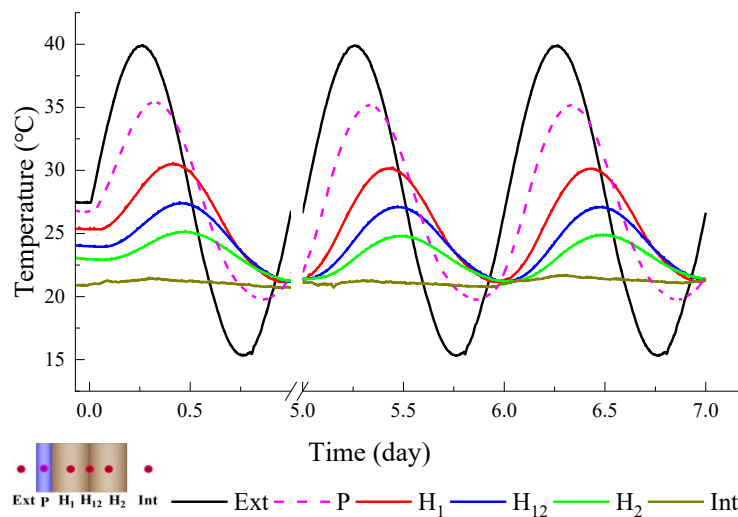


Fig. 3.27. Temperature behavior of the configuration  $X = 0$  L

For the relative humidity behavior shown in Fig. 3.28, the amplitudes at  $H_{12}$  and  $H_2$  were 2.9% and 1.9%, which was 2.2% and 0.1% less than in the configuration without PCM. As mentioned above, the relative humidity at  $H_{12}$  and  $H_2$  was mainly influenced by temperature variation, so their relative humidity amplitudes decreased with the reduction of the temperature amplitude.

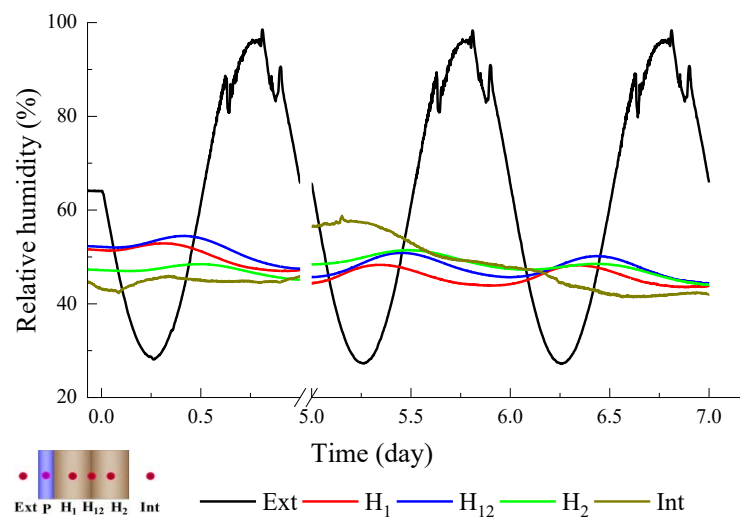


Fig. 3.28. Relative humidity behavior of the configuration  $X = 0$  L

### 3.5.2.2 PCM placed on the interior side ( $X = 1$ L)

The temperature behavior of configuration  $X = 1$  L is shown in Fig. 3.29. The temperature amplitudes at  $H_1$  and  $H_{12}$  were slightly smaller (0.1–0.2 °C) than in the configuration without PCM. Since there was little heat transfer between the interior environment and the PCM, the PCM thermal inertia had little effect on the temperature distribution at  $H_1$  and  $H_{12}$ . Inversely, the amplitude at  $H_2$  was 0.1 °C higher than in the configuration without PCM, which was caused by the thermal accumulation at  $H_2$ . Although there was little change in temperature amplitude compared to the

configuration without PCM, time delays were still extended by 0.3, 0.7, and 1.2 h at points H<sub>1</sub>, H<sub>12</sub>, and H<sub>2</sub>.

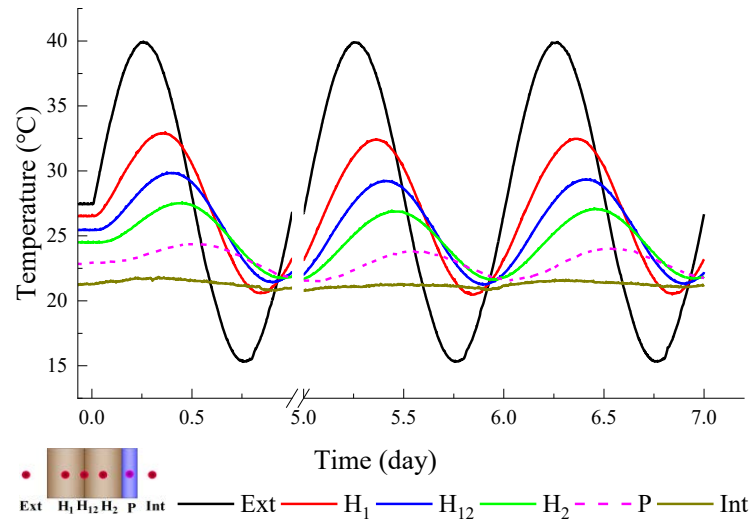


Fig. 3.29. Temperature behavior of the configuration X = 1 L

Fig. 3.30 shows the relative humidity behavior. Compared with configuration without PCM, the relative humidity amplitude was lower at H<sub>12</sub> (3.7%), and slightly higher at H<sub>2</sub> (2.1%) because the PCM's impermeability caused moisture to accumulate around H<sub>2</sub>. Therefore, the configuration X = 1 L should be avoided in practice because the moisture transfer between the envelope and the interior environment was completely blocked by the PCM.

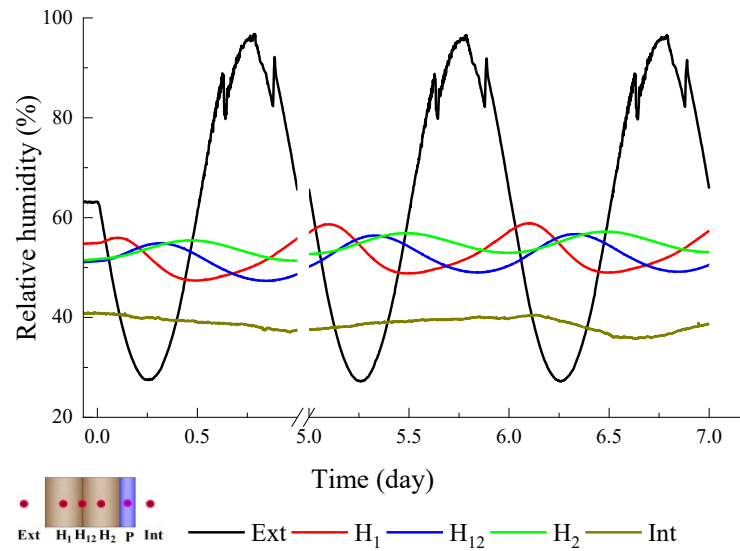


Fig. 3.30. Relative humidity behavior of the configuration  $X = 1$  L

### 3.5.2.3 PCM placed between two HC layers ( $X = 0.5$ L)

In Fig. 3.31, the temperature amplitudes of configuration  $X = 0.5$  L at  $H_1$  and  $H_2$  were 5.7 and 2.1 °C, respectively, both smaller than in the configuration without PCM. However, the amplitude at  $H_1$  was reduced by only 6.5%, while at  $H_2$  it was as high as 50%, because the PCM's thermal inertia had a greater effect on  $H_2$ . Likewise, the time delay at  $H_2$  was more noticeable, which is extended by 2.3 h compared to the configuration without PCM.

Due to the effect of temperature amplitude, the relative humidity at  $H_2$  was significantly reduced, from 2.0 to 0.8% compared to the configuration without PCM (Fig. 3.32).

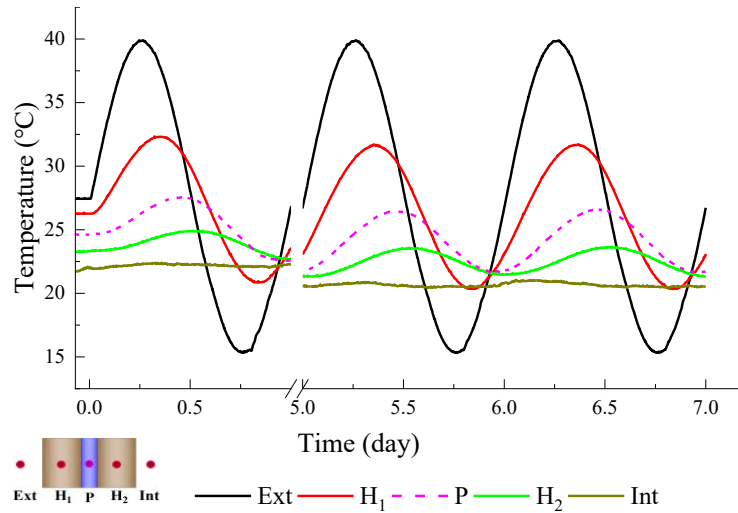


Fig. 3.31. Temperature behavior of the configuration X = 0.5 L

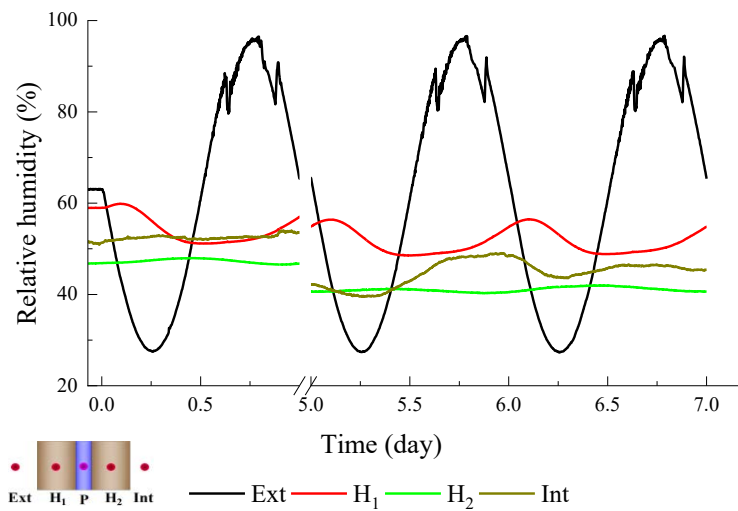


Fig. 3.32. Relative humidity behavior of the configuration X = 0.5 L

### 3.5.3 Summary of temperature/relative humidity amplitudes and time delay

Fig. 3.33 shows the mean daily temperature and relative humidity amplitudes at  $H_1$ ,  $H_{12}$ , and  $H_2$  in the different configurations. Due to the complex superposition effect at  $H_1$ , the magnitude order of relative humidity and temperature amplitude at different configurations was not consistent. However, for points  $H_{12}$  and  $H_2$ , higher temperature amplitudes meant higher relative humidity amplitudes.

To reduce interior temperature/relative humidity fluctuations, the temperature/relative humidity

amplitudes should ideally be low in the layer closest to the interior environment. Therefore, configuration  $X = 0.5 L$  was optimal, with the smallest temperature and relative humidity amplitudes (1.2 °C and 0.8%, respectively) at  $H_2$ , which were 50% and 60% less than in the configuration without PCM (2.4 °C and 2.0%). Furthermore, compared with the exterior temperature and relative humidity amplitudes, the reduction was as high as 90.4% and 97.7%, respectively, ensuring interior hygrothermal comfort under a wide range of exterior temperature/relative humidity fluctuations.

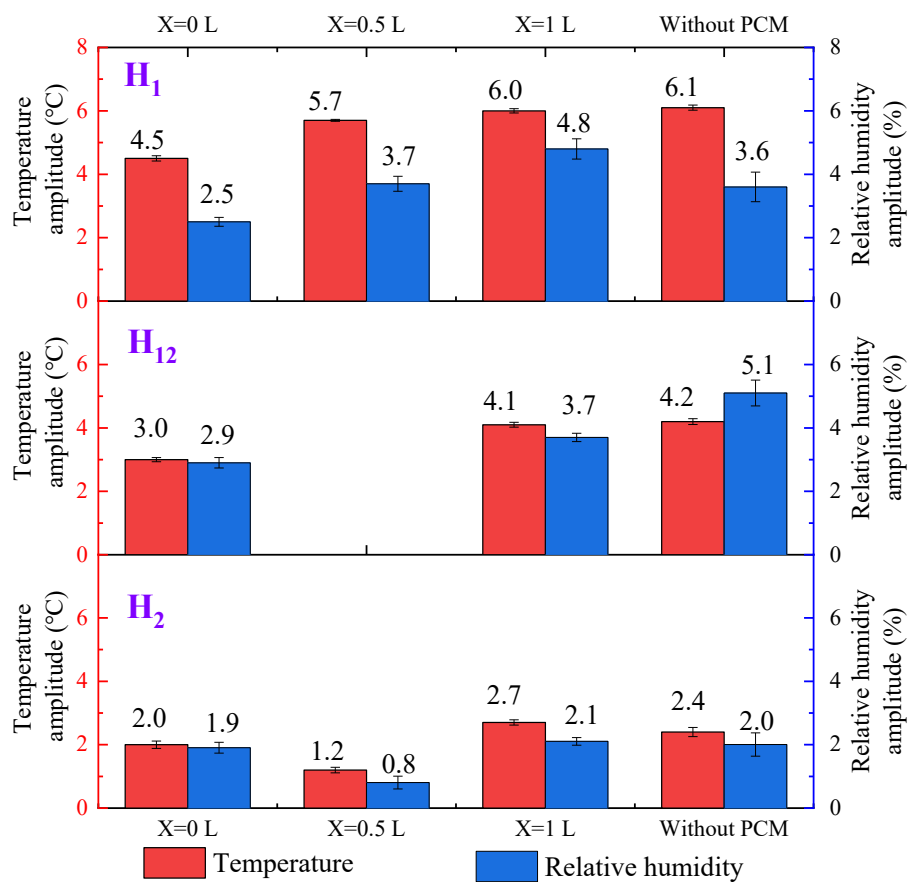


Fig. 3.33. Temperature and relative humidity amplitudes of HC in different configurations

Fig. 3.34 presents the relationship between the temperature amplitude and time delay. The time delay decreased almost linearly as the temperature amplitude increased from the exterior side to the interior side, reflecting the decay in temperature fluctuation over time. Both parameters were affected

by the PCM, but the effect was different on the two sides of the PCM. Compared to the configuration without PCM, the temperature amplitude was reduced significantly at points between the PCM and the interior side ( $H_1$ ,  $H_{12}$ , and  $H_2$  of configuration  $X = 0$  L— reduced by 26.2%, 28.6%, and 16.7%;  $H_2$  of configuration  $X = 0.5$  L— reduced by as much as 50%). In contrast, for points between the PCM and the exterior side ( $H_1$  of configuration  $X = 0.5$  L;  $H_1$  and  $H_{12}$  of configuration  $X = 1$  L), the reduction was less than 6.5%. Similarly, the time delays at points between the PCM and the interior side were extended by 56.8% to 114.3% compared to the configuration without PCM. But on the other side, the time delay was extended by less than 35%. Thus, the PCM had a significant effect on the temperature amplitude and time delay at points between the PCM and the interior side, which explains the small temperature/relative humidity amplitude at  $H_2$  for the configuration  $X = 0.5$  L.

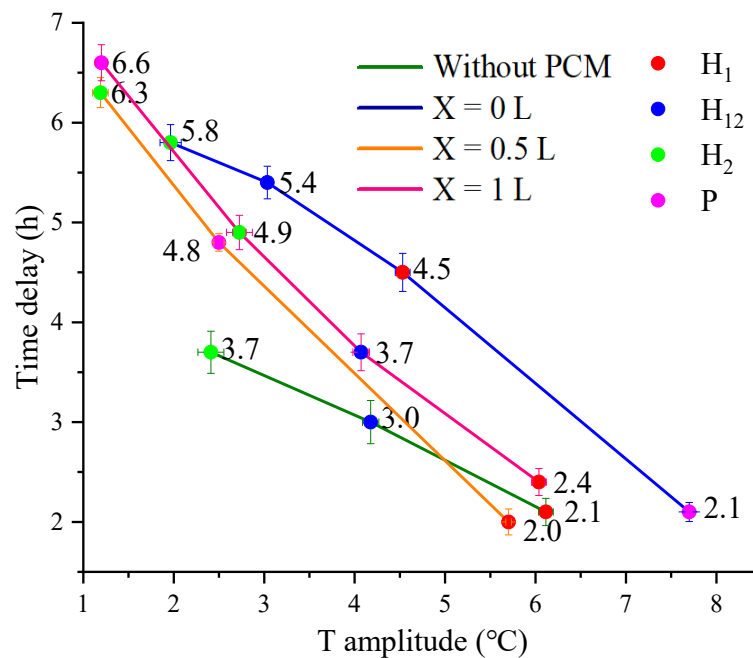


Fig. 3.34. Temperature amplitude and time delay at different configurations and measurement points

It is worth noting that the closest layers to the interior environment for configuration  $X = 1$  L and  $X = 0.5$  L (PCM layer and second HC layer, respectively) had the smallest temperature amplitudes

(1.2 °C for both) and almost the longest time delays (6.6 and 6.3 h, which were 78.4% and 70.3% longer than the configuration without PCM, respectively). In real buildings, these behaviors would have provided thermal comfort and shifted peak energy demand. However, due to the moisture impermeability of the PCM located between the envelope and the interior environment, the configuration  $X = 1$  L should be avoided. Therefore, configuration  $X = 0.5$  L was considerable in terms of temperature/relative humidity amplitude and time delay.

#### **3.5.4 Heat flux and released/absorbed heat on the interior/exterior surface**

Fig. 3.35 (a) shows the heat flux on the interior and exterior surface of the envelope for different configurations. On the interior surface, the configuration without PCM showed negative values for 6 h per day, indicating that the envelope released heat into the interior environment for 18 h of the day. In comparison, the remaining configurations released heat for almost 24 h. For the heat flux amplitudes, the configuration without PCM was high because of its low thermal inertia. With the presence of PCM, the thermal inertia of the envelope was significantly improved, and the heat flux fluctuation was reduced. Configuration  $X = 0.5$  L had the smallest amplitude at  $4.4 \text{ W/m}^2$ , which was 53.7%, 36.2%, and 36.2% less than configuration without PCM,  $X = 0$  L, and  $X = 1$  L.

As for the exterior surface, the heat flux fluctuation of configuration  $X = 0$  L was the highest, indicating a great capacity to absorb/release energy when PCM is in direct contact with the exterior thermal environment. In contrast, the remaining three configurations are clearly different from the configuration  $X = 0$  L. Configurations  $X = 0.5$  L and  $X = 1$  L had similar fluctuations and were slightly higher than the configuration without PCM.

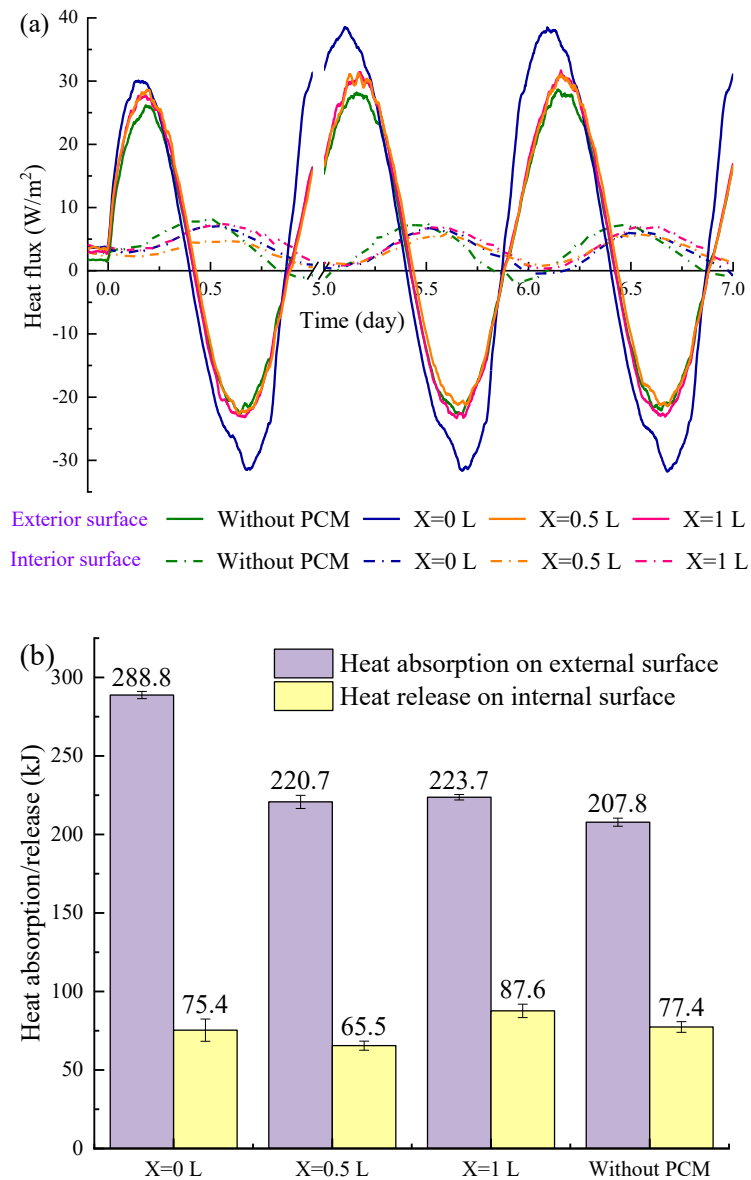


Fig. 3.35. (a) Heat flux on the exterior and interior surface; (b) heat absorption/release on the exterior/interior surface

Fig. 3.35 (b) summarizes the daily released heat on the interior surface and the absorbed heat on the exterior surface for different configurations. The heat released on the interior surface represents a part of the building cooling load and affects the building's energy consumption. The released heat of the configuration without PCM was 77.4 kJ, which was higher than that of the configurations  $X = 0$  L and  $X = 0.5$  L. That is to say, the configuration without PCM released more heat in 18 h than the

configurations  $X = 0$  L and  $X = 0.5$  L did in 24 h, which indirectly demonstrated the energy-saving potential of the PCM. For the configurations with PCM, their released heat changed in a non-linear manner as the PCM's location changed from the exterior to the interior side. Configuration  $X = 0.5$  L released the least heat at 65.5 kJ, which was 13.1, 25.2, and 15.3% less than the configurations  $X = 0$  L,  $X = 1$  L, and without PCM, respectively. Therefore, the placement of the PCM in the middle of the envelope is promising based on its energy-saving potential.

As for the absorbed heat on the exterior surface, the heat of configuration  $X = 0$  L (288.8 kJ) was significantly higher than those of the other configurations. The heat absorption of configurations  $X = 0.5$  L and  $X = 1$  L (220.7 and 223.7 kJ) was almost the same and slightly higher than the configuration without PCM (207.8 kJ). Therefore, the configuration with the PCM directly exposed to the exterior environment adsorbed the most heat due to its higher thermal inertia, while the remaining three configurations with HC facing the exterior environment adsorbed almost identical amounts of heat.

### **3.5.5 Energy storage/release by the whole envelope and the PCM**

The heat flux difference on both sides of the envelope and PCM for different configurations is plotted in Fig. 3.36 (a). The configuration  $X = 0$  L has the highest fluctuations of heat flux difference the envelope and the PCM, indicating a high energy storage/release potential. The daily thermal energy storage/release by the envelope and PCM for different configurations is plotted in Fig. 3.36 (b). For the envelope, the energy storage/release was very similar for the configurations  $X = 0.5$  L,  $X = 1$  L, and without PCM, while the configuration  $X = 0$  L had the highest value. For the PCM, the energy storage/release capacity decreased significantly as the PCM moved away from the exterior side. This trend is consistent with the proportion of energy storage/release by the PCM (on the right axis), which showed a linear downward trend from configuration  $X = 0$  L to  $X = 0.5$  L to  $X = 1$  L. Therefore, when PCM was placed closer to the exterior side, it had a greater role in participating the thermal energy

management in the envelope.

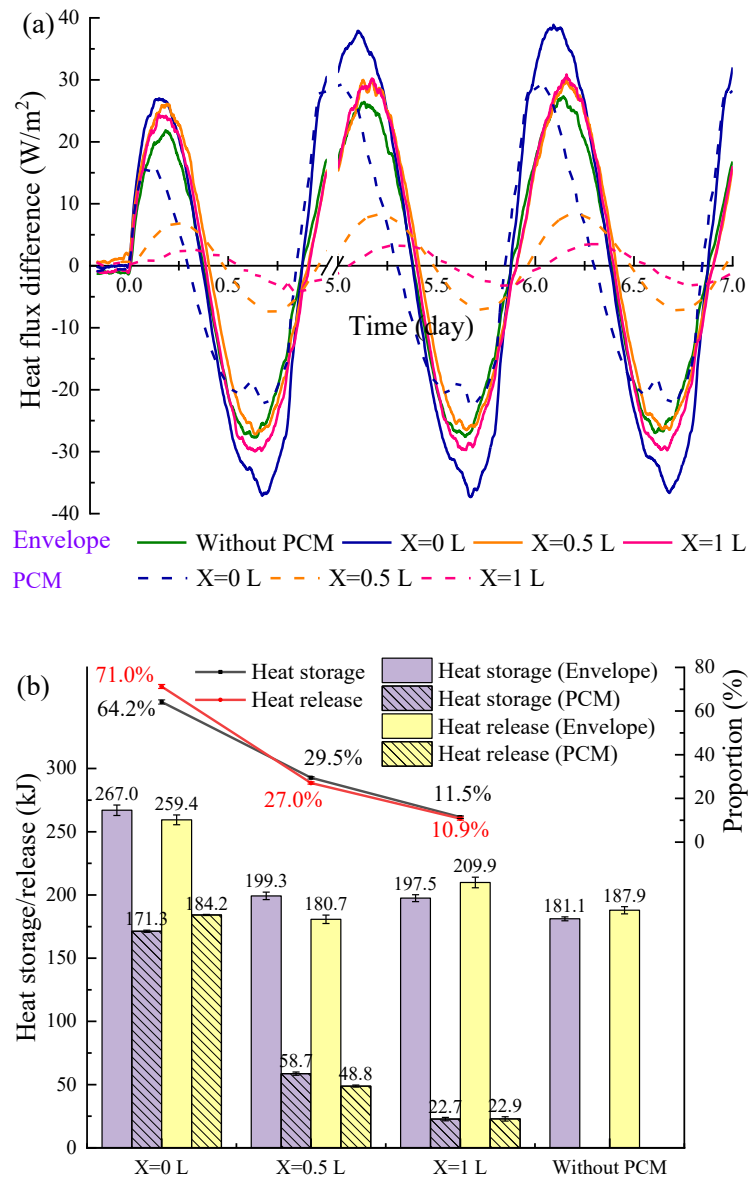


Fig. 3.36. (a) Heat flux difference of the envelope and the PCM; (b) energy storage/release and the proportion of the PCM

As mentioned previously, the absorbed heat on the exterior surface of the configuration  $X = 0$  L was the highest, while the other three configurations were similar to each other (see Fig. 3.35). The

released heat on the exterior surface also followed this pattern (204.8, 140.4, 136.6, and 147.3 kJ for configurations  $X = 0$  L, without PCM,  $X = 0.5$  L, and  $X = 1$  L, respectively). Therefore, when the PCM was placed on the exterior side and interacted with the exterior environment directly, the envelope and PCM tended to store/release more energy, and the energy participation of the PCM in the envelope was high. In contrast, when the PCM was far away from the exterior side, the thermal interaction between the PCM and the exterior environment was damped by one or two HC layers, which reduced the stored/released energy and the PCM's energy participation.

### 3.5.6 PCM activation and storage/release efficiency

This section discussed the performance of PCM utilization, including its phase change activation and energy efficiency. The melt fraction ( $f$ ) represents the percentage of the activated (melted) PCM that has undergone the phase change. The PCM's thermal storage/release efficiency ( $\eta$ ) allows an evaluation of how much latent heat has been utilized. They were expressed as:

$$f = \frac{T - T_{fin}}{T_{fin} - T_{ini}} \quad (3.5)$$

$$\eta = \frac{E_{st}}{L} = \frac{\int_{t_1}^{t_2} \Delta q A dt}{\int_{T_{ini}}^{T_{fin}} m_{pcm} c_{pcm} dT_{pcm}} \quad (3.6)$$

where

$T_{ini}, T_{fin}$  = initial and final temperature of melting, (°C);

$E_{st}$  = actual latent thermal energy stored/released by the PCM, (J/kg);

$L$  = PCM's total latent thermal energy, (J/kg);

$t_1, t_2$  = start and end time of calculation, (s);

$\Delta q$  = heat flux difference between the inflow and outflow of the PCM, (W/m<sup>2</sup>);

$A$  = transversal envelope area, ( $m^2$ );

$m_{pcm}$  = mass of the PCM, (kg);

$T_{pcm}$  = mean temperature of the PCM, ( $^{\circ}C$ );

$C_{pcm}$  = specific heat capacity of the PCM, ( $J/(kg/K)$ ).

The middle temperature of the PCM (point P) is considered the mean temperature of the PCM and is shown on the left axis of Fig. 3.37. On the right axis, the corresponding melt fraction is plotted. Since the phase change temperature ranges from 10 to 28  $^{\circ}C$ , the mean temperature of the configurations  $X = 0.5$  and  $X = 1$  L both lie within the phase transition range. Their corresponding melt fractions were below 100% (80.1–97.7% and 64.8–69.2%, respectively), indicating that the PCM was partially melted and the configurations  $X = 0.5$  L was more activated. Under the circumstances, phase change continued throughout the experiment period and energy was stored/released only in the latent heat mode. For the configuration  $X = 0$  L, the PCM's melt fraction was equal to 100% for almost half the day (11.5 h), implying that it remained in the liquid state and the energy storage/release was mainly taking place by the sensible heat mode during this period. For the remaining 12.5 h, with the melt fraction below 100%, the PCM was in a liquid-solid coexistence state and the energy storage/release was in latent heat mode.

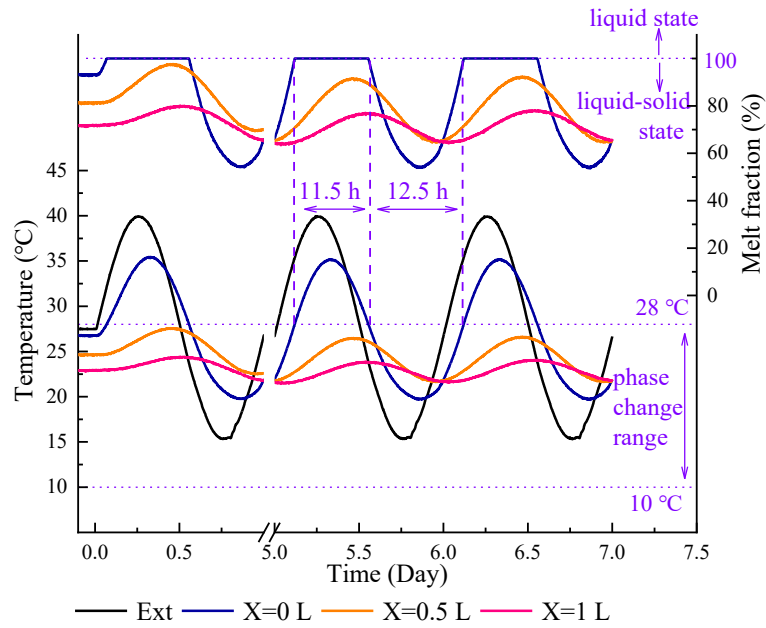


Fig. 3.37. PCM's mean T and melt fraction

The PCM's daily storage/release efficiency for the integrated configurations is plotted in Fig. 3.38. It is noted that these values were significantly lower than the melt fraction due to the non-uniformity between the specific heat capacity and temperature. Furthermore, the PCM storage/release efficiency in this study was not high: the highest value was only 21.5%. This is because its value is affected by several factors, such as the convective heat transfer coefficient, boundary temperature, and peak melt temperature [108, 230-232]. Since the experiment was done with the given boundary conditions, PCM, etc., the efficiency could not reach its optimal value. Nevertheless, this study concerns the relationship between the PCM's efficiency and its location in the envelope. For the values, the highest PCM storage/release efficiency was 21.5%/18.8% for configuration  $X = 0$  L, which was 2.2/2.3 and 5.7/4.9 times higher than the configurations  $X = 0.5$  L and  $X = 1$  L, respectively. It should be remembered that the efficiency of configuration  $X = 0$  L was only generated for about half of the day (latent heat mode for 12.5 h, see Fig. 3.37). Hence, when located close to the exterior side, the PCM was more likely to be activated and had a higher efficiency.

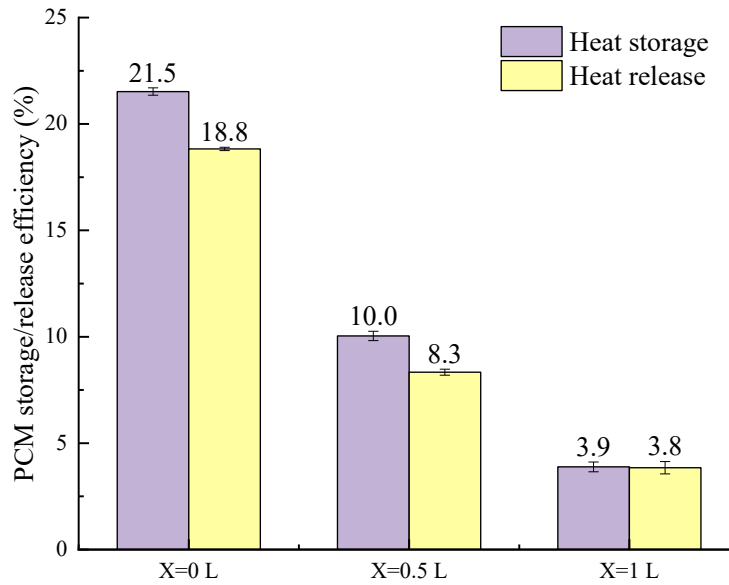


Fig. 3.38. PCM's storage/release efficiency

However, although the PCM had a high efficiency when it was exposed to the exterior environment directly (configuration  $X = 0$  L), it was liable to overactivation (overmelting, 11.5 h a day), which may increase the risk of leakage [233, 234]. The configuration  $X = 0.5$  L is preferable because the PCM was kept in a partially melted state throughout the experimental period. Besides, the PCM's efficiency was more than twice as high as that of configuration  $X = 1$  L for the same heat absorption on the exterior surface.

### 3.6 Conclusion

In this chapter, PCM and HC were combined into a multilayer integrated building envelope on an experimental scale. Four envelope configurations were considered and studied: one configuration without a PCM layer and three configurations with a PCM layer located in different locations. The hygrothermal behavior and energy performance of the envelopes were investigated experimentally.

Two types of boundary conditions were conducted to imitate the exterior condition. The main results and conclusions with different boundary conditions are summarized as below.

### **3.6.1 Results of static boundary condition**

The variation consistency of relative humidity and temperature within the HC over the four days indicates that temperature plays a dominant role in the mechanism of moisture transfer. Besides, the slight difference between the relative humidity variation within the HC on the first and third day (or the second and fourth day) demonstrates the coupling of heat and moisture transfer.

With inclusion of PCM, the characteristic times of temperature and relative humidity both increase, indicating an increase in thermal inertia and hygric inertia of the envelope.

When the PCM is placed on the interior side, the moisture transfer between envelope and interior is blocked. Moisture accumulation may occur inside the envelope due to the exterior environment's high relative humidity. The PCM placed in the middle of the envelope ensures that both sides of the envelope are subject to heat and moisture transfer with the environment. The envelope's hygric inertia is beneficial to the interior side but the risk of moisture accumulation on the exterior side is accentuated. The PCM placed on the exterior side protects against condensation and mold growth risk caused by the high relative humidity fluctuation. It also ensures that the envelope's hygric inertia has a major effect on the interior environment.

As regards thermal energy, heating and cooling loads are effectively decreased when PCM is placed on the exterior side and middle of the envelope. Besides, when PCM is placed close to the exterior side, its heat store/release capacity is enhanced, which is closely related to the PCM's temperature distribution and its corresponding specific heat capacity.

### 3.6.2 Results of dynamic boundary condition

The temperature and relative humidity response in the HC emphasize the high coupling between heat and moisture transfer. The relative humidity is affected mainly by temperature due to evaporation and condensation, especially at points close to the interior side.

Since the moisture-buffering capacity of HC increases as temperature decreases, the presence of the PCM damps the temperature fluctuation, and thus increases the moisture retention capacity of the HC. Notably, the configuration with the PCM placed in the middle of the envelope has the smallest temperature/relative humidity amplitudes of 1.2 °C/0.8% and a significant time delay of 6.3 h at measurement point H<sub>2</sub>. The placement of the PCM in direct exposure to the interior environment should be avoided because of the moisture impermeability of the PCM.

As for the energy performance, when the PCM is placed on the exterior side, it has the highest energy participation (64.2%/71.0%) in the envelope during the energy storage/release process. Furthermore, it has the highest activation and the highest storage/release efficiency (21.5%/18.8%). However, the PCM absorbs more heat from the exterior than other configurations, which makes it prone to overmelting during high-temperature periods (nearly 11.5 h a day). For the placement of the PCM in the middle of the envelope, the interaction between the PCM and the exterior is damped by a HC layer, so that the PCM has a smaller energy participation, activation, and efficiency than the PCM on the exterior side. Nevertheless, the PCM stays in the phase transition range with a melt fraction between 80.1 and 97.7% (partially melted, full latent heat mode), making this location the optimum for energy saving. There are minimal heat flux fluctuations and released heat on the interior surface with the values of 4.4 W/m<sup>2</sup> and 65.5 kJ, which are 53.7% and 15.3% less than those for the envelope with HC only.

### 3.6.3 Over conclusion and recommendation

Experimental results demonstrate the heat and moisture coupling and the dominant role of temperature within the HC, which provides the theoretical feasibility to change the hygrothermal behavior by adding PCM to change the temperature distribution and variation of the envelope.

When PCM is placed on the exterior side, it absorbs/releases the most thermal energy from/to the surrounding environment and therefore is more likely to be activated with a high melt fraction. As a result, PCM has the highest storage/release efficiency and the highest energy participation in the envelope during the energy storage/release process. However, there is a potential downside of overmelting for PCM directly exposed to the exterior environment.

Due to the moisture impermeability of PCM, the placement directly to the interior environment is not recommended because this configuration loses the benefit of HC as a hygroscopic material to regulate the interior humidity. Nevertheless, some advantages of this configuration are still notable. The PCM is often in the phase transition range, making the PCM layer have the smallest temperature fluctuation and the longest time delay.

The placement of PCM in the middle ensures that both sides of the envelope can transfer heat and moisture with their respective environment. Besides, PCM is kept in the phase transition range for most of the time, which contributes to energy savings and ensures less temperature/relative humidity fluctuation with long temperature time delay in the HC layer near the interior environment. However, moisture accumulation on both sides of the PCM may cause the condensation risk.

In summary, the multilayer integration of PCM and HC has proven to have the ability to improve the hygrothermal performance of the envelope. There are several advantages and disadvantages to placing PCM anywhere in the envelope. Therefore, it is necessary to identify the configuration with the best performance and avoid its shortcomings.

# **Chapter 4      Numerical study on hygrothermal performance of integrated envelope**

## **4.1 Objectives of numerical study**

In Chapter 3, the hygrothermal performance of the integrated envelope consisting of HC and PCM was experimentally investigated. Preliminary results, conclusions, and recommendations were obtained from four different configurations. However, each configuration has advantages and disadvantages. It is necessary to further expand more configurations and fully exploit their advantages. Moreover, due to the limitations of experimental conditions and sensors, it is difficult to study in detail some important parameters that cannot be measured, such as moisture flux and load. In addition, it is interesting and valuable to study the hygrothermal and energy performance of the integrated envelope in real climates, both from a short-term perspective (days and weeks) and from a long-term perspective (months and years). In this context, numerical studies are carried out in this chapter to investigate the performance of the integrated envelope in real climatic environments.

Furthermore, as mentioned in Section 2.4, the studies focusing on the integration of PCM and hygroscopic materials were divided into two categories. These two categories are of great interest from the perspective of sample characterization and basic hygrothermal behavior evaluation. However, an overall analysis of energy performance (total, sensible, and latent heat load) and the quantification of hygric performance are also important. Moreover, because of the coupling between heat and moisture transfer, it is necessary to comprehensively study the thermal, hygric, and energy performances. First, the principle that PCMs affect the hygric performance of the envelope by influencing its thermal performance needs to be investigated. Further, the effect of hygroscopic materials on hygric and energy performance is also worth studying. In addition, considering that the location of the PCM affects the

temperature distribution in the envelope, it is meaningful to explore the performance of the integrated envelope with PCM placed in more different locations.

Based on the above motivation, the main objectives are presented as follows:

- 1) Establish and validate a multilayer envelope model that couples heat and moisture transfer and considers the temperature dependence of HC's hygroscopic characteristic.
- 2) Study the hygrothermal and energy performance of the integrated envelope in summer and winter seasons.
- 3) Prove the importance of moisture transfer on the hygrothermal and energy performance of the envelope.
- 4) Analyze the relationship between energy, thermal, and hygric performance.
- 5) Investigate the impact of PCM and its location on the performance of the integrated envelope and identify the optimal location.
- 6) Evaluate annual energy and hygric performance.

## **4.2 Description of the integrated envelope**

### **4.2.1 Multilayer envelope**

As with the experimental study in the previous chapter, two types of envelope configurations (with and without PCM) are presented in this chapter. However, unlike the experimental study, the envelope thicknesses of all configurations were set to be consistent for better accuracy of the analysis. The first type is the configuration without PCM, which is named configuration baseline. The second type is the integrated configuration with the PCM placed in different locations.

Fig. 4.1 shows the two types of envelope configurations. The configuration baseline is a single layer of HC. For the integrated configurations, the HC layer was assumed to be divided into four

uniform parts by three gaps along the thickness direction, and PCMs were inserted into the gaps; the resulting configurations were simplistically named configuration 2/5, 3/5, and 4/5, respectively. The configuration with PCM on the outermost layer was named configuration 1/5. Notably, as concluded in Section 3.4 and Section 3.5, the configuration with the PCM in direct contact with the interior environment was eliminated because the moisture impermeability of the PCM caused the loss of the moisture regulation ability of the HC.

The thickness of the configuration baseline was 25 cm. The integrated configurations comprised a 24-cm HC layer and a 1-cm PCM layer. The distance between the PCM and the interior surface in configuration 4/5 was 6 cm, which was thicker than the penetration depth of the HC [235].

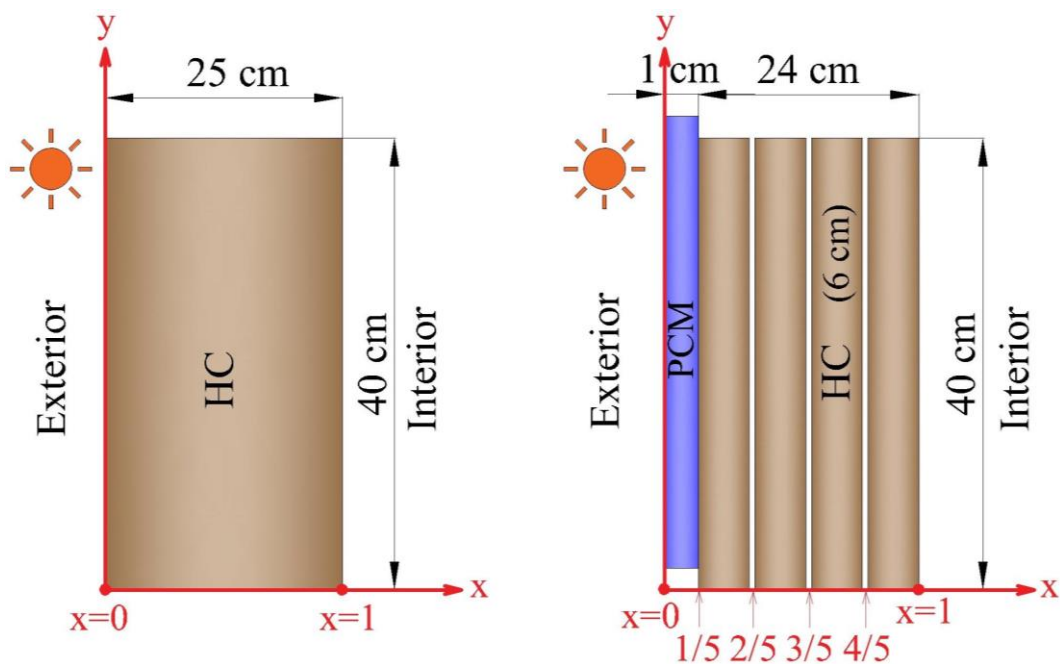


Fig. 4.1. Two-dimensional layout of envelope: Baseline and integrated configurations

#### 4.2.2 Properties of materials

Table 4.1 shows the physical properties of HC and PCM. HC is the one used in Chapter 3, and its physical properties are expressed as a function of some basic parameters such as temperature, relative

humidity, and volumetric moisture content.

	HC <sup>a</sup>	PCM
Density (kg/m <sup>3</sup> )	478	810
Specific heat capacity (kJ/(kg·K))	$1.08 + 8.8 \times 10^{-3}w$	Fig. 4.2 (a)
Thermal conductivity (W/(m·K))	$0.125 + 3.36 \times 10^{-4}w$	Fig. 4.2 (b)
Latent heat (kJ/kg)	—	90.4
Phase transition range (°C)	—	24–28
Water vapor permeability (kg/(Pa·m·s))	$1.26 \times 10^{-11} \times \exp(2.26\varphi)$	—
Volumetric moisture content (kg/m <sup>3</sup> )	$\frac{\varphi}{-0.08\varphi^2 + 0.06\varphi + 0.03} - (0.4 - 0.26\varphi)(T - 23)$	—

<sup>a</sup> In the expression of the physical properties of HC,  $w$ ,  $\varphi$ , and  $T$  are the volumetric moisture content, relative humidity (expressed in decimal form), and temperature, respectively.

Table 4.1 Physical properties of HC [94, 236] and PCM [222]

In order to better analyze the impact of PCM on the envelope in this chapter and to conduct the parametric analysis in the next chapter, a PCM with ideal specific heat capacity and thermal conductivity is proposed. As the most important parameter of the PCM, the specific heat capacity curve is ideally symmetric about the center of the phase transition range. The curves of specific heat capacity and thermal conductivity of the PCM can be seen in Fig. 4.2, and the equations are referred to Section 4.3.3. The phase transition range is 24–28 °C with the maximum specific heat capacity (62 (kJ/(kg·K)) achieved at 26 °C in the center of the phase transition range. For the solid state PCM with the temperature below 24 °C or the liquid state PCM with the temperature above 28 °C, the specific heat capacity is 2 kJ/(kg·K). The thermal conductivity of the solid and liquid PCM is 0.18 and 0.14 (W/(m·K)), respectively. In the phase transition range, the thermal conductivity shows a linear

decrease trend.

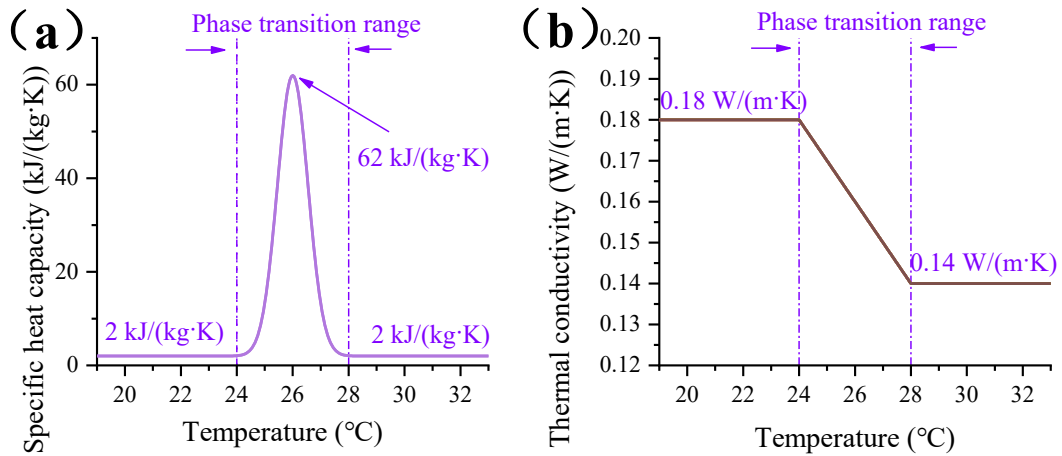


Fig. 4.2. Thermal properties of PCM: (a) specific heat capacity; (b) thermal conductivity

### 4.3 Model derivation and boundary conditions

The coupled heat and moisture transfer in the envelope is a complex unsteady process, influenced by boundary conditions and its own physical properties. In order to simplify the physical model with guaranteed computational accuracy, the following assumptions are considered:

- 1) Every element and layer of the envelope is non-deformable, homogeneous, and isotropic.
- 2) Thermal resistance on the interface between the layers is neglected.
- 3) Radiative heat transfer between the interior and the envelope is neglected.
- 4) The air in the pores of the porous structure of the HC is considered an ideal gas.
- 5) No heat or moisture sources exist in the envelope.
- 6) A local thermodynamic equilibrium exists between heat and moisture in the envelope.

#### 4.3.1 Moisture transfer equation of HC

In the model presented, relative humidity ( $\varphi$ ) and temperature ( $T$ ) are chosen as driving potentials

of moisture and heat transfer, respectively. The total moisture transfer in porous materials includes vapor diffusion and liquid transport. The total moisture flux and mass conservation equation [191] can be written as

$$j = j_v + j_l \quad (4.1)$$

$$\frac{\partial w}{\partial t} = -\nabla j \quad (4.2)$$

where

$j$  = total moisture flux, (kg/(m<sup>2</sup>.s));

$j_v$  = vapor moisture flux, (kg/(m<sup>2</sup>.s));

$j_l$  = liquid moisture flux, (kg/(m<sup>2</sup>.s));

$w$  = volumetric moisture content, (kg/m<sup>3</sup>).

Vapor diffusion in porous materials follows Fick's law [186], the vapor moisture flux is

$$j_v = -\delta_p \nabla p_v \quad (4.3)$$

where

$\delta_p$  = water vapor permeability, (kg/(Pa·m·s));

$p_v$  = partial water vapor pressure, (Pa).

Liquid transport in porous materials follows Darcy's law [190], the liquid moisture flux is

$$j_l = -K_w \nabla p_c \quad (4.4)$$

where

$K_w$  = liquid water permeability, (kg/(Pa·m·s));

$p_c$  = capillary pressure, (Pa).

Therefore, the total moisture flux in porous materials is

$$j = j_v + j_l = -\delta_p \nabla p_v - K_w \nabla p_c \quad (4.5)$$

According to the statements in Section 2.2.4, the sorption moisture retention curve is dependent on both relative humidity and temperature [89-91]. Therefore, the left term of the mass conservation equation is expressed by

$$\frac{\partial w}{\partial t} = \left. \frac{\partial w}{\partial \varphi} \right|_T \frac{\partial \varphi}{\partial t} + \left. \frac{\partial w}{\partial T} \right|_\varphi \frac{\partial T}{\partial t} = \xi_\varphi \frac{\partial \varphi}{\partial t} + \xi_T \frac{\partial T}{\partial t} \quad (4.6)$$

where

$\varphi$  = relative humidity, (%);

$T$  = temperature, (°C);

$\xi$  = sorption capacity.

The vapor pressure of moisture can be expressed in terms of relative humidity and saturation pressure

$$p_v = \varphi p_{v,sat} \quad (4.7)$$

$$\nabla p_v = \nabla(\varphi p_{v,sat}) = \varphi \nabla p_{v,sat} + p_{v,sat} \nabla \varphi = \varphi \frac{dp_{v,sat}}{dT} \nabla T + p_{v,sat} \nabla \varphi \quad (4.8)$$

The saturation pressure can be expressed by [237]

$$p_{v,sat} = 610.5 \exp\left(\frac{17.269T}{237.3+T}\right) \quad (4.9)$$

where

$p_{v,sat}$  = saturation pressure, (Pa).

The capillary pressure is calculated by Kelvin equation [238]:

$$p_c = \frac{\rho_w R}{M_w} \ln(\varphi) \quad (4.10)$$

$$\nabla p_c = \frac{\rho_w R}{M_w} \ln(\varphi) \nabla T + \frac{\rho_w R T}{M_w \varphi} \nabla \varphi \quad (4.11)$$

where

$\rho_w$  = density of water, (kg/m<sup>3</sup>);

$R$  = universal gas constant, (J/(kg·K));

$M_w$  = molar mass of water, (kg/mol).

Therefore, the mass conservation equation Eq. (4.2) can be expressed by

$$\xi_\varphi \frac{\partial \varphi}{\partial t} + \xi_T \frac{\partial T}{\partial t} = \nabla \left( \left( \delta_p p_{v,sat} + K_w \frac{\rho_w R T}{\varphi M_w} \right) \nabla \varphi + \left( \delta_p \varphi \frac{dp_{v,sat}}{dT} + K_w \frac{\rho_w R \ln(\varphi)}{M_w} \right) \nabla T \right) \quad (4.12)$$

Eq. (4.12) can be simplified as

$$\xi_\varphi \frac{\partial \varphi}{\partial t} + \xi_T \frac{\partial T}{\partial t} = \nabla (D_\varphi \nabla \varphi + D_T \nabla T) \quad (4.13)$$

$$D_\varphi = \delta_p p_{v,sat} + K_w \frac{\rho_w R T}{\varphi M_w} \quad (4.14)$$

$$D_T = \delta_p \varphi \frac{dp_{v,sat}}{dT} + K_w \frac{\rho_w R \ln(\varphi)}{M_w} \quad (4.15)$$

The liquid water permeability can be written as [239]:

$$K_w = \frac{\delta_p \varphi M_w p_{v,sat}}{RT \rho_w} \quad (4.16)$$

### 4.3.2 Heat transfer equation of HC

Heat transfer in the HC can be described as a change in enthalpy caused by a change in temperature, and it consists of two parts. First, the heat flux gradient is directly proportional to the temperature gradient and the conductivity as defined by Fourier's law. Second, the heat flux gradient can also be transported by the moisture flux, defined as a source term in the general heat equation [96].

Thus, the energy conservation equation [191] can be expressed by

$$\rho_{hc} C_{hc} \frac{\partial T}{\partial t} = \nabla (\lambda_{hc} \nabla T) - L_v \nabla j_v \quad (4.17)$$

where

$\rho_{hc}$  = density of HC, (kg/m<sup>3</sup>);

$C_{hc}$  = specific heat capacity of HC, (J/(kg·K));

$\lambda_{hc}$  = thermal conductivity of HC, (W/(m·K));

$L_v$  = latent heat of evaporation, (J/kg).

According to Eqs. (4.3) and (4.8),

$$\nabla j_v = -(\delta_p \nabla p_v) = -\nabla \left( \delta_p p_{v,sat} \nabla \varphi + \delta_p \varphi \frac{dp_{v,sat}}{dT} \nabla T \right) \quad (4.18)$$

Thus, Eq. (4.17) can be expressed as

$$\rho_{hc} C_{hc} \frac{\partial T}{\partial t} = \nabla (\lambda_{hc} \nabla T) + L_v \nabla (\delta_p p_{v,sat} \nabla \varphi + \delta_p \varphi \frac{dp_{v,sat}}{dT} \nabla T) \quad (4.19)$$

Eq. (4.19) can be simplified as

$$\rho_{hc} C_{hc} \frac{\partial T}{\partial t} = \nabla (\lambda_{hc} \nabla T) + L_v \nabla (D_{\varphi,v} \nabla \varphi + D_{T,v} \nabla T) \quad (4.20)$$

$$D_{\varphi,v} = \delta_p p_{v,sat} \quad (4.21)$$

$$D_{T,v} = \delta_p \varphi \frac{dp_{v,sat}}{dT} \quad (4.22)$$

Here, the latent heat of evaporation is the function of temperature [240]:

$$L_v = (2500 - 2.4T) \times 10^3 \quad (4.23)$$

### 4.3.3 Heat transfer equation of PCM

The effective heat capacity model [241] was chosen to describe the heat transfer of the PCM. This model deals with heat capacity and thermal conductivity as a function of temperature; their curves are shown in Fig. 4.2 (a) and (b) in Section 4.2.2. The heat transfer equation of the PCM can be expressed by

$$\rho_{pcm} C^* \frac{\partial T}{\partial t} = \nabla(\lambda^* \nabla T) \quad (4.24)$$

$$C^* = \begin{cases} C_s & T < T_{ini} \\ \frac{C_s + C_l}{2} + 60 \times \exp\left(-1.67 \times \left(T - \frac{T_{ini} + T_{fin}}{2}\right)^2\right) & T_{ini} \ll T \ll T_{fin} \\ C_l & T > T_{fin} \end{cases} \quad (4.25)$$

$$\lambda^* = \begin{cases} \lambda_s & T < T_{ini} \\ \lambda_l + 0.01 \times (T_{fin} - T) & T_{ini} \ll T \ll T_{fin} \\ \lambda_l & T > T_{fin} \end{cases} \quad (4.26)$$

where

$\rho_{pcm}$  = density of PCM, (kg/m<sup>3</sup>);

$C^*$  = effective heat capacity of PCM, (J/(kg·K));

$\lambda^*$  = effective thermal conductivity of PCM, (W/(m·K));

$C_s, C_l$  = specific heat capacity of solid and liquid PCM, (J/(kg·K)),  $C_s = C_l = 2$  kJ/(kg·K);

$\lambda_s, \lambda_l$  = thermal conductivity of solid and liquid PCM, (W/(m·K)),  $\lambda_s = 0.18$  W/(m·K) and  $\lambda_l = 0.14$  W/(m·K);

$T_{ini}, T_{fin}$  = initial and final temperatures of the phase transition range, (°C), in this chapter,  $T_{ini} = 24$  °C and  $T_{fin} = 28$  °C.

#### 4.3.4 Boundary conditions

Since the outermost layer comprised the PCM in configuration 1/5 and HC in the remaining configurations, the boundary conditions were different on the exterior surface.

When HC is the outermost layer, the moisture and heat transfer boundary conditions on the exterior surface are

$$-(D_\varphi \nabla \varphi + D_T \nabla T)|_{x=0} = h_{m,e} (p_{v,e} - p_{v,x=0}) \quad (4.27)$$

$$-\left(\lambda_{hc}\nabla T + L_v(D_{T,v}\nabla T + D_{\phi,v}\nabla\phi)\right)\Big|_{x=0} = h_{t,e}(T_e - T_{x=0}) + L_v h_{m,e}(p_{v,e} - p_{v,x=0}) + \alpha I_{rad} + \varepsilon\sigma\left[(1 - F_{sky})(T_e^4 - T_{x=0}^4) + F_{sky}(T_{sky}^4 - T_{x=0}^4)\right] \quad (4.28)$$

When PCM is the outermost layer, no moisture transfer happens on the exterior surface and the boundary conditions are expressed as

$$j|_{x=0} = 0 \quad (4.29)$$

$$-(\lambda^*\nabla T)|_{x=0} = h_{t,e}(T_e - T_{x=0}) + \alpha I_{rad} + \varepsilon\sigma\left[(1 - F_{sky})(T_e^4 - T_{x=0}^4) + F_{sky}(T_{sky}^4 - T_{x=0}^4)\right] \quad (4.30)$$

For interior surface, the moisture and heat transfer boundary conditions remain coincident for all configurations:

$$-(D_\phi\nabla\phi + D_T\nabla T)\Big|_{x=l} = h_{m,i}(p_{v,x=l} - p_{v,i}) \quad (4.31)$$

$$-\left(\lambda_{hc}\nabla T + L_v(D_{T,v}\nabla T + D_{\phi,v}\nabla\phi)\right)\Big|_{x=l} = h_{t,i}(T_{x=l} - T_i) + L_v h_{m,i}(p_{v,x=l} - p_{v,i}) \quad (4.32)$$

where

$h_{t,e}, h_{t,i}$  = convective heat transfer coefficients on the exterior and interior surface, ( $W/(m^2\cdot K)$ ),

assumed to be constant with the value of 23.26 and 8.72  $W/m^2\cdot K$  [242];

$h_{m,e}, h_{m,i}$  = convective mass transfer coefficients on the exterior and interior surface, ( $kg/(m^2\cdot s\cdot Pa)$ );

$p_{v,e}, p_{v,i}$  = partial water vapor pressure of exterior and interior, (Pa);

$p_{v,x=0}, p_{v,x=l}$  = partial water vapor pressure on the exterior and interior surface, (Pa);

$T_e, T_i$  = temperature of exterior and interior, ( $^{\circ}C$ );

$T_{x=0}, T_{x=l}$  = temperature on the exterior and interior surface, ( $^{\circ}C$ );

$\alpha$  = solar absorptivity, assumed to be 0.8;

$\varepsilon$  = infrared emittance, assumed to be 0.8;

$I_{rad}$  = solar radiation, (W/m<sup>2</sup>);

$\sigma$  = Stefan-Boltzmann constant, (W/(m<sup>2</sup>·K<sup>4</sup>));

$F_{sky}$  = radiation view factor from sky to the envelope [243]:  $F_{sky} = \beta[0.5(1 + \cos\gamma)]$ . Here,  $\gamma = 90^\circ$  for vertical envelope;  $\beta = \sqrt{0.5(1 + \cos\gamma)}$ ;

$T_{sky}$  = sky temperature [244],  $T_{sky} = 0.0552T_e^{1.5}$ , (°C).

The mass transfer coefficient is related to the heat transfer coefficient by using Lewis relationship [245]:

$$h_m = \frac{h_t}{\rho_a c_a Le} \quad (4.33)$$

where

$\rho_a$  = density of air, (kg/m<sup>3</sup>);

$C_a$  = specific heat capacity of air, (J/(kg·K));

$Le$  = Lewis number.

#### 4.4 Numerical principle and tool

Generally, partial differential equations (PDEs) can be solved by analytical or numerical methods. Analytical methods can obtain the exact solution of the model, while numerical methods can only obtain an approximate solution of the model at discrete points. However, the models of the integrated envelope contain both the coupled heat and moisture transfer model of the HC and the heat transfer model of the PCM. The coupled heat and moisture models of the HC are PDEs with variable coefficients, which are highly nonlinear and mutually coupled and are difficult to solve analytically. Thus, numerical methods are used in this study.

#### **4.4.1 Commonly used numerical methods**

There are three common numerical methods for the numerical solution of PDEs, including the finite difference method, the finite volume method, and the finite element method.

##### **4.4.1.1 Finite difference method**

The finite difference method (FDM) is the earliest numerical method in history and the most classical method in numerical solution. The PDE is a class of numerical techniques for solving differential equations by approximating derivatives with finite differences. The principle is to employ a Taylor series expansion for the discretization of the derivatives of the flow variables. The advantage of FDM is its computational simplicity and flexibility. The disadvantage is that it is limited to conventional differential meshes and is poorly adapted to solve problems in complex regions.

The application of FDM in solving the coupled heat and moisture transfer model of building structures is described in the literature [246-248]. For PCM, the FDM has been used in the literature [249-251]. A representative software that uses FDM is Energy Plus.

##### **4.4.1.2 Finite volume method**

The finite volume method (FVM) is also known as the control volume method. The basic principle is to divide the computational region into a series of non-repeating control volumes. The integration of the PDE over each control volume results in a balance equation. The set of balance equations is then discretized with respect to a set of discrete unknowns. The advantages of FVM are that the physical concept of the derivation process is clear, the coefficients of the discrete equations are physically meaningful, and the conservation properties of the discrete equations are guaranteed. The disadvantage of FVM is the difficulty in analyzing the mathematical properties of the equations.

The studies of heat and moisture transfer in buildings using FVM can be found in literature [252-254], and the studies of PCM heat transfer using FVM can be found in literature [255-257]. WUFI is a representative software that uses FVM.

#### **4.4.1.3 Finite element method**

The development of finite element method (FEM) can be traced back to the idea of piecewise linear approximation on triangles proposed by Courant in 1943, which is a numerical method based on the classical Ritz-Galerkin variational method. The basic principle of FEM [258] is to discretize the domain of interest in which the PDE is defined in order to obtain an approximate solution of the PDE by a linear combination of basic functions defined within each subdomain. The subdomains are then assembled in the process of putting the finite element back in place to obtain a discrete set of equations similar to the original mathematical problem. In each finite element, these equations are solved by assuming basis functions that interpolate unknown variables over the finite element to approximate the problem within the element. Then, the local element equations for all finite elements are assembled together and solved simultaneously to obtain a continuous solution of their values at the nodes, with appropriate loads, boundaries and initial conditions applied to the elements/nodes. The advantage of the FEM is the wide adaptability, especially for edge value problems with complex geometric and physical conditions. The disadvantage is that the variation law of the dependent variable between grid points needs to be assumed, and the solution speed is much slower than that of the FDM and the FVM.

The literatures on heat and mass transfer in buildings using FEM are [259-261] and on PCM heat transfer are [262-264]. A representative software that uses FEM is COMSOL Multiphysics.

#### **4.4.2 COMSOL Multiphysics**

In this study, the numerical analysis method chosen is the FEM, and the corresponding software

is COMSOL Multiphysics. COMSOL Multiphysics is widely used as finite element analysis software for direct coupling of multiple physical fields and for numerical calculations. Its boundary conditions can be set in a wide range of modes, either as a constant or as a function of any variable or as a logical expression, or as an interpolation function. In addition, users can also choose physical fields according to their needs or define their own PDEs to finally complete the coupling between multiple physical fields.

The mathematical model of the envelope in this study includes heat and moisture transfer inside the HC, heat transfer inside the PCM, and heat/moisture transfer between the interior/exterior surface and boundary environment. The heat and moisture transfer inside and on the surfaces of the envelope are related to the interior/exterior boundary conditions and the physical parameters of the envelope materials. Since these equations exhibit a high degree of nonlinearity, the general form PDE interface in COMSOL Multiphysics was used to program the control equations. The general form PDE form is shown below:

$$e_a \frac{\partial^2 u}{\partial t^2} + d_a \frac{\partial u}{\partial t} + \nabla \cdot \Gamma = f \quad \text{in } \Omega \quad (4.34)$$

$$-n \cdot \Gamma = g - qu + h^T \mu \quad \text{on } \partial\Omega \quad (4.35)$$

$$0 = R \quad \text{on } \partial\Omega_c \quad (4.36)$$

$$u = r \quad \text{on } \partial\Omega_d \quad (4.37)$$

where

$\Omega$  = computational domain (the union of all domains);

$\partial\Omega$  = domain boundary;

$n$  = outward unit normal vector on  $\partial\Omega$ .

The first equation is the PDE, which must be satisfied in domain  $\Omega$ . The second, third, and fourth equations are the boundary conditions, which must hold on  $\partial\Omega$ . The second equation is a generalization

of a Neumann boundary condition. In the PDE interfaces, the corresponding condition is called a flux or source, because it specifies the value of the numerical flux  $\Gamma$  at the boundary. The general constraint of the third equation specifies that an arbitrary expression is equal to zero on the boundary:  $R = 0$ . The Dirichlet condition of the fourth equation is a special case directly specifying the value of the dependent variable at the boundary:  $u = r$ , which makes the constraint a more general boundary condition.

The terms  $\Gamma$ ,  $f$ ,  $g$ ,  $q$ ,  $R$ , and  $r$  are user-defined coefficients. The coefficients  $f$ ,  $g$ ,  $q$ ,  $R$ , and  $r$  are scalar. In practical applications,  $\Gamma$  typically represents the flux of a conserved quantity such as heat, charge, mass, or momentum. In this paper,  $u$  presents the variables temperature and relative humidity,  $\Gamma$  represents the heat flux and the moisture flux.

## 4.5 Model validation

The model validation is based on the experimental results in the previous chapter. The dynamic boundary conditions (see Section 3.2.6.2) were used as the experimental boundary conditions; the configuration without PCM and configuration  $X = 0.5$  L were used as experimental configurations; the temperature and relative humidity variations for two days (48 h) in Sections 3.5.1 and 3.5.2.3 were used as the experimental results; the point  $H_{12}$  in the configuration without PCM as well as the points  $H_2$  and  $P$  in the configuration  $X = 0.5$  L were used as compared points.

To compare the experimental and simulation results and ensure the validation accuracy, the relative error, the root mean square error (RMSE), and the coefficient of variation of the root mean square error ( $CV_{(RMSE)}$ ) were calculated.

$$\theta = \frac{R_e - R_s}{R_e} \times 100\% \quad (4.38)$$

$$RMSE = \sqrt{\frac{\sum_{i=1}^n (R_{e_i} - R_{s_i})^2}{n}} \quad (4.39)$$

$$CV_{(RMSE)} = \frac{RMSE}{\bar{R}_e} \times 100\% \quad (4.40)$$

where

$\theta$  = relative error;

$R_e$  = experimental results;

$R_s$  = simulation results;

RMSE = root mean square error;

$CV_{(RMSE)}$  = coefficient of variation of the root mean square error;

$n$  = number of data points;

$\bar{R}_e$  = average value of the experimental result,  $\bar{R}_e = (\sum_{i=1}^n R_{e_i})/n$ .

Fig. 4.3 (a) and (b) show the simulation and experimental results and their relative errors (right axis) of configuration without PCM and  $X = 0.5 L$ , respectively. It can be seen that the simulation results are in good agreement with the experimental results in both configurations.

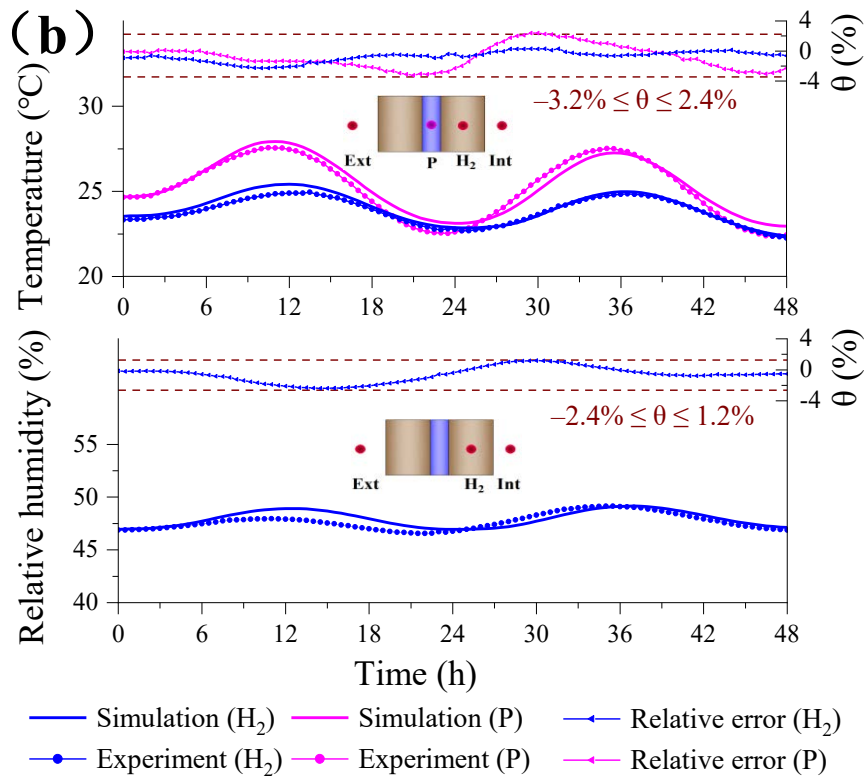
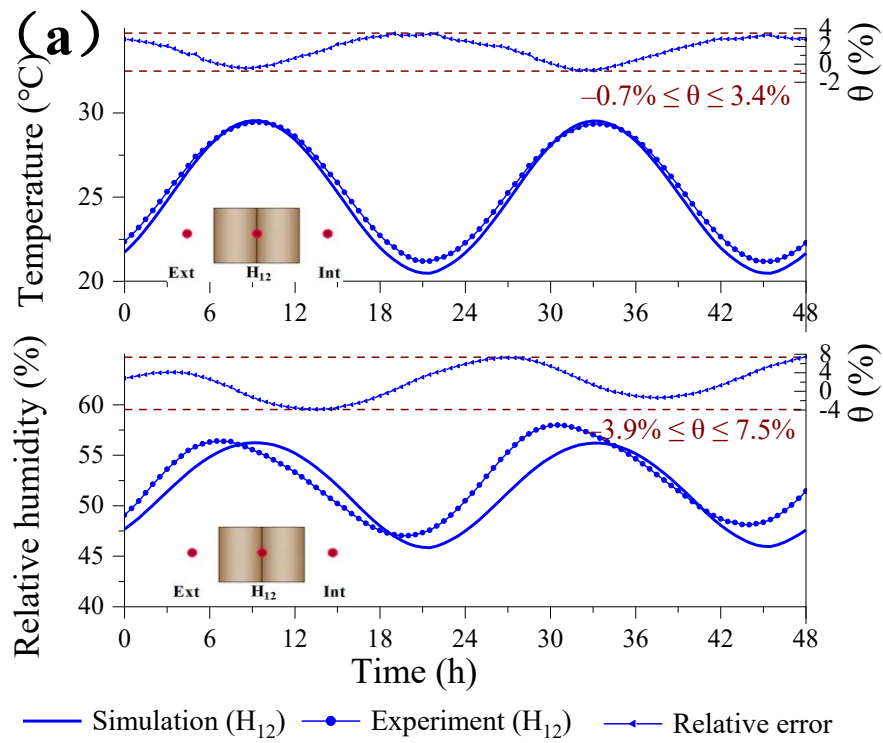


Fig. 4.3. Comparison between the simulation and experimental results of (a) configuration without PCM and (b) configuration X = 0.5 L

Table 4.2 summarizes the average, maximum, and minimum relative errors, RMSE, and  $CV_{(RMSE)}$ . The relative humidity of configuration without PCM has the maximum relative error, but it is only 7.5%, while the relative errors for the remaining parameters are less than 3.4%. Moreover, the RMSEs of temperature and relative humidity are less than 0.6 °C and 2.2%, respectively, and all  $CV_{(RMSE)}$ s are less than 4%. These data suggested that the model exhibits high accuracy compared to the experiment, and it can be considered validated and used to support further simulation studies.

	Configuration without PCM		Configuration X = 0.5 L		
	$T_{h_{12}}$	$\varphi_{h_{12}}$	$T_{h_2}$	$\varphi_{h_2}$	$T_p$
Average $\theta$	1.6%	1.9%	-0.7%	-0.6%	-0.8%
Max $\theta$	3.4%	7.5%	0.3%	1.2%	2.4%
Min $\theta$	-0.7%	-3.9%	-2.3%	-2.4%	-3.2%
RMSE	0.5 °C	2.1%	0.2 °C	0.6%	0.4 °C
$CV_{(RMSE)}$	1.9%	3.9%	1.0%	1.2%	1.7%

Table 4.2 Summary of relative error, RMSE, and  $CV_{(RMSE)}$  for configurations without PCM and X = 0.5 L

## 4.6 Climate and interior conditions

Fig. 4.4 (a) depicts the studied climate in Rome, Italy, which is characterized as a Mediterranean climate (according to the Köppen-Geiger climate classification system shown in Fig. 2.4 [24]: Csa). It is mild but humid in winter, and hot with temperate humidity in summer. The interior temperature was determined according to International Standard ISO 13788-2012 [265], which proposes a simplified approach to determining interior conditions based on climate temperature. Fig. 4.4 (b) shows the seasonally dependent interior temperature, which was set to 25 and 20 °C in summer and winter,

respectively, and to vary linearly between 20 and 25 °C in spring and autumn. The interior relative humidity was taken as 50% throughout the year.

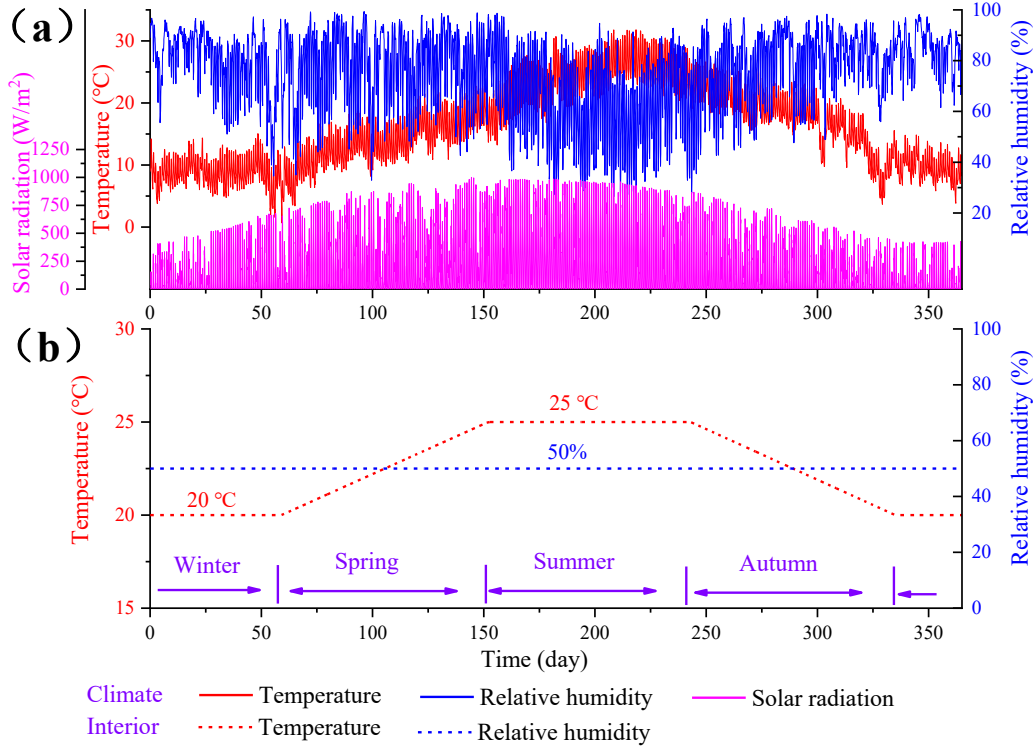


Fig. 4.4. Annual climate and interior conditions: (a) exterior climate in Rome; (b) interior temperature and relative humidity

Fig. 4.5 (a) and (b) show the representative climate variation during one week in summer (August 1 to 7) and in winter (January 10 to 17), respectively, in terms of climate temperature, relative humidity, and sol-air temperature ( $T_{sol-air}$ ). The sol-air temperature reflects the superposition effect of ambient temperature and radiation on the exterior envelope surface [266]:

$$T_{sol-air} = T_e + \frac{\alpha I_{rad}}{h_{t,e}} \quad (4.41)$$

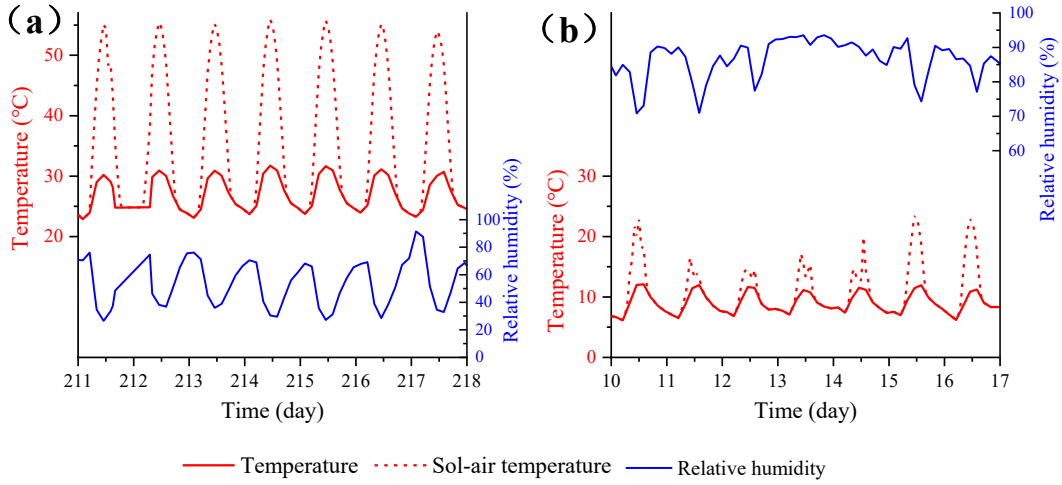


Fig. 4.5. Representative climate during one week in (a) summer and (b) winter

## 4.7 Metric parameters

The metric parameters used in this study comprise three aspects of the interior envelope surface: energy, hygric, and thermal performance.

Energy performance refers to the cumulative heat load over a time duration of  $t_2 - t_1$ :

$$Q_{gain/loss} = \int_{t_1}^{t_2} q_{gain/loss} dt \quad (4.42)$$

where

$Q_{gain/loss}$  = cumulative heat load, ( $W \cdot h/m^2$ );

$q_{gain/loss}$  = heat gain/loss flux, ( $W/m^2$ );

$t_1, t_2$  = start and end time of calculation, (s);

The heat gain/loss flux ( $q_{gain/loss}$ ) comprises total, sensible, and latent heat flux:

$$q_{total} = q_{sensible} + q_{latent} \quad (4.43)$$

$$q_{sensible} = h_{t,i}(T_{x=l} - T_i) \quad (4.44)$$

$$q_{latent} = L_v h_{m,i}(p_{v,x=l} - p_{v,i}) \quad (4.45)$$

where

$q_{\text{total}}$  = total heat gain/loss flux, (W/m<sup>2</sup>);

$q_{\text{sensible}}$  = sensible heat gain/loss flux, (W/m<sup>2</sup>);

$q_{\text{latent}}$  = latent heat gain/loss flux, (W/m<sup>2</sup>).

The hygric and thermal performances comprise cumulative moisture load ( $J_{\text{gain/loss}}$ ) over a time duration of  $t_2 - t_1$ , partial water vapor pressure amplitude and temperature amplitude:

$$J_{\text{gain/loss}} = \int_{t_1}^{t_2} j_{\text{gain/loss}} dt \quad (4.46)$$

$$p_{v \text{ amp}} = (p_{v \text{ peak}} - p_{v \text{ valley}})/2 \quad (4.47)$$

$$T_{\text{amp}} = (T_{\text{peak}} - T_{\text{valley}})/2 \quad (4.48)$$

where

$J_{\text{gain/loss}}$  = cumulative moisture load, (kg/m<sup>2</sup>);

$j_{\text{gain/loss}}$  = moisture gain/loss flux, (kg/(m<sup>2</sup>·s));

$p_{v \text{ amp}}$  = partial water vapor pressure amplitude, (Pa);

$T_{\text{amp}}$  = temperature amplitude, (°C);

$p_{v \text{ peak}}, p_{v \text{ valley}}$  = peak and valley partial water vapor pressure, (Pa);

$T_{\text{peak}}, T_{\text{valley}}$  = peak and valley temperature, (°C);

The moisture gain/loss flux ( $j_{\text{gain/loss}}$ ) between the envelope and the interior is driven by the concentration difference in partial water vapor pressure, which can be expressed by

$$j = h_{m,i}(p_{v,x=l} - p_{v,i}) \quad (4.49)$$

## 4.8 Results, analysis, and discussion

In Section 4.8.1, the impact of moisture transfer on the envelope is analyzed with respect to the configuration baseline. The relationship between energy, thermal, and hygric performance is analyzed in Section 4.8.2. Sections 4.8.3 consider the impact of the PCM's location in the envelope. In these sections, the results of the numerical calculations for the third year are used. The heat and moisture loads for seven representative days in summer and winter (see Fig. 4.5 (a) and (b)) are presented. When the figures express the evolution of the parameters over time (such as Fig. 4.6 (a), Fig. 4.7, Fig. 4.8 (b)), the two-day evolution from a single week is presented for better observation. In Section 4.8.4, energy and hygric performance are evaluated based on the calculations for the entire third year.

### 4.8.1 Impact of moisture transfer on energy and hygrothermal performance

To study the impact of moisture transfer, the numerical results calculated using the heat and moisture transfer (HMT) model and the heat transfer (HT) model were compared based on the configuration baseline. Table 4.3 shows the difference between the HMT and HT models. The HMT model considered the heat and moisture transfer in the HC and heat transfer in the PCM. The HT model considered only heat transfer in the HC and the PCM. The thermophysical parameters of the HC in the HT model were the constant terms shown in Table 4.1.

	HMT model	HT model
PCM	Heat transfer	Heat transfer
HC	Heat and moisture transfer	Heat transfer

Table 4.3 Difference between the HMT and HT models

Fig. 4.6 (a) presents the heat fluxes of the HMT and HT models in summer and winter. By

focusing on sensible heat in the HMT model and total heat in the HT model, it can be seen that their variations and values are similar. The slight difference between these is caused by the thermophysical parameters of HC: The thermal conductivity and heat capacity of HC are higher in the HMT model due to the consideration of moisture. In addition, these values are both lower than the total heat flux in the HMT model. As for the latent heat flux in the HMT model, it is small and fluctuates around the x-axis ( $0 \text{ W/m}^2$ ) in both seasons.

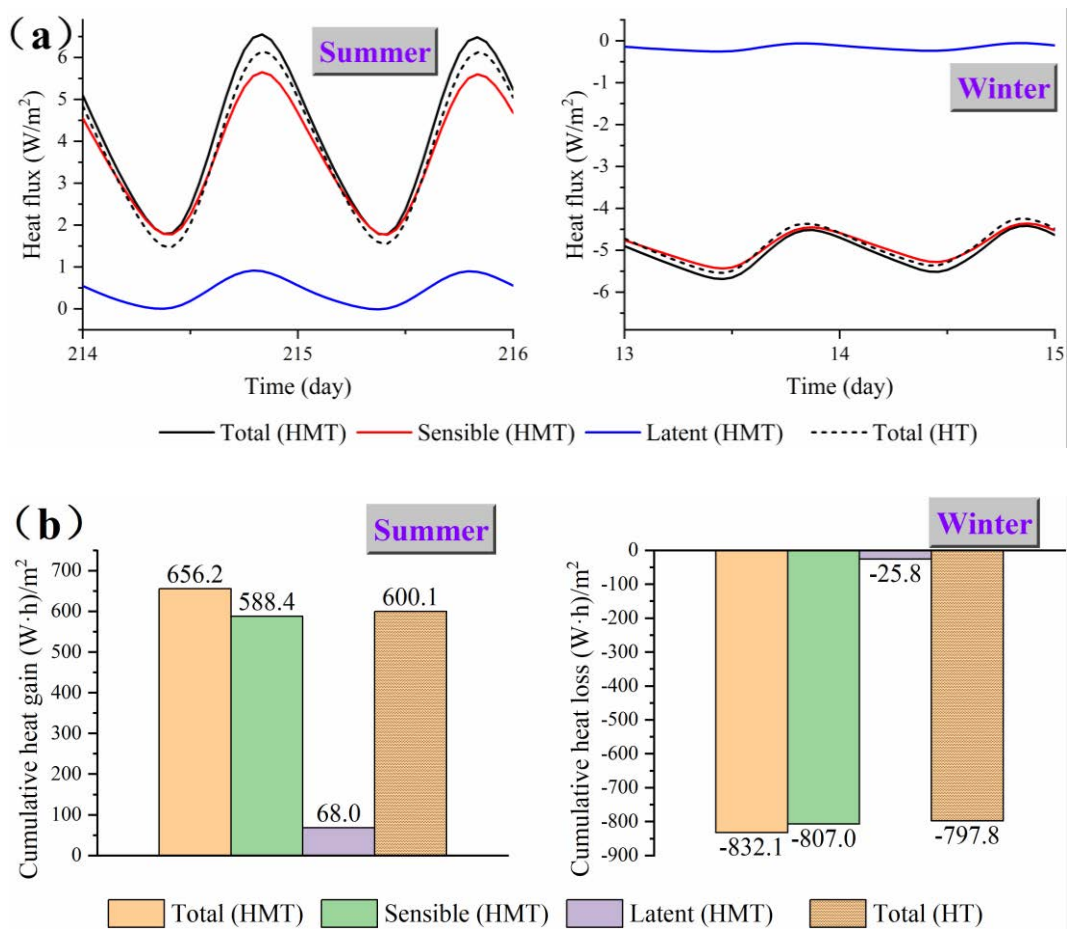


Fig. 4.6. Comparison between HMT and HT models: (a) heat fluxes; (b) heat loads

The heat loads of the HMT and HT models are shown in Fig. 4.6 (b). The total heat load in the HT model is less than that in the HMT model for both seasons, indicating that the total heat load was

underestimated without considering moisture transfer. Further, since the sensible heat in the HMT model is close to the total heat in the HT model, and the total heat is the superposition of the sensible and latent heats in the HMT model, it can be inferred that the latent heat load is the main reason for the total heat load difference between the two models. Based on the calculations, the latent heats are 10.4% and 3.1% of the total heat load in summer and winter, respectively, showing that the impact of latent heat on the total heat is greater in summer.

To sum up, moisture transfer is crucial since it correlates with the indoor humid environment and significantly affects the latent/total heat and, thus, the energy performance.

#### **4.8.2 Relationship between energy, thermal, and hygric performance**

Fig. 4.7 illustrates the transformation between moisture transfer and latent heat transfer by analyzing the relationship between partial water vapor pressure, moisture flux, and latent heat flux. The driving force for moisture transfer between the envelope surface and the interior is the concentration difference in partial water vapor pressure, and the partial water vapor pressure on the interior surface is jointly affected by temperature and relative humidity, with temperature playing the dominant role. On the one hand, the partial water vapor pressure variation is highly consistent with temperature variation, indicating the dominant role of temperature. On the other hand, a slight time delay (1.6 and 1.7 h in summer and winter, respectively) is observed between changes in partial water vapor pressure and changes in temperature, suggesting a weak effect of relative humidity on partial water vapor pressure.

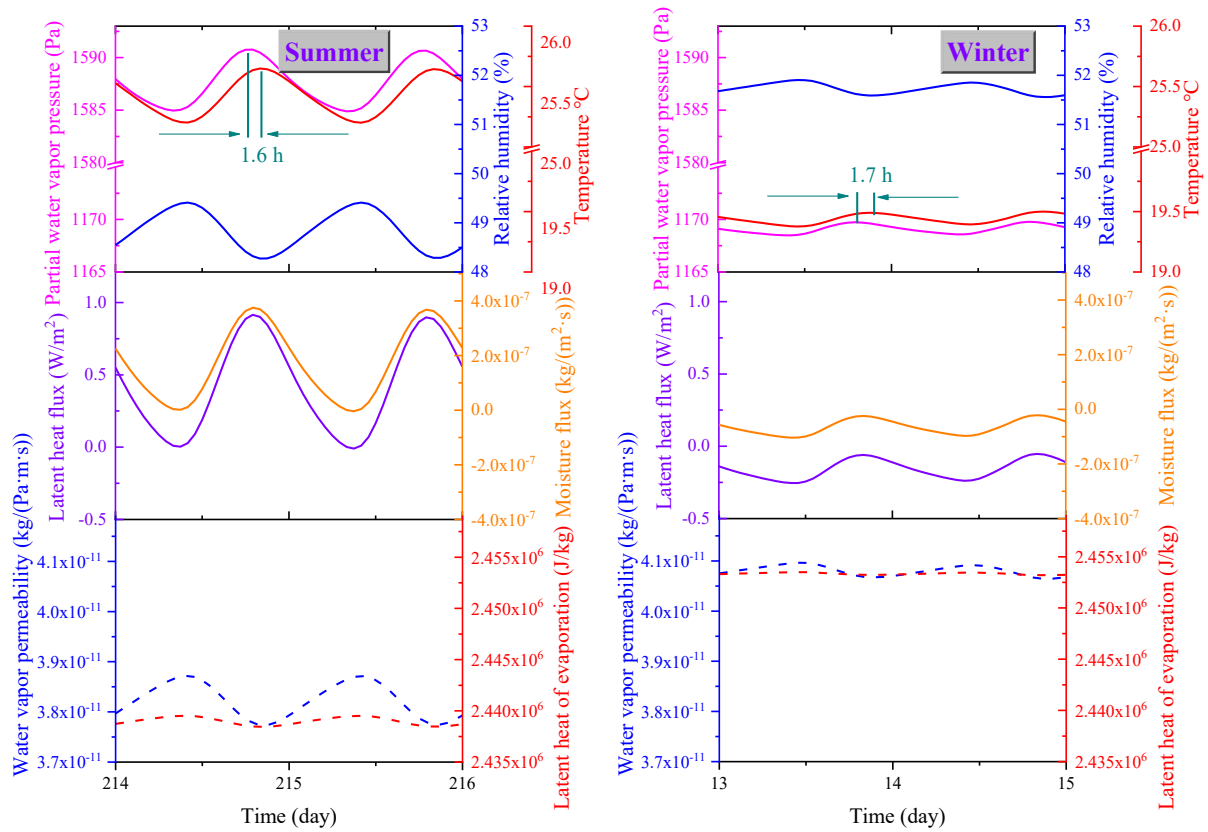


Fig. 4.7. Relationship between temperature, relative humidity, partial water vapor pressure, moisture flux, and latent heat flux

Concerning partial water vapor pressure, moisture flux, and latent heat flux, they show similar variation trends. The conversion factors between the partial water vapor pressure gradient and moisture flux and between the moisture flux gradient and latent heat flux are water vapor permeability (a function of relative humidity) and latent heat of evaporation (a function of temperature), respectively. In summer, the water vapor permeability fluctuates from  $3.8 \times 10^{-11}$  to  $3.9 \times 10^{-11}$  kg/(Pa·m·s) and the latent heat of evaporation fluctuates from  $2.438 \times 10^6$  to  $2.440 \times 10^6$  J/kg, while in winter, they fluctuate even less. Since the orders of magnitude of water vapor permeability and latent heat of evaporation are lower than those of the partial water vapor pressure gradient and the moisture flux gradient, respectively, they can be regarded as constant, which explains the similar variation trends between partial water vapor pressure, moisture flux, and latent heat flux. Thus, the moisture flux/load

is highly correlated with the latent heat flux/load, and both are mainly dominated by temperature.

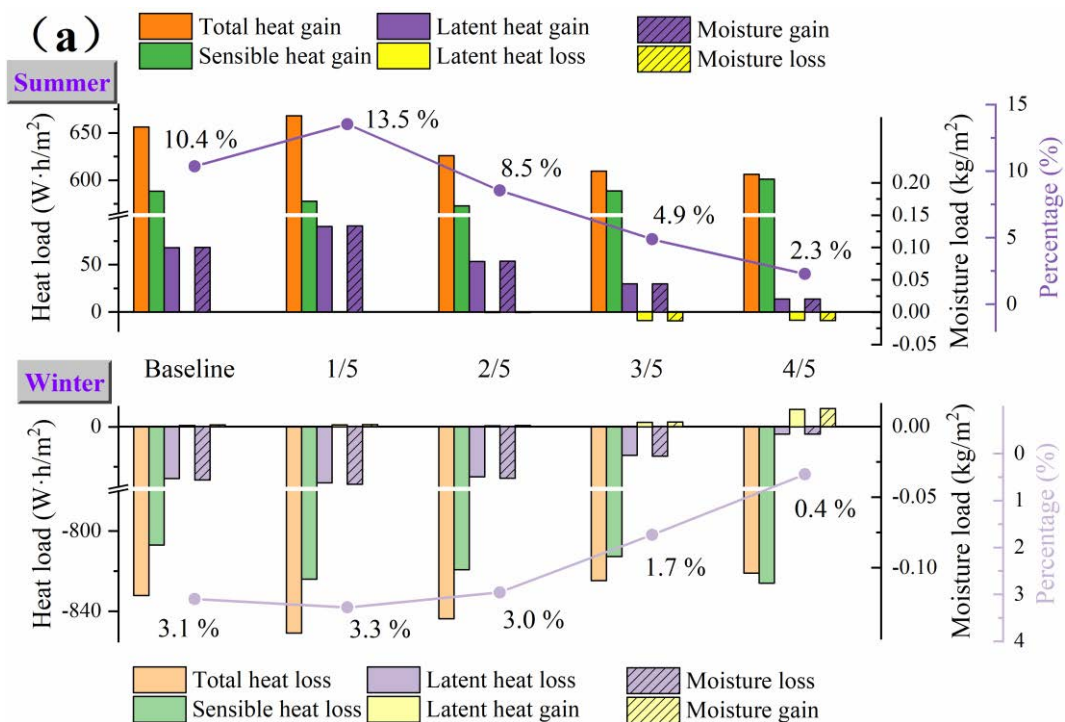
### 4.8.3 Impact of PCM and its location on energy and hygrothermal performance

The energy and hygrothermal performance of different configurations is investigated in this subsection. Fig. 4.8 (a) shows the cumulative heat load and moisture load in summer and winter for the five configurations. For the integrated configurations, the total heat gain decreases with the movement of the PCM toward the interior, and its values are mostly lower than that of the configuration baseline. Fig. 4.8 (c) summarizes the heat load reductions of the integrated configurations compared to the configuration baseline. In summer, the total heat gain is reduced for all integrated configurations except configuration 1/5, since the PCM placed on the outermost layer absorbs/releases more energy than does the HC as explained in Section 3.5.4. The heat load reductions for configurations 2/5, 3/5, and 4/5 are 3.6%, 6.6%, and 8.2%, respectively. In winter, the heat load is less affected by the PCM, with a reduction of less than 1.5%. Notably, as illustrated in Fig. 4.8 (a), configuration 4/5 has the largest sensible heat load but the smallest total heat load in both seasons. Moreover, the latent heat difference among the configurations is higher than the sensible heat difference: The maximum difference among the latent heat loads is about 3.6 and 1.3 times that for sensible heat loads in summer and winter, respectively. This indicates that the latent heat loads play a crucial role in determining the magnitude of the total heat loads in different configurations; as the PCM moves toward the interior, the latent heat and its percentage (ratio of latent heat load to total heat load; right axis) decrease. The latent heat percentages for configuration 4/5 (2.3% in summer and 0.4% in winter) are much smaller than those for configuration 1/5 (13.5% in summer and 3.3% in winter).

Several prior studies have reported similar results in terms of PCM location [165, 167, 267]. However, these studies focused only on the heat transfer and thermal performance (sensible heat load) of the envelope. In this study, due to the presence of hygroscopic HC, the latent heat load caused by

moisture transfer increases the complexity of the total heat load. If only the sensible heat load is considered, the configurations with the smallest heat gain in summer and the smallest heat loss in winter are 2/5 and 3/5, respectively, either of which would undoubtedly be the wrong choice. When considering the effect of latent heat load, the optimal PCM location moves to the interior in both seasons because of the decreasing latent heat percentage. Therefore, when evaluating the energy performance of an envelope that can transfer moisture with the interior environment, the superposition effect of the sensible and latent heat loads, rather than just sensible heat loads, needs to be considered.

Concerning the moisture loads, they are highly consistent with the latent heat loads. For the integrated configurations, the closer the PCM is to the interior, the lower the moisture gain in summer and the lower the moisture loss in winter. Further, the difference between the moisture gain and moisture loss decreases as the PCM moves closer to the interior, which is favorable in terms of the moisture equilibrium within the HC.



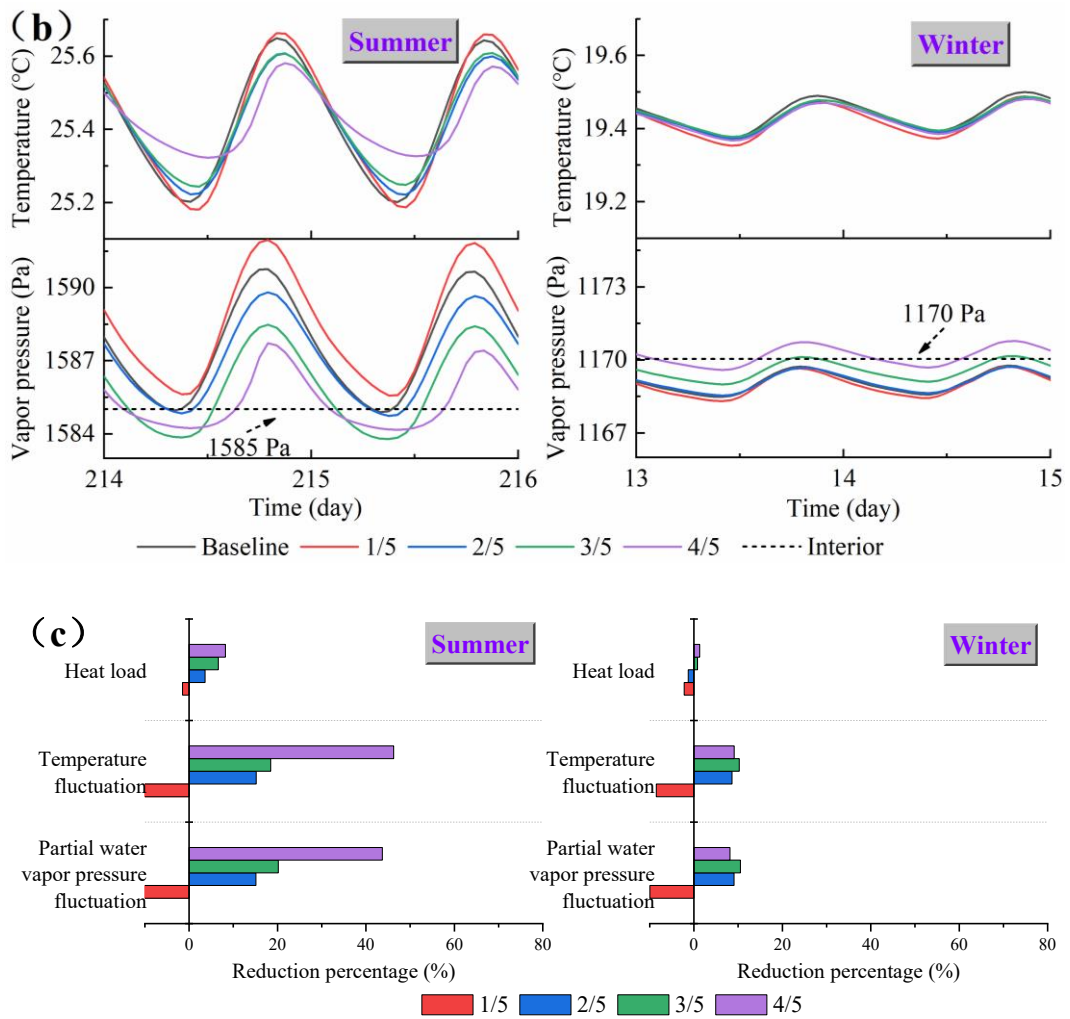


Fig. 4.8. Impact of PCM presence and location: (a) cumulative heat load and moisture load; (b) variation of temperature and partial water vapor pressure; (c) reduction of heat load, temperature fluctuation, and partial water vapor pressure fluctuation compared to configuration baseline

Fig. 4.8 (b) shows the variations of temperature and partial water vapor pressure and explains the different moisture and latent heat loads among the configurations. First, the temperature and partial water vapor pressure amplitudes decrease with the presence of the PCM, except in configuration 1/5; these also decrease as the PCM moves closer to the interior, especially in summer. Fig. 4.8 (c) shows the temperature and partial water vapor pressure amplitude reductions compared to the configuration baseline. In summer, the temperature fluctuations in configurations 2/5, 3/5, and 4/5 are reduced by

15.2%, 18.5%, and 46.3%, respectively, and the partial water vapor pressure fluctuations are reduced by 15.1%, 20.2%, and 43.7%, respectively. In winter, the corresponding reductions in configurations 2/5, 3/5, and 4/5 are small and similar, with a mean reduction of 9.3%. Hence, configurations 2/5, 3/5, and 4/5 can reduce indoor temperature and relative humidity fluctuations to improve thermal and hygric comfort, especially in summer.

Furthermore, the partial water vapor pressure moves gradually toward the reference line (interior) from configuration 1/5 to configuration 4/5, meaning that their values gradually decrease in summer and increase in winter. In particular, the curves for configurations 3/5 and 4/5 move to such a situation that they fluctuate repeatedly around the reference line, especially for configuration 4/5. As explained previously, the moisture flux and latent heat flux between the envelope and the interior environment are affected by partial water vapor pressure. Therefore, with the movement of the PCM closer to the interior, the moisture and latent heat loads' gains in summer and losses in winter gradually decrease.

In sum, among the configurations, configuration 4/5 shows the greatest advantage in terms of improving indoor hygrothermal comfort and saving energy.

#### **4.8.4 Evaluation of annual energy and hygric performance**

Fig. 4.9 shows the annual heat loads of the HMT and HT models. For the HMT model, the heat loads for the integrated configurations decrease as the PCM moves closer to the interior. Most of these are lower than the heat loads for the configuration baseline, and the reduction of heat gain is more obvious than the reduction of heat loss. Configuration 4/5 has the smallest heat gain and loss, and the reduction of heat gain is 13.3% compared to the baseline, which is much higher than the heat loss reduction of only 0.5%. Hence, PCMs are more capable of reducing heat gain, and the closer the PCM to the interior, the more the heat gain reduction.

Concerning the difference between the HMT and HT models, the heat gains and losses are

always higher in the HMT model than in the HT model due to moisture transfer. Thus, failing to consider moisture transfer leads to an underestimation of the annual heat load, which is reflected by the heat load reduction percentage in the HT model (right axis) compared to the HMT model. The heat gain underestimation for the configuration baseline is as high as 12.1%. For the integrated configurations, the underestimation decreases as the PCM moves toward the interior, with the lowest underestimation being 2.6% for configuration 4/5. For heat loss, the underestimations are all below 5%.

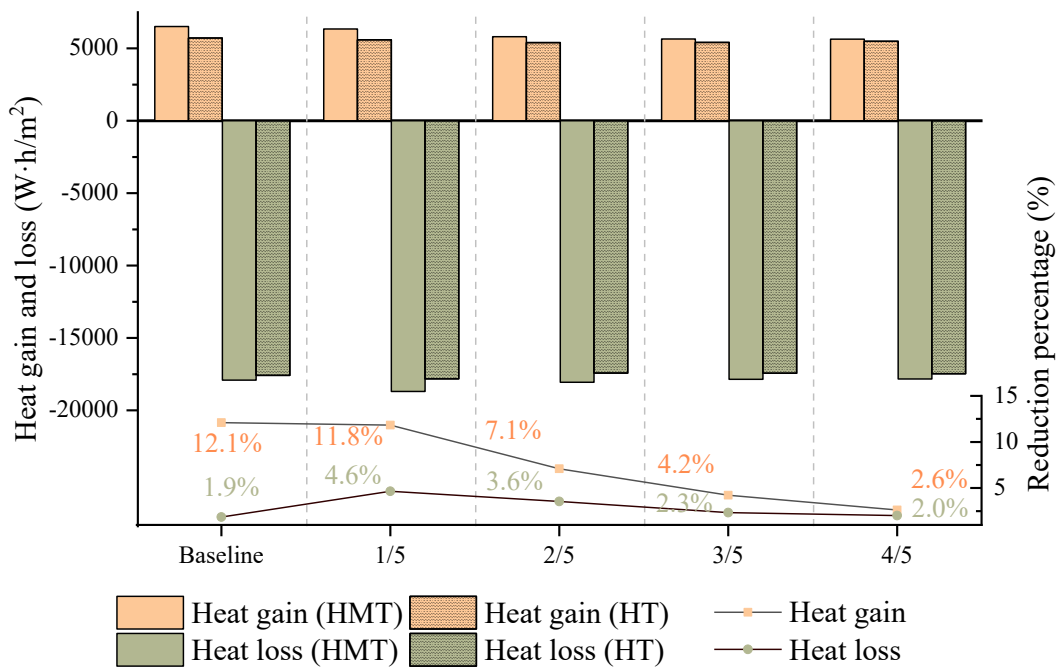


Fig. 4.9. Annual heat gain and loss for HMT and HT models

Fig. 4.10 presents the annual heat load expressed in a seasonal format. Concerning the temperature change over the year first, it can be observed that heat gain is predominant in summer, while heat loss is predominant in spring, autumn, and winter. In any event, configuration 4/5 is noteworthy in almost every season. In summer, configuration 4/5 has the smallest heat gain and the largest energy savings of all configurations. Compared to the configuration baseline, the heat gain

reductions are 0.34%, 5.93%, 11.0%, and 11.5% for configurations 1/5, 2/5, 3/5, and 4/5, respectively. In winter, configuration 4/5 also has the smallest heat loss, but the heat loss reduction is less pronounced than in summer, with 0.70% energy savings compared to the configuration baseline. Similarly, in spring and autumn, configuration 4/5 also slightly reduces heat loss.

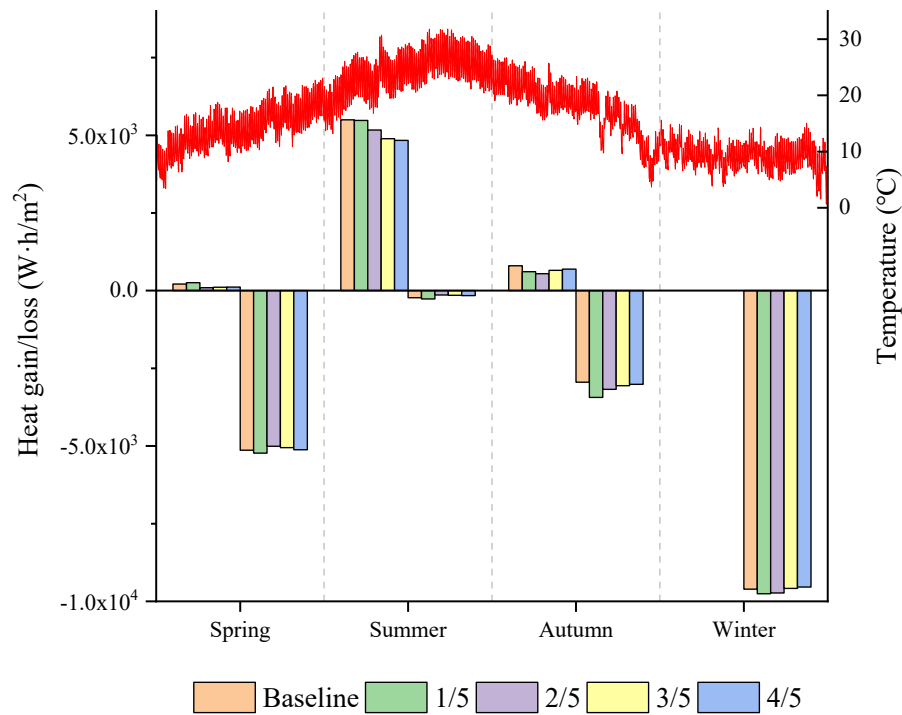
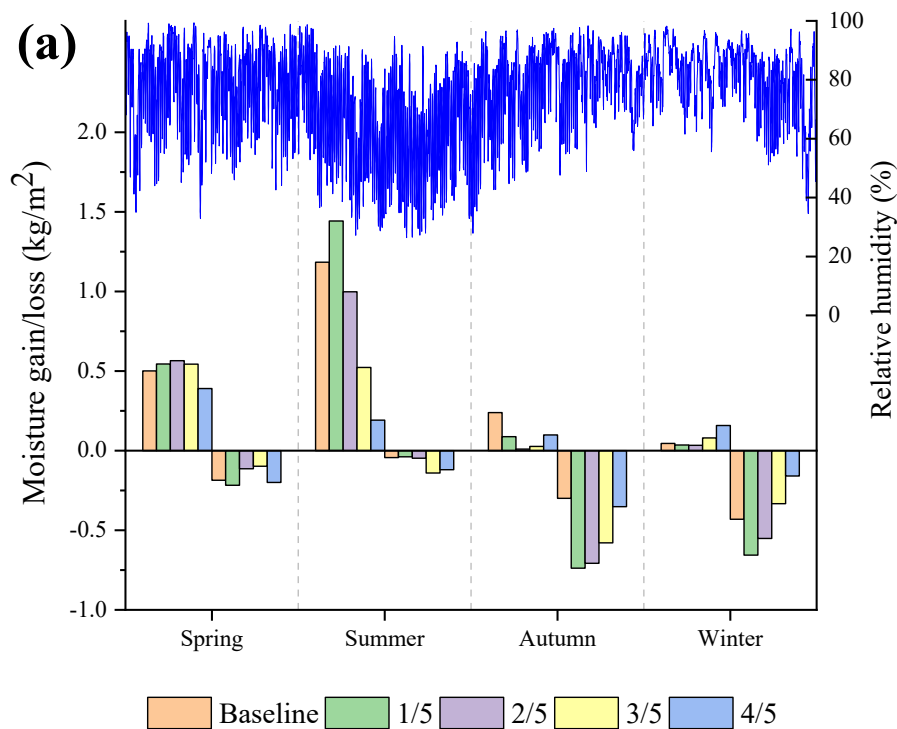


Fig. 4.10. Annual heat load for different configurations

Fig. 4.11 (a) shows the annual moisture load expressed in a seasonal format. The moisture performance is evaluated from two aspects. First, the climate relative humidity is moderate in summer (average relative humidity of 63.9%) and high in spring, autumn, and winter (average relative humidities of 77.9%, 78.9%, and 81.5%, respectively). Hence, an ideal situation for the interior would involve less moisture gain in summer and more moisture loss in spring, autumn, and winter. From this point of view, configuration 4/5 is the optimum configuration. Second, the moisture content within the HC in contact with the interior needs to be well equilibrated, which requires a slight difference between

moisture gain and loss. The configuration baseline and configurations 1/5 and 2/5 have almost no moisture loss in summer and almost no moisture gain in winter. Similarly, configurations 2/5 and 3/5 have almost no moisture gain in autumn. In contrast, configuration 4/5 better meets this requirement in all seasons as it has both moisture gain and loss, and the difference between moisture gain and loss is smaller than in the other configurations. Fig. 4.11 (b) shows the seasonal and annual net moisture load, which is calculated by the difference between moisture gain and loss. The net moisture load of configuration 4/5 is the smallest in spring, summer, winter, and even the whole year. The configuration baseline has the highest annual net moisture load, which means that the configuration baseline hardly ensures the moisture equilibration within the HC. For the integrated configuration, the annual net moisture load decreases with the PCM towards the interior. As a result, configuration 4/5 has the smallest annual net moisture load with a value of only 0.0096 kg/m<sup>2</sup>, which ensures the moisture equilibration within the HC.

Therefore, the configuration 4/5 is valuable in terms of annual energy and hygric performance.



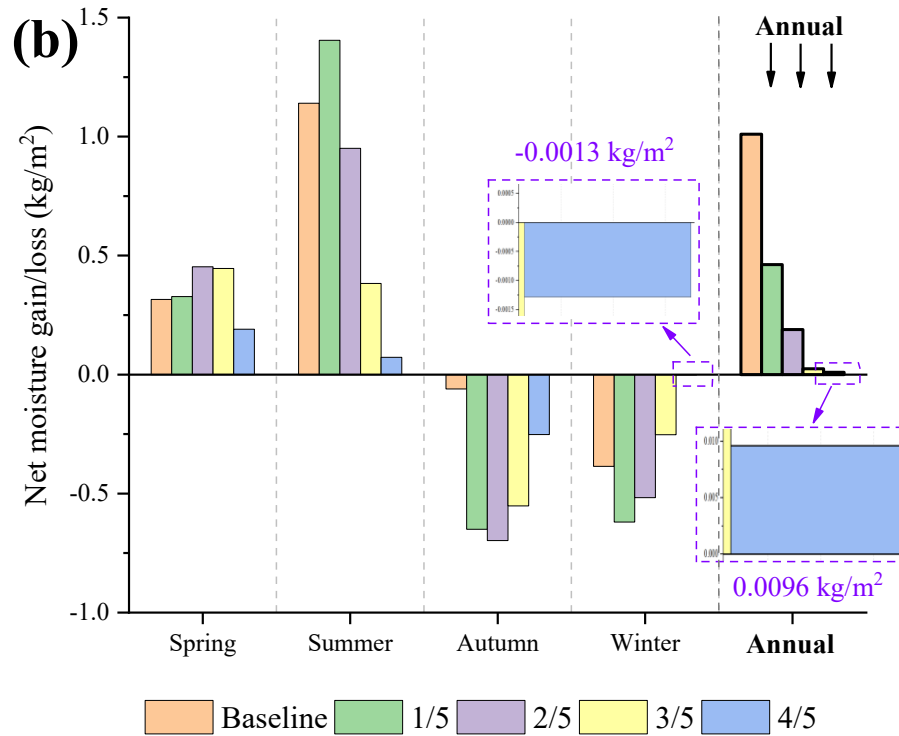


Fig. 4.11. Annual hygric performance for different configurations: (a) moisture load and (b) net moisture load

## 4.9 Conclusion

In this chapter, the integrated envelope assembled by PCM and HC is further investigated by numerical methods based on the preliminary experimental study in Chapter 3. More configurations are proposed according to the location of the PCM in the HC. The configurations with the PCM in direct contact with the indoor environment are specifically avoided due to the moisture impermeability of PCM. The mathematical model of the integrated envelope that couples heat and moisture transfer and considers the temperature dependence of HC's hygroscopic characteristic is proposed and validated based on the experimental results. The experimental and simulation results show high agreement, with small relative errors (less than 7.5%), RMSEs (less than 0.6 °C and 2.2% for temperature and relative humidity), and  $CV_{(RMSE)S}$  (less than 4%). Based on the validated model, the thermal, hygric, and energy performance of this integrated envelope under real climate conditions (Rome, Italy) is studied. The

key findings and conclusions of the study are presented below.

The high coupling between moisture and heat transfer in the HC affects the energy and hygrothermal performance of the integrated envelope. On the one hand, temperature dominates the partial water vapor pressure and affects the variation of moisture flux/load, which ultimately affects the indoor thermal and hygric environment. On the other hand, moisture transfer is important for energy performance since the moisture load affects the latent heat load and thus the total heat load. The latent heats are 10.4% and 3.1% of the total heat load in summer and winter, respectively.

The location of PCM has a great impact on the energy and hygrothermal performance of the integrated envelope. As the PCM moves toward the interior, the latent heat percentage decrease from 13.5% to 2.3% in summer and from 3.3% to 0.4% in winter, which makes configuration 4/5 to have the lowest heat gain in summer and heat loss in winter. Compared to the configuration baseline, the total heat load, temperature amplitude, and partial water vapor pressure amplitude of configuration 4/5 are reduced by 8.2%, 46.3%, and 43.7%, respectively, in summer and 1.3%, 9.1%, and 8.2%, respectively, in winter. Thus, placing the PCM close to the interior is recommended as the energy and hygrothermal performance are both improved.

From a year-round perspective, the PCM reduces the heat gain in most configurations compared to the configuration baseline, especially configuration 4/5, which showed the biggest annual heat gain reduction, 13.3%. In contrast, the PCM hardly affects annual heat loss with the heat loss reduction of only 0.5% compared to the configuration baseline. In addition, the annual energy performance comparison between HMT and HT models also emphasizes the importance of moisture transfer. Neglecting moisture transfer leads to an underestimation of annual heat gain by 2.6% to 12.1% and of annual heat loss by 1.9% to 4.6% for different configurations. Moreover, configuration 4/5 is noteworthy in every season. On the one hand, it saves 11.5% and 0.7% of energy in summer and winter, respectively, compared to the baseline configuration. On the other hand, it shows adaptability in

dealing with climatic relative humidity while guaranteeing moisture equilibrium within the HC with an annual net moisture load of  $0.0096 \text{ kg/m}^2$ .

Overall, this section discussed more integrated configurations, conducted a comprehensive analysis of the energy and thermal performance, and explored more advantages of the integrated envelopes. On this basis, it is necessary to further conduct the parametric analysis and practical application risk of the integrated envelope.

# **Chapter 5      Parametric analysis and application risk evaluation of integrated envelope**

## **5.1    Objectives of parametric analysis and risk evaluation**

In Chapter 4, a detailed study is conducted on the thermal, hygric, and energy performance of the integrated envelopes. The results highlight more advantages of the integrated envelope by studying the impact of PCM and its location on performance. In addition to the location of the PCM, some other properties such as the thickness, latent heat, and phase transition range of the PCM also have an impact on the thermal performance of the envelope (see Section 2.3.3). Therefore, it is interesting and meaningful to conduct the parametric analysis by studying the impact of PCM properties on the energy and hygrothermal performance of the integrated envelope.

Furthermore, according to the phenomena described in Section 3.4.2, the overall increasing or decreasing trend of relative humidity at some key locations proves that there is a potential moisture accumulation in the integrated envelope due to the moisture impermeability of the PCM. If the relative humidity in these key locations is chronically too high, it creates a risk of condensation, which is certainly disadvantageous for the service life of the integrated envelope. In addition, once the relative humidity is too high and the temperature is suitable, this will promote the mold growth, which affects the performance of the envelope and even poses a threat to the health of the occupants. Based on these reasons, it is necessary to investigate the characteristics and laws of the long-term variations in relative humidity within the integrated envelope. Therefore, the condensation and mold growth risks were evaluated to determine the application risk in this chapter.

Based on the above motivations, the main objectives of this chapter are introduced as follows:

- 1) Conduct the parametric analysis of the integrated envelope from the perspective of the PCM properties, i.e., thickness, latent heat, and phase transition range.
- 2) Study the law of variation in relative humidity and evaluate the application risk of the integrated envelope, i.e., condensation and mold growth risk.

## 5.2 Methodology of parametric analysis and application risk evaluation

### 5.2.1 Methodology of parametric analysis

The thickness, phase transition range, and latent heat of PCM were shown to affect the thermal performance of PCM. Therefore, parametric analysis of the integrated envelope was conducted from these properties of PCM. The parametric analysis was based on the configuration 4/5 with PCM placed 6 cm from the interior, who was proven to be the optimal configuration in Section 4.8.

The physical properties of the base PCM refer to Chapter 4 with a thickness of 0.01m, a latent heat of 90.4 kJ/kg, and a phase transition range of 24–28 °C. On this basis, three additional phase transition ranges (16–20, 20–24, and 28–32 °C), three additional latent heats (62.9, 117.8, and 145.3 kJ/kg), and two additional thicknesses (0.02 and 0.03 m) were considered. The equations for the effective specific heat capacities and effective thermal conductivities of these PCMs from solid to liquid phase are expressed as follows:

$$C^* = \begin{cases} C_s & T < T_{ini} \\ \frac{C_s + C_l}{2} + \beta \times \exp\left(-1.67 \times \left(T - \frac{T_{ini} + T_{fin}}{2}\right)^2\right) & T_{ini} \ll T \ll T_{fin} \\ C_l & T > T_{fin} \end{cases} \quad (5.1)$$

$$\lambda^* = \begin{cases} \lambda_s & T < T_{ini} \\ \lambda_l + 0.01 \times (T_{fin} - T) & T_{ini} \ll T \ll T_{fin} \\ \lambda_l & T > T_{fin} \end{cases} \quad (5.2)$$

The initial and final temperatures ( $T_{ini}$  and  $T_{fin}$ ) of the phase transition range for the four cases are listed in Table 5.1.  $\beta$  is the factor that determines latent heat level, with the relationship between

$\beta$  and latent heat shown in Table 5.2. Therefore, by changing the  $T_{ini}$ ,  $T_{fin}$ , and  $\beta$  in the above equations, the different latent heats and phase transition ranges of PCM can be obtained. Fig. 5.1 plots the curves for the effective specific heat capacities and effective thermal conductivities of these PCMs.

Phase transition range	16–20 °C	20–24 °C	24–28 °C	28–32 °C
$T_{ini}$ (°C)	16	20	24	28
$T_{fin}$ (°C)	20	24	28	32

Table 5.1 Initial and final temperature of different phase transition ranges

Latent heat of PCM (kJ/kg)	62.9	90.4	117.8	145.3
$\beta$	40	60	80	100

Table 5.2 Relationship between  $\beta$  and latent heat of PCM

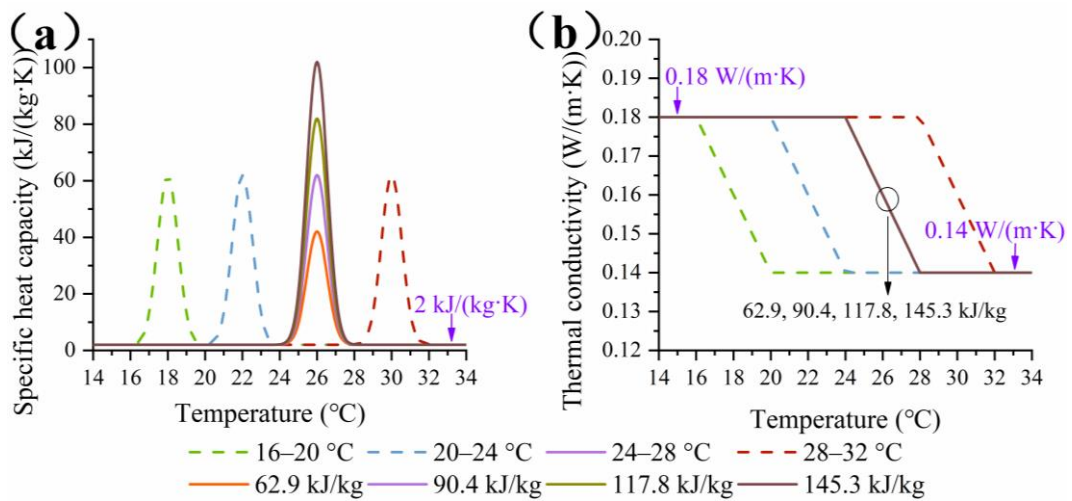


Fig. 5.1. Thermal properties of PCMs with different phase transition ranges and latent heats: (a) specific heat capacity; (b) thermal conductivity

Table 5.3 shows the detailed PCM properties settings used for parametric analysis in the following

study. When one of these properties is studied, the remaining two properties remain unchanged.

	Thickness (Section 5.3.1)	Latent heat (Section 5.3.2)	Phase transition range (Section 5.3.3)
Thickness (m)	0.01, 0.02, 0.03	0.01	0.01
Latent heat (kJ/(kg·K))	90.4	62.9, 90.4, 117.8, 145.3	90.4
Phase transition range (°C)	24–28	24–28	16–20, 20–24, 24–28, 28–32

Table 5.3 PCM properties settings for parametric analysis

The main metric parameters concerned in parametric analysis are the total heat load, temperature, and partial water vapor pressure fluctuations (refer to Section 4.7), as well as their reductions compared to the configuration baseline.

### 5.2.2 Methodology of application risk evaluation

Condensation risk evaluation was based on ASHRAE Standard 160-2009 [268], which includes the following three criteria for running average surface temperature between 5 and 40 °C:

- 1) The 30-day running average surface relative humidity is less than 80%;
- 2) The 7-day running average surface relative humidity is less than 98%;
- 3) The 1-day running average surface relative humidity is less than 100%.

It has been noted that these criteria should be guaranteed at the interior surface and the interfaces between the layers. This logic does not apply to the exterior surface due to its direct exposure to the exterior environment.

Mold growth risk evaluation is based on an empirical VTT model developed by Hukka and Viitanen [269], by which a critical relative humidity ( $\varphi_{crit}$ ) can be found, defined as the minimum

relative humidity at which mold growth will occur if the material is exposed for a long enough period of time.

$$\varphi_{crit} = \begin{cases} -2.67 \times 10^{-3} \times T^3 + 1.60 \times 10^{-1} \times T^2 - 3.13 \times T + 100, & T \leq 20 \text{ }^\circ\text{C} \\ 80, & T > 20 \text{ }^\circ\text{C} \end{cases} \quad (5.3)$$

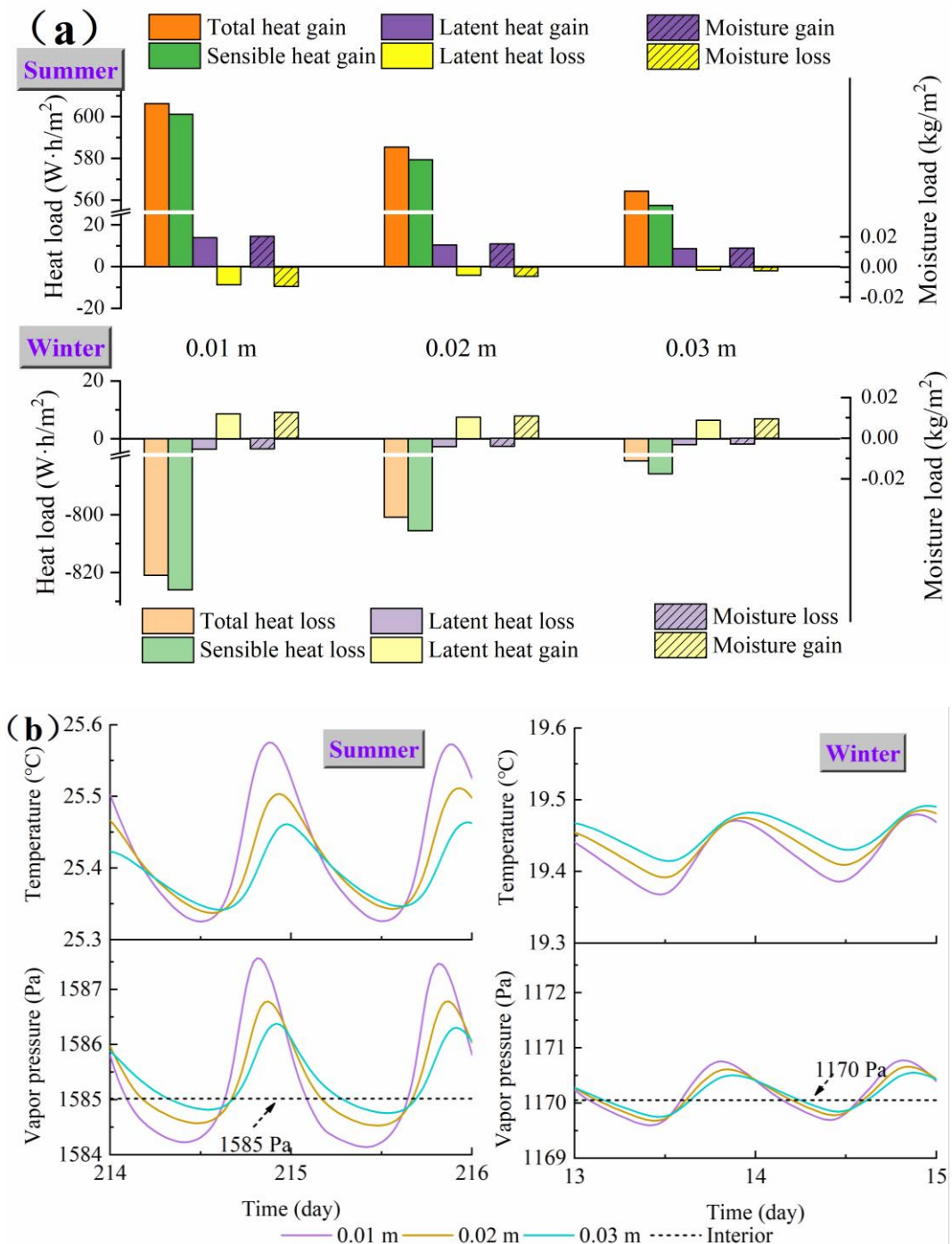
## 5.3 Parametric analysis of integrated envelope

### 5.3.1 Impact of PCM thickness

The impact of different PCM thicknesses (0.01, 0.02, and 0.03 m) on the energy and hygrothermal performance of the integrated envelope is investigated in this subsection. Fig. 5.2 (a) shows the heat and moisture loads for different PCM thicknesses. Fig. 5.2 (b) shows the variations of temperature and partial water vapor pressure. With the increase in PCM thickness, the total heat/moisture load, temperature fluctuation, and partial water vapor pressure fluctuations all decrease, especially in summer. This is because the increase in PCM thickness enhances the heat storage capacity and thermal resistance of the envelope, and the thermal storage capacity enhancement is greater in summer, thus dampening the heat transfer between the exterior and interior.

Fig. 5.2 (c) shows the percentage reduction in heat load and partial water vapor pressure/temperature fluctuations for PCM thicknesses of 0.01, 0.02, and 0.03 m, compared to the configuration baseline. It can be observed that a thicker PCM is more conducive to improving energy and hygrothermal performance, especially in summer. In summer, the heat loads of 0.01, 0.02, and 0.03 m are reduced by 7.8%, 10.5%, and 13.9%, respectively, and the partial water vapor pressure/temperature fluctuations are reduced by more than 43.6%, 64.2%, and 76.5%, respectively. In winter, the reductions are 1.2%, 2.4%, and 5.0% for heat load and approximately 8.6%, 25.8%, and 38.8% for the partial water vapor pressure/temperature fluctuations. Although the reductions are smaller in winter than in summer, they still contribute to energy savings and the stability of indoor

temperature and relative humidity. Hence, the energy and hygrothermal performance of the integrated envelope can be improved by increasing PCM thickness, especially in summer.



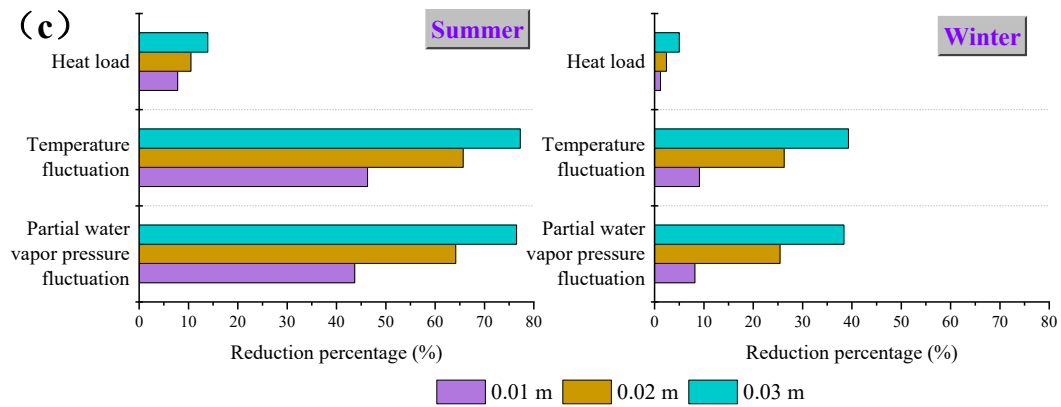


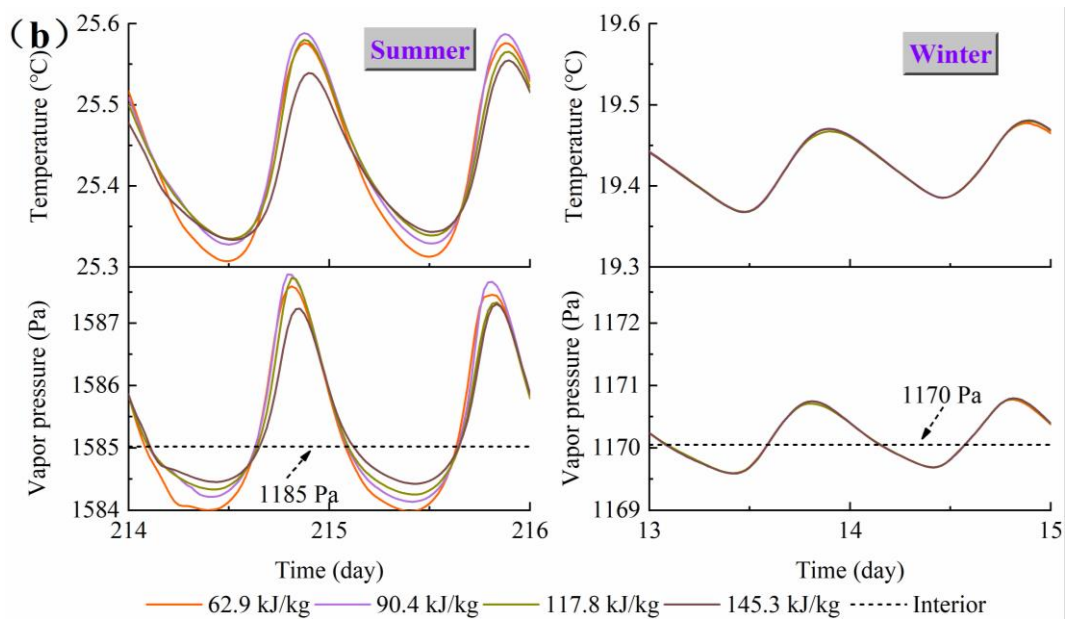
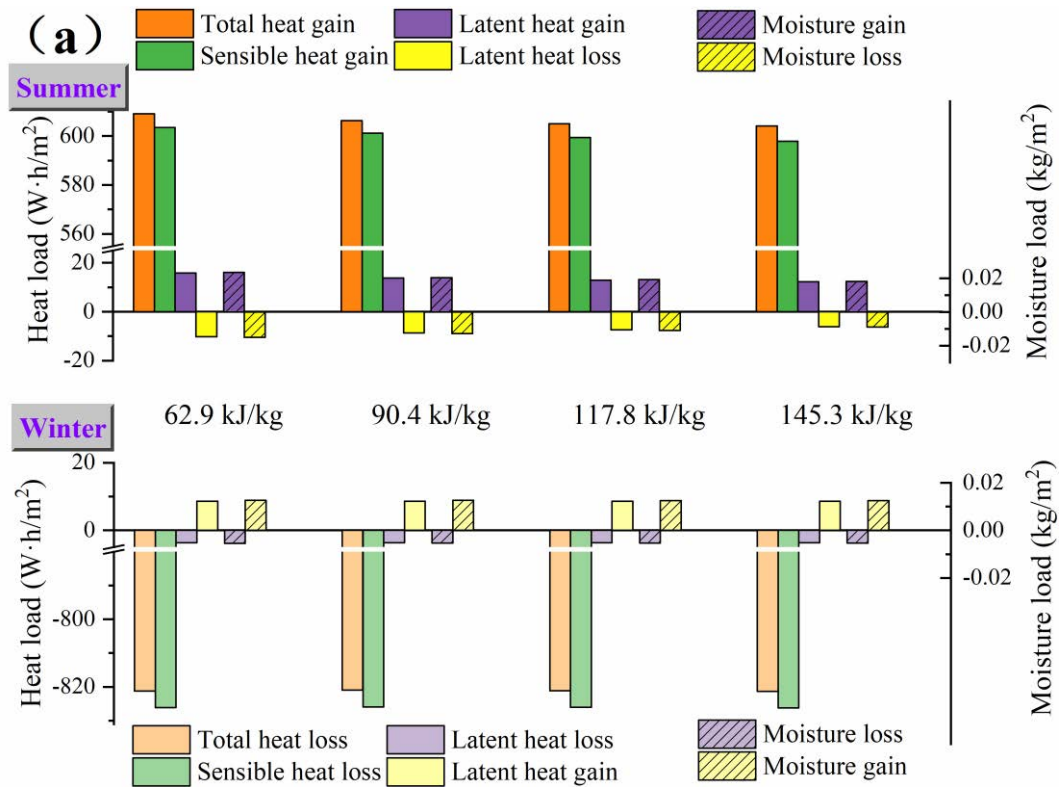
Fig. 5.2. Impact of PCM thickness: (a) cumulative heat load and moisture load; (b) variation of temperature and partial water vapor pressure; (c) reduction of heat load, temperature fluctuation, and partial water vapor pressure fluctuation compared to configuration baseline

### 5.3.2 Impact of PCM latent heat

In this subsection, the impact of four different latent heats, 62.9, 90.4, 117.8, and 145.3 kJ/kg, on the energy and hygrothermal performance is studied. Fig. 5.3 (a) shows the heat and moisture load for different PCM latent heats. In summer, both the heat and moisture loads decrease with the increase in latent heat. As presented in Fig. 5.3 (c), the heat load reductions for 62.9, 90.4, 117.8, and 145.3 kJ/kg are 7.1%, 7.5%, 7.7%, and 8.0%, respectively, compared to the baseline. However, in winter, the heat loads are less affected by the PCM latent heat load, with almost identical reductions of less than 1.5%. This is because the PCM with a phase transition range of 24–28 °C is in a solid state and thus not activated in winter.

Fig. 5.3 (b) presents the variations of temperature and partial water vapor pressure. In summer, a clear difference can be observed: The temperature and partial water vapor pressure amplitudes decrease with the increase in PCM latent heat. Compared to the configuration baseline, the temperature amplitudes of 62.9, 90.4, 117.8, and 145.3 kJ/kg are reduced by 40.3%, 46.3%, 51.2%, and 57.2%, respectively, and the partial water vapor pressure amplitudes are reduced by 38.3%, 43.7%, 48.4%, and 55.2%, respectively (see Fig. 5.3 (c)). However, in winter, the temperature and partial water vapor

pressure curves for the different PCM latent heats almost overlap and the reductions are similar, reflecting the negligible effect of latent heat on hygrothermal performance. Hence, increasing PCM latent heat to improve envelope performance is more likely to be suggested in summer.



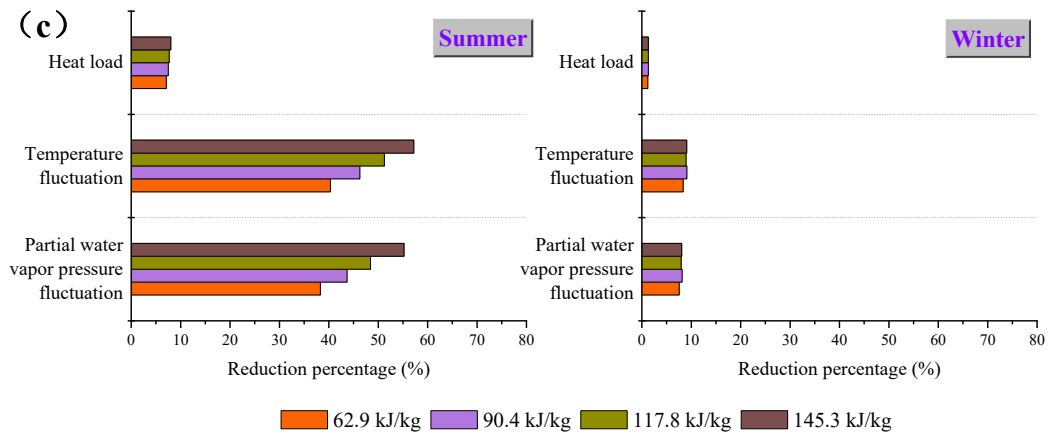


Fig. 5.3. Impact of PCM latent heat: (a) cumulative heat load and moisture load; (b) variation of temperature and partial water vapor pressure; (c) reduction of heat load, temperature fluctuation, and partial water vapor pressure fluctuation compared to configuration baseline

### 5.3.3 Impact of PCM phase transition range

In this subsection, the impact of the PCM phase transition range is studied; the different ranges are 16–20, 20–24, 24–28, and 28–32 °C. Fig. 5.4 shows the middle temperature and melt fraction of PCM for these phase transition ranges. The PCM temperatures for the phase transition ranges of 24–28 °C in summer and 16–20 °C in winter differ significantly from the temperatures for the remaining phase transition ranges, which are characterized by fewer temperature fluctuations since their PCMs are undergoing a phase change process with a melt fraction mostly between 0 and 100%. In contrast, the PCMs in the remaining phase transition ranges are in the solid or liquid state with a melt fraction of mostly 0 or 100%, which does not take full advantage of the PCM.

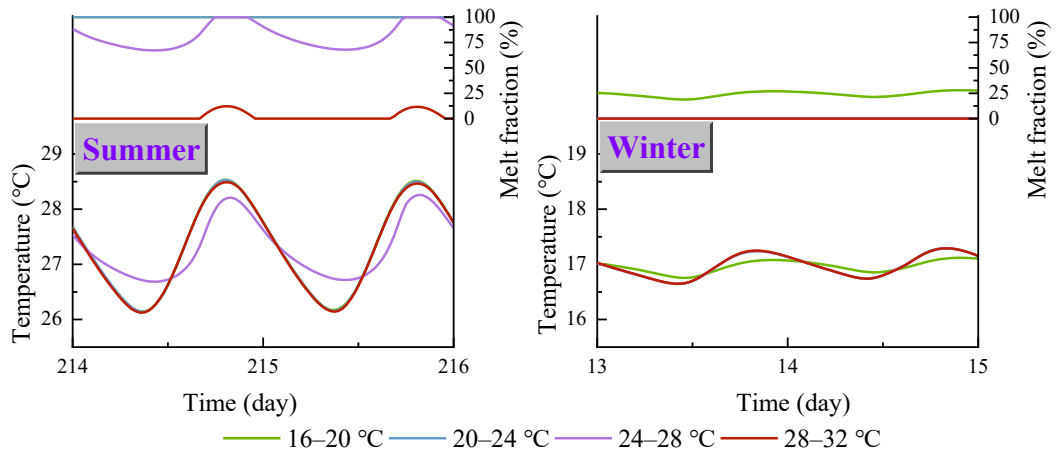
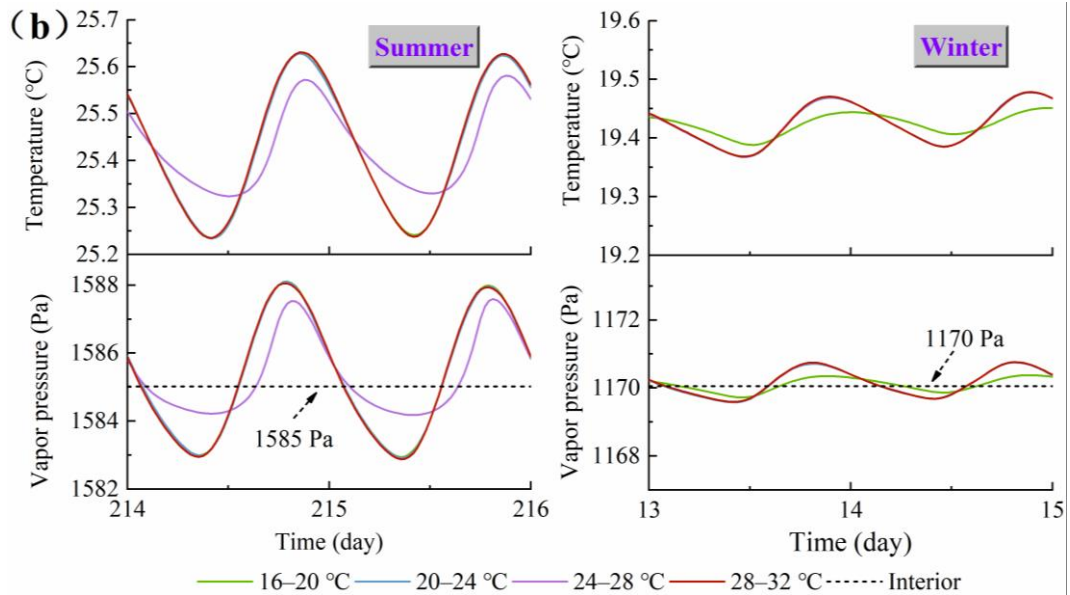
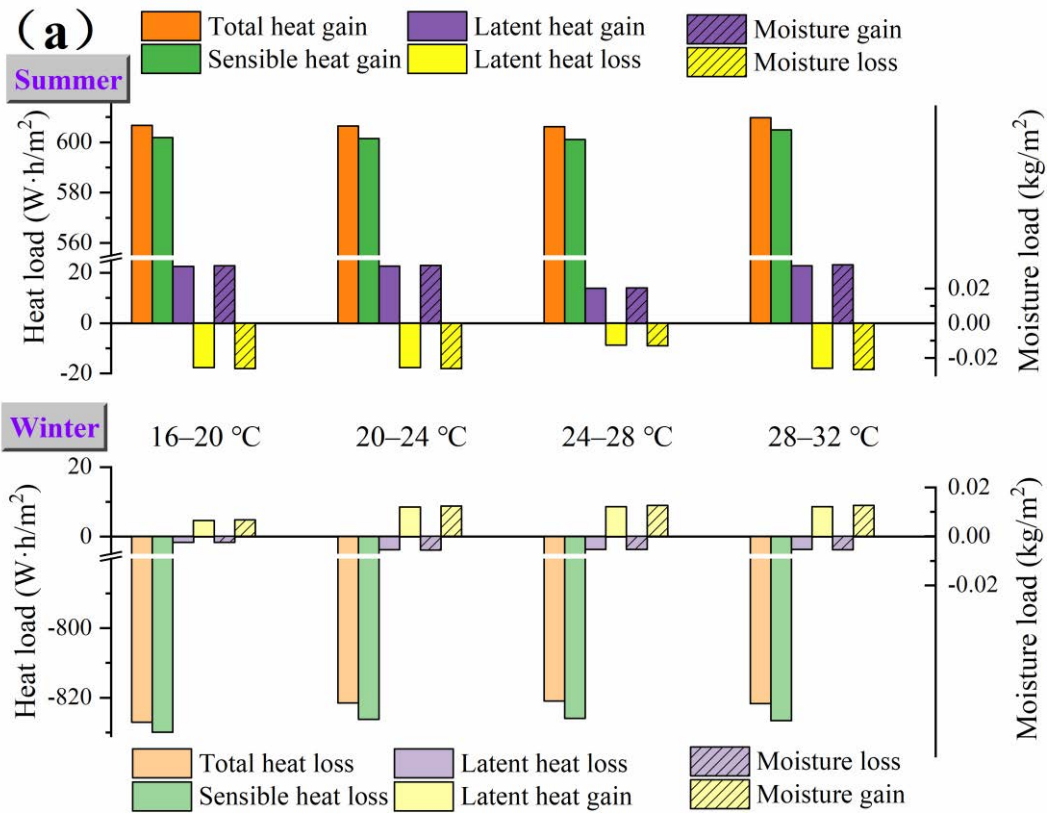


Fig. 5.4. Middle temperature and melt fraction of PCMs for different PCM phase transition ranges

Fig. 5.5 (a) depicts the heat and moisture loads. In summer, the smallest total heat gain occurs in the 24–28 °C phase transition range. Inversely, the largest heat loss corresponds to the 16–20 °C phase transition range in winter, as the innermost PCM layer easily absorbs energy from the high temperature side (interior). Fig. 5.5 (c) summarizes the total heat load reduction compared to the configuration baseline. The reductions for 16–20, 20–24, 24–28, and 28–32 °C are 7.5%, 7.6%, 7.7%, and 7.1%, respectively, in summer and 0.6%, 1.3%, 1.3%, and 1.3%, respectively, in winter. Thus, the 24–28 °C phase transition range in summer contributes to energy savings. As for the improvement of hygrothermal performance, the phase transition ranges of 24–28 °C in summer and 16–20 °C in winter both make contributions. In Fig. 5.5 (b), the corresponding temperature and partial water vapor pressure fluctuations are reduced in both seasons. Compared to the configuration baseline, the temperature and partial water vapor pressure amplitude reductions are 46.2% and 43.7% for the 24–28 °C phase transition range in summer, almost three times the reductions for the remaining phase transition ranges. Similarly, the temperature and partial water vapor pressure amplitude reductions are as high as 55.8% and 55.9% for the 16–20 °C phase transition range in winter (see Fig. 5.5 (c)). Therefore, when the phase transition range ensures that the PCM undergoes a phase change, indoor hygrothermal comfort can be improved in both seasons and energy savings can be achieved in summer.



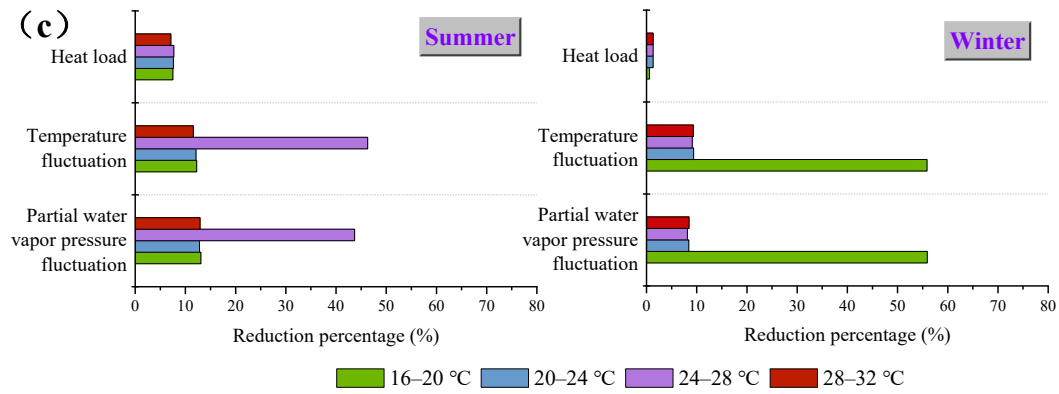


Fig. 5.5. Impact of PCM phase transition range: (a) cumulative heat load and moisture load; (b) variation of temperature and partial water vapor pressure; (c) reduction of heat load, temperature fluctuation, and partial water vapor pressure fluctuation compared to configuration baseline

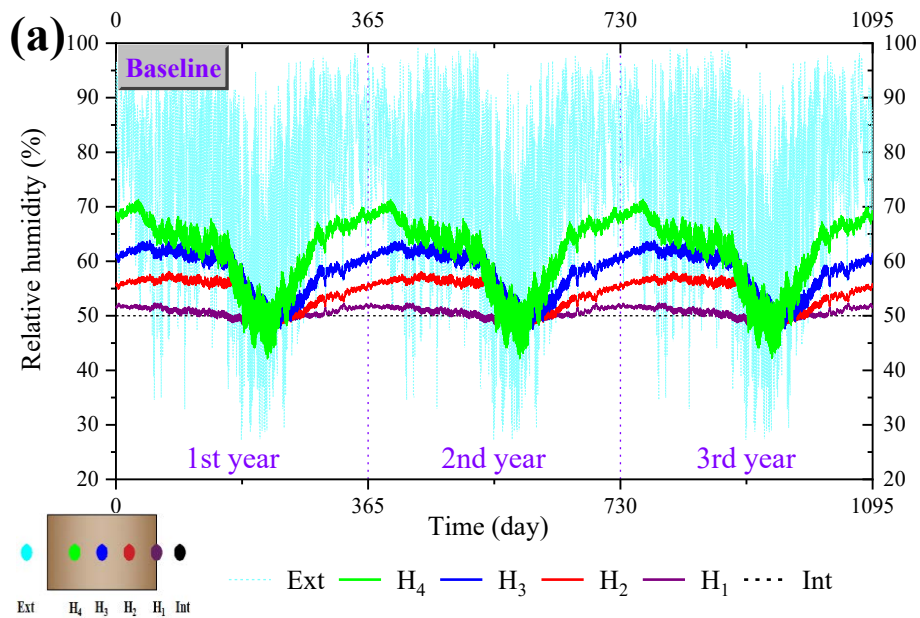
## 5.4 Evaluation of condensation and mold growth risk

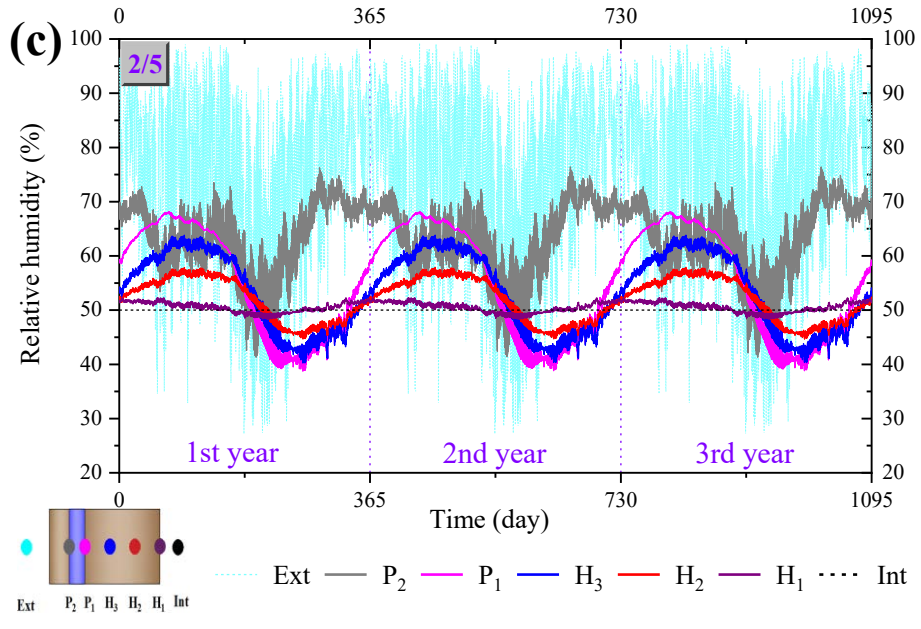
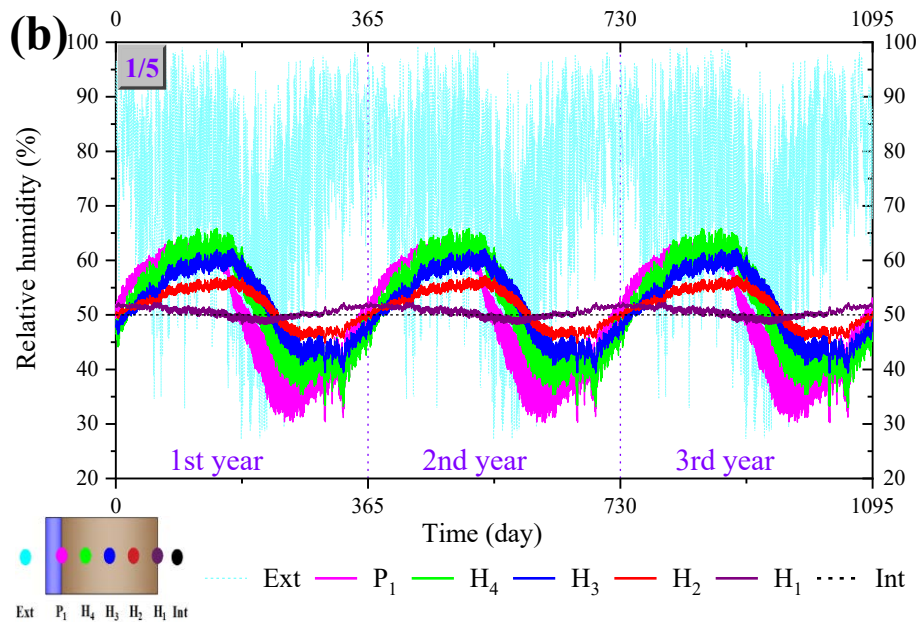
PCM is a moisture impermeable material and seems to cause high relative humidity in localized locations of the integrated configurations. This section covers the three-year simulation conducted to evaluate the relative humidity and temperature behaviors at different locations for the different configurations to evaluate the risk of condensation and mold growth.

### 5.4.1 Evaluation of condensation risk

Fig. 5.6 shows the relative humidity variation during the three years. Generally, the relative humidity at each location under different configurations shows periodic variation with a one-year cycle, fixing the relative humidity within a certain range year after year. Taking location P<sub>1</sub> in configuration 4/5 as an example, its relative humidity increases starting in autumn and reaches its highest values in winter, and then it decreases in spring and drops to its lowest values in summer, with an overall relative humidity range of 44.0% to 60.9%. Concerning the locations of each configuration, location H<sub>1</sub> (interior surface) in each configuration has the most stable relative humidity throughout the year.

Conversely, the locations close to the exterior (such as location H<sub>4</sub> in the configuration baseline, location P<sub>1</sub> in configuration 1/5, etc.) are more likely to experience a large relative humidity fluctuation both yearly and daily. Because the relative humidity variation within the HC is highly affected by temperature, an increase/decrease in temperature leads to the evaporation/condensation of moisture within the HC, which increases/decreases the relative humidity. Thus, the locations with high temperature fluctuations always have high relative humidity fluctuations, both daily and annually. For these configurations, the maximal relative humidity is always below 75% at each location. Therefore, criteria a, b, and c in ASHRAE Standard 160-2009 are confirmed.





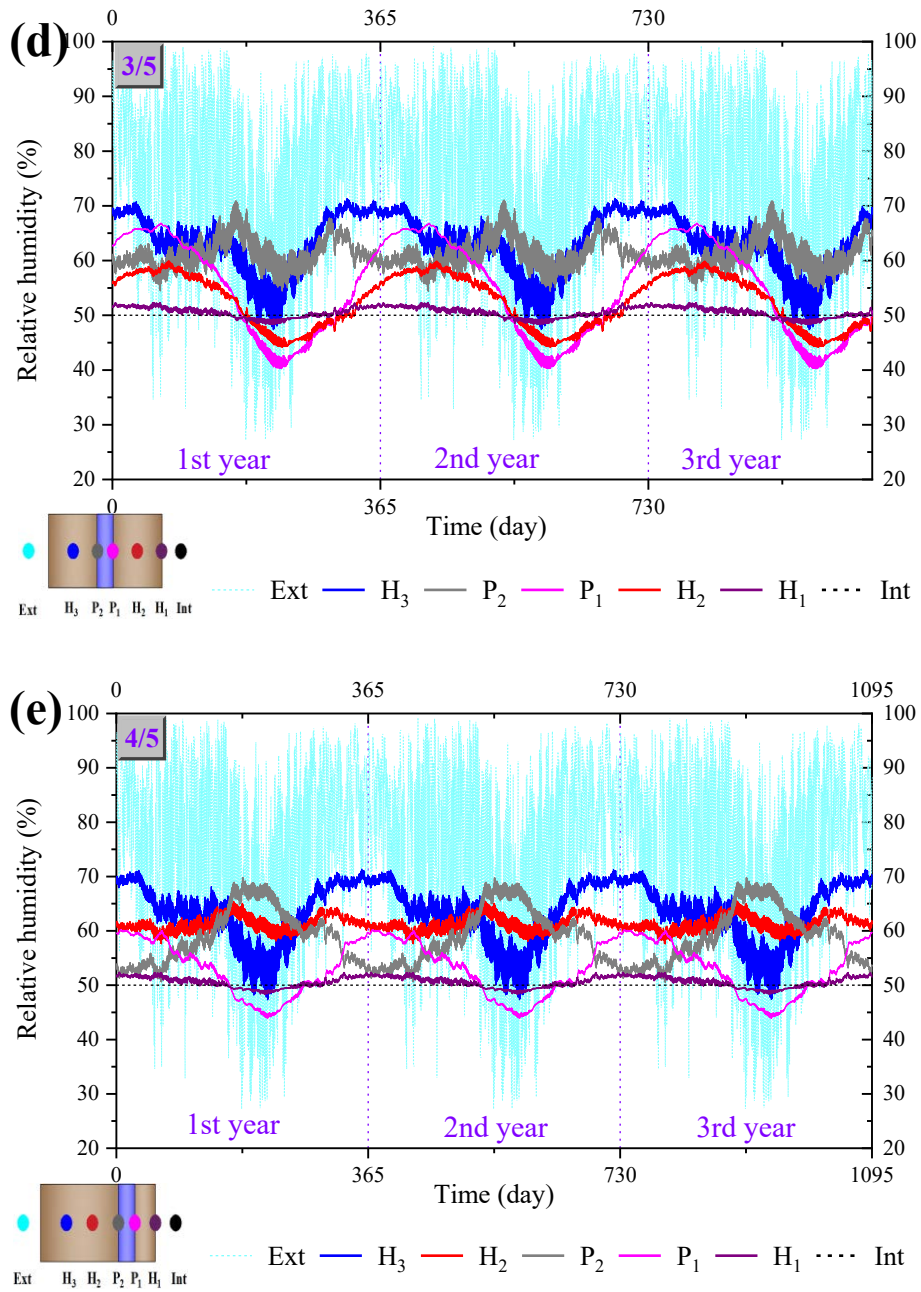


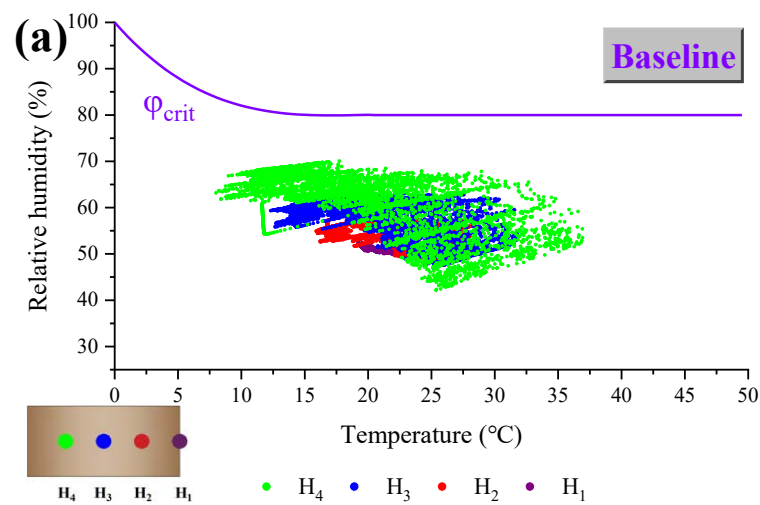
Fig. 5.6. Condensation risk evaluation of (a) configuration baseline; (b) configuration 1/5; (c) configuration 2/5; (d) configuration 3/5; (e) configuration 4/5

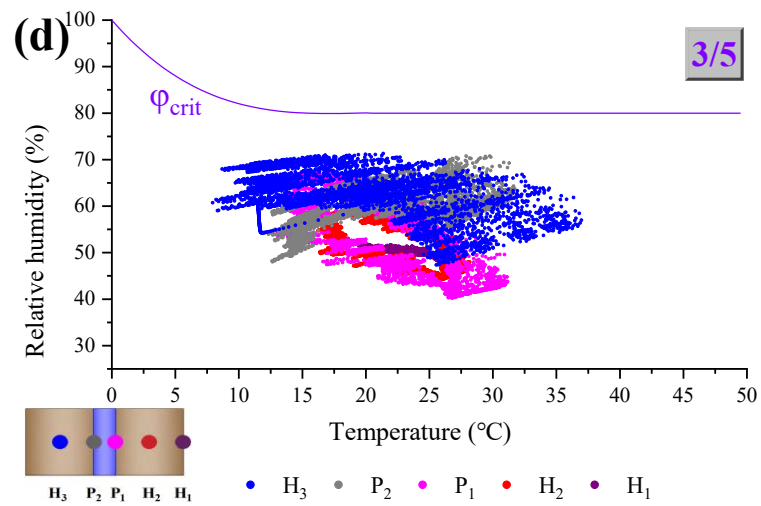
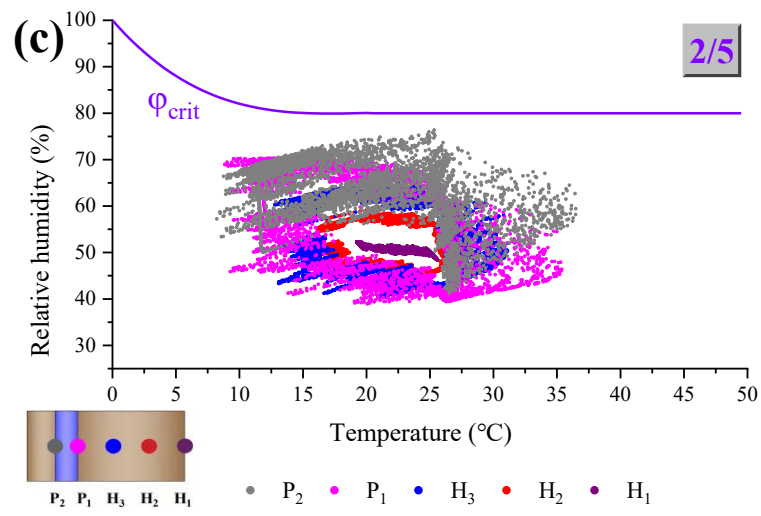
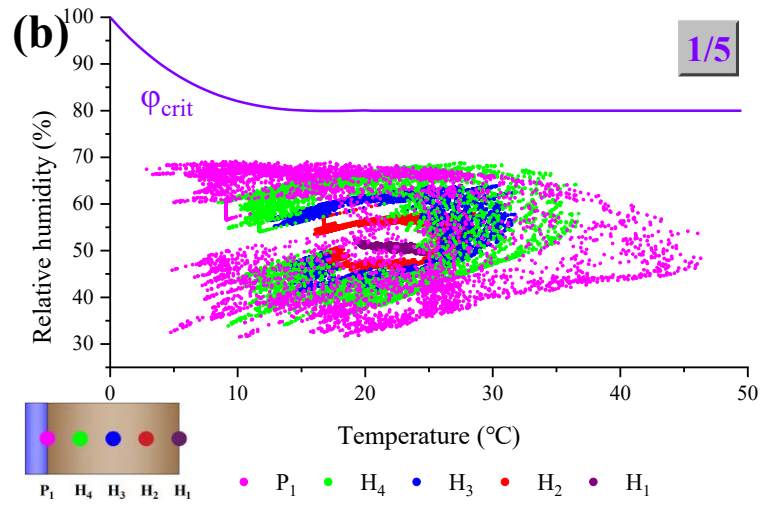
### 5.4.2 Evaluation of mold growth risk

Fig. 5.7 presents the point group of temperature and relative humidity on a three-year scale to evaluate the risk of mold growth. A visually expansive range of temperatures and relative humidities

can also be observed at locations close to the exterior of each configuration, especially configuration 1/5. Because the configuration 1/5 with PCM as the outermost layer can absorb and release the most energy from the exterior environment compared to the remaining configurations. Location P<sub>2</sub> in configuration 2/5 has the highest mold growth risk with a relative humidity slightly below the  $\varphi_{crit}$ . Because the moisture impermeable PCM causes the moisture accumulation. However, due to the periodic variation of relative humidity, the relative humidity at P<sub>2</sub> is always below the  $\varphi_{crit}$  and is free from the risk of mold growth. Configuration 4/5 remains particularly far from the  $\varphi_{crit}$  with the smallest temperature and relative humidity variations, indicating the smallest risk of mold growth. Thus, the integrated configurations ensure that the relative humidity is always below  $\varphi_{crit}$ .

Consequently, considering the periodic variations, a low risk of condensation and mold growth can be guaranteed for a long time.





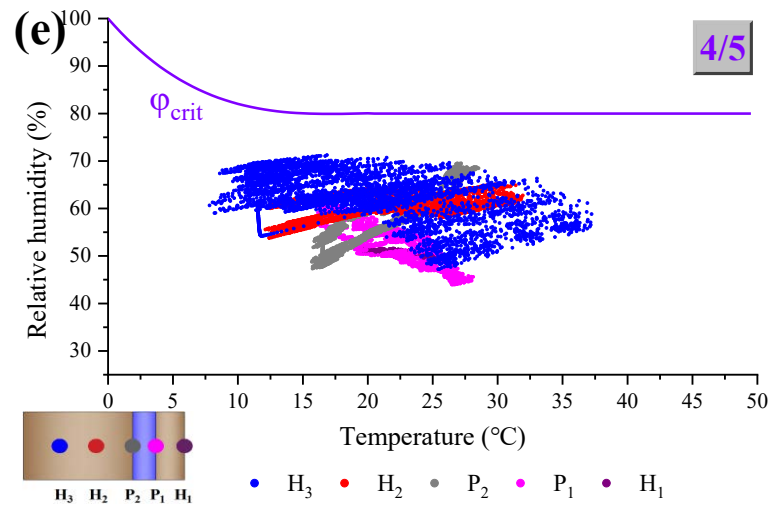


Fig. 5.7. Mold growth risk evaluation of (a) configuration baseline; (b) configuration 1/5; (c) configuration 2/5; (d) configuration 3/5; (e) configuration 4/5

## 5.5 Conclusion

In this chapter, the parametric analysis is conducted, and the application risk is evaluated for the integrated envelope. The parametric analysis is conducted based on configuration 4/5 by studying the impact of three important properties of PCM, i.e., thickness, latent heat, and phase transition range. The application risk evaluation is conducted by studying the temperature and relative humidity in key locations within the integrated envelope of all configurations. The results, conclusions, and recommendations are summarized below.

With the increase in thickness and latent heat, the temperature amplitude, partial water vapor pressure amplitude, and heat load were reduced, especially in summer. In summer, the heat loads of 0.01, 0.02, and 0.03 m are reduced by 7.8%, 10.5%, and 13.9%, respectively, and the partial water vapor pressure/temperature fluctuations are reduced by more than 43.6%, 64.2%, and 76.5%, respectively. In winter, the reduction in heat load is less (less than 5%), but the reduction in partial water vapor pressure/temperature fluctuation is significant (although lower than that in summer), being about 8.6%, 25.8%, and 38.8% for 0.01, 0.02, and 0.03 m, respectively. The impact of PCM latent heat

on the heat load is not significant compared to the thickness. Increasing the PCM latent heat to improve the performance is more effective in summer. With the increase in latent heat in summer, the reductions in heat load, temperature fluctuation, and partial water vapor pressure fluctuation increase from 7.1% to 8.0%, from 40.3% to 57.2%, and from 38.3% to 55.2%, respectively.

As for improving performance by changing the phase transition range, the key point is to ensure that the PCM is activated, i.e., undergoes a phase change. The phase transition range of 24–28 °C in summer and 16–20 °C in winter is remarkable for interior hygrothermal comfort in both seasons and for energy savings in summer (7.7% reduction). Compared to the configuration baseline, the temperature and partial water vapor pressure amplitude reductions are 46.2% and 43.7% for 24–28 °C in summer and 55.8% and 55.9% for 16–20 °C in winter.

The application risk evaluation shows that the integrated envelope is free from the risk of condensation and mold growth in the climate of Roma, Italy. During the three-year evaluation, the relative humidity at each location in each configuration shows a periodic variation with a one-year cycle. The temperature highly influences the relative humidity fluctuation; the locations with high temperature fluctuations always have high relative humidity fluctuations, both daily and annually. Although the relative humidity tends to increase or decrease during certain periods of the year, the overall relative humidity is always below 75% because of the cyclical variation of relative humidity.

In short, this chapter investigates the further strengths and potential weaknesses of the integration envelope and demonstrates its promising applications.

## **Chapter 6            Conclusions, contributions and future work**

Under the urgent need for energy saving, carbon emission reduction, and indoor hygrothermal comfort improvement, a novel passive building envelope was proposed in this thesis. PCM and bio-based concrete (i.e., HC) were integrated into a multilayer envelope to exploit the thermal inertia of PCM and the hygric inertia of bio-based concrete. The integrated envelope is expected to simultaneously improve the thermal, hygric, and energy performance of the building. In Chapter 1, the background, motivation, and objectives of the study are presented. In Chapter 2, the literature review and basic theory are introduced. In Chapter 3, an experimental study is performed to analyze the hygrothermal and energy performance of the integrated envelope as well as the advantages/disadvantages of different configurations. In Chapter 4, the integrated envelope is analyzed in depth by numerical approach. More detailed and comprehensive performance is investigated, and richer advantages are explored. In Chapter 5, further simulation studies are conducted to build on the strengths and avoid the weaknesses of the integrated envelope. Parametric analysis is developed, and potential application risk is evaluated.

The following sections summarize the conclusions, contributions, and future work of this research.

### **6.1 Findings and conclusions**

Findings and conclusions obtained from experimental study:

- 1) The hygrothermal behavior within the HC is a coupled effect of heat and moisture transfer with temperature plays a dominant role. With the presence of PCM, the characteristic times of temperature and relative humidity increase, the thermal and hygric

inertia of the integrated envelope increases. Besides, the time delay increases and the amplitude of temperature/relative humidity decreases at locations close to the interior.

- 2) When PCM is placed on the exterior side, it absorbs/releases the most thermal energy from/to the surrounding environment and therefore is more likely to be activated with a high melt fraction. As a result, PCM has the highest efficiency of 21.5%/18.8% and energy participation of 64.2%/71.0% in the envelope during the energy storage/release process. However, the PCM has the downside of overmelting.
- 3) Due to the moisture impermeability, PCM is not recommended to be placed on the interior side as it loses the benefit of hygroscopic HC to regulate the interior humidity. However, some advantages of this configuration are notable. The PCM is often in the phase transition range, making the PCM layer have the smallest temperature fluctuation of 1.2 °C and the longest time delay of 6.6 h.
- 4) The placement of PCM in the middle of the HC ensures the heat and moisture transfer on both sides of the envelope. PCM stays in the phase transition range most of the time, which ensures less temperature/relative humidity fluctuation of 1.2 °C/0.8% with long temperature time delay of 6.3 h in the HC layer near the interior. Besides, this configuration has the greatest energy savings, with 15.3% less than the envelope with HC only. However, moisture accumulation on both sides of the PCM may cause the potential condensation risk.

Findings and conclusions obtained from simulation study:

- 1) The high coupling between moisture and heat transfer within the HC affects the energy and hygrothermal performance of the integrated envelope. On the one hand, temperature dominates the partial water vapor pressure and affects the variation of moisture flux/load, which ultimately affects the indoor thermal and hygric environment. On the other hand,

moisture transfer is important for energy performance since the moisture load affects the latent heat load and thus the total heat load. The latent heats are 10.4% and 3.1% of the total heat load in summer and winter.

- 2) The location of PCM has a significant impact on the energy and hygrothermal performance of the integrated envelope. As the PCM moves toward the interior, the latent heat percentage decreases from 13.5% to 2.3% in summer and from 3.3% to 0.4% in winter, which makes configuration 4/5 to have the lowest heat gain in summer and heat loss in winter. Compared to the configuration baseline, the total heat load, temperature amplitude, and partial water vapor pressure amplitude of configuration 4/5 are reduced by 8.2%, 46.3%, and 43.7%, respectively, in summer and 1.3%, 9.1%, and 8.2%, respectively, in winter. Thus, configuration 4/5 is recommended because of its optimal energy and hygrothermal performance.
- 3) From a year-round perspective, the PCM reduces the heat gain in most configurations compared to the configuration baseline, especially configuration 4/5, which showed the biggest annual heat gain reduction of 13.3%. In contrast, the PCM hardly affects the annual heat loss with a reduction of only 0.5%. Moreover, the annual energy performance comparison between HMT and HT models emphasizes the importance of moisture transfer. Neglecting moisture transfer leads to an underestimation of annual heat gain and annual heat loss by 2.6% to 12.1% and 1.9% to 4.6%, respectively.
- 4) Configuration 4/5 is noteworthy from a long-term perspective. On the one hand, it saves 11.5% and 0.7% of energy in summer and winter, respectively, compared to the baseline configuration. On the other hand, it shows adaptability in dealing with climatic relative humidity while guaranteeing moisture equilibrium within the HC with an annual net moisture load of  $0.0096 \text{ kg/m}^2$ .

- 5) With the increase in thickness, the temperature amplitude, partial water vapor pressure amplitude, and heat load were reduced, especially in summer. In summer, the heat loads of 0.01, 0.02, and 0.03 m are reduced by 7.8%, 10.5%, and 13.9%, respectively, and the partial water vapor pressure/temperature fluctuations are reduced by more than 43.6%, 64.2%, and 76.5%, respectively. In winter, the reduction in heat load is less (less than 5%), but the reduction in partial water vapor pressure/temperature fluctuation is significant (although lower than that in summer), being about 8.6%, 25.8%, and 38.8% for 0.01, 0.02, and 0.03 m, respectively.
- 6) Increasing the PCM latent heat to improve the performance is more effective in summer. With the increase in latent heat, the reductions in heat load, temperature fluctuation, and partial water vapor pressure fluctuation increase from 7.1% to 8.0%, from 40.3% to 57.2%, and from 38.3% to 55.2%, respectively.
- 7) The key point in selecting the phase transition range to improve the performance is to ensure that the PCM is activated, i.e., undergoes a phase change. The phase transition range of 24–28 °C in summer and 16–20 °C in winter is remarkable for interior hygrothermal comfort in both seasons and energy savings (7.7% reduction) in summer. Compared to the baseline configuration, the temperature and partial water vapor pressure amplitude reductions are 46.2% and 43.7% for 24–28 °C in summer and 55.8% and 55.9% for 16–20 °C in winter.
- 8) The application risk evaluation shows that the integrated envelope is free from the risk of condensation and mold growth in Roma, Italy. During the three-year evaluation, the relative humidity at each location in each configuration showed a periodic variation with a one-year cycle. Although the relative humidity tends to increase or decrease during certain periods of the year, the overall relative humidity is always below 75%.

## 6.2 Contributions

The main contributions of the present research are summarized as follows:

- 1) A novel passive building envelope integrating PCM and bio-based hygroscopic concrete by multilayer assembly approach is proposed. Compared to the PCM capsulation form, multilayer assembly has the advantages of easy installation, large utilization of PCM thermal storage capacity, and high mechanical strength. The integrated envelope conforms to the concept of green and low-carbon of buildings as well as has the ability of energy saving and temperature/humidity regulation. This is an innovative and promising building envelope.
- 2) The feasibility, advantages, and disadvantages of different integrated configurations are experimentally investigated. The principle of PCM to affect the thermal performance, especially the hygric performance of the HC, is quantitatively explained. The principle can be used as a reference for the integration of PCM with other materials.
- 3) The mathematical model of the integrated envelope that couples heat and moisture transfer and considers the temperature dependence of HC's hygroscopic characteristic is developed. The relationship between energy, thermal, and hygric performance as well as the impact of the PCM's location are comprehensively investigated. The energy and hygrothermal performance are studied in the short-term (days and weeks) and long-term (months and years). Such results have not been found in the literature review.
- 4) The parametric analysis of the integrated envelope are proposed from the perspective of PCM properties. The law of long-term variation in relative humidity is studied, and the risk of condensation and mold growth is evaluated. These results are guideline for the design, optimization, and evaluation of multilayer envelopes assembled with PCM.

### 6.3 Future work

This study confirms the ability of the integrated envelope to improve the energy and hygrothermal performance of buildings and provides potential optimization strategies. The current work is a start, and several potential investigations have been identified:

- 1) The integrated envelope has been shown to affect the indoor thermal and humidity environment. Further investigation is needed to study the hygrothermal and energy performance by considering the heat and moisture transfer models for indoor air.
- 2) The integrated envelope contributes to the energy savings of the building, but the life-cycle cost and payback period of buildings assembled with the integrated envelope are unknown. Therefore, it is necessary to determine the economic feasibility of the integrated envelope by conducting an economic analysis.
- 3) There are many parameters that affect the performance of the integrated envelope, such as the thermophysical properties of HC (specific heat capacity, thermal conductivity, etc.), the hygric physical properties of HC (water vapor permeability, sorption capacity, etc.), and the thermophysical properties of PCM (latent heat capacity, phase transition range, thermal conductivity, etc.). Thus, the study can be extended to perform a sensitivity analysis of these parameters and identify how much the performance is sensitive to the changes of these parameters.

# Appendix

## Appendix A: Résumé de la thèse en français

### A.1 Résumé

Les économies d'énergie et la réduction des émissions des gaz à effet de serre dans le secteur du bâtiment ainsi que le maintien d'un confort hygrométrique prennent une importance majeure ces dernières décennies. L'utilisation de matériaux à changement de phase (MCP) ou de matériaux hygroscopiques d'origine végétale pour l'enveloppe des bâtiments est une solution prometteuse. Les MCP conduisent à améliorer le confort thermique intérieur et à réduire la consommation d'énergie, tandis que les matériaux hygroscopiques biosourcés sont des matériaux respectueux de l'environnement et permettent la régulation de l'humidité intérieure et assure une isolation thermique optimale. Cependant, seules quelques études ont exploré l'application l'intégration de ces deux types de matériaux et analysé de manière exhaustive les performances énergétiques et hygrothermiques. Cette thèse propose une solution d'enveloppe passive qui intègre le PCM et le béton de chanvre biosourcé pour améliorer simultanément les performances énergétiques, et hygrothermiques du bâtiment. Les principaux objectifs de cette étude sont d'examiner la faisabilité des enveloppes intégrées, d'étudier de manière exhaustive les performances hygrothermiques et énergétiques ainsi que les avantages et les inconvénients de différentes configurations avec le PCM placé à différents endroits du béton de chanvre.

Tout d'abord, des expériences ont été menées en comparant les performances hygrothermiques d'une enveloppe de référence (béton de chanvre uniquement) et de trois enveloppes intégrées avec du MCP placé à différents endroits dans deux conditions limites typiques. Les résultats ont montré la faisabilité des enveloppes intégrées. La présence de PCM a augmenté les inerties thermique et hygrique de l'enveloppe. Par conséquent, le déphasage a été augmenté et l'amplitude de la température et de

l'humidité relative a été réduite. Les différentes configurations présentaient des avantages et des inconvénients différents. La configuration dans laquelle le MCP est placé au milieu du béton de chanvre est intéressante car elle présente une faible fluctuation et un déphasage intéressant à la fois pour les variations de la température et de l'humidité relative, et conduit ainsi à de grandes économies d'énergie.

Ensuite, le modèle physique  $i$ , de transfert de la chaleur et de l'humidité, à l'échelle de l'enveloppe a été développé. Ce modèle intègre la dépendance de la température et de la caractéristique hygroscopique du béton de chanvre. La précision du modèle a été validée par comparaison avec les données expérimentales. Sur la base du modèle validé, les simulations ont été effectuées dans un climat méditerranéen afin d'étudier de manière exhaustive les performances hygrothermiques et énergétiques de l'enveloppe intégrée. Les résultats ont mis en évidence le rôle indispensable du transfert d'humidité dans la détermination de la charge hygrothermique, ainsi que l'effet précieux de l'enveloppe sur l'amélioration des performances énergétiques et hygrothermiques. En outre, l'enveloppe intégrée avec le PCM proche de (mais pas en contact avec) l'intérieur a montré un grand potentiel pour économiser de l'énergie et s'adapter aux variations d'humidité du climat tout en garantissant l'équilibre de l'humidité dans le béton de chanvre.

Enfin, l'analyse paramétrique a été réalisée du point de vue des propriétés du MCP (épaisseur, chaleur latente et plage de transition de phase), et le risque d'application (condensation et développement de moisissures) a été évalué. Les résultats de l'analyse paramétrique ont montré que les performances de l'enveloppe pouvaient être améliorées en augmentant l'épaisseur et la chaleur latente de MCP et en identifiant la plage de transition de phase appropriée du MCP. Les résultats de l'évaluation des risques ont confirmé que l'enveloppe ne présentait aucun risque de condensation et de développement de moisissures.

**Mots clés:** Matériau à changement de phase (MCP); Béton biosourcé; Enveloppe passive du bâtiment;

Transfert de chaleur et d'humidité; Performances hygrothermiques et énergétiques; Analyse paramétrique; Évaluation du risque

## A.2 Constatations et conclusions

Constatations et conclusions tirées de l'étude expérimentale :

- 1) La température jouant un rôle dominant dans le comportement hygrothermique au sein du béton de chanvre. Avec la présence de PCM favorise l'augmentation des inerties thermique et hygrique de l'enveloppe . En outre, le déphasage augmente et l'amplitude de variation de la température et de l'humidité relative diminue aux endroits proches de l'intérieur.
- 2) Lorsque le MCP est placé à l'extérieur, il absorbe/libère le plus d'énergie thermique de/vers le milieu environnant et est donc plus susceptible d'être activé avec une fraction élevée. En conséquence, le MCP présente le rendement le plus élevé (21.5 %/18.8 %) et une participation énergétique de 64.2 %/71.0 % dans l'enveloppe pendant le processus de stockage/libération de l'énergie.
- 3) En raison de l'imperméabilité à l'humidité, il n'est pas recommandé de placer le MCP sur le côté intérieur car béton de chanvre hygroscopique perd l'avantage pour réguler l'humidité intérieure. Cependant, certains avantages de cette configuration sont notables car le PCM se trouve souvent dans la plage de transition de phase, ce qui fait que la couche de PCM présente la plus petite fluctuation de température de 1.2 ° et le plus long délai de 6.6 h.
- 4) Le placement du PCM au milieu du béton de chanvre assure le transfert de chaleur et d'humidité des deux côtés de l'enveloppe. Le MCP reste dans la plage de transition de phase la plupart du temps, ce qui assure une moindre fluctuation de la température et de

l'humidité relative de 1.2 °/ 0.8% avec un long délai de température de 6.3 h dans la couche de béton de chanvre près de l'intérieur. En outre, cette configuration présente les plus grandes économies d'énergie, avec 15.3% de moins que l'enveloppe avec le béton de chanvre uniquement. Cependant, l'accumulation d'humidité sur les deux faces du PCM peut entraîner un risque potentiel de condensation.

Constatations et conclusions de l'étude de simulation:

- 1) Le couplage élevé entre le transfert de chaleur et de masse dans le béton de chanvre affecte les performances énergétiques et hygrothermiques de l'enveloppe intégrée. D'une part, la température domine la pression partielle de la vapeur d'eau et affecte la variation du flux/charge d'humidité, ce qui affecte finalement l'environnement thermique et hygrique intérieur. D'autre part, le transfert d'humidité est important pour la performance énergétique car la charge d'humidité affecte la charge de chaleur latente et donc la charge thermique totale. Les chaleurs latentes représentent 10.4 % et 3.1 % de la charge thermique totale en été et en hiver.
- 2) L'emplacement du MCP a un impact important sur les performances énergétiques et hygrothermiques de l'enveloppe intégrée. Lorsque le MCP se déplace vers l'intérieur, le pourcentage de chaleur latente diminue de 13.5 % à 2.3 % en été et de 3.3 % à 0.4 % en hiver, ce qui fait que la configuration 4/5 présente le gain de chaleur le plus faible en été et la perte de chaleur la plus faible en hiver. Par rapport à la configuration de base, la charge thermique totale, l'amplitude de la température et l'amplitude de la pression partielle de vapeur d'eau de la configuration 4/5 sont réduites de 8.2 %, 46.3 % et 43.7 %, respectivement, en été et de 1.3 %, 9.1 % et 8.2 %, respectivement, en hiver. Ainsi, la configuration 4/5 est recommandée en raison de ses performances énergétiques et hygrothermiques optimales.

- 3) D'un point de vue annuel, le MCP réduit le gain de chaleur dans la plupart des configurations par rapport à la configuration de base, en particulier la configuration 4/5, qui présente la plus grande réduction annuelle du gain de chaleur de 13.3 %. En revanche, le MCP n'affecte pratiquement pas les pertes de chaleur annuelles, avec une réduction de seulement 0.5 %. De plus, la comparaison des performances énergétiques annuelles entre les modèles HMT et HT souligne l'importance du transfert d'humidité. Négliger le transfert d'humidité conduit à une sous-estimation du gain de chaleur annuel et de la perte de chaleur annuelle de 2.6 % à 12.1 % et de 1.9 % à 4.6 %, respectivement.
- 4) La configuration 4/5 est remarquable dans une perspective à long terme. D'une part, elle permet d'économiser 11.5 % et 0.7 % d'énergie en été et en hiver, respectivement, par rapport à la configuration de référence. D'autre part, elle montre une adaptabilité face à l'humidité relative climatique tout en garantissant l'équilibre de l'humidité dans le béton de chanvre avec une charge d'humidité nette annuelle de 0.0096 kg/m<sup>2</sup>.
- 5) Avec l'augmentation de l'épaisseur, l'amplitude de la température, l'amplitude de la pression partielle de vapeur d'eau et la charge thermique ont été réduites, surtout en été. En été, les charges thermiques de 0.01, 0.02 et 0.03 m sont réduites de 7.8 %, 10.5 % et 13.9 % respectivement, et les fluctuations de pression partielle de vapeur d'eau/température sont réduites de plus de 43.6 %, 64.2 % et 76.5 % respectivement. En hiver, la réduction de la charge thermique est moindre (moins de 5 %), mais la réduction de la pression partielle de vapeur d'eau/des fluctuations de température est significative (bien que plus faible qu'en été), soit environ 8.6 %, 25.8 % et 38.8 % pour 0.01, 0.02 et 0.03 m, respectivement.
- 6) L'augmentation de la chaleur latente du MCP pour améliorer les performances est plus efficace en été. Avec l'augmentation de la chaleur latente, les réductions de la charge thermique, de la fluctuation de température et de la fluctuation de la pression partielle de

la vapeur d'eau, passent respectivement de 7.1 % à 8.0 %, de 40.3 % à 57.2 % et de 38.3 % à 55.2 %.

- 7) Le point clé dans le choix de la plage de transition de phase pour améliorer les performances, est de s'assurer que le MCP est activé, c'est-à-dire qu'il subit un changement de phase. La plage de transition de phase de 24-28 °C en été, et de 16-20 °C en hiver, est remarquable pour le confort hygrothermique intérieur pendant les deux saisons, et les économies d'énergie (réduction de 7.7 %) en été. Par rapport à la configuration de référence, les réductions d'amplitude de température et de pression partielle de vapeur d'eau sont de 46.2 % et 43.7 % pour 24-28 °C en été et de 55.8 % et 55.9 % pour 16-20 ° en hiver.
- 8) L'évaluation du risque d'application montre que l'enveloppe avec PCM est exempte de risque de condensation et de développement de moisissures à Rome, en Italie. Au cours de l'évaluation de trois ans, l'humidité relative à chaque emplacement dans chaque configuration a montré une variation périodique avec un cycle d'un an. Bien que l'humidité relative ait tendance à augmenter ou à diminuer pendant certaines périodes de l'année, l'humidité relative globale est toujours inférieure à 75 %.

### **A.3 Contributions**

Les principales contributions de la présente recherche sont résumées comme suit:

- 1) Une nouvelle enveloppe de bâtiment passive intégrant le MCP et le béton hygroscopique biosourcé par une approche d'assemblage multicouche est proposée. Par rapport à la forme de capsulation du MCP, l'assemblage multicouche présente les avantages d'une installation facile, d'une grande utilisation de la capacité de stockage thermique du MCP et d'une résistance mécanique élevée. L'enveloppe avec MCP est conforme au concept

de bâtiments verts et à faible émission de gaz à effet de serre et conduit à des économies d'énergie et la réduction des fluctuations et des bonnes régulations de la température et de l'humidité. Il s'agit d'une enveloppe de bâtiment innovante et prometteuse.

- 2) La faisabilité, les avantages et les inconvénients de différentes configurations intégrées sont étudiés expérimentalement. Le principe de l'influence du PCM sur la performance thermique, et en particulier sur la performance hygrique du béton de chanvre, est expliqué quantitativement. Ce principe peut être utilisé comme référence pour l'intégration du PCM avec d'autres matériaux.
- 3) Le modèle hygrothermique couplé de chaleur et de masse à l'échelle de l'enveloppe intégrant la dépendance à la température de la caractéristique hygroscopique du béton de chanvre, est développé. La relation entre les performances énergétiques, thermiques et hygriques ainsi que l'impact de l'emplacement du MCP sont étudiés de manière approfondie. Les performances énergétiques et hygrothermiques sont étudiées à court terme (jours et semaines) et à long terme (mois et années). De tels résultats n'ont pas été trouvés dans la revue de la littérature.
- 4) L'analyse paramétrique de l'enveloppe avec PCM est proposée du point de vue des propriétés du PCM. La loi de variation de l'humidité relative est étudiée, et le risque de condensation et de développement de moisissures est évalué. Ces résultats constituent une ligne directrice pour la conception, l'optimisation et l'évaluation des enveloppes multicouches assemblées avec du PCM.

#### **A.4 Travaux futurs**

Cette étude confirme la capacité de l'enveloppe intégrée à améliorer les performances énergétiques et hygrothermiques des bâtiments et fournit des stratégies d'optimisation potentielles. Le

travail actuel est un début, et plusieurs investigations potentielles ont été identifiées :

- 1) Il a été démontré que l'enveloppe avec PCM affecte l'environnement thermique et hygrométrique intérieur. Des recherches supplémentaires sont nécessaires pour étudier les performances hygrothermiques et énergétiques en considérant les modèles de transfert de chaleur et d'humidité pour l'air intérieur.
- 2) L'enveloppe avec PCM contribue aux économies d'énergie du bâtiment, mais le coût du cycle de vie et la période de récupération des bâtiments assemblés avec l'enveloppe intégrée sont inconnus. Par conséquent, il est nécessaire de déterminer la faisabilité économique de l'enveloppe intégrée en effectuant une analyse économique.
- 3) Il existe de nombreux paramètres qui affectent les performances de l'enveloppe intégrée, tels que les propriétés thermophysiques du béton de chanvre (capacité thermique spécifique, conductivité thermique, etc.), les propriétés physiques hygiéniques du béton de chanvre (perméabilité à la vapeur d'eau, capacité de sorption, etc.), et les propriétés thermophysiques du PCM (capacité thermique latente, plage de transition de phase, conductivité thermique, etc.) Ainsi, l'étude peut être étendue pour effectuer une analyse de sensibilité de ces paramètres et identifier dans quelle mesure la performance est sensible aux changements de ces paramètres.

## **Appendix B: List of publications**

- **D. Wu**, M. Rahim, M. El Ganaoui, R. Bennacer, B. Liu, Multilayer assembly of phase change material and bio-based concrete: A passive envelope to improve the energy and hygrothermal performance of buildings, *Energy Conversion and Management* 257 (2022) 115454. <https://doi.org/10.1016/j.enconman.2022.115454> (Article, IF=11.533)

- **D. Wu**, M. Rahim, M. El Ganaoui, R. Djedjig, R. Bennacer, B. Liu, Experimental investigation on the hygrothermal behavior of a new multilayer building envelope integrating PCM with bio-based material, *Building and Environment* 201 (2021) 107995. <https://doi.org/10.1016/j.buildenv.2021.107995> (Article, IF=7.693)
- **D. Wu**, M. Rahim, M. El Ganaoui, R. Bennacer, R. Djedjig, B. Liu, Dynamic hygrothermal behavior and energy performance analysis of a novel multilayer building envelope based on PCM and hemp concrete, *Construction and Building Materials* (2022). <https://doi.org/10.1016/j.conbuildmat.2022.127739> (Article, IF=7.093)
- **D. Wu**, M. Rahim, W. Li, M.E. Ganaoui, R. Bennacer, Simulation Study of the Hygrothermal Behavior of a Building Envelope Combining PCM and Bio-Based Concrete, *Fluid Dynamics & Materials Processing* (2022) <http://dx.doi.org/10.32604/fdmp.2022.021917> (Article, IF=1.9)
- **D. Wu**, M. Rahim, M. El Ganaoui, R. Bennacer, Numerical study of a novel building envelope integrating PCM and bio-based material, *06th International Conference on Materials & Energy*, Metz, France (2021). (Conference with oral presentation and poster)
- **D. Wu**, M. Rahim, W. Li, M.E. Ganaoui, R. Bennacer, B. Liu, Effect of PCM on the energy and hygrothermal performance of a multilayer building envelope, *07th International Conference on Materials & Energy*, Baku, Azerbaijan (2022). (Conference with oral presentation)
- M. Rahim, R. Djedjig, **D. Wu**, R. Bennacer, M.E.L. Ganaoui, Experimental investigation of hygrothermal behavior of wooden-frame house under real climate conditions, *Energy and Built Environment* (2021). <https://doi.org/10.1016/j.enbenv.2021.09.002> (Article)

## Reference

- [1] K. Lyu, X. Zhang, J.A. Church, A.B.A. Slangen, J. Hu, Time of emergence for regional sea-level change, *Nature Climate Change*, 4 (2014) 1006-1010.
- [2] S. Dale, BP Energy Outlook-2019 edition, in: BP Energy Outlook, Vol. (accessed 01 April 2021, <https://www.bp.com/content/dam/bp/business-sites/en/global/corporate/pdfs/energy-economics/energy-outlook/bp-energy-outlook-2019.pdf>), 2019.
- [3] G.A.f.B.a. Construction, 2021 Global Status Report for Building and Construction, in: Towards a zero-emissions, efficient and resilient buildings and construction sector, 2021.
- [4] IEA, World Energy Outlook 2019, in: international energy agency, Vol. (accessed 04 December 2021, 2019).
- [5] M.L. Rivera, H.L. MacLean, B. McCabe, Implications of passive energy efficiency measures on life cycle greenhouse gas emissions of high-rise residential building envelopes, *Energy and Buildings*, 249 (2021) 111202.
- [6] S. DING, Passive house in China, (2018).
- [7] Y. Lin, L. Zhao, W. Yang, X. Hao, C.-Q. Li, A review on research and development of passive building in China, *Journal of Building Engineering*, 42 (2021) 102509.
- [8] J. Liang, X. Zhang, J. Ji, Hygroscopic phase change composite material——A review, *Journal of Energy Storage*, 36 (2021) 102395.
- [9] M. Helm, C. Keil, S. Hiebler, H. Mehling, C. Schweigler, Solar heating and cooling system with absorption chiller and low temperature latent heat storage: Energetic performance and operational experience, *International Journal of Refrigeration*, 32 (2009) 596-606.
- [10] C.-Y. Zhao, G.H.J.R. Zhang, S.E. Reviews, Review on microencapsulated phase change materials (MEPCMs): fabrication, characterization and applications, 15 (2011) 3813-3832.
- [11] K.C. Parsons, Environmental ergonomics: a review of principles, methods and models, *Applied Ergonomics*, 31 (2000) 581-594.
- [12] D. Enescu, A review of thermal comfort models and indicators for indoor environments, *Renewable and Sustainable Energy Reviews*, 79 (2017) 1353-1379.
- [13] A.A.S. 55, Thermal environmental conditions for human occupancy, 5 (2014).
- [14] B.P. Ho, Thermal comfort, (2011).
- [15] R.J.A.S.R. MacPherson, Studies in the preferred thermal environment, 6 (1963) 183-189.
- [16] H.J. Moon, S.H. Ryu, J.T. Kim, The effect of moisture transportation on energy efficiency and IAQ in residential buildings, *Energy and Buildings*, 75 (2014) 439-446.
- [17] K. Abe, Assessment of the environmental conditions in a museum storehouse by use of a fungal index, *International Biodeterioration & Biodegradation*, 64 (2010) 32-40.
- [18] A. K, Comparison of computed measured fungal index in field, *Proc Healthy Buildings, II* (2006).
- [19] P. Wolkoff, Indoor air humidity, air quality, and health – An overview, *International Journal of Hygiene and Environmental Health*, 221 (2018) 376-390.
- [20] A.V. Arundel, E.M. Sterling, J.H. Biggin, T.D.J.E.h.p. Sterling, Indirect health effects of relative humidity in indoor environments, 65 (1986) 351-361.
- [21] Fanger, O.J.T.C.A. P., A.i.E. Engineering, Thermal comfort: analysis and applications in environmental engineering, (1972).
- [22] E. European Standard, Indoor Environmental Input Parameters for Design and Assessment of Energy Performance of Buildings—Addressing Indoor Air Quality, Thermal Environment, Lighting and Acoustics, (2007).
- [23] A.A.S. RAA-C.E, Thermal Environmental Conditions for Human Occupancy, , American Society of Heating, Refrigerating and Air-Conditioning Engineers, (2013).
- [24] M. Kottek, J. Grieser, C. Beck, B. Rudolf, F. Rubel, World map of the Köppen-Geiger climate

classification updated, (2006).

- [25] M. Napp, T. Kalamees, T. Tark, E. Arumägi, Integrated Design of Museum's Indoor Climate in Medieval Episcopal Castle of Haapsalu, *Energy Procedia*, 96 (2016) 592-600.
- [26] B. Li, C. Du, R. Yao, W. Yu, V. Costanzo, Indoor thermal environments in Chinese residential buildings responding to the diversity of climates, *Applied Thermal Engineering*, 129 (2018) 693-708.
- [27] M. Qin, P. Hou, Z. Wu, J. Wang, Precise humidity control materials for autonomous regulation of indoor moisture, *Building and Environment*, 169 (2020) 106581.
- [28] X. Ju, Application of Building Integrated Active and Passive Solar Technology in Harsher Climate Area--Design of the Central Control Building of PV Demonstration Area in Turpan Area, Xinjiang Uygur Autonomous Region, China, *Energy Procedia*, 57 (2014) 1659-1668.
- [29] Y. Ren, L. Yang, W. Zheng, X. Song, W. He, Levels of Adaptation in Dry-Hot and Dry-Cold Climate Zone and its Implications in Evaluation for Indoor Thermal Environment, *Procedia Engineering*, 121 (2015) 143-150.
- [30] L. Zhang, G. Sang, W. Han, Effect of hygrothermal behaviour of earth brick on indoor environment in a desert climate, *Sustainable Cities and Society*, 55 (2020) 102070.
- [31] C. Kilbert, Establishing principles and a model for sustainable construction, First International Conference of CIB TG 16 on Sustainable Construction, Tampa, Florida (November 1994), (1994).
- [32] M. Yadav, M.J.M.T.P. Agarwal, Biobased building materials for sustainable future: An overview, (2021).
- [33] R. Sathre, L. Gustavsson, Using wood products to mitigate climate change: External costs and structural change, *Applied Energy*, 86 (2009) 251-257.
- [34] L. Wang, A. Toppinen, H. Juslin, Use of wood in green building: a study of expert perspectives from the UK, *Journal of Cleaner Production*, 65 (2014) 350-361.
- [35] F.-T.F.a.A.O.o.t.U. Nations, World consultation on the use of wood in housing, *An International Review of Forestry and Forest Products*, 25 (1971).
- [36] U.S.T. Association, Market report 2012 Prepared by Timber Trends, Structural Timber Association, (2013).
- [37] J. Hildebrandt, N. Hagemann, D. Thrän, The contribution of wood-based construction materials for leveraging a low carbon building sector in europe, *Sustainable Cities and Society*, 34 (2017) 405-418.
- [38] I. Cetiner, A.D. Shea, Wood waste as an alternative thermal insulation for buildings, *Energy and Buildings*, 168 (2018) 374-384.
- [39] H. Zhang, H. Yoshino, K. Hasegawa, J. Liu, W. Zhang, H. Xuan, Practical moisture buffering effect of three hygroscopic materials in real-world conditions, *Energy and Buildings*, 139 (2017) 214-223.
- [40] I. Hartley, M. Hamza, Wood: Moisture content, hygroscopicity, and sorption, (2016).
- [41] M. Yadav, M. Agarwal, Biobased building materials for sustainable future: An overview, *Materials Today: Proceedings*, 43 (2021) 2895-2902.
- [42] M. Degrave-Lemeurs, P. Glé, A. Hellouin de Menibus, Acoustical properties of hemp concretes for buildings thermal insulation: Application to clay and lime binders, *Construction and Building Materials*, 160 (2018) 462-474.
- [43] Z. Zhang, J. Chen, E.M.A. Elbashiry, Z. Guo, X. Yu, Effects of changes in the structural parameters of bionic straw sandwich concrete beetle elytron plates on their mechanical and thermal insulation properties, *Journal of the Mechanical Behavior of Biomedical Materials*, 90 (2019) 217-225.
- [44] M. Asli, F. Brachelet, E. Sassine, E. Antczak, Thermal and hygroscopic study of hemp concrete in real ambient conditions, *Journal of Building Engineering*, 44 (2021) 102612.
- [45] C. Rabbat, S. Awad, A. Villot, D. Rollet, Y. André, Sustainability of biomass-based insulation materials in buildings: Current status in France, end-of-life projections and energy recovery potentials, *Renewable and Sustainable Energy Reviews*, 156 (2022) 111962.

- [46] B. Ismail, N. Belayachi, D. Hoxha, Hygric properties of wheat straw biocomposite containing natural additives intended for thermal insulation of buildings, *Construction and Building Materials*, 317 (2022) 126049.
- [47] L. Liu, H. Li, A. Lazzaretto, G. Manente, C. Tong, Q. Liu, N. Li, The development history and prospects of biomass-based insulation materials for buildings, *Renewable and Sustainable Energy Reviews*, 69 (2017) 912-932.
- [48] I. Ferguson, B. La Fontaine, P. Vinden, L. Bren, R. Hateley, B.J.R.P.c.b.t.F. Hermesec, W.P. Research, D.w.f.o. au/publications/online/epotbrochure/manufacture, Environmental properties of timber, (1996).
- [49] P. Gupta, P.K. Maji, Characterization of Wood, Cork and Their Composites for Building Insulation, in: S. Hashmi, I.A. Choudhury (eds.) *Encyclopedia of Renewable and Sustainable Materials*, Elsevier, Oxford, 2020, pp. 44-59.
- [50] E. Sassoni, S. Manzi, A. Motori, M. Montecchi, M. Canti, Novel sustainable hemp-based composites for application in the building industry: Physical, thermal and mechanical characterization, *Energy and Buildings*, 77 (2014) 219-226.
- [51] F. Bennai, M.Y. Ferroukhi, F. Benmahiddine, R. Belarbi, A. Nouviaire, Assessment of hygrothermal performance of hemp concrete compared to conventional building materials at overall building scale, *Construction and Building Materials*, 316 (2022) 126007.
- [52] L. Liu, S. Zou, H. Li, L. Deng, C. Bai, X. Zhang, S. Wang, N. Li, Experimental physical properties of an eco-friendly bio-insulation material based on wheat straw for buildings, *Energy and Buildings*, 201 (2019) 19-36.
- [53] B. Belhadj, M. Bederina, Z. Makhloufi, A. Goullieux, M. Quéneudec, Study of the thermal performances of an exterior wall of barley straw sand concrete in an arid environment, *Energy and Buildings*, 87 (2015) 166-175.
- [54] F. Benmahiddine, R. Cherif, F. Bennai, R. Belarbi, A. Tahakourt, K. Abahri, Effect of flax shives content and size on the hygrothermal and mechanical properties of flax concrete, *Construction and Building Materials*, 262 (2020) 120077.
- [55] H.-R. Kymäläinen, A.-M. Sjöberg, Flax and hemp fibres as raw materials for thermal insulations, *Building and Environment*, 43 (2008) 1261-1269.
- [56] T. Li, J. Song, X. Zhao, Z. Yang, G. Pastel, S. Xu, C. Jia, J. Dai, C. Chen, A.J.S.a. Gong, Anisotropic, lightweight, strong, and super thermally insulating nanowood with naturally aligned nanocellulose, 4 (2018) eaar3724.
- [57] L. Bianco, R. Pollo, V. Serra, Wood Fiber vs Synthetic Thermal Insulation for Roofs Energy Retrofit: A Case Study in Turin, Italy, *Energy Procedia*, 111 (2017) 347-356.
- [58] V. Kočí, M. Jerman, Z. Pavlík, J. Maděra, J. Žák, R. Černý, Interior thermal insulation systems based on wood fiberboards: experimental analysis and computational assessment of hygrothermal and energy performance in the Central European climate, *Energy and Buildings*, 222 (2020) 110093.
- [59] X.-y. Zhou, F. Zheng, H.-g. Li, C.-l. Lu, An environment-friendly thermal insulation material from cotton stalk fibers, *Energy and Buildings*, 42 (2010) 1070-1074.
- [60] S. Panyakaew, S. Fotios, New thermal insulation boards made from coconut husk and bagasse, *Energy and Buildings*, 43 (2011) 1732-1739.
- [61] K. Wei, C. Lv, M. Chen, X. Zhou, Z. Dai, D. Shen, Development and performance evaluation of a new thermal insulation material from rice straw using high frequency hot-pressing, *Energy and Buildings*, 87 (2015) 116-122.
- [62] M.E. Ali, A. Alabdulkarem, On thermal characteristics and microstructure of a new insulation material extracted from date palm trees surface fibers, *Construction and Building Materials*, 138 (2017) 276-284.
- [63] S. Zou, H. Li, S. Wang, R. Jiang, J. Zou, X. Zhang, L. Liu, G. Zhang, Experimental research on an innovative sawdust biomass-based insulation material for buildings, *Journal of Cleaner Production*,

260 (2020) 121029.

- [64] K. Manohar, J. Ramroopsingh, D.W. Yarbrough, Use of Sugarcane Fiber as Building Insulation, in: A.O. Desjarlais, R.R. Zarr (eds.), ASTM International, West Conshohocken, PA, 2002, pp. 299-313.
- [65] J. Pinto, D. Cruz, A. Paiva, S. Pereira, P. Tavares, L. Fernandes, H. Varum, Characterization of corn cob as a possible raw building material, *Construction and Building Materials*, 34 (2012) 28-33.
- [66] P. Evon, V. Vandenbossche, P.-Y. Pontalier, L. Rigal, New thermal insulation fiberboards from cake generated during biorefinery of sunflower whole plant in a twin-screw extruder, *Industrial Crops and Products*, 52 (2014) 354-362.
- [67] N. Benmansour, B. Agoudjil, A. Gherabli, A. Kareche, A. Boudenne, Thermal and mechanical performance of natural mortar reinforced with date palm fibers for use as insulating materials in building, *Energy and Buildings*, 81 (2014) 98-104.
- [68] A.-b. Cherki, B. Remy, A. Khabbazi, Y. Jannot, D. Baillis, Experimental thermal properties characterization of insulating cork–gypsum composite, *Construction and Building Materials*, 54 (2014) 202-209.
- [69] H. Binici, O. Aksogan, Eco-friendly insulation material production with waste olive seeds, ground PVC and wood chips, *Journal of Building Engineering*, 5 (2016) 260-266.
- [70] B. Time, *Hygroscopic moisture transport in wood*, in, Norwegian University of Science and Technology Trondheim, 1998.
- [71] R. Shmulsky, P.D. Jones, *Forest products and wood science: an introduction*, John Wiley & Sons, 2019.
- [72] T.J.D.o.S.E. Padfield, L. Materials, Technical University of Denmark, The role of absorbent building materials in moderating changes of relative humidity, 150 (1998).
- [73] C. Rode, R. Peuhkuri, B. Time, K. Svennberg, T.J.J.o.A.I. Ojanen, Moisture buffer value of building materials, 4 (2007) 1-12.
- [74] Z. Chen, M. Qin, J. Yang, Synthesis and characteristics of hygroscopic phase change material: Composite microencapsulated phase change material (MPCM) and diatomite, *Energy and Buildings*, 106 (2015) 175-182.
- [75] N. Chennouf, B. Agoudjil, A. Boudenne, K. Benzarti, F. Bouras, Hygrothermal characterization of a new bio-based construction material: Concrete reinforced with date palm fibers, *Construction and Building Materials*, 192 (2018) 348-356.
- [76] M. Rahim, O. Douzane, A.D. Tran Le, G. Promis, B. Laidoudi, A. Crigny, B. Dupre, T. Langlet, Characterization of flax lime and hemp lime concretes: Hygric properties and moisture buffer capacity, *Energy and Buildings*, 88 (2015) 91-99.
- [77] F. Collet, S. Pretot, Experimental highlight of hygrothermal phenomena in hemp concrete wall, *Building and Environment*, 82 (2014) 459-466.
- [78] M. Rahim, O. Douzane, A.D. Tran Le, G. Promis, T. Langlet, Experimental investigation of hygrothermal behavior of two bio-based building envelopes, *Energy and Buildings*, 139 (2017) 608-615.
- [79] C. Maalouf, A.D.T. Le, S.B. Umurigirwa, M. Lachi, O. Douzane, Study of hygrothermal behaviour of a hemp concrete building envelope under summer conditions in France, *Energy and Buildings*, 77 (2014) 48-57.
- [80] A.D. Tran Le, C. Maalouf, T.H. Mai, E. Wurtz, F. Collet, Transient hygrothermal behaviour of a hemp concrete building envelope, *Energy and Buildings*, 42 (2010) 1797-1806.
- [81] B. Moujalled, Y. Aït Ouméziane, S. Moissette, M. Bart, C. Lanos, D. Samri, Experimental and numerical evaluation of the hygrothermal performance of a hemp lime concrete building: A long term case study, *Building and Environment*, 136 (2018) 11-27.
- [82] N. Chennouf, B. Agoudjil, T. Alioua, A. Boudenne, K. Benzarti, Experimental investigation on hygrothermal performance of a bio-based wall made of cement mortar filled with date palm fibers,

Energy and Buildings, 202 (2019) 109413.

- [83] D. Wu, M. Rahim, M. El Ganaoui, R. Djedjig, R. Bennacer, B. Liu, Experimental investigation on the hygrothermal behavior of a new multilayer building envelope integrating PCM with bio-based material, *Building and Environment*, 201 (2021) 107995.
- [84] D. Lelievre, T. Colinart, P. Glouannec, Hygrothermal behavior of bio-based building materials including hysteresis effects: Experimental and numerical analyses, *Energy and Buildings*, 84 (2014) 617-627.
- [85] C. Feng, H. Janssen, Hygric properties of porous building materials (II): Analysis of temperature influence, *Building and Environment*, 99 (2016) 107-118.
- [86] J. Hundt, Kantelberg, Hans, Sorption behavior of concrete Blocks, mortar and concrete, *Dtsch Ausschuss Stahlbeton*, (1978) 25-39.
- [87] J.-F.J.T.i.p.m. Daian, Condensation and isothermal water transfer in cement mortar Part I—Pore size distribution, equilibrium water condensation and imbibition, 3 (1988) 563-589.
- [88] S.J.C. Poyet, C. Research, Experimental investigation of the effect of temperature on the first desorption isotherm of concrete, 39 (2009) 1052-1059.
- [89] S. Poyet, Experimental investigation of the effect of temperature on the first desorption isotherm of concrete, *Cement and Concrete Research*, 39 (2009) 1052-1059.
- [90] S. Poyet, S. Charles, Temperature dependence of the sorption isotherms of cement-based materials: Heat of sorption and Clausius–Clapeyron formula, *Cement and Concrete Research*, 39 (2009) 1060-1067.
- [91] T. Colinart, P. Glouannec, Temperature dependence of sorption isotherm of hygroscopic building materials. Part 1: Experimental evidence and modeling, *Energy and Buildings*, 139 (2017) 360-370.
- [92] T. Colinart, P. Glouannec, M. Bendouma, P. Chauvelon, Temperature dependence of sorption isotherm of hygroscopic building materials. Part 2: Influence on hygrothermal behavior of hemp concrete, *Energy and Buildings*, 152 (2017) 42-51.
- [93] Y. Aït Oumeziane, S. Moissette, M. Bart, C. Lanos, Influence of temperature on sorption process in hemp concrete, *Construction and Building Materials*, 106 (2016) 600-607.
- [94] M. Rahim, A.D. Tran Le, O. Douzane, G. Promis, T. Langlet, Numerical investigation of the effect of non-isotherme sorption characteristics on hygrothermal behavior of two bio-based building walls, *Journal of Building Engineering*, 7 (2016) 263-272.
- [95] A.D.T. Le, D. Samri, O. Douzane, G. Promis, A.T. Nguyen, T.J.E.o.R. Langlet, E. Sustainable Materials, Effect of Temperature Dependence of Sorption on Hygrothermal Performance of a Hemp Concrete Building Envelope, 2 (2020) 68-77.
- [96] N. Mendes, P.C. Philippi, R. Lamberts, A new mathematical method to solve highly coupled equations of heat and mass transfer in porous media, *International Journal of Heat and Mass Transfer*, 45 (2002) 509-518.
- [97] N. Mendes, F.C. Winkelmann, R. Lamberts, P.C. Philippi, Moisture effects on conduction loads, *Energy and Buildings*, 35 (2003) 631-644.
- [98] O.F. Osanyintola, C.J. Simonson, Moisture buffering capacity of hygroscopic building materials: Experimental facilities and energy impact, *Energy and Buildings*, 38 (2006) 1270-1282.
- [99] R.M. Barbosa, N. Mendes, Combined simulation of central HVAC systems with a whole-building hygrothermal model, *Energy and Buildings*, 40 (2008) 276-288.
- [100] X. Liu, Y. Chen, H. Ge, P. Fazio, G. Chen, Numerical investigation for thermal performance of exterior walls of residential buildings with moisture transfer in hot summer and cold winter zone of China, *Energy and Buildings*, 93 (2015) 259-268.
- [101] X. Liu, Y. Chen, H. Ge, P. Fazio, G. Chen, X. Guo, Determination of optimum insulation thickness for building walls with moisture transfer in hot summer and cold winter zone of China, *Energy and Buildings*, 109 (2015) 361-368.
- [102] M. Woloszyn, T. Kalamees, M. Olivier Abadie, M. Steeman, A. Sasic Kalagasidis, The effect

of combining a relative-humidity-sensitive ventilation system with the moisture-buffering capacity of materials on indoor climate and energy efficiency of buildings, *Building and Environment*, 44 (2009) 515-524.

[103] Y. Liu, Y. Wang, D. Wang, J. Liu, Effect of moisture transfer on internal surface temperature, *Energy and Buildings*, 60 (2013) 83-91.

[104] Y. Wang, Y. Liu, D. Wang, J. Liu, Effect of the night ventilation rate on the indoor environment and air-conditioning load while considering wall inner surface moisture transfer, *Energy and Buildings*, 80 (2014) 366-374.

[105] R. Saxena, D. Rakshit, S.C. Kaushik, Experimental assessment of Phase Change Material (PCM) embedded bricks for passive conditioning in buildings, *Renewable Energy*, 149 (2020) 587-599.

[106] L. Yang, J.-n. Huang, F. Zhou, Thermophysical properties and applications of nano-enhanced PCMs: An update review, *Energy Conversion and Management*, 214 (2020) 112876.

[107] D.A. Neeper, Potential benefits of distributed PCM thermal, in, United States, 1989.

[108] D.A. Neeper, Thermal dynamics of wallboard with latent heat storage, *Solar Energy*, 68 (2000) 393-403.

[109] R.J. Kedl, T.K. Stovall, Activities in support of the wax-impregnated wallboard concept, in, United States, 1989.

[110] A. Pasupathy, R. Velraj, R.V. Seeniraj, Phase change material-based building architecture for thermal management in residential and commercial establishments, *Renewable and Sustainable Energy Reviews*, 12 (2008) 39-64.

[111] A.F. Regin, S.C. Solanki, J.S. Saini, Heat transfer characteristics of thermal energy storage system using PCM capsules: A review, *Renewable and Sustainable Energy Reviews*, 12 (2008) 2438-2458.

[112] A. Sharma, V.V. Tyagi, C.R. Chen, D. Buddhi, Review on thermal energy storage with phase change materials and applications, *Renewable and Sustainable Energy Reviews*, 13 (2009) 318-345.

[113] R. Baetens, B.P. Jelle, A. Gustavsen, Phase change materials for building applications: A state-of-the-art review, *Energy and Buildings*, 42 (2010) 1361-1368.

[114] D. Zhou, C.Y. Zhao, Y. Tian, Review on thermal energy storage with phase change materials (PCMs) in building applications, *Applied Energy*, 92 (2012) 593-605.

[115] N. Soares, J.J. Costa, A.R. Gaspar, P. Santos, Review of passive PCM latent heat thermal energy storage systems towards buildings' energy efficiency, *Energy and Buildings*, 59 (2013) 82-103.

[116] A. Waqas, Z. Ud Din, Phase change material (PCM) storage for free cooling of buildings—A review, *Renewable and Sustainable Energy Reviews*, 18 (2013) 607-625.

[117] S.A. Memon, Phase change materials integrated in building walls: A state of the art review, *Renewable and Sustainable Energy Reviews*, 31 (2014) 870-906.

[118] D. Feldman, D. Banu, D. Hawes, E. Ghanbari, Obtaining an energy storing building material by direct incorporation of an organic phase change material in gypsum wallboard, *Solar Energy Materials*, 22 (1991) 231-242.

[119] D. Zhou, C.Y. Zhao, Y. Tian, Review on thermal energy storage with phase change materials (PCMs) in building applications, *Applied Energy*, 92 (2012) 593-605.

[120] M.N.A. Hawlader, M.S. Uddin, M.M. Khin, Microencapsulated PCM thermal-energy storage system, *Applied Energy*, 74 (2003) 195-202.

[121] V.V. Tyagi, D. Buddhi, Thermal cycle testing of calcium chloride hexahydrate as a possible PCM for latent heat storage, *Solar Energy Materials and Solar Cells*, 92 (2008) 891-899.

[122] M. Koschenz, B. Lehmann, Development of a thermally activated ceiling panel with PCM for application in lightweight and retrofitted buildings, *Energy and Buildings*, 36 (2004) 567-578.

[123] N. Arconada, L. Arribas, B. Lucio, J. González-Aguilar, M. Romero, Macroencapsulation of sodium chloride as phase change materials for thermal energy storage, *Solar Energy*, 167 (2018) 1-9.

[124] L. Erlbeck, P. Schreiner, F. Fasel, F.J. Methner, M. Rädle, Investigation of different materials

for macroencapsulation of salt hydrate phase change materials for building purposes, *Construction and Building Materials*, 180 (2018) 512-518.

[125] M.-J. Li, B. Jin, Z. Ma, F. Yuan, Experimental and numerical study on the performance of a new high-temperature packed-bed thermal energy storage system with macroencapsulation of molten salt phase change material, *Applied Energy*, 221 (2018) 1-15.

[126] H. Inaba, P. Tu, Evaluation of thermophysical characteristics on shape-stabilized paraffin as a solid-liquid phase change material, *Heat and Mass Transfer*, 32 (1997) 307-312.

[127] W.-l. Cheng, R.-m. Zhang, K. Xie, N. Liu, J. Wang, Heat conduction enhanced shape-stabilized paraffin/HDPE composite PCMs by graphite addition: Preparation and thermal properties, *Solar Energy Materials and Solar Cells*, 94 (2010) 1636-1642.

[128] Y. Yang, W. Wu, S. Fu, H. Zhang, Study of a novel ceramsite-based shape-stabilized composite phase change material (PCM) for energy conservation in buildings, *Construction and Building Materials*, 246 (2020) 118479.

[129] B. Xu, Z. Li, Paraffin/diatomite composite phase change material incorporated cement-based composite for thermal energy storage, *Applied Energy*, 105 (2013) 229-237.

[130] A. Sarı, A. Karaipekli, C. Alkan, Preparation, characterization and thermal properties of lauric acid/expanded perlite as novel form-stable composite phase change material, *Chemical Engineering Journal*, 155 (2009) 899-904.

[131] T.-C. Ling, C.-S. Poon, S.-C. Kou, Feasibility of using recycled glass in architectural cement mortars, *Cement and Concrete Composites*, 33 (2011) 848-854.

[132] P. Schossig, H.M. Henning, S. Gschwander, T. Haussmann, Micro-encapsulated phase-change materials integrated into construction materials, *Solar Energy Materials and Solar Cells*, 89 (2005) 297-306.

[133] F. Kuznik, D. David, K. Johannes, J.J. Roux, A review on phase change materials integrated in building walls, *Renewable & Sustainable Energy Reviews*, 15 (2011) 379-391.

[134] Y.P. Zhang, K.P. Lin, R. Yang, H.F. Di, Y. Jiang, Preparation, thermal performance and application of shape-stabilized PCM in energy efficient buildings, *Energy and Buildings*, 38 (2006) 1262-1269.

[135] M. Zhu, Z. Wang, H. Zhang, X. Sun, B. Dou, W. Wu, G. Zhang, L. Jiang, Experimental investigation of the comprehensive heat transfer performance of PCMs filled with CMF in a heat storage device, *International Journal of Heat and Mass Transfer*, 188 (2022) 122582.

[136] T. Silva, R. Vicente, N. Soares, V. Ferreira, Experimental testing and numerical modelling of masonry wall solution with PCM incorporation: A passive construction solution, *Energy and Buildings*, 49 (2012) 235-245.

[137] M. Kenisarin, K. Mahkamov, Solar energy storage using phase change materials, *Renewable and Sustainable Energy Reviews*, 11 (2007) 1913-1965.

[138] F. Kuznik, J. Virgone, K. Johannes, In-situ study of thermal comfort enhancement in a renovated building equipped with phase change material wallboard, *Renewable Energy*, 36 (2011) 1458-1462.

[139] C. Li, H. Yu, Y. Song, Experimental investigation of thermal performance of microencapsulated PCM-contained wallboard by two measurement modes, *Energy and Buildings*, 184 (2019) 34-43.

[140] J. Guo, G. Zhang, Investigating the performance of the PCM-integrated building envelope on a seasonal basis, *Journal of the Taiwan Institute of Chemical Engineers*, 124 (2021) 91-97.

[141] L. Karim, F. Barbeon, P. Gegout, A. Bontemps, L. Royon, New phase-change material components for thermal management of the light weight envelope of buildings, *Energy and Buildings*, 68 (2014) 703-706.

[142] L. Royon, L. Karim, A. Bontemps, Optimization of PCM embedded in a floor panel developed for thermal management of the lightweight envelope of buildings, *Energy and Buildings*, 82 (2014) 385-390.

[143] J. Kośny, K. Biswas, W. Miller, S. Kriner, Field thermal performance of naturally ventilated

solar roof with PCM heat sink, *Solar Energy*, 86 (2012) 2504-2514.

- [144] D. Li, Y. Zheng, C. Liu, G. Wu, Numerical analysis on thermal performance of roof contained PCM of a single residential building, *Energy Conversion and Management*, 100 (2015) 147-156.
- [145] J. Xamán, A. Rodríguez-Ake, I. Zavala-Guillén, I. Hernández-Pérez, J. Arce, D. Saucedo, Thermal performance analysis of a roof with a PCM-layer under Mexican weather conditions, *Renewable Energy*, 149 (2020) 773-785.
- [146] N.A. Yahay, H. Ahmad, Numerical Investigation of Indoor Air Temperature with the Application of PCM Gypsum Board as Ceiling Panels in Buildings, *Procedia Engineering*, 20 (2011) 238-248.
- [147] M.J. Abden, Z. Tao, Z. Pan, L. George, R. Wuhler, Inclusion of methyl stearate/diatomite composite in gypsum board ceiling for building energy conservation, *Applied Energy*, 259 (2020) 114113.
- [148] H. Weinläder, F. Klinker, M. Yasin, PCM cooling ceilings in the Energy Efficiency Center—passive cooling potential of two different system designs, *Energy and Buildings*, 119 (2016) 93-100.
- [149] H. Weinläder, F. Klinker, M. Yasin, PCM cooling ceilings in the Energy Efficiency Center – Regeneration behaviour of two different system designs, *Energy and Buildings*, 156 (2017) 70-77.
- [150] H. Weinläder, W. Körner, B. Strieder, A ventilated cooling ceiling with integrated latent heat storage—Monitoring results, *Energy and Buildings*, 82 (2014) 65-72.
- [151] E.M. Alawadhi, Using phase change materials in window shutter to reduce the solar heat gain, *Energy and Buildings*, 47 (2012) 421-429.
- [152] F. Goia, M. Perino, V. Serra, Improving thermal comfort conditions by means of PCM glazing systems, *Energy & Buildings*, 60 (2013) 442-452.
- [153] F. Goia, M. Perino, V. Serra, Experimental analysis of the energy performance of a full-scale PCM glazing prototype, *Solar Energy*, 100 (2014) 217-233.
- [154] D. Li, Y. Wu, C. Liu, G. Zhang, M. Arıcı, Energy investigation of glazed windows containing Nano-PCM in different seasons, *Energy Conversion and Management*, 172 (2018) 119-128.
- [155] M.F.L. King, P.N. Rao, A. Sivakumar, V.K. Mamidi, S. Richard, M. Vijayakumar, K. Arunprasath, P.M. Kumar, Thermal performance of a double-glazed window integrated with a phase change material (PCM), *Materials Today: Proceedings*, (2021).
- [156] C. Piselli, V.L. Castaldo, A.L. Pisello, How to enhance thermal energy storage effect of PCM in roofs with varying solar reflectance: Experimental and numerical assessment of a new roof system for passive cooling in different climate conditions, *Solar Energy*, 192 (2019) 106-119.
- [157] A. Fateh, D. Borelli, H. Weinläder, F. Devia, Cardinal orientation and melting temperature effects for PCM-enhanced light-walls in different climates, *Sustainable Cities and Society*, 51 (2019) 101766.
- [158] F. Souayfane, P.H. Biwolé, F. Fardoun, P. Achard, Energy performance and economic analysis of a TIM-PCM wall under different climates, *Energy*, 169 (2019) 1274-1291.
- [159] M. Ahangari, M. Maerefat, An innovative PCM system for thermal comfort improvement and energy demand reduction in building under different climate conditions, *Sustainable Cities and Society*, 44 (2019) 120-129.
- [160] J. Yu, K. Leng, H. Ye, X. Xu, Y. Luo, J. Wang, X. Yang, Q. Yang, W. Gang, Study on thermal insulation characteristics and optimized design of pipe-embedded ventilation roof with outer-layer shape-stabilized PCM in different climate zones, *Renewable Energy*, 147 (2020) 1609-1622.
- [161] X. Jin, S. Zhang, X. Xu, X. Zhang, Effects of PCM state on its phase change performance and the thermal performance of building walls, *Building and Environment*, 81 (2014) 334-339.
- [162] X. Jin, M.A. Medina, X. Zhang, Numerical analysis for the optimal location of a thin PCM layer in frame walls, *Applied Thermal Engineering*, 103 (2016) 1057-1063.
- [163] X. Jin, M.A. Medina, X. Zhang, On the importance of the location of PCMs in building walls for enhanced thermal performance, *Applied Energy*, 106 (2013) 72-78.

- [164] X. Jin, D. Shi, M.A. Medina, X. Shi, X. Zhou, X. Zhang, Optimal location of PCM layer in building walls under Nanjing (China) weather conditions, *Journal of Thermal Analysis and Calorimetry*, 129 (2017) 1767-1778.
- [165] K.O. Lee, M.A. Medina, E. Raith, X. Sun, Assessing the integration of a thin phase change material (PCM) layer in a residential building wall for heat transfer reduction and management, *Applied Energy*, 137 (2015) 699-706.
- [166] A. Lagou, A. Kylili, J. Šadauskienė, P.A. Fokaides, Numerical investigation of phase change materials (PCM) optimal melting properties and position in building elements under diverse conditions, *Construction and Building Materials*, 225 (2019) 452-464.
- [167] R.A. Kishore, M.V.A. Bianchi, C. Booten, J. Vidal, R. Jackson, Optimizing PCM-integrated walls for potential energy savings in U.S. Buildings, *Energy and Buildings*, 226 (2020) 110355.
- [168] R.A. Kishore, M.V.A. Bianchi, C. Booten, J. Vidal, R. Jackson, Parametric and sensitivity analysis of a PCM-integrated wall for optimal thermal load modulation in lightweight buildings, *Applied Thermal Engineering*, 187 (2021) 116568.
- [169] Z.X. Li, A.A.A.A. Al-Rashed, M. Rostamzadeh, R. Kalbasi, A. Shahsavari, M. Afrand, Heat transfer reduction in buildings by embedding phase change material in multi-layer walls: Effects of repositioning, thermophysical properties and thickness of PCM, *Energy Conversion and Management*, 195 (2019) 43-56.
- [170] E. Köse Murathan, G. Manioğlu, Evaluation of phase change materials used in building components for conservation of energy in buildings in hot dry climatic regions, *Renewable Energy*, 162 (2020) 1919-1930.
- [171] A.C. Rai, Energy performance of phase change materials integrated into brick masonry walls for cooling load management in residential buildings, *Building and Environment*, 199 (2021) 107930.
- [172] J. Yu, Q. Yang, H. Ye, Y. Luo, J. Huang, X. Xu, W. Gang, J. Wang, Thermal performance evaluation and optimal design of building roof with outer-layer shape-stabilized PCM, *Renewable Energy*, 145 (2020) 2538-2549.
- [173] E. Mohseni, W. Tang, Parametric analysis and optimisation of energy efficiency of a lightweight building integrated with different configurations and types of PCM, *Renewable Energy*, 168 (2021) 865-877.
- [174] M. Li, Q. Cao, H. Pan, X. Wang, Z. Lin, Effect of melting point on thermodynamics of thin PCM reinforced residential frame walls in different climate zones, *Applied Thermal Engineering*, 188 (2021) 116615.
- [175] J. Lei, J. Yang, E.-H. Yang, Energy performance of building envelopes integrated with phase change materials for cooling load reduction in tropical Singapore, *Applied Energy*, 162 (2016) 207-217.
- [176] X. He, H. Zhang, L. Qiu, Z. Mao, C. Shi, Hygrothermal performance of temperature-humidity controlling materials with different compositions, *Energy and Buildings*, 236 (2021) 110792.
- [177] Z. Wu, M. Qin, Z. Chen, Phase Change Humidity Control Material and its Application in Buildings, *Procedia Engineering*, 205 (2017) 1011-1018.
- [178] Z. Chen, M. Qin, Preparation and hygrothermal properties of composite phase change humidity control materials, *Applied Thermal Engineering*, 98 (2016) 1150-1157.
- [179] P. Hou, M. Qin, S. Cui, K. Zu, Preparation and characterization of metal-organic framework /microencapsulated phase change material composites for indoor hygrothermal control, *Journal of Building Engineering*, 31 (2020) 101345.
- [180] J.H. Park, Y. Kang, J. Lee, S. Wi, J.D. Chang, S. Kim, Analysis of walls of functional gypsum board added with porous material and phase change material to improve hygrothermal performance, *Energy and Buildings*, 183 (2019) 803-816.
- [181] S.J. Chang, Y. Kang, S. Wi, S.-G. Jeong, S. Kim, Hygrothermal performance improvement of the Korean wood frame walls using macro-packed phase change materials (MPPCM), *Applied*

Thermal Engineering, 114 (2017) 457-465.

- [182] X. Shi, S.A. Memon, W. Tang, H. Cui, F. Xing, Experimental assessment of position of macro encapsulated phase change material in concrete walls on indoor temperatures and humidity levels, *Energy and Buildings*, 71 (2014) 80-87.
- [183] Y. Fraine, C. Seladji, A. Aït-Mokhtar, Effect of microencapsulation phase change material and diatomite composite filling on hygrothermal performance of sintered hollow bricks, *Building and Environment*, 154 (2019) 145-154.
- [184] Z. Wu, M. Qin, M. Zhang, Phase change humidity control material and its impact on building energy consumption, *Energy and Buildings*, 174 (2018) 254-261.
- [185] N. Zhu, X. Li, P. Hu, F. Lei, S. Wei, W. Wang, An exploration on the performance of using phase change humidity control material wallboards in office buildings, *Energy*, 239 (2022) 122433.
- [186] A. Fick, *Ueber Diffusion*, 170 (1855) 59-86.
- [187] H.M.J.O.-a.t.-d.c.u.s.p.I.-V.S. Kunzel, Simultaneous heat and moisture transport in building components, 65 (1995).
- [188] G. Promis, O. Douzane, A.D. Tran Le, T. Langlet, Moisture hysteresis influence on mass transfer through bio-based building materials in dynamic state, *Energy and Buildings*, 166 (2018) 450-459.
- [189] A. Tadeu, L. Škerget, N. Simões, R. Fino, Simulation of heat and moisture flow through walls covered with uncoated medium density expanded cork, *Building and Environment*, 142 (2018) 195-210.
- [190] S. Whitaker, Flow in porous media I: A theoretical derivation of Darcy's law, *Transport in Porous Media*, 1 (1986) 3-25.
- [191] H.M.J.F.I.o.b.p. Kunzel, *Allemagne*, Simultaneous heat and moisture transport in building components, (1995).
- [192] M.-A. Hamdaoui, M.-H. Benzaama, Y. El Mendili, D. Chateigner, A review on physical and data-driven modeling of buildings hygrothermal behavior: Models, approaches and simulation tools, *Energy and Buildings*, 251 (2021) 111343.
- [193] J.R.P.D.A.D. Vries, Moisture movement in porous materials under temperature gradients, 38 (1957) 222-232.
- [194] D.A.D. Vries, Simultaneous transfer of heat and moisture in porous media, 39 (1958) 909-916.
- [195] D.A. De Vries, The theory of heat and moisture transfer in porous media revisited, *International Journal of Heat and Mass Transfer*, 30 (1987) 1343-1350.
- [196] A.V. Luikov, Heat and Mass Transfer in Capillary-Porous Bodies, in: T.F. Irvine, J.P. Hartnett (eds.) *Advances in Heat Transfer*, Vol. 1, Elsevier, 1964, pp. 123-184.
- [197] A.V. Luikov, A.G. Shashkov, L.L. Vasiliev, Y.E. Fraiman, Thermal conductivity of porous systems, *International Journal of Heat and Mass Transfer*, 11 (1968) 117-140.
- [198] A.V. Luikov, Systems of differential equations of heat and mass transfer in capillary-porous bodies (review), *International Journal of Heat and Mass Transfer*, 18 (1975) 1-14.
- [199] S. Whitaker, Simultaneous heat, mass, and momentum transfer in porous media: a theory of drying, in: *Advances in heat transfer*, Vol. 13, Elsevier, 1977, pp. 119-203.
- [200] N. Mendes, I. Ridley, R. Lamberts, P.C. Philippi, K. Budag, UMIDUS: a PC program for the prediction of heat and moisture transfer in porous building elements, in: *Building Simulation Conference—IBPSA*, Vol. 99, 1999, pp. 277-283.
- [201] R. El Diasty, P. Fazio, I. Budaiwi, Dynamic modelling of moisture absorption and desorption in buildings, *Building and Environment*, 28 (1993) 21-32.
- [202] G.H. dos Santos, N. Mendes, Heat, air and moisture transfer through hollow porous blocks, *International Journal of Heat and Mass Transfer*, 52 (2009) 2390-2398.
- [203] P. Häupl, J. Grunewald, H. Fechner, H. Stopp, Coupled heat air and moisture transfer in building structures, *International Journal of Heat and Mass Transfer*, 40 (1997) 1633-1642.
- [204] M. Matsumoto, S. Hokoi, M. Hatano, Model for simulation of freezing and thawing processes

- in building materials, *Building and Environment*, 36 (2001) 733-742.
- [205] C. Vuik, Some historical notes about the Stefan problem, (1993).
- [206] C. Chen, H. Guo, Y. Liu, H. Yue, C. Wang, A new kind of phase change material (PCM) for energy-storing wallboard, *Energy and Buildings*, 40 (2008) 882-890.
- [207] F. Kuznik, D. David, K. Johannes, J.-J. Roux, A review on phase change materials integrated in building walls, *Renewable and Sustainable Energy Reviews*, 15 (2011) 379-391.
- [208] S.E. Kalnæs, B.P. Jelle, Phase change materials and products for building applications: A state-of-the-art review and future research opportunities, *Energy and Buildings*, 94 (2015) 150-176.
- [209] P.J. Haines, M. Reading, F.W. Wilburn, Chapter 5 - Differential Thermal Analysis and Differential Scanning Calorimetry, in: M.E. Brown (ed.) *Handbook of Thermal Analysis and Calorimetry*, Vol. 1, Elsevier Science B.V., 1998, pp. 279-361.
- [210] Z. Yinping, J. Yi, J. Yi, A simple method, the -history method, of determining the heat of fusion, specific heat and thermal conductivity of phase-change materials, *Measurement Science and Technology*, 10 (1999) 201-205.
- [211] A. Solé, L. Miró, C. Barreneche, I. Martorell, L.F. Cabeza, Review of the T-history method to determine thermophysical properties of phase change materials (PCM), *Renewable and Sustainable Energy Reviews*, 26 (2013) 425-436.
- [212] J.M. Marín, B. Zalba, L.F. Cabeza, H. Mehling, Determination of enthalpy temperature curves of phase change materials with the temperature-history method: improvement to temperature dependent properties, *Measurement Science and Technology*, 14 (2003) 184-189.
- [213] ASTM, Standard test method for steady-state thermal transmission properties by means of the heat flow meter apparatus, ASTM International, (2010) 15.
- [214] F. Frusteri, V. Leonardi, S. Vasta, G. Restuccia, Thermal conductivity measurement of a PCM based storage system containing carbon fibers, *Applied Thermal Engineering*, 25 (2005) 1623-1633.
- [215] A. Karaipekli, A. Sarı, K. Kaygusuz, Thermal conductivity improvement of stearic acid using expanded graphite and carbon fiber for energy storage applications, *Renewable Energy*, 32 (2007) 2201-2210.
- [216] V.R. Voller, L. Shadabi, Enthalpy methods for tracking a phase change boundary in two dimensions, *International Communications in Heat and Mass Transfer*, 11 (1984) 239-249.
- [217] P. Verma, Varun, S.K. Singal, Review of mathematical modeling on latent heat thermal energy storage systems using phase-change material, *Renewable and Sustainable Energy Reviews*, 12 (2008) 999-1031.
- [218] S. Karthikeyan, R. Velraj, Numerical investigation of packed bed storage unit filled with PCM encapsulated spherical containers – A comparison between various mathematical models, *International Journal of Thermal Sciences*, 60 (2012) 153-160.
- [219] D. Poirier, M. Salcudean, On numerical methods used in mathematical modeling of phase change in liquid metals, (1988).
- [220] H. Yang, Y. He, Solving heat transfer problems with phase change via smoothed effective heat capacity and element-free Galerkin methods, *International Communications in Heat and Mass Transfer*, 37 (2010) 385-392.
- [221] C. Tzivanidis, K. Antonopoulos, E.J.I.j.o.e.r. Kravvaritis, Parametric analysis of space cooling systems based on night ceiling cooling with PCM-embedded piping, 36 (2012) 18-35.
- [222] D. Energain®, Hydrocarbon-based PCM Applications, in, Vol. (accessed 04 December 2021, 2010).
- [223] G. Costantine, C. Maalouf, T. Moussa, G. Polidori, Experimental and numerical investigations of thermal performance of a Hemp Lime external building insulation, *Building and Environment*, 131 (2018) 140-153.
- [224] H. Djamil, Indoor thermal comfort predictions: Selected issues and trends, *Renewable and Sustainable Energy Reviews*, 74 (2017) 569-580.

- [225] Y. Aït Oumeziane, S. Moissette, M. Bart, F. Collet, S. Pretot, C. Lanos, Influence of hysteresis on the transient hygrothermal response of a hemp concrete wall, *Journal of Building Performance Simulation*, 10 (2017) 256-271.
- [226] G. Stefanovich, A. Pergament, D. Stefanovich, Electrical switching and Mott transition in VO<sub>2</sub>, *Journal of Physics: Condensed Matter*, 12 (2000) 8837-8845.
- [227] J. Cape, G.J.J.o.a.p. Lehman, Temperature and finite pulse-time effects in the flash method for measuring thermal diffusivity, 34 (1963) 1909-1913.
- [228] G. Gilboa, R. Chen, N.J.J.o.N. Brenner, History-dependent multiple-time-scale dynamics in a single-neuron model, 25 (2005) 6479-6489.
- [229] R.W. Lewis, P. Nithiarasu, K.N. Seetharamu, *Fundamentals of the finite element method for heat and fluid flow*, John Wiley & Sons, 2004.
- [230] I. Adilkhanova, S.A. Memon, J. Kim, A. Sheriyev, A novel approach to investigate the thermal comfort of the lightweight relocatable building integrated with PCM in different climates of Kazakhstan during summertime, *Energy*, 217 (2021) 119390.
- [231] G. Evola, L. Marletta, F. Sicurella, A methodology for investigating the effectiveness of PCM wallboards for summer thermal comfort in buildings, *Building and Environment*, 59 (2013) 517-527.
- [232] K. Peippo, P. Kauranen, P.D. Lund, A multicomponent PCM wall optimized for passive solar heating, *Energy and Buildings*, 17 (1991) 259-270.
- [233] P.K.S. Rathore, S.K. Shukla, Enhanced thermophysical properties of organic PCM through shape stabilization for thermal energy storage in buildings: A state of the art review, *Energy and Buildings*, 236 (2021) 110799.
- [234] S. Drissi, T.-C. Ling, K.H. Mo, Thermal performance of a solar energy storage concrete panel incorporating phase change material aggregates developed for thermal regulation in buildings, *Renewable Energy*, 160 (2020) 817-829.
- [235] F. Benmahiddine, F. Bennai, R. Cherif, R. Belarbi, A. Tahakourt, K. Abahri, Experimental investigation on the influence of immersion/drying cycles on the hygrothermal and mechanical properties of hemp concrete, *Journal of Building Engineering*, 32 (2020) 101758.
- [236] M. Rahim, Analysis and characterization of the hygrothermal behavior of bio based walls at real scale: experimentation and modeling
- Analyse et caractérisation du comportement hygrothermique de parois agro-sourcées à l'échelle 1 : expérimentation et modélisation, in, Université de Picardie Jules Verne (UPJV), Amiens, FRA. Ecole doctorale en Sciences Technologie et Santé, 2015.
- [237] R. Peuhkuri, *Moisture Dynamics in Building Envelopes*, (2003).
- [238] K.P. Galvin, A conceptually simple derivation of the Kelvin equation, *Chemical Engineering Science*, 60 (2005) 4659-4660.
- [239] Y. Wang, Y. Fan, D. Wang, Y. Liu, J. Liu, The effect of moisture transfer on the inner surface thermal performance and the thermal transmittance of the roof-wall corner building node in high-temperature and high-humidity areas, *Journal of Building Engineering*, 44 (2021) 102949.
- [240] S. Zhou, R. Zhang, Z. Zhang, *Climatology and meteorology*, (2002).
- [241] S. Wijesuriya, P.C. Tabares-Velasco, K. Biswas, D. Heim, Empirical validation and comparison of PCM modeling algorithms commonly used in building energy and hygrothermal software, *Building and Environment*, 173 (2020) 106750.
- [242] L.P. Li, Z.G. Wu, Y.L. He, G. Lauriat, W.Q. Tao, Optimization of the configuration of 290×140×90 hollow clay bricks with 3-D numerical simulation by finite volume method, *Energy and Buildings*, 40 (2008) 1790-1798.
- [243] G.N. Walton, *Thermal Analysis Research Program Reference Manual*, National Bureau of Standards, March, (1983).
- [244] W.C. Swinbank, Long-wave radiation from clear skies, *Quarterly Journal of the Royal*

Meteorological Society, 89 (1963) 339-348.

- [245] C. Rode, R. Peuhkuri, H. Lone, B. Time, A. Gustavsen, T. Ojanen, J. Ahonen, K. Svennberg, L.-E. Harderup, J. Arfvidsson, Moisture buffering of building materials, (2006).
- [246] V.Y. Borodulin, M.I. Nizovtsev, Modeling heat and moisture transfer of building facades thermally insulated by the panels with ventilated channels, *Journal of Building Engineering*, 40 (2021) 102391.
- [247] M. Simo-Tagne, R. Remond, R. Kharchi, L. Bennamoun, M.C. Ndukwu, Y. Rogaume, Modeling, numerical simulation and validation of the hygrothermal transfer through a wooden building wall in Nancy, France, *Thermal Science and Engineering Progress*, 22 (2021) 100808.
- [248] X. Wang, X. Jin, Y. Yin, X. Shi, X. Zhou, A transient heat and moisture transfer model for building materials based on phase change criterion under isothermal and non-isothermal conditions, *Energy*, 224 (2021) 120112.
- [249] M. Kabdrakhmanova, S.A. Memon, A. Saurbayeva, Implementation of the panel data regression analysis in PCM integrated buildings located in a humid subtropical climate, *Energy*, 237 (2021) 121651.
- [250] Y. Qu, D. Zhou, F. Xue, L. Cui, Multi-factor analysis on thermal comfort and energy saving potential for PCM-integrated buildings in summer, *Energy and Buildings*, 241 (2021) 110966.
- [251] A. Sarri, D. Bechki, H. Bouguettaia, S.N. Al-Saadi, S. Boughali, M.M. Farid, Effect of using PCMs and shading devices on the thermal performance of buildings in different Algerian climates. A simulation-based optimization, *Solar Energy*, 217 (2021) 375-389.
- [252] X.D. Hang, W. Sun, C. Ye, Finite volume solution of heat and moisture transfer through three-dimensional textile materials, *Computers & Fluids*, 57 (2012) 25-39.
- [253] K. Taurines, S. Giroux-Julien, M. Farid, C. Ménézo, Numerical modelling of a building integrated earth-to-air heat exchanger, *Applied Energy*, 296 (2021) 117030.
- [254] C. Xu, S. Li, K. Zou, Study of heat and moisture transfer in internal and external wall insulation configurations, *Journal of Building Engineering*, 24 (2019) 100724.
- [255] S.N. Al-Saadi, Z. Zhai, Systematic evaluation of mathematical methods and numerical schemes for modeling PCM-enhanced building enclosure, *Energy and Buildings*, 92 (2015) 374-388.
- [256] M. Mahdaoui, S. Hamdaoui, A. Ait Msaad, T. Kousksou, T. El Rhafiki, A. Jamil, M. Ahachad, Building bricks with phase change material (PCM): Thermal performances, *Construction and Building Materials*, 269 (2021) 121315.
- [257] H.M. Abbas, J.M. Jalil, S.T. Ahmed, Experimental and numerical investigation of PCM capsules as insulation materials inserted into a hollow brick wall, *Energy and Buildings*, 246 (2021) 111127.
- [258] M. Rovitto, Electromigration reliability issue in interconnects for three-dimensional integration technologies, in, *Wien*, 2016.
- [259] B. Cho, D. Park, J. Kim, H. Hamasaki, Study on the heat-moisture transfer in concrete under real environment, *Construction and Building Materials*, 132 (2017) 124-129.
- [260] M. Autengruber, M. Lukacevic, J. Füssl, Finite-element-based moisture transport model for wood including free water above the fiber saturation point, *International Journal of Heat and Mass Transfer*, 161 (2020) 120228.
- [261] T. Alioua, B. Agoudjil, A. Boudenne, K. Benzarti, Sensitivity analysis of transient heat and moisture transfer in a bio-based date palm concrete wall, *Building and Environment*, 202 (2021) 108019.
- [262] A.N. Desai, H. Shah, V.K. Singh, Novel inverted fin configurations for enhancing the thermal performance of PCM based thermal control unit: A numerical study, *Applied Thermal Engineering*, 195 (2021) 117155.
- [263] Z. Xiao, P. Mishra, A. Mahdavi Nejad, M. Tao, S. Granados-Focil, S. Van Dessel, Thermal optimization of a novel thermo-optically responsive SS-PCM coatings for building enclosures, *Energy and Buildings*, 247 (2021) 111129.

- [264] K.J. Kontoleon, M. Stefanidou, S. Saboor, D. Mazzeo, A. Karaoulis, D. Zeggini, D. Kraniotis, Defensive behaviour of building envelopes in terms of mechanical and thermal responsiveness by incorporating PCMs in cement mortar layers, *Sustainable Energy Technologies and Assessments*, 47 (2021) 101349.
- [265] E.I. 13788:, Hygrothermal performance of building components and building elements–internal surface temperature to avoid critical surface humidity and interstitial condensation–calculation methods (European Committee for Standardization), (2012).
- [266] P.W. O'Callaghan, S.D. Probert, Sol-air temperature, *Applied Energy*, 3 (1977) 307-311.
- [267] A. Fateh, F. Klinker, M. Brütting, H. Weinläder, F. Devia, Numerical and experimental investigation of an insulation layer with phase change materials (PCMs), *Energy and Buildings*, 153 (2017) 231-240.
- [268] A.J.A.S.o.H. Standard, Refrigerating, I. Air-Conditioning Engineers, Criteria for Moisture-Control Design Analysis in Buildings, (2009).
- [269] A. Hukka, H.A. Viitanen, A mathematical model of mould growth on wooden material, *Wood Science and Technology*, 33 (1999) 475-485.